Bangor University

DOCTOR OF PHILOSOPHY

The distribution and dynamics of particulate matter at the Hebridean shelf edge

McCandliss, Robin Rita

Award date:
2000

Awarding institution:
University of Wales, Bangor

[Link to publication](#)

Title: The distribution and dynamics of particulate matter at the Hebridean shelf edge

A thesis submitted in accordance with the requirements of the University of Wales for the degree of Doctor of Philosophy

by Robin Rita McCandliss

University of Wales, Bangor
School of Ocean Sciences,
Menai Bridge,
Wales LL59 5EY
Great Britain

December 2000

ABSTRACT

The SES experimental campaign took place over a 16 month period between March 1995 and August 1996 along the Hebridean continental slope (56° - 58° N), to the west of Scotland. This study was associated with, in particular, examining the distribution and fluxes of particulate matter based on observations with moored instrumentation and regular water column surveys. Despite the poor performance of some of the instruments during the study, a valuable dataset was collected comprising PMC, current velocity, particle size and settling velocity data, substantially enhancing the existing database.

A seasonal cycle in PM distribution was observed at the Hebridean shelf edge, which is dominated by phytoplankton production in Spring and storm-driven resuspension in Winter. Despite strong tidal currents and internal wave activity in the summer months no significant resuspension due to these agents was observed. PM distribution at the upper slope is influenced by the poleward flowing slope current. This is confined to the upper 500 m and is characterised by a core of warmer, more saline water with higher PMC than the surrounding water. Further down the slope, benthic nepheloid layers form a typical feature throughout the year, but especially in Winter and late Spring. Intermediate nepheloid layers, following density surfaces were also observed in the aftermath of a storm.

Near-bed PM flux calculations indicate that PM is persistently transported northwards along-slope by the slope current, and off-shelf by Ekman transport in the benthic boundary layer, even at depths of 1500 m. Along-slope fluxes are 2-3 times greater than across-slope fluxes and are greatest on the shelf and upper slope.

Intermittent resuspension by storms of PM on the shelf and slope enhances near-bed PMC and off-shelf flux, albeit for relatively short periods (days). Cross-slope fluxes are also enhanced by phytodetritus settling into the benthic boundary layer in the aftermath of phytoplankton blooms, this time over longer periods (weeks).

Estimates of off-shelf PM flux in the benthic boundary layer are three orders of magnitude greater than the estimated vertical flux. This lateral source of carbon may account for discrepancies observed by other SES workers between the sediment community demand for carbon and the vertical supply, and represents an important transfer of organic matter to the deep ocean.

ACKNOWLEDGEMENTS

For my Dad and Mom

TABLE OF CONTENTS

...

LIST OF FIGURES

Appendix

LIST OF TABLES

CHAPTER 1

Introduction

1.1 Background and motivation for the study

Particulate matter (PM) is present in all natural waters of the world. It may be a very small amount, as in some parts of the ocean, but microscopic inspection to date has always indicated the presence of at least some particulate material in suspension. Because of this ubiquitous presence, and because of the physical and chemical properties of the particulate material itself, PM forms an integral part of the world-wide geochemical, biological, and geological cycles in the marine environment.

Quantifying particle transport is a fundamental requirement for understanding of contaminant dispersal and water quality. Many pollutants and contaminants are associated with particulate matter. They interact with material in suspension or on the sea bed and become adsorbed onto the particle surfaces (Duursma and Eisma, 1973). Exchange rates tend to be higher with PM than with the sea bed due to the greater surface area exposed by particles in suspension.

Particulate matter plays a significant role in the productivity of shelf waters. Particulate organic matter is a major source of food for many marine organisms. The fate and sink of this material is presently not well quantified. The living organic fraction of PM makes up the base of the food web and accounts for the fact that continental shelves are the most productive areas in the world's oceans (Emery & Honjo, 1979). On the other hand, PM may restrict productivity as particles influence turbidity and hence the light available for primary production.

Virtually all particulate matter is supplied either by terrestrial input or through the production of organic matter. It is estimated that 73 % of the total supply to the marine environment arises from production of biogenic particles, while rivers supply 8 % (Eisma, 1993). The remainder is supplied by a variety of sources: the

1

atmosphere, coastal erosion, sea floor erosion, direct run-off from land, ice flows and ice rafting, submarine volcanism and interplanetary space (cosmic dust).

Phytoplankton and zooplankton dominate the particles present in the surface waters. Their skeletons and pellets sink, comprising a large fraction of the material in transit through the water column. Other components, such as volcanic and wind-blown detritus, are regionally important constituents of particulate matter. Particle surfaces provide micro-habitats allowing colonisation by bacteria. These bacteria may break down less soluble molecules and contribute to remineralisation of certain components.

The contrasting differences in the physical, chemical and biological properties between the coastal zone and the open ocean lead to marked gradients that strongly influence the exchanges between the two systems. Continental margins are the transitional zone at which contrasting deep ocean and shelf sea regimes adjust to one another. Distinctive processes operate at the shelf edge, which control interchanges between the shelf and ocean.

Because of the diversity of processes occurring at continental margins, the exchanges of energy, and of particulate matter between the shelf and the open ocean remain poorly understood. The quantification of exchanges (e.g. sediments, nutrients) across the continental slope is fundamental to determining shelf sea budgets. Major processes and factors controlling fluxes at the shelf edge are depicted in Figure 1.1.

1.2 Previous studies of PM dynamics at continental margins
1.2.1 SEEP

The growing awareness of the importance of continental margins in shelf-ocean exchange processes has given rise to a number of experiments. The most extended study of fluxes of particulate matter on the continental slope has been produced by the Shelf Edge Exchange Processes (SEEP) I and II programmes (Biscaye *et al*, 1988; Walsh, 1988; Biscaye and Anderson, 1994; Falkowski *et al*, 1994, Walsh, 1994). Both programmes focused on the Middle Atlantic Bight: SEEP-I at the northern end and SEEP-II at the southern end.

The SEEP-I experiment took place at the Middle Atlantic Bight (MAB) off New England between July 1983 and October 1984. Investigations prior to SEEP-I suggested that a large proportion of shelf primary production was exported to the continental slope: as much as 90% of spring bloom primary production could not be traced either to burial on the sea bed or to immediate respiration by the food chain (Walsh, 1983). This interest in the fate of particles in the continental shelf water column and the slope water dynamics that affect sedimentation of particles onto the slope, led to the formation of the general hypothesis that there was a substantial export of particles in general, and organic carbon in particular, from the continental shelf to the continental slope sediments (Biscaye *et al*, 1988). The mid-slope region was presumed to be a 'sink' for both biogenic and abiogenic particles, with quiescent bottom currents creating favourable conditions for particle deposition on the slope.

The overall SEEP project working hypothesis was that most of the biogenic and abiogenic PM that is formed on and introduced to the shelf, and not consumed there, is not deposited on the shelf. It is either transported alongshore to the southern end of the MAB where it exits the shelf adjacent to the Gulf Stream, and/or it is transported by several mechanisms across the shelf-slope front at the shelf break into the relatively quiescent waters of the continental slope, where it undergoes deposition (Biscaye *et al*, 1988). It was expected that the flux of particles across the shelf break would increase towards the south from New England to Cape Hatteras since the Mid Atlantic shelf becomes narrower, and primary productivity is expected to increase to the south. The SEEP-I experiment was designed to measure the exchange of particles from shelf to slope waters at a location where it might be at a minimum, in contrast with the SEEP-II experiment off Cape Hatteras where it might be at a maximum.

Datasets obtained during SEEP-I from moored current meters across the shelf and slope showed that conditions at the slope were indeed favourable for deposition and accumulation of fine-grained sediment and organic carbon. Near bottom currents greater than 20 cm s^{-1} occurred frequently over the outer shelf (<200 m) but very rarely between bottom depths of 500 m and 2000 m over the slope (Csanady *et al*, 1988). Asymmetry was observed in the near-bed cross-isobath current, with

maximum downslope flow exceeding maximum upslope flow by a factor of two to three, favouring net downslope transport of particles (Butman, 1988).

Evidence for downslope transport of material emerged from particle fluxes measured by sediment traps. Near-bed traps consistently measured greater fluxes than the traps overlying them. This implied that, in addition to the vertical supply of particles, there was near-bed lateral transport of particulate matter from the waters and sediment of the shelf, shelf break and upper slope (Biscaye *et al*, 1988). With regards to the export of organic carbon, while export of particulates to the slope had been measured, there was evidence that the bulk of the unused shelf primary production was not available for export. Rather, it was remineralised on the shelf and that which was exported (<10%) was a small part of the total organic carbon productivity (Biscaye *et al*, 1988).

The second experiment, SEEP II, took place at the southern MAB from February 1988 to June 1989. All of the observational data provided strong evidence that the original hypothesis was false (Biscaye *et al*, 1994). Most of the biological particulate matter was shown to be recycled by consumption and oxidation on the shelf, and only a small proportion (of the order of <<5%) was exported to the adjacent slope. Most of the carbon flux to the upper slope sediments in the Middle Atlantic Bight is supplied by lateral transport rather than vertical settling (Anderson *et al*, 1994). Much of the carbon supplied to the slope sediments was found to be refractory, having originated by reworking of older deposits. The depocentre was found to be a site of preferential deposition of new labile carbon as well as old refractory carbon but the labile carbon disappears rapidly and contributes nothing to the organic rich nature of the depocentre sediments (Anderson *et al*, 1994).

1.2.2 ECOMARGE

On the eastern side of the Atlantic, the ECOMARGE (ECOsystèmes de MARGE continental) experiment aimed to quantify the transport of particulate matter from the shelf to the slope and deep sea (Monaco *et al*, 1990), with particular emphasis on the roles that canyons play in particle transfer. The first experiment, ECOMARGE-I, was carried out in the north-western Mediterranean from 1985-1988. The characteristics

of this site differed from the SEEP site in that the Rhône River was a major direct source of material onto a narrow shelf and canyon-incised slope. The second ECOMARGE experiment, ECOsystème du canyon du cap-FERret (ECOFER) took place on the Atlantic margin at the Bay of Biscay from 1987 to 1991. As the dominant feature on the French Atlantic margin, the Cap Ferret Canyon was chosen as the focus of the ECOFER experiment because of its obviously erosive origin, and because of its proximity to the Gironde Estuary, the major modern source of freshwater and of fluvial particles to the Aquitanian continental shelf (Monaco *et al*, 1999).

ECOMARGE-I results showed that of the particles formed in the waters of the continental shelf and those introduced by rivers, some are deposited on the shelf and some are transported offshore to the slope and deep sea (Monaco *et al*, 1990a). Observed variations in lithogenic and biogenic fluxes were attributed to seasonal factors such as river input and current intensity, and high frequency variations related to forcing events such as internal waves, storm resuspension and phytoplankton blooms (Monaco *et al*, 1990b). Offshelf distributions of particles were typically layered (Durrieu de Madron *et al*, 1990). The surface layer was dominated by biogenic particles; the near-bed layer dominated by abiogenic particles introduced by rivers or resuspended from bottom sediments (Monaco *et al*, 1990b). Intermediate layers formed where the benthic layer detached from the slope or canyon.

Two transport components and principal sources were differentiated during ECOMARGE-I: the vertical component, controlled by biological production, and the predominantly horizontal shelf-slope transport of continental input. The horizontal transfer of material consistently occurred from the north-east to the south-west of the study area, influenced by the prevailing cyclonic current, characteristic of the region (Monaco *et al*, 1990b). The large Lacaze-Duthiers Canyon at the south-eastern end of the study area served both as a sink and as a conduit for particle transfer, focusing the flux of material down the canyon.

The ECOFER experiment provided the opportunity to compare a relatively open Atlantic margin with the enclosed north-western Mediterranean margin. Circulation

in the Bay of Biscay is characterised by a predominantly northward flowing along slope current, though reversals in the current's direction can occur in summer (Durrieu de Madron *et al*, 1999). Results from this margin experiment showed similarities and differences to other margin studies.

Like SEEP and ECOMARGE-I, the ECOFER slope was found to be a depocentre for organic carbon and other particulates (Etcheber *et al*, 1999). Additionally, sediment trap studies exhibited typical margin patterns of fluxes decreasing offshore and increasing with depth, revealing the importance of advective transport (Heussner *et al*, 1999). However, in contrast to ECOMARGE-I, there was no clear seasonal trend in the variations of the total mass and particle composition in the water column and surficial sediment (Monaco *et al*, 1999; Etcheber *et al*, 1999). The Mediterranean canyon system studied in ECOMARGE-I is close to land and has well identified sources of material from phytoplankton blooms and direct continental supply at times of high river discharge. The Cap Ferret Canyon, on the other hand, is relatively distant from the main continental sources preventing direct supply of material to the canyon. There was evidence that internal tides caused resuspension on the slope, and resulting intermediate nepheloid layers (INLs) were advected along-slope by the slope current (Durrieu de Madron *et al*, 1999).

1.2.3 OMEX

Another experiment took place more recently in the north-eastern Atlantic: the Ocean Margin Exchange (OMEX) study. The first phase of this study focused on the Goban Spur, south-west of Ireland, from 1993-1996, with particular attention to biogeochemical cycling. This site has a gradual and extended slope leading to the North Atlantic abyssal plain. The dominant physical processes contributing to sediment transport and energy dissipation at the Goban Spur margin include a poleward-flowing along-slope current, and internal waves and tides (Huthnance, 1995). The second phase, 1997-2000, shifted its focus to the Iberian margin, which is characterised by a narrow shelf and steep, canyon-incised slope subject to seasonal wind-driven upwelling.

The general aim of OMEX I was to study the physical, chemical, geological, and biological processes at ocean margins that determine the transport of matter from the shelf to the deep sea (van Weering *et al*, 1998a). Sediment trap studies showed an increase in bulk flux with depth (Antia *et al*, 1999), following the trend of previous margin studies. Seasonal variability was observed in the flux of biogenic material, and there was evidence that resuspension occurred on the slope (Antia *et al*, 1999).

It was anticipated that lateral mass fluxes of particulate matter would significantly exceed the vertical fluxes, and it was found that even under low flow conditions, the horizontal fluxes of particulate organic carbon were two to three orders of magnitude higher than the vertical fluxes (Thomsen & van Weering, 1998). The north-west European continental margin at Goban Spur is characterised by enhanced flow conditions at mid-slope areas, especially during autumn and winter. At the lower slope, weak currents support the deposition of material (Thomsen & van Weering, 1998). It was concluded that the foot of the continental slope rather than the slope itself was the site of preferential deposition, and that the Goban spur slope was not considered to be a major carbon depocentre (van Weering *et al*, 1998b). The Goban Spur has a lower organic carbon burial flux than the Gulf of Lions and the MAB (van Weering *et al*, 1998b). In contrast with the SEEP MAB depocentre at 1000 m, the Goban Spur slope at 1000 m is likely to act as a source, rather than a sink, for off- and along-slope directed transport of fine particles in intermediate or benthic nepheloid layers (Thomsen & van Weering, 1998; van Weering *et al*, 1998b).

An important common conclusion to all of these studies is that lateral transport must account for a significant proportion of material exported from the slope to the ocean. The Shelf Edge Study, based at a location north of the OMEX I site, serves to complement the database of observations from the north-west European continental margin and add to the knowledge already gained from previous margin studies.

1.3 The LOIS Shelf Edge Study

This thesis considers the dynamics and distribution of PM at a continental margin in the north-eastern Atlantic, west of the Hebrides. The study was made as part of the Land-Ocean Interaction Study (LOIS) Shelf Edge Study (SES) funded by the Natural

Environment Research Council (NERC). This was an integrated interdisciplinary study to establish the basis for the estimation of fluxes between the north-west European shelf and the Atlantic ocean across the Hebridean shelf edge. The objectives of SES were (Simpson, 1994):

- To identify the time and space scales of ocean-shelf momentum transmission and to quantify the contributions to ocean-shelf water exchange by physical processes.

- To estimate fluxes of water, heat and certain dissolved and suspended constituents across a section of the shelf edge with special emphasis on net organic carbon export from and nutrient import to the shelf.

- To incorporate process understanding into models which will be tested by comparison with observations and provide a basis for estimation of fluxes integrated over time and the length of the shelf edge.

Within this programme an intensive data collection campaign involving cross-slope mooring arrays, and hydrographic surveys was undertaken, over a 16 month period during 1995 and 1996, along the Hebridean slope. A significant proportion of the instrumentation was lost or damaged, falling victim to the multitude of trawling vessels that frequent the area. Consequently, the times series data are patchy both in space and time. Nonetheless, an extensive new data set has been collected that greatly enhances the available database.

1.4 Aims and specific objectives

The broad aims of this component of the SES programme were to gain an insight into the characteristics and dynamics of PM at this continental margin. More specifically, this study aimed to achieve the following objectives:

- To quantify the vertical and horizontal distribution of PM.

- To characterise PM in terms of the constituent populations and settling velocity.

- To investigate the temporal variability of PM on tidal, lunar, episodic and seasonal time scales.

- To identify, investigate and compare the impact of

  i) resuspension due to tides, storms and internal waves

  ii) the downslope transport of nepheloid layers.

1.5 Thesis layout

Following the introduction presented in this chapter, the remainder of this thesis is organised as follows:

Chapter 2: Basic particle dynamics, factors affecting particle size, particle settling and deposition, and resuspension of PM are reviewed along with some of the physical processes affecting the distribution and transport of particles in the shelf edge environment.

Chapter 3: The study area and sampling strategy are described and the instrumentation used in this study is introduced.

Chapter 4: Data collection and processing methods are described, including a section describing the method adopted to rectify CTD transmissometer data affected by instrumentation faults.

Chapter 5: The calibration procedure used to convert optical data into PM mass concentration is described.

Chapter 6: The results obtained from the study are presented. Spatial surveys are presented and cross-shelf features and seasonal variations are described. Time series observations of currents and PM concentration are presented. Following this, particle size and particle settling velocity distributions are presented.

Chapter 7: Lateral fluxes calculated from the time series data and the results from harmonic analysis of the PM concentration signal are presented.

Chapter 8: The results presented in the previous two chapters are discussed with particular emphasis on biological processes, resuspension and lateral fluxes. The chapter closes with the main conclusions drawn from this study.
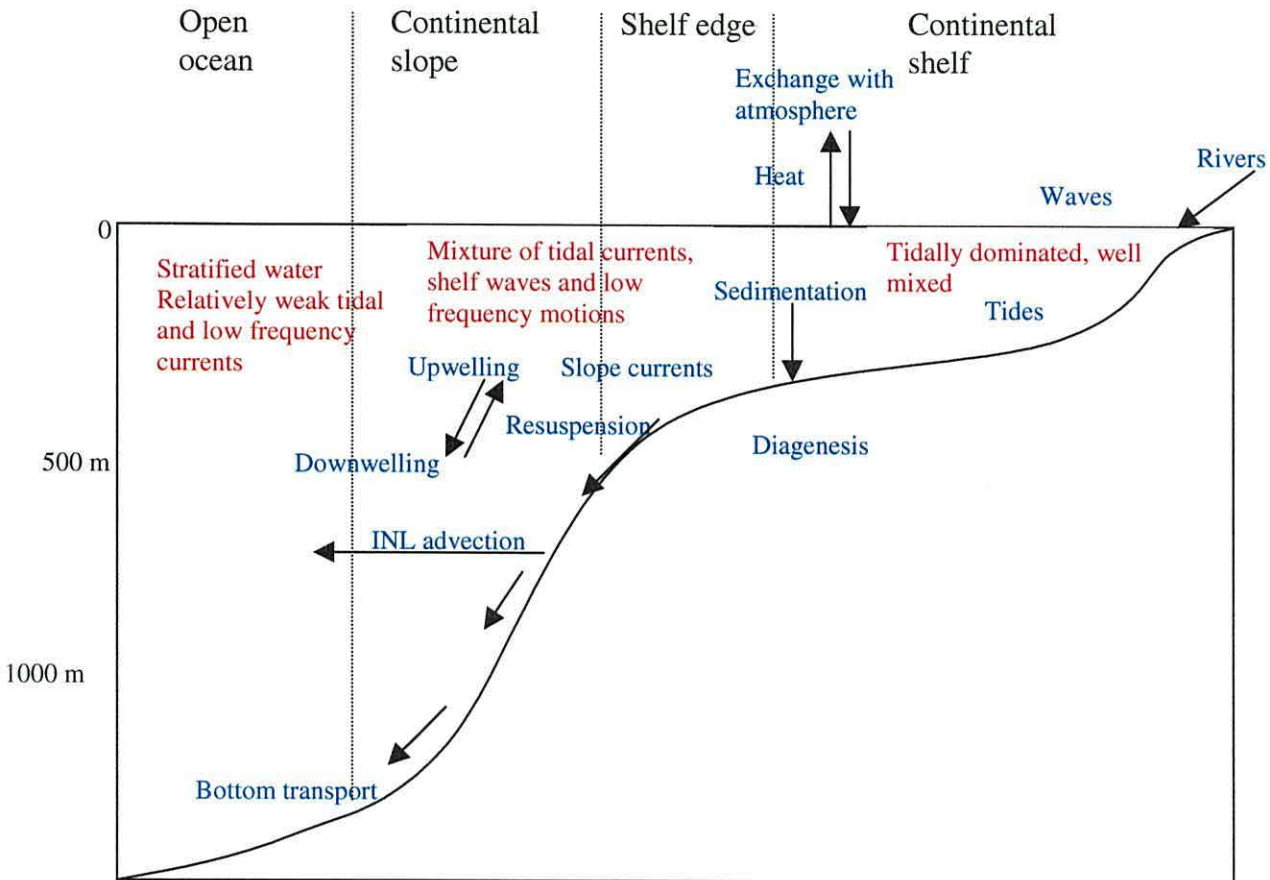
Figure 1.1: Cross section of the continental shelf and slope showing the energetic regimes (red text) and major processes affecting the fluxes of material (blue text).

CHAPTER 2

Particle dynamics and physical processes at the shelf edge

2.1 Introduction

The distribution of PM in the seas and oceans depends on many factors such as the origin and nature of the PM population, the tidal regime, meteorological conditions and seasons. As a result, PM concentrations fluctuate at many different frequencies over time scales ranging from minutes to years. The PM population in the marine environment is usually composed of several individual populations from a number of diverse sources and varies widely in composition, size and shape. In general, inorganic particles in suspension range from clays, characterized by a flat, plate-like structure, to fine sands that are more rounded. Sources of inorganic particles include coastal erosion, river run-off and erosion of sea bed sediments so that the concentration of such particles tends to decrease seawards. Levels of organic particles, on the other hand, tend to be dependent on the seasonal cycle. Such particles include phytoplankton and zooplankton and can be living matter or detritus. Particulate matter concentration (PMC) in the open ocean varies from less than 5 mg m^{-3} to *ca.* 1000 mg m^{-3} but may be as high as 100,000 mg m^{-3} in coastal waters (Eisma, 1993).

Having introduced the project and its specific aims within the LOIS framework in the previous chapter, the aim of this chapter is to present some general background information on suspended particle dynamics followed by a brief introduction to some of the physical mechanisms that affect transport of PM in the marine environment.

2.2 Factors controlling particle size

Particle size is one of the fundamental properties that determines distribution of PM in the water column. Particle size influences settling velocity and hence the degree of suspension, resuspension and deposition of the PM population. The size distribution of suspended particles is a function of several variables, including source and nature of the particles, and physical or biological processes of flocculation. Published

observations of marine particle size range from 1 μm to stringers tens of centimetres in length (Eisma, 1993). Lambert *et al* (1981) found individual aluminosilicate particles dominated size classes below 10 μm while aggregated or flocculated particles dominated size classes greater than 10 μm in the open ocean. Generally, two particle populations have been distinguished in the ocean: a common population of particles with sizes smaller than 5 μm and a rarer population of large particles > 50 μm (Lal, 1977). The fine particle population dominates the standing stock of suspended particles and is transported horizontally over large distances. The larger particles (> 50 μm) are mainly flocs and, with relatively rapid settling velocities, vertical transport dominates.

The flocculation of particles has a pronounced effect on particle transport and on the transport of particle-associated substances. It results in the formation of large particles from small ones and may increase the settling rate as a result of the larger particle diameter, although this can depend on the density. Larger particles do not necessarily settle more rapidly than small ones if they are loosely packed, with high water content and relatively low density. Concentration of a large number of fine particles into a small number of large ones may enhance primary production through increased water clarity (Eisma, 1993).

For flocculation to occur, two conditions must be fulfilled. Some process must bring particles close enough to collide and some of the collisions must result in the particles sticking together. Collision rates depend on particle concentration and a combination of processes causing the relative movement. These processes are:
- Turbulence
- Brownian motion
- Differential settling

Random turbulent eddies contribute to particle collision. The frequency depends on the concentration and volume of the particles, and the turbulent dissipation rate. A more detailed description of turbulence is given later in the chapter in section 2.3.1. Brownian motion results from the thermal motion of the particles. Krone (1978) showed that under estuarine conditions Brownian motion controlled flocculation of particles < 1 μm in diameter, and shear controlled flocculation of larger ones. Flocs

resulting from Brownian motion tend to be irregular and weak, which are easily broken up by turbulence. In contrast, flocs resulting from velocity shear tend to be spherical and are stronger than those formed by other methods. Differential settling is important for large particles. However, because there is little stress placed on the particles during collision they tend to be irregular and weak (Krone, 1978).

For the formation of flocs a considerable number of processes have been indicated:

2.2.1 Salt flocculation

Particles in natural waters are usually negatively charged (Hunter & Liss 1979, 1982) and repel each other. In saline water, however, colloidal suspensions form a double layer and the negative charge is neutralized. This allows Van der Waals forces to operate between particles close enough to one another, and cause flocculation. Salt flocculation was once believed to be the main agent for depositional processes in the coastal boundary zone, but new techniques for observing flocs revealed that other factors are involved which, in fact, inhibit salt flocculation including micro-organisms and organic coatings. Coating of a particle by organic compounds changes the surface characteristics and inhibits double-layer formation (Hunter & Liss, 1979, 1982).

2.2.2 Particle coatings

In natural waters, particulate matter is coated with organic matter, such as saccharides and humic compounds. The coatings can be formed in different ways: by direct adsorption of dissolved compounds onto the particle surface, or by flocculation or polymerization of dissolved compounds in the water followed by adsorption. Coatings can also be produced by microorganisms associated with the particles. The mucus produced by these organisms provides a surface suitable for adsorption (Trent *et al*, 1978; Alldredge, 1979). It is postulated that flocculation is facilitated because the particles have increased stickiness and polymer chains can form 'bridges' between adsorption sites on different particles.

2.2.3 Flocculation by organisms

It is now thought that biological processes play the most important role in flocculation. Mass flocculation of spring phytoplankton blooms (marine snow formation) has been observed in Nova Scotia (Kranck and Milligan, 1988), Californian coastal waters (Alldredge & Gotschalk, 1989), and in the southern North Sea (Riebesell, 1991 a, b). Flocs as large as 5 cm in diameter can form during the decline of the bloom and result in diatoms settling to deep water.

Bacteria produce slime films on immersed surfaces, enhancing flocculation (Riley, 1963,1970). Microorganisms, including bacteria, phytoplankton and zooplankton, are themselves coated with secretions which promote flocculation and can act as nuclei for the flocculation of other particles.

Larger organisms, both planktonic and benthic, actively produce flocs by binding particles together, usually within a membrane (Alldredge & Silver, 1988). The pellets produced are faeces or pseudofaeces, the former have passed through the digestive tract, the latter consist of particles that were not taken in but were rejected and enveloped in mucus on the gills. Both types of pellets have much larger settling velocities than those of the constituent particles.

A major part of the matter sinking out of the euphotic zone consists of amorphous aggregates (Olsen & Lundsgaard, 1991), and preliminary studies indicate that transparent exopolymer particles (TEP) are important in the aggregation of diatom blooms. These TEP provide the matrix of marine snow, serving as a substrate and microhabitat for attached bacteria, and representing an important pathway for the transformation of dissolved to particulate material (Alldredge *et al*, 1993; Passow *et al*, 1994). TEP is apparently formed from polysaccharides exuded by phytoplankton and bacteria (Alldredge *et al,* 1993).

2.2.4 Floc formation by bubbles

Bubbles are formed by gas escaping from organisms or bottom sediments, but principally from breaking waves at the surface. Dissolved organic matter can be converted into particles through adsorption onto the bubbles and aggregation when

the bubbles burst or dissolve (Riley, 1970). Bubbles can also aggregate existing particles. It is unknown how important this process is in the flocculation of suspended matter relative to the other flocculation processes. It is probable that bubbles become more important in oceanic surface waters where particle concentrations and biological activity are low.

2.2.5 Floc break-up

For any suspension, the degree of flocculation is a dynamic balance between floc formation and floc break-up processes. Flocs may either break up completely or be eroded through surface shear or turbulent drag. The break-up process depends on the turbulent dissipation rate, floc size relative to the turbulent microscale, floc cross-sectional area and floc strength (Eisma, 1993). Collision of flocs can result in break-up as well as flocculation.

2.3 Vertical flux and deposition of PM

The rate of deposition of PM depends on settling velocity, the mean flow velocity and on the concentration of material in suspension near the sea bed. In the oceans much of the PMC lies in relatively small sized particles with low descent rates, but the vertical flux is dominated by large, relatively rare particles settling rapidly (McCave, 1975). Certain small particles, for example calcareous nanoplankton, would dissolve before reaching the bottom unless they fell rapidly in aggregates (Honjo, 1976). In areas where bottom currents are weak this vertical flux of large particles is the principal means of sedimentation (McCave, 1984).

In areas of low concentration, such as continental margins, there is less flocculation compared with high concentration areas such as estuaries. Thus the rate of deposition tends to be lower. Observations in nature have shown that flocculated material usually starts to settle out of suspension at flow velocities of 10-15 cm s^{-1}. Those flocs which are strong enough to withstand the maximum shear at the bottom will deposit, but the weaker ones will break apart and be re-entrained into the main flow (Mehta & Partheniades, 1975). In the open ocean, settling rates for fine aluminosilicate particles range between 0.08-0.41 m day^{-1} (0.0009-0.005 mm s^{-1}) (Lambert *et al*, 1981) and thus are unlikely to be deposited unless incorporated into

flocs. Settling velocities of flocs vary widely depending on the size, composition and density. Published examples include 1 m day^{-1} (Asper, 1987), 4 m day^{-1} (McCave, 1985), 45-79 m day^{-1} (Gardner & Walsh, 1990), 150 m day^{-1} (Thomsen & van Weering, 1998) and 50-200 m day^{-1} (Alldredge & Silver, 1988).

2.3.1 Factors controlling particle settling velocity

The settling velocity of particles in quiescent seawater is controlled by size, density, shape and roughness. In natural waters, turbulent fluctuations provide an additional vertical component of velocity, which can counteract settling velocity and prevent deposition.

A particle falling in laminar flow conditions reaches terminal velocity when the drag force F_D equals the immersed weight. Drag force can be written as:

$$F_D = C_D \pi \frac{D^2}{4} \rho \frac{w_s^2}{2}$$

(2.1)

where C_D is the drag coefficient, D is the particle diameter, ρ is the fluid density and w_s is the settling velocity. The immersed weight F_B of a particle is shown by:

$$F_B = \frac{4}{3} \pi \frac{D^3}{8} (\rho_P - \rho) g$$

(2.2)

where ρ_P is the particle density and g is the gravitational acceleration. When $F_D = F_B$:

$$w_s^2 = \frac{4}{3} D \frac{(\rho_P - \rho)}{\rho} \frac{g}{C_D}$$

(2.3)

The drag coefficient C_D is a function of the particle's Reynold's number Re_p:

$$Re_p = \frac{D w_s}{v}$$

(2.4)

where v is the kinematic viscosity of the water. In laminar flow, where the particle moves through the water leaving no turbulent wake, the settling velocity can be written as (Eisma, 1993):

$$w_s = \frac{2 \pi (\rho_P - \rho) g D^2}{9 \quad 4v}$$

(2.5)

This is Stokes Law: the settling velocity is proportional to the diameter squared when flow is laminar. Experiments have shown that Stokes law is only valid for spherical particles with diameters smaller than 0.1 mm. Settling rate, then, depends on:

- Particle diameter: large diameter results in a faster settling rate.
- Particle density: high particle density results in a faster settling rate.
- Fluid density and viscosity, properties dependent on composition and temperature.

High concentrations of particles also affect the settling rate as there is increased frequency of particle collisions and flocculation may be enhanced.

The shape of particles influences the way in which they settle. Most natural particles have shapes that can be approximated to regular geometric forms, for example, spheres, disks and cylinders. The shape of particles can be expressed in terms of the Corey shape factor SF (Dyer, 1986):

$$SF = \frac{D_1}{(D_2 * D_3)^{1/2}}$$

(2.6)

where D_1, D_2, and D_3 are the shortest, intermediate, and longest diameters on mutually perpendicular axes. A value of $SF = 1$ indicates a sphere or cube. Decreasing SF indicates increasing platiness, which in turn increases the drag coefficient. Particle roughness also increases the drag coefficient due to turbulence induced, and reduces the settling rate.

The considerations of settling velocity have, thus far, been for quiescent flow conditions. In natural waters, turbulence may counteract particles settling and prevent deposition. Turbulence is characterized by random, disorganized motion that results in dissipation of energy and is a necessary preliminary to mixing processes in the marine environment. A statistical description of turbulence can be given by applying Cartesian coordinates; the velocity components in the x, y, and z directions of the flow are given by:

$$u = U + u' ; v = V + v' ; w = W + w'$$

(2.7)

where U, V and W indicate the mean flow along the x, y and z directions and u', v' and w' are the turbulent fluctuations. The high frequency turbulent components do

not contribute to any advective transport. Steady or stationary flow is characterized by values for U, V and W that do not change with time at any fixed point through which the fluid moves. When the mean flow is in the x-direction, the turbulent fluctuations are stronger in that direction than in the other directions.

The energy in turbulent motion is continually being transferred from large scales of motion to smaller scales. The small turbulent eddies get their energy from larger ones, which in turn get their energy from still larger ones. This process, the energy cascade, does not change the total amount of energy in the turbulence, nor does it convert the kinetic energy of the turbulent motion to another form of energy.

With the decrease in size of the turbulent eddies comes an increase in the velocity gradient across the eddies. When the eddies are sufficiently small and the velocity shear great enough, then molecular viscosity acts to resist and smooth the gradients in velocity. This smoothing of the flow by viscosity is the way the energy in turbulence is finally converted to heat and dissipated.

Turbulence in the ocean is controlled by the ratio of inertial forces to viscous forces, Reynold's dimensionless number:

$$\text{Re} = \frac{(uD)}{v} \tag{2.8}$$

where u is the velocity of the flow (m s^{-1}), D is the length scale (m), and v is the kinematic viscosity (m^2 s^{-1}). Flow becomes turbulent when Re $\approx$ 2200. To maintain turbulence the energy supply must exceed the energy demand. The supply arises from velocity shear and must be sufficient to overcome the stability or buoyancy forces in the water column.

In turbulent flow there is transport of material because of the turbulent velocity fluctuations as well as through mixing. The result is diffusion of material whereby the transfer is in the direction of decreasing concentration. The rates of turbulent dispersal and mixing are much larger, and the time scales shorter, than the rates of molecular diffusion. If the upward components of turbulence are strong enough to counteract particle settling velocity then the particle will not be deposited and will

remain in suspension. The main contributors to turbulence, friction and mixing processes at the northwest European shelf are tides and wind-driven currents, which commonly exceed 0.5 m s^{-1} (Huthnance, 1995).

2.3.2 Factors controlling particle resuspension

Resuspension of particles is controlled by a variety of factors including bed shear stress, particle size, shape and density, cohesion of the sea bed and biological processes. The extent of resuspension through the water column is controlled by the bottom boundary layer (BBL) which can coincide with the height of the pycnocline or extend through the entire water column in shelf seas.

The bottom boundary layer is defined as the region in which the flow is influenced by the presence of the sea-bed. The average velocity of the flow increases away from the boundary until the 'free-stream velocity' is reached, that is, the velocity that it would have if the boundary were not present. This is a simplified description, as if the water in a particular layer is moving at a constant velocity and always in the same direction. In natural waters flows are turbulent and exhibit fluctuations perpendicular to the direction of the mean flow. The amplitude of these fluctuations decreases towards the boundary as there can be no flow into or out of the boundary.

The decrease in the magnitude of the mean flow is caused by the stress exerted on the water by the solid boundary. The transmission of this stress across the layer of water is accomplished, in turbulent flow, by eddy diffusion. As the boundary is approached the flow decreases until a level is reached where viscosity smoothes out almost all turbulence and the stress between the water and the boundary is transmitted by viscous stresses. A vertical profile of mean water velocity through the boundary layer above a smooth surface will show a linear sublayer where viscous stresses dominate and a logarithmic layer where turbulent stresses dominate. For the logarithmic layer, the mean velocity is given by the von Karman-Prandtl relation:

$$u(z) = \frac{u_*}{k} \ln \frac{z}{z_0}$$

(2.9)

where u is the velocity at height z, u_* is the friction or shear velocity, k is the Von Karman constant (0.4), and z_0 is the roughness length scale, dependent on the bed

form. In this layer velocity increases logarithmically with distance from the boundary. Elements of roughness in the surface of the boundary are liable to generate turbulent wakes in the sublayer. If viscosity does not smooth out this turbulence then the whole sublayer becomes turbulent and the flow is 'rough'. This has two consequences. First, the boundary exerts more stress on the water because there is more friction. Second, the relationship between velocity and distance from the boundary layer becomes logarithmic throughout the boundary layer and the laminar sublayer controlled by viscosity disappears.

In order to resuspend recently deposited particles, the threshold for erosion must first be exceeded. The quantity most commonly used to describe the potential that a certain flow has for the erosion of sediment is the bed shear stress (τ_b), with the value for the onset of erosion given by the critical bed shear stress (τ_c).

The drag force the flow exerts on a particle at the sea bed is the product of the shear stress τ_b and the surface area of the particle exposed to this stress. This force is counteracted by the weight of the particle in the water. The critical shear stress τ_c occurs when the upward component of the drag is equal to the particle weight. If the bed shear stress exceeds the threshold value τ_c, then the sediment will move. The critical shear stress increases with cohesiveness of the sediment.

The bed shear stress for a particular flow is commonly determined by assuming that the velocity profile can be described by the von Karman-Prandtl velocity profile given by equation 2.9, allowing calculation of u_*, the friction or shear velocity. u_* is defined in terms of the bed shear stress by:

$$\tau_b \equiv \rho u_*^2 \tag{2.10}$$

where ρ is the density of seawater. Thus, if u_* is known, τ_b can be calculated. Another common method for predicting the bed shear stress is through a quadratic friction law:

$$\tau_b = \rho C_D u^2 \tag{2.11}$$

where u is the measured velocity and C_D is the drag coefficient dependent on the roughness of the bed.

Several oceanographic processes cause increases in bed shear stress and hence resuspension on the continental shelf and slope. Storms are one important mechanism for increasing bed shear stress and if severe enough may cause shelf-wide episodes of resuspension (Churchill *et* al, 1994). The effect of storms diminishes with depth, so that resuspension at the outer shelf is generally less than that at the middle and inner shelf. High frequency internal waves and internal tides are also possible agents in initiating sediment motion at the shelf edge (Huthnance, 1981). Bottom trawling by fishing boats is an increasingly common anthropogenic cause of resuspension both on the shelf and over the slope (Churchill *et al* , 1994).

Although a variety of physical factors at the sediment-water interface influences the magnitude of resuspension, biological factors are also important. Most marine sediments contain biota which may destabilize sediment during feeding and locomotor activities, facilitating resuspension, or stabilize them with tubes, roots and mucus (Eckman *et al*, 1981; Grant *et al*, 1982) making it harder for resuspension to occur. The benthic population can actively incorporate particles into the sediment by biodeposition as well as resuspend material into the water column by bioentrainment.

Benthic organisms play a significant role in modifying the conditions for sediment entrainment (Jumars & Nowell, 1984) by:
- altering the individual particle characteristics, their vertical and horizontal distribution and, therefore, their availability for entrainment.
- changing the bulk characteristics of the sediment, such as its permeability and cohesiveness.
- varying the boundary properties of the flow by altering the surface roughness of the bed.

Biological effects are variable and depend, for example, on organism density, sediment composition and the lifestyle of the organisms in the community. Polychaete tubes, which protrude from the bed, can entrain higher-velocity fluid

down to the sediment surface causing local scour. The tracks of small mobile organisms increase the small scale roughness of the boundary. This increases z_0, the boundary roughness length scale, which may enhance entrainment of sediment.

Once sediment has been resuspended, it may be transported as either bed load or suspended load. Particles are supported by turbulence in suspended load transport, whereas in bed load transport the particles are supported intermittently by grain to grain contact. Particles in bedload transport move in a series of short hops and jumps along the bed at a fraction of the flow speed (Bridge & Dominic, 1984). Generally, grains of sand size and larger tend to be transported as bedload while suspended loads tend to consist of fine silts, clays and other particles with low settling velocities.

2.4 Factors controlling the vertical distribution of PMC

The vertical distribution of PMC depends on the degree of resuspension occurring, settling velocity of the particles, turbulence in the water column and biological production. This normally results in surface and bottom layers of PM with, in some areas, several layers at intermediate depths (Drake *et al*, 1972; Meade *et al*, 1975). These turbid layers found on the shelf and in the deep ocean are termed nepheloid (cloudy) layers.

2.4.1 Water column structure: stratification and mixing

The difference between shelf sea and oceanic regimes, has implications for the distribution of PM in the water column. Coastal waters tend generally to be fully mixed as shallow depths allow tidal stirring and surface windstress to penetrate through the water column. Away from the coast, in the shelf seas seasonal stratification occurs. Solar heating at the surface increases in Spring resulting in a warmer, less dense surface layer overlying a colder bottom layer, separated by a thermocline. In Autumn heat is lost from the surface layer making it less stable and eventually the water column is overturned and becomes fully mixed.

Stratification is classified by the potential energy anomaly (ϕ) which is the work required to bring about complete vertical mixing (Simpson & Hunter, 1974). In a

mixed water column ϕ is zero and increases in value as stratification develops. It is the key parameter in the competition between stabilizing and stirring effects in the water column (Simpson & Hunter, 1974). Stratification will only develop if the buoyancy term due to heat input is greater than the stirring term. In continental shelf seas, where buoyancy changes are primarily due to heating, and this rate of heat input is spatially uniform, the controlling parameter for stratification is found to be h/U^3 where h is the water depth and U is the amplitude of the tidal current (Simpson & Hunter, 1974).

The shelf seas alternate seasonally between mixed and stratified regimes. Across the continental slope, oceanic waters are permanently stratified as the water column is too deep for complete mixing to occur. The structure of the water column influences the vertical distribution of PM. In fully mixed waters, turbulent activity results in dispersal of PM through the water column. Mixing may also cause PMC to increase if primary production occurs as a result of increased nutrient availability, providing light is not a limiting factor. In stratified conditions the surface and bottom mixed layers can be dominated by completely different populations of particles, depending on the season. In Spring and Summer, when nutrient and light conditions are favourable, phytoplankton blooms occur causing PMC to increase in the surface layer. With the decline of the bloom, particles may flocculate and settle to the bed, resulting in temporally varying concentrations in both layers. Stratification significantly reduces the flux of particulates into the surface layer as turbulence is inhibited by the presence of the pycnocline (Weeks, 1989). The role of the pycnocline acting as a barrier to the upward flux of particulates has also been reported by Jones *et al* (1998) from observations at a seasonally stratified site in the southern North Sea.

2.4.2 Nepheloid layers

Layers in the ocean in which light is less well transmitted because of the presence of suspended matter are termed nepheloid layers. They are frequently tens, or even hundreds of metres in thickness. Benthic nepheloid layers (BNLs) are often found adjacent to the seabed above the continental shelf (Newberger & Caldwell, 1981; Shideler, 1981) and the deep ocean floor (e.g. Jerlov, 1953; Gardner & Sullivan,

1981; Nyfeller *et al*, 1985), or in other regions where rapid bottom currents are locally scouring and transporting sediment (eg. Thorpe, 1972; Gross *et al* , 1988).

Intermediate nepheloid layers (INLs), separated from immediate contact with the seabed below them, occur in deep water at the level of a nearby shelf-break (Drake, 1971; Pak *et al*, 1980a; Hickey *et al*, 1986; Azetzu-Scott *et al,* 1995), due to the advection of suspended material off the continental shelf. They can also be found at greater depths, for example, where currents carry suspended material from a BNL over a deep ocean trench (Tucholke & Eittreim, 1974) and occasionally have been identified optically in mid-water adjacent to the continental slope and rise (e.g. Ewing & Thorndike, 1965; Pak *et al*, 1980b; McCave, 1983; Dickson & McCave, 1986; Richardson, 1987). Intermediate nepheloid layers are considered very important for transporting particulate matter from the ocean margins to the ocean interior (Murray, 1987).

2.5 Physical processes at the shelf break

The deep ocean and shelf sea physical regimes meet at the shelf edge. The relatively sharp change in bathymetry has implications for the general hydrodynamics that operate at the ocean-shelf margin. The remainder of this chapter gives a brief description of some of the physical mechanisms that affect transport of PM in the marine environment, in general, and at shelf-break regions in particular.

2.5.1 Tides

Tidal motion, generated by the gravitational forces of the sun and moon, occurs on the global scale. Resonance, bathymetry and friction affect surface elevations and currents due to the tide. These effects are greatest in shelf seas. Enhanced response of the water column to tidal forcing occurs at shelves that are sufficiently broad. The northwest European shelf, the Argentine shelf and the Gulf of Maine are examples of such wide shelves.

Cross-slope transport induced by the tide may be large but may not result in significant exchange as most of the water returns each tidal period and gives little time for a constituent to undergo non-conservative processes. Vertical mixing

between waters experiencing different tidal displacements gives rise to shear dispersion, which tends to be the main process of lateral exchange in these circumstances (Huthnance, 1995). Tidal currents may be effective in moving PM when the ebb flow may transport PM from the more energetic shelf with subsequent settling in quieter slope waters.

2.5.2 Along-slope currents

Slope currents are observed at many continental slopes along the eastern boundary of the ocean basins. They are steady or slowly varying currents flowing along the continental slope with shallower water on the right in the northern hemisphere. Along-slope currents contribute significantly to shelf edge circulation (Huthnance 1995). The distribution of the flow depends on the character of the forcing, balanced by the along-shore pressure gradient, friction and acceleration. Along-shore pressure gradients are typically imposed by the ocean and may incorporate density forcing. In general, temporally and spatially varying wind-stress acts in combination with the joint effect of baroclinicity and relief (JEBAR) (Huthnance 1984), waves and eddies with some degree of nonlinearity and a reactive barotropic pressure gradient. This barotropic pressure gradient acts equally throughout the water depth and is therefore most effective in deep water where it tends to give a return flow balancing the forward flow driven by the other agencies over the shelf and slope.

With respect to the exchange of bottom sediment, a strong along-slope current prevents sedimentation except in deeper areas which are preferentially filled to inhibit slope failure (Kenyon, 1987). As well as potentially introducing a different water mass from 'upstream', the bottom boundary Ekman layer associated with a slope current can also affect mixing over the slope. White (1994) reports changes of stratification in the bottom 100 m associated with changes in the mean slope current and consistent with the effect of Ekman flow up/down slope.

2.5.3 Wind-driven flows

The upwelling of deeper ocean waters onshore to the shelf is a consequence of offshore transport of upper waters. For example, northerly winds along western European shelves drive a surface (Ekman) transport offshore. At the European ocean

margin, upwelling is most prominent west of Iberia where there is a very strong seasonal signal, a complete reversal of the slope and shelf circulation between summer upwelling and a northward flow along the slope in winter (Huthnance 1995). There is also evidence of occasional upwelling west of Scotland and Ireland (Booth & Ellett, 1983; Dickson & McCave, 1986). Upwelling has important implications for the productivity and thus amount of biogenic PM in the surface waters above the thermocline, as it injects new supplies of nutrients into the euphotic zone. With winds in the opposite direction, surface transport is landward which causes downwelling flows. Results from the outer shelf of the Middle Atlantic Bight obtained via the SEEP I field study showed that net transport was seaward in the surface and bottom layers and landward flow of slope water took place at mid depth (Walsh *et al*, 1988).

2.5.4 Cascading

Cascading may be regarded as a special form of downwelling. It occurs when shallow waters on the shelf are cooled in winter to lower temperatures and greater density than adjacent waters over the slope. The dense shelf waters flow down the slope under gravity, aided by friction and any topographic channeling counteracting the geostrophic tendency for along-slope flow. The down-slope flow entrains ambient water, reaches a depth where the density is the same, and spreads off-slope (Price & Baringer, 1994). Cascading is an irreversible exchange of oceanic and shelf waters and may be distinctive in moving sediment downslope, off the shelf. It is a process sensitive to the hydrographic conditions and degree of winter cooling in any one year. Cascading events have been observed in the Gulf of Lions (Millot,1990), eastern Spain (Andrie & Merlivat, 1988), the Celtic Sea (Cooper & Vaux, 1949) and at the Hebridean shelf (Hill *et al*, 1998).

2.5.5 Internal waves

Internal waves are formed when vertical displacements and associated pressure fields are induced in tidal flow across the steep continental slope. The precise form of the waves and possible bottom-intensified currents are very sensitive to the distribution of bathymetry and density at the shelf edge (Baines, 1986).

Internal tides propagate slowly and thus are affected by strong advective tidal currents. The presence of strong cross-slope barotropic tidal currents gives rise to large amplitude internal tides. Internal tides with sufficient vertical displacements steepen and form solitons, as seen from satellites by Synthetic Aperture Radar (SAR) (e.g. New, 1988). Enhanced mixing is usually the main impact of internal waves at the ocean margin. Sediment movement may be increased with the reinforcement of bottom currents by internal waves. Internal waves have been observed to propagate both on-shelf and off-shelf at the outer shelf of the Celtic Sea (Heathershaw, 1985). Flow velocities associated with these waves are 30-40 cm s^{-1} and are superimposed on other local currents (Heathershaw, 1985). These velocities are sufficient to affect cross-shelf sediment transport rates (Nittrouer & Wright, 1994).

2.5.6 Coastal trapped waves

The steep change in bathymetry at the shelf edge provides conditions that lead to trapping of certain wave motions called coastal trapped waves. These waves are commonly generated by transient winds and propagate along the edge of the shelf. They tend to decay off-shelf but some may be at their most energetic over the slope (Huthnance, 1995). A review of observations up to 1986 (Huthnance *et al*, 1986) shows that coastal trapped waves occur along shelves of various orientation and in both hemispheres. Coastal trapped waves underlie and control phenomena important to ocean margin circulation exchange and mixing rather than making an independent contribution (Huthnance, 1995). They may contribute to the magnitude of circulation and exchange if the waves are near-resonant, causing increased motion on the shelf and by propagation to a shelf or slope sector of a different character, e.g. narrower.

2.6 Summary

Transport of suspended sediments on continental shelves involves several complex processes dependent not only on the properties of the particles but also on the physical processes operating in the water column. Particle size affects the settling velocity of particles and hence deposition and resuspension processes. Turbulence provides a means for evolution of particle size and density by the formation and breaking of flocs, as well as vertical transport of suspended particles. Tidal motion provides a primary source of turbulence in the bottom boundary layer but other

events such as internal waves and storms intermittently enhance mixing processes. The onset of stratification inhibits upward fluxes of PM but provides light favourable conditions for phytoplankton blooms, causing changes in the particle population. Slope currents transport PM along the slope, and upwelling and downwelling flows in response to along-slope winds facilitate cross-slope exchange. It is imperative to consider all of these variables, and the interactions and feedback effects that occur, in order to meet the objectives set out in Chapter 1 and gain an understanding of the dynamics and distribution of PM at the Hebridean shelf edge.

CHAPTER 3

The study area and observational strategy

3.1 Introduction

The Hebridean shelf edge was chosen as the site for the present study because it has a well-defined shelf break and a simple topography. The system studied would be two-dimensional with variations only in the cross-slope and vertical directions. The area can be considered representative of many shelf edge regions at the eastern boundary of the ocean where there are no complicated topographic features such as submarine canyons, shallow banks or ridges. This chapter introduces the study area in more detail and outlines the observational strategy and instrumentation used during the data collection campaign.

3.2 The study area

3.2.1 Location and description

The shelf bounded by the Hebridean margin is relatively broad and the continental slope is relatively distant from direct terrestrial influence. The region has a regular topography with isobaths running almost parallel to the meridians and depth increasing from the 140 m to the 1500 m isobaths in a distance of about 30 km. The steepest gradients, of the order of 1:10, occur between 200 m and 500 m (Holmes, 1994).

The detailed study region during the SES experiment is known as the SES box. This is a large rectangular area bounded by the North (N) and South (S) primary transects with secondary transects R and P between them (Figure 3.1). The co-ordinates of these lines are shown in Table 3.1. The transects run east-west from ~ 8 ° 55 ' W (140 m water depth) to ~ 9 ° 40 ' W (1500 m water depth) over a distance of approximately 30 km. The shelf break is situated at ~ 9 ° W and is orientated ~ 15 ° clockwise from true North.

28

Table 3.1: Positions of the regular survey lines within the SES box.

Transect	Longitude (° W)		Latitude (°N)	
	Shallow water	Deep water	Shallow water	Deep water
N	-8.954	-9.390	56.588	56.735
P	-8.936	-9.284	56.551	56.591
R	-8.933	-9.292	56.502	56.519
S	-8.977	-9.658	56.470	56.453

3.2.2 Features of the Hebridean margin

The Hebridean shelf edge is an accessible but exposed region which experiences moderate tidal currents, some internal tides and a well defined slope current. Of these characteristics, the most pronounced feature of the Scottish continental slope is the poleward flowing current confined to the upper 500 m of the slope. This current is characterised by warmer, more saline water than surrounding waters with velocities of the order 15-20 cm s^{-1} (Harikrishnan, 1998). Tidal currents in the region diminish in magnitude from 15 cm s^{-1} on the shelf to ~5 cm s^{-1} in deep water (Souza *et al*, 1999). The winds in this region are predominantly from the south-west with mean speeds of ~8 m s^{-1} and exhibit large variability as Atlantic depressions track in from the west (Souza *et al*, 1999).

The sharp change in bathymetry at the slope changes the tidal regime as the deep ocean tide moves onto the shelf. This leads to the formation of internal waves, which have the potential to enhance vertical mixing and exchange at the shelf edge (Sherwin & Huthnance, 1994). It is thought that enhanced primary production occurs at this margin due to nutrient injection into surface waters when internal tides interact with the slope (Jones, 1994). Exchanges of water column properties may also occur with cascading events. Cascades are intermittent phenomena that occur when dense water formed on the shelf (usually in winter) spills over the shelf edge and descends the continental slope as a gravity current (Whitehead, 1987). There is evidence to suggest that cascading occurred at the Hebridean margin in 1985 (Hill & Simpson, 1994) providing a sudden, if infrequent, method of transporting shelf sediments down the slope.

3.3.3 Sea bed sediments

Some information on the seabed within the SES box was obtained through photographs taken with the Proudman Oceanographic Laboratory (POL) seabed camera (Humphery, 1998). At the shelfbreak (140-200 m) there were few biota present. Large cobbles 10-40 cm in diameter were common, and coarse sand was formed into ripples and furrows by strong northerly currents. At 300 m pebbles from 3-5 cm were present, and the sand was still formed into north-south oriented ripples. At 700 m there were no current induced bedforms, but the fine sand bed was colonised by dense communities of sea urchins and brittle stars. Indistinct north-west facing ripples formed by weak benthic currents shaped the silt bed at 1000 m, where there was a rich and varied benthic community. The bed at 1500 m was composed of mud and there were no current induced bedforms in evidence. The biota at this location was dominated by burrowers (Humphery, 1998).

3.3 The observational program

In order to meet the project objectives, transmissometers, most with attached current meters, were deployed on moorings across the shelf edge, mainly concentrated on the southern transect (S) line and to a lesser extent along the northern (N) line. Maintenance of the moorings and intensive spatial surveys were carried out over a sixteen month period between March 1995 and August 1996. This involved seven cruises, occurring approximately every two months with a duration of about 30 days. Most of the cruises consisted of a mooring deployment/maintenance leg and a fast-track conductivity-temperature-depth (CTD) survey leg. CTD profiling was carried out during the mooring legs of the cruises, but to a much lesser extent. Cruise legs that were not devoted to mooring work involved repeated CTD surveys and water sampling. Along the transect lines, settling velocity tubes (SVTs) were deployed to determine particle settling velocity distributions, and additional water samples were collected for analysis by a Galai Cis-100 laser particle sizer with video-microscope.

3.3.1 Cruise details

The cruise schedule for the SES period is summarised in Table 3.2. Cruise vessels are indicated by the letters in the cruise code. Codes commencing with the letters CD indicate *RRS Charles Darwin* and CH indicates *RRS Challenger*.

Table 3.2: Summary of cruises during the Shelf Edge Study.

Cruise no.	Cruise code	Start	End	Lines surveyed
SES 1	CD91 A	02/03/95	22/03/95	selected stations only
	CD91 B	22/03/95	02/04/95	selected stations only
SES 2	CD93 A	07/05/95	16/05/95	N, S
	CD93 B	16/05/95	30/05/95	N, P, R, S
SES 3	CH121 A	10/08/95	18/08/95	N, S
	CH121B	18/08/95	01/09/95	N, S
	CH121 C	01/09/95	10/09/95	R
SES 4	CH123 A	15/11/95	29/11/95	selected stations only
	CH123 B	29/11/95	16/12/95	N, P, R, S
SES 5	CH125 A	31/01/96	12/02/96	N, P, R, S
	CH125 B	12/02/96	03/03/96	N, R, S, Upstream sections
SES 6	CH126 A	11/04/96	27/04/96	N, S
	CH126 B	27/04/96	12/05/96	N, P, R, S
SES 7	CH128 A	10/07/96	25/07/96	N, P, R, S
	CH128 B	26/07/96	08/08/96	N, S

3.3.2 Mooring details

The principal mooring array across the shelf break was located on the S line with moorings at depths of 140, 200, 300, and 700 m (Figure 3.1). A secondary array was located on the N line at 140, 300 and 1500 m. Three additional moorings (CC1, CC2, CC3) were deployed in a depression to the north of the N line at a location where cascading events might occur. Positions of the mooring sites are given in Table 3.3. Dates of individual deployment periods are given in Chapter 6 Table 6.1.

Table 3.3: Mooring sites and approximate positions in the SES box.

Mooring sites	Positions	
	Latitude (° N)	Longitude (° W)
S140	56 28	08 58
S200	56 27	09 03
S300	56 28	09 04
S700	56 27	09 10
N140	56 37	08 56
N200	56 38	09 00
N300	56 38	09 01
N1500	56 43	09 24
CC1	56 37	09 01
CC2	56 38	09 02
CC3	56 43	09 00

Each mooring was equipped with a variety of instrumentation but for the purposes of this study only transmissometers and current meters will be referred to. An example of a typical SES mooring with current meters and transmissometers located at near-surface, mid-water and near-bed positions is shown in Figure 3.2. During the regular cruise periods the moorings were recovered to allow downloading of the data and instrument maintenance.

The original aim, to obtain comprehensive time series observations across the slope for a 16 month period, was severely impeded with frequent disruption of the moorings by trawling activities. Many instruments were lost. The dataset was further reduced by poor instrument performance in some cases. Despite these setbacks and considerable gaps in the time series, the resulting datasets from the moorings and the hydrographic surveys have provided an important contribution to the available database on conditions at the shelf edge.

3.4 Instrument description

The range of instrumentation used during this study has been briefly referred to up to this point in the chapter. The remainder of this chapter presents a more detailed description of the instruments. The CTD unit is described first, followed by the SVTs and Galai Cis-100 particle sizer. This is followed by a section describing the Sea-Tech transmissometer used on the CTD and mid-water and near-bed moorings, the UWB moored transmissometers and the Aanderaa current meter.

3.4.1 The CTD package

Hydrographic casts were performed with a lowered instrument package consisting of a Neil Brown Mk IIIB CTD equipped with a 25 cm path length Sea-Tech transmissometer, Chelsea Instruments Aquatracka Mk III fluorometer and a rosette sampler carrying 10 litre capacity General Oceanics Go-Flo bottles. Data were transmitted in real time on both the down and upcasts via a single conductor armoured cable.

Pressure was measured using a high performance strain gauge bridge transducer. The temperature sensor was a platinum resistance sensor coupled with a fast response thermistor. Conductivity was measured using a four-electrode conductivity cell. Sensor specifications (from Harikrishnan, 1998) are shown in Table 3.4.

Table 3.4: Sensor specifications for the Neil Brown MkIIIb CTD unit.

Sensor	Range	Accuracy	Resolution	Response time (ms)
Pressure (dBar)	0 to 3000	±0.5	0.005	20
Temperature (°C)	-3 to +32	±0.005	0.0005	200
Conductivity (mmho cm^{-1})	1 to 65	±0.005	0.001	30

Temperature was calibrated with reversing thermometers and salinity was calibrated from bottle samples taken throughout the cruises. These calibrations were carried by RVS personnel and the data were initially quality controlled by the British Oceanographic Data Centre (BODC).

3.4.2 The Settling Velocity Tube (SVT)

The Owen tube (1976) was the first instrument developed to measure the settling velocity distribution of natural suspensions of PM under field conditions. This comprised a 1 x 0.25 m tube sampler open at both ends, which was lowered into the water, aligned horizontally and closed by trigger at the required depth. On recovery, it is rotated into the vertical position and placed on a stand. Sub-samples are withdrawn from a funnel-shaped tap at the bottom of the tube at specified intervals, and these are then filtered through pre-weighed filters for gravimetric determination of concentration. Volumes and sub-sample weights can then be converted to cumulative settling velocity curves and hence to median settling velocity.

The SVT was developed at the University of Wales, Bangor, specifically for deployment in continental shelf waters. It represents a modification from an earlier design by I.N. McCave at Cambridge University and is a bottom withdrawal tube with novel sampling and triggering features.

The SVT (Figure 3.3) comprises a 2 m stainless steel frame that supports the sampling tube, held at one end in the open position against stretched elastic cords. The frame is lowered horizontally into the water from the ship's winch.

The tube can either be triggered automatically at 1 m above the bed by means of a spring mechanism released when a suspended weight comes into contact with the bed, or at any depth in the water column by means of an acoustic release system. The latter was more appropriate for obtaining samples at the shelf edge since it allowed firing of the tubes at any specified depth. The release system works as follows: the tubes are cocked open and the trigger mechanism locked into place by means of elastic cords held taut by the acoustic release in the 'closed' position. When the required depth is reached, a transponder sends a signal to the release allowing it to open, releasing the elastics allowing the tubes to be pulled shut. This novel release system meant that the SVTs were not limited to sampling only surface or near-bed, but anywhere throughout the water column.

These tubes were developed specifically for deployment in PMC ranges of 1 to 50 mg dm^{-3}. Since concentrations at the shelf edge are typically an order of magnitude lower, the tubes were deployed as pairs, allowing double the sample volume to be obtained. On triggering, the tubes move horizontally past a piston to seal at a 60° conical tap end. This closure mechanism, combined with the relatively large tube diameter, ensures a more natural turbulent environment at the moment of sampling (Jones and Jago, 1996). The steep cone angle, combined with relatively fast withdrawal rates is designed to minimise settlement of PM onto the cone sides during analysis.

3.4.3 The Galai Cis-100 laser system for particle size and shape analysis

The Galai Cis-100 is a bench-based particle size analysis system which provides particle size distributions and shape characterisations. The system combines two distinct data acquisition and processing channels: a laser based size analyser and a video based shape analyser.

Particle size analysis employs the 'time-of-transition' theory. According to this theory, the time it takes a laser beam moving at a fixed velocity to interact with a particle and cause a shadow on the detector is directly dependent on the particle's diameter. Particle-laser interactions can be processed to yield diameter size. The size analysis program in the software provides statistical data on particle diameter, area and volume, and the number and concentration of particles sampled. Each water sample can be directly visualised and recorded on video allowing re-examination frame by frame for particle shape analysis. Data from the particle size and shape analysis programs are stored on the computer.

3.4.4 The beam transmissometer

Two types of transmissometer were used for deployment on moorings. Near bed and mid water optical measurements were made with the Sea-Tech transmissometer. These instruments were interfaced with Aanderaa Type 7 and 8 recording current meters (RCM). Surface measurements were made with transmissometers built at UW Bangor (UWB) and will be referred to in the text as TRB transmissometers. The optics of the TRB transmissometer are similar to those of the Sea-Tech instrument, described below. Instantaneous values are logged at one minute intervals on a solid state memory card capable of storing 3 months worth of data. These instruments were not interfaced with current meters.

The 25 cm pathlength Sea-Tech transmissometer measures transmission using a modulated Light Emitting Diode (LED), and a synchronous detector. The instrument is not sensitive to ambient light, is temperature compensated, and has excellent long term stability (Bartz *et al*, 1978). The Sea-Tech 25 cm pathlength transmissometer has been designed to provide accurate *in-situ* measurements of beam transmission and the concentration of suspended matter in relatively clear waters. Optical design features a collimated LED transmitter with a beam divergence of less than 3 milliradians, and the optical receiver acceptance angle is less than eighteen milliradians in water. This well-collimated optical design minimises errors caused by scattered light. Specifications are shown in Table 3.5.

Table 3.5: Specifications for the Sea-Tech transmissometer

Water path length	25 cm
Beam diameter	15 mm
Transmitted beam collimation	< 3 milliradians
Light source wavelength	LED 660 nm
Range (in water)	0 to 100 %
Accuracy	± 0.5 %
Linearity	± 0.1 %
Temperature stability	± 0.3 % (0 to 25 °C)
Depth capability	5000 m

The two basic processes that alter the underwater distribution of light are absorption and scattering. Absorption is a change of light energy into other forms of energy whereas scattering entails a change in direction of light without loss of energy.

In a pure absorbing medium, the loss of light due to absorption in a well-collimated beam of monochromatic light will be given by:

$$I_{(z)} = I_{(o)} e^{-az} \tag{3.1}$$

where $I_{(o)}$ is the source intensity, $I_{(z)}$ is the received intensity, a is the absorption coefficient (m^{-1}) and z is the pathlength (m). Similarly, in a pure scattering medium, the light redirected from a well-collimated beam of monochromatic light will be given by:

$$I_{(z)} = I_{(o)} e^{-bz} \tag{3.2}$$

where b is the volume scattering coefficient (m^{-1}). Since attenuation is defined as the sum of absorption and scattering, thus a + b = c, where c is the beam attenuation coefficient (m^{-1}).

The light lost from a well-collimated monochromatic beam of light in a scattering and absorbing medium is thus given by:

$$I_{(z)} = I_{(o)} e^{-cz} \tag{3.3}$$

This can be rewritten as:

$$T_{(z)} = \frac{I_{(z)}}{I_{(o)}} = e^{-cz} \tag{3.4}$$

where $T_{(z)}$ is the percentage of light transmitted over a distance z.

36

It should be noted that transmission is always given over a distance, whereas beam attenuation coefficient, c, is independent of distance. Beam attenuation coefficient is given by:

$$c = -\frac{1}{z}\ln\left(\frac{I_{(z)}}{I_{(o)}}\right)$$ (3.5)

where z is the pathlength of the instrument.

The simple exponential relationship holds only if the light is monochromatic. The Sea Tech transmissometer employs a light emitting diode (LED) light source with a wavelength of 660 nm, which is in the red part of the spectrum. This LED is nearly monochromatic (Sea Tech, 1990).

A beam attenuation coefficient, c, can be divided into three parts:
1) That due to water c_w
2) that due to suspended particulate matter c_p
3) that due to dissolved materials such as yellow substance, c_y

Hence, $c = c_w + c_p + c_y$. Each of these components has distinct spectral characteristics. Yellow matter absorbs strongly in the blue part of the spectrum. This absorption decreases exponentially with increasing wavelengths. The beam attenuation coefficient for particulate matter is much less wavelength dependent. The attenuation spectrum of natural waters is a composite of the three components, depending on the relative concentrations. Yellow substance is a by-product of organic decay and can be present in large amounts in lakes, reservoirs, and near-shore waters. At 660 nm, the attenuation of yellow substance is negligible, however, so that the attenuation is due to particulate matter and sea water only (Jerlov, 1976).

The above text describes the theory behind the Sea-Tech transmissometer and the specifications of the instrument. The CTD transmissometer recorded during the down and upcasts in real time via a microcomputer. These data were processed into beam attenuation units and quality controlled at BODC before release to the SES database for use by this project. However, problems with the CTD transmissometer over several of the data collection cruises resulted in corrections being required on a

cruise-by-cruise and sometimes cast-by-cast basis. The moored transmissometer calibrations, both from raw data into beam attenuation units (stage 1), and from these units into PMC (stage 2) were the responsibility of this project. Details of the CTD transmissometer corrections and stage 1 processing of the moored transmissometers will be described in the next chapter. Calibration for PMC (stage 2) for both the CTD and moored transmissometers will be presented in Chapter 5.

All of the moored instruments were deployed and recovered by Proudman Oceanographic Laboratory (POL) personnel who, prior to most deployments, checked and recorded the reading when the transmissometer light path was blocked (Blocked path) and when the transmissometer was recording in air with clean windows (Free path). Instruments were calibrated against the CTD transmissometer by suspending them below the CTD and lowering the entire assembly to ~ 30 m for 10 to 15 minutes. Data from the recovered instruments were downloaded at POL and, along with the calibration cast data from the CTD and the moored transmissometer, sent to UWB for processing and quality control.

3.4.5 The Aanderaa Recording Current Meter (RCM)

The RCMs used were self-recording current meters which are capable of monitoring vector-averaged speed, direction and temperature. Conductivity and water pressure sensors were fitted on some but not all of the instruments. The current meter aligns itself in the current and an internal compass measures the orientation of the instrument. A rotor at the top of the instrument is used to measure current speed. Rotor revolutions are magnetically transferred to an electronic counter that counts every half revolution. A vector-averaging method is used for recording the speed and direction of the current.

The current meter consists of two main parts, a vane assembly including tail fins and balance weights to ensure the meter orientates itself with the flow and a pressure case housing all the electronics and data storage equipment. The two are attached to a spindle through which the mooring wire runs. The entire instrument is gimballed allowing it to deviate up to 27 ° in any direction. Calibration of the sensors in the

instrument was carried out by POL and RVS. The manufacturer quotes the accuracy to which the speed can be measured as either $\pm$ 1 cm s^{-1} or $\pm$ 2% of the measured speed, whichever is the greater. The error in the direction from the RCM compass is given as $\pm$ 5 $^\circ$ (Aanderaa, 1992).

3.5 Summary

Seven cruises were carried out over a 16 month period at the edge of the north-west European shelf. Four main transects (S, R, P, N) were surveyed and water samples taken with a profiling CTD. Moored transmissometers and current meters obtained time series at sites on the S line and to a lesser extent on the N line. A range of instrumentation was used to collect data on the distribution and characteristics of SPM in the SES box. A CTD with attached transmissometer was used to profile the water column during survey cruises. SVTs were used to collect information on the settling velocities of the particle population. A laser particle sizer processed water samples from the CTD bottles to obtain information on particle size distributions and particle shape characteristics. Moored transmissometers and current meters obtained time series of the beam attenuation and velocity field. The methods used to obtain and process the various water samples, and processing of raw data into calibrated data, and any data correction procedures are presented in the next chapter.
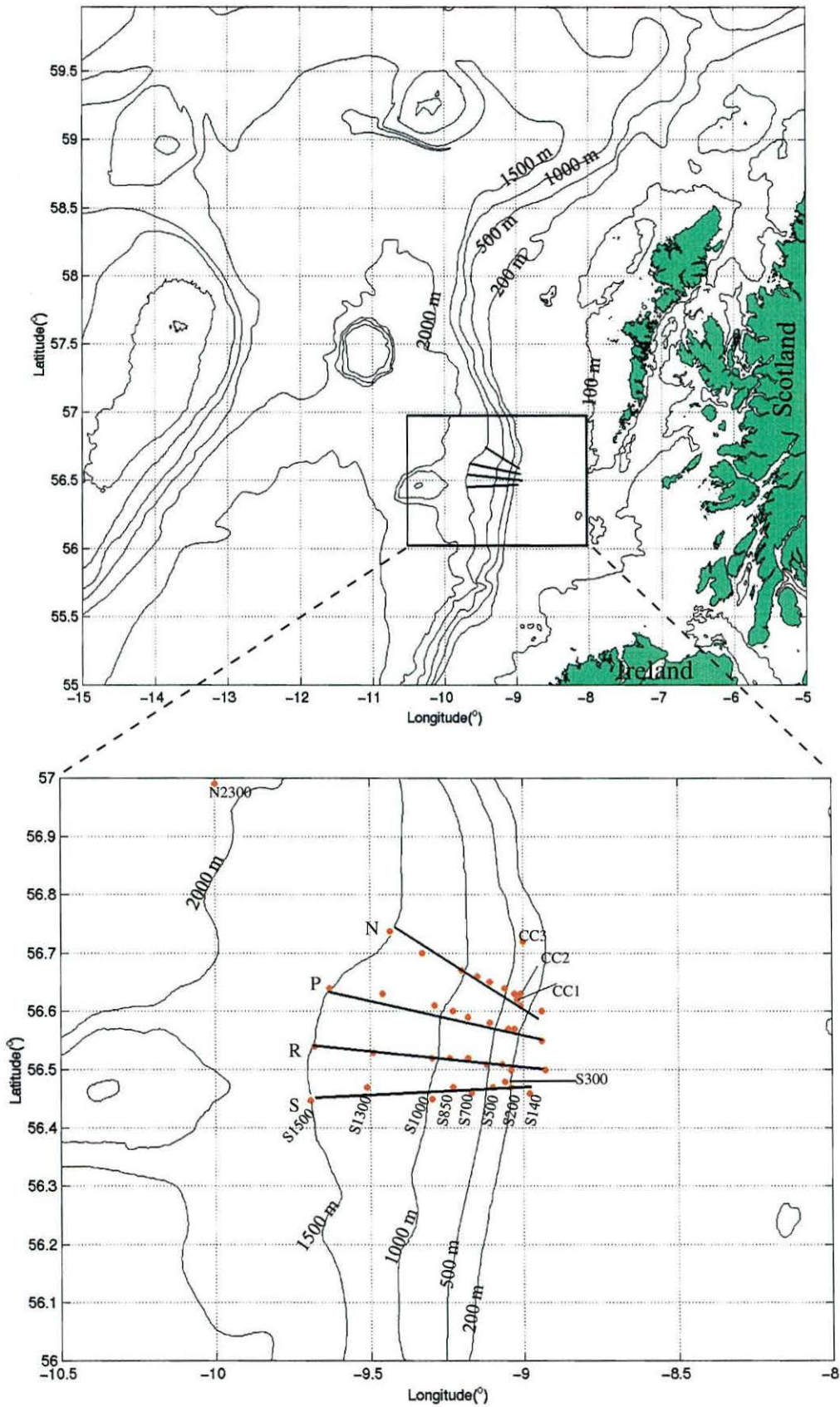
Figure 3.1: Map showing the location of the SES study area with an expanded view of the SES box detailing the station positions.

S 300 South section (sub-surface mooring)

Deployed 9 May '95
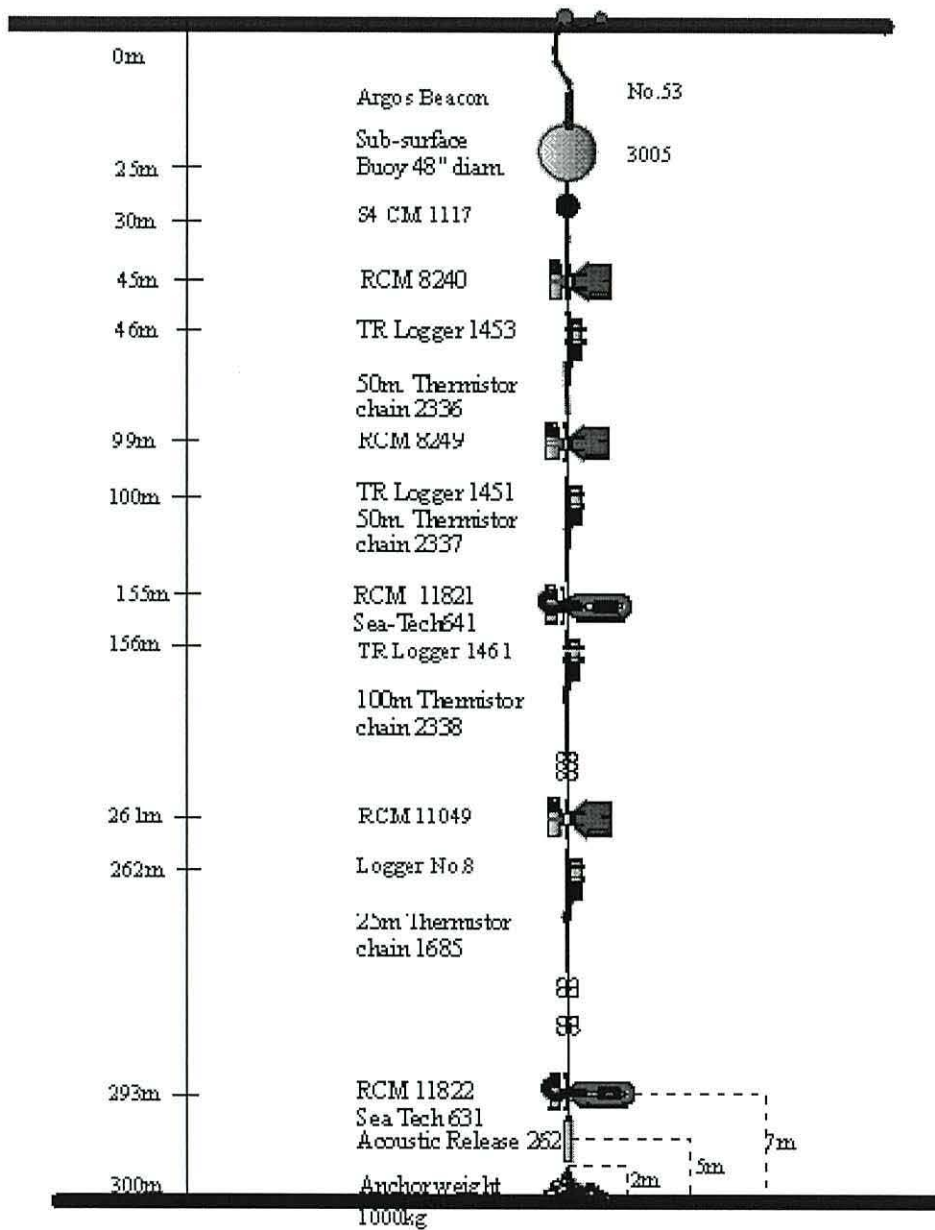
Figure 3.2: An example diagram of a mooring equipped with current meters and transmissometers used during SES. This image was downloaded from the SES web page (maintained by A. Coates, P. Knight and J.Richards of Proudman Oceanographic Laboratory) and modifed. Current meters are indicated by RCM7 and RCM8 while Sea-Tech refers to Sea-Tech transmissometers.
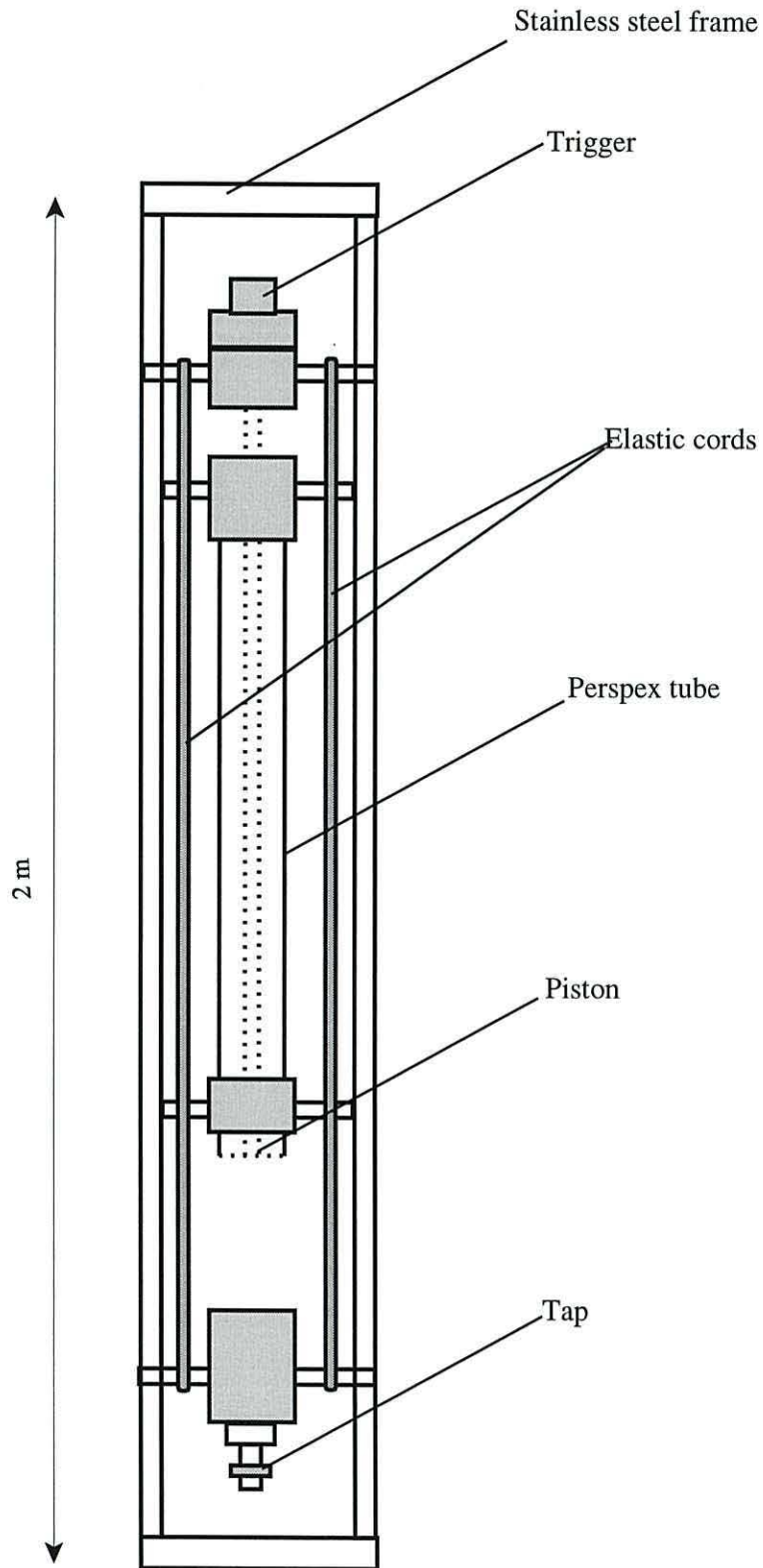
Figure 3.3: Schematic diagram (plan view) of the SVT (not to scale) adapted from Jones and Jago (1996).

CHAPTER 4

Data collection and processing

4.1 Introduction

The study area, observational strategy and range of instrumentation used in this project were described in detail in Chapter 3. This chapter details the scientific method involved in obtaining and processing water samples for suspended particle concentration, particle settling velocity distribution and particle size distribution. The remainder of the chapter is devoted to the improvement of data obtained with the CTD transmissometers, concluding with a section describing the preliminary data processing procedures for the moored transmissometers and current meters.

4.2 Determination of PM mass concentration

Direct measurement of PM mass concentration was carried out during the SES data collection campaign for the purpose of calibrating the beam transmissometers for the estimation of PMC throughout the water column, wherever beam attenuation measurements were made. CTD water samples were filtered and gravimetrically analysed for determination of PMC over six SES cruises. CTD stations ranged from 60 m on the shelf to 2000 m across the shelf edge. However, data were used from only five cruises as both beam attenuation and PMC data were unreliable for cruise CH121B and have been omitted.

The method for determination of particulate matter concentration involved filtering 5-10 (usually 10) dm^3 of seawater taken at surface, mid-water and near-bed locations in the water column. Water samples were taken from the CTD rosette by opening the end of the bottle into a container that had been rinsed previously with some of the sample water. Taking the sample in this way ensured any rapidly settling material (dregs) was included. The sample was then transferred into a Nalgene bottle, which had also been rinsed with sample water, and the lid closed until filtration took place. Some samples were stored for a few hours in the Nalgenes but the majority of

samples were filtered as soon as they were obtained from the CTD rosette. Known sample volumes were filtered by gentle vacuum through pre-washed and pre-weighed 47 mm diameter Whatman GF/C glass microfibre filters with 1.2 μm retention capabilities.

Each filter was rinsed of salt with a 200 cm^3 aliquot of Milli-Q water. As much moisture as possible was removed with the vacuum pump before storage in the freezer until return to the laboratory. Approximately every 10 samples, an extra filter was placed on the filtering apparatus, one on top of the other, with the bottom filter acting as a blank for procedural error. The blank filters were taken through all steps in the procedure that the upper filters underwent. The used filters were frozen until return to the laboratory. Back at the laboratory, the filters were oven dried overnight at 60 °C. The dried filters were re-weighed under ambient humidity on an Ohaus 5 decimal place balance. The value for each blank filter was calculated by subtracting the pre-usage filter weight from the post-usage weight. This is called the blank weight, from this point onwards.

Using the GraphPad Instat statistical package, an analysis of variance was performed on the blanks to see if the mean blanks from each cruise were statistically different from one another. It was found that the mean from CH125B was significantly different from the CH128A mean, but all other means were statistically similar. It was decided subtract a mean blank for each cruise from each cruise's data, instead of using an overall SES mean blank. Details of mean blank weights for all the cruises are shown in Table 4.1.

Table 4.1: Details of blank GFC filters during SES.

Cruise	Mean (mg)	St. Dev. (mg)	Min. (mg)	Max. (mg)	n
CD93B	3.32	Not known	Not known	Not known	13
CH123B	3.51	0.88	2.60	5.30	10
CH125B	4.45	1.92	1.99	7.95	15
CH126B	3.18	0.96	0.89	4.94	18
CH128A	2.73	0.72	1.12	4.17	12

3.9

PMC was calculated by subtracting the pre-usage weight from the post-usage weight, then subtracting the mean blank weight for that particular cruise and dividing by the volume filtered. The mean blank weight was sometimes greater than the weight of material on the filter, resulting in negative values. Although it could be argued that the concentration is not measurable if the procedural error is greater than the weight of material on the filter, the negative values have not been removed from the regression analysis in the next chapter, as this would have the effect of biasing the data.

4.3 Determination of particle settling velocity

4.3.1 Obtaining the sample

The settling velocity tubes were lowered horizontally, as an attached pair, from the side of the ship using the winch, which had a depth gauge accurate to 1 m. The transponder used to communicate with the acoustic release also gave a readout of the depth of the instrument. When the required depth was reached, a signal was sent via the transponder to the release, which fired the tubes. After triggering, the tubes were recovered as rapidly as possible and set vertically on a stand. They were then encased in insulating neoprene jackets to avoid the effects of sunlight on the temperature of the sample and on the phytoplankton population.

4.3.2 Processing the sample

Sub-samples were collected from the bottom tap at ten specified intervals. For this study, the sample times were at longer intervals than those used in shelf waters (Jones and Jago, 1996) because of the low concentrations and relatively large amount of very slow settling material present. Generally, the sample times used were 2, 10, 20, 40, 80, 160, 300, 420, 600 minutes. Sub-sample volumes were ~ 550 cm^3 from each tube, so the total sub-sample obtained for filtration was approximately 1100 cm^3.

For determination of settling rates of total PM the entire sub-sample was filtered through a pre-weighed 47 mm Cyclopore etched polycarbonate membrane filter of pore size 0.4 μm. Membranes were rinsed using 50 cm^3 of distilled water, then air

dried before storage in the freezer. After each set of ten sub-samples, an additional membrane was inserted beneath the last one before filtering and rinsing, thereby acting as a blank. In the laboratory, the membranes were oven-dried overnight at 40° C, then brought to room temperature at ambient humidity before re-weighing. The blank weight was subtracted from the weight on the filters to correct for any 'handling' error.

Summary statistics for the blanks are shown in Table 4.2. For cruises CH125 and CH128, where there was more than one blank, an analysis of variance was performed using Instat statistical package to see if there was any significant difference between the mean blanks from these cruises. The tests showed no significant difference, indicating a relatively constant handling error and thus consistency in the method used.

Table 4.2: Summary statistics for total PM Cyclopore blank filters.

Cruise	Mean (mg)	St. Dev. (mg)	n
CH123B	0.110	N/A	1
CH125B	0.592	0.278	6
CH128A	0.237	0.198	5

In Spring and Summer, sub-samples were also used to determine the settling rates of the phytoplankton population. 100 cm^3 to 250 cm^3 of sub-sample was filtered through a 25 mm Whatman GF/F glass-fibre filter with a nominal pore size of 0.7 μm. Replicate measurements were made on each sample removed from the settling tube. The pigments on the filter were extracted for a minimum of 18 hours and a maximum of 72 hours (Tett, 1987) in 8 ml 90 % acetone (made up of nine parts Analar grade acetone, one part distilled water and neutralised with sodium bicarbonate). The extractions took place in a refrigerator in darkness. After extraction, the sample was shaken, centrifuged for 5 minutes, re-shaken and re-centrifuged for a further 5 minutes to ensure complete solution of the pigments.

The chlorophyll a and phaeopigments of the supernatant were measured using a Turner Design Model 10 fluorometer. The fluorescence was measured before and after acidification with 2N HCl (approximately 8 % concentrated HCl by volume).

Blanks were also measured to give correction factors and the fluorescence measured was corrected for the appropriate blanks and range used.

If f_o* and f_a* are original fluorometer readings before and after acidification, and $f_{o(b)}$ and $f_{a(b)}$ are the equivalent blank readings, then

$$f_o = \frac{\left(f_o^* - f_{o(b)}\right)}{R}$$ (4.1)

$$f_a = \frac{\left(f_a^* - f_{a(b)}\right)}{R}$$ (4.2)

where R is the range factor for the scale used on the fluorometer.

Pigment concentrations (mg m^{-3}) can be calculated as follows:

$$[Chl] = K_f \left(f_o - f_a\right)\left(\frac{E}{V}\right)$$ (4.3)

$$[Phaeo] = K_f \left(H_f \left(f_a - f_o\right)\right)\left(\frac{E}{V}\right)$$ (4.4)

where E is the extracted volume (cm^3) and V is the sample volume (dm^3). K_f and H_f are constants for the fluorometer, 0.08 and 2.02, respectively during the SES cruises.

The replicate measurements were examined for similarity using the GraphPad Instat statistics package. Where two replicates were made on each sample, a paired t-test was performed to see if the mean from one set of replicates was significantly different from the other. For samples where more than two replicates were made, a repeated measures ANOVA was used. In all cases, the replicates were not statistically different from one another, indicating that the method used was precise and consistent.

4.3.3 Data analysis

The raw data were analysed and interpreted using an interactive computerised procedure developed at the University of Wales, Bangor (Jones and Jago, 1996). If the percentage frequency distribution of settling velocity W_s is $F(W_s)$, then after time

t the proportion of a particular settling velocity class which has settled to the bottom of a tube of height h is:

$$\frac{W_s t}{h}, \quad W_s < \frac{h}{t} \qquad\qquad 1, W_s \geq \frac{h}{t} \qquad\qquad (4.5)$$

So, integrating over all settling velocity classes the total percentage $P(t)$ remaining in suspension after time t is given by:

$$P(t) = \int_0^{W_s = h/t} F(W_s)\left(1 - \frac{W_s t}{h}\right) dW_s \qquad\qquad (4.6)$$

It then follows that the cumulative weight percentage settling velocity distribution can be obtained as:

$$\int_0^{W_s = h/t} F(W_s) dW_s = P(t) - \frac{dP}{d\log_e(t)} \qquad\qquad (4.7)$$

A computer-automated version of the manual/graphical procedure for solving equation 4.7 (Owen, 1976) performs the following steps and an example of the graphical output is shown in Figure 4.1.

- PM or pigment masses and volumes for each of the ten sub-samples are used to compute $P(t)$, after correction to allow for time variation in water column height as sub-samples are removed.

- $P(t)$ is plotted against $\log_{10}(t)$ (Figure 4.1(a)).

- A smooth 'best-fit' curve is then fitted through these data points by an interactive cubic-spline procedure. The user selects both number of splines and the intersection points, viewing the result and repeating until satisfied.

- This curve is transformed using equation 4.7 into a cumulative weight percentage versus log (settling velocity) curve. Where necessary (for samples containing significant proportions of very low or very high settling velocity) this is extrapolated assuming log-normal tail-end distributions, between 10^{-6} and 10^2 mm s^{-1}. The extrapolated portion is clearly identified in graphical output from the procedure (Figure 4.1(b)).
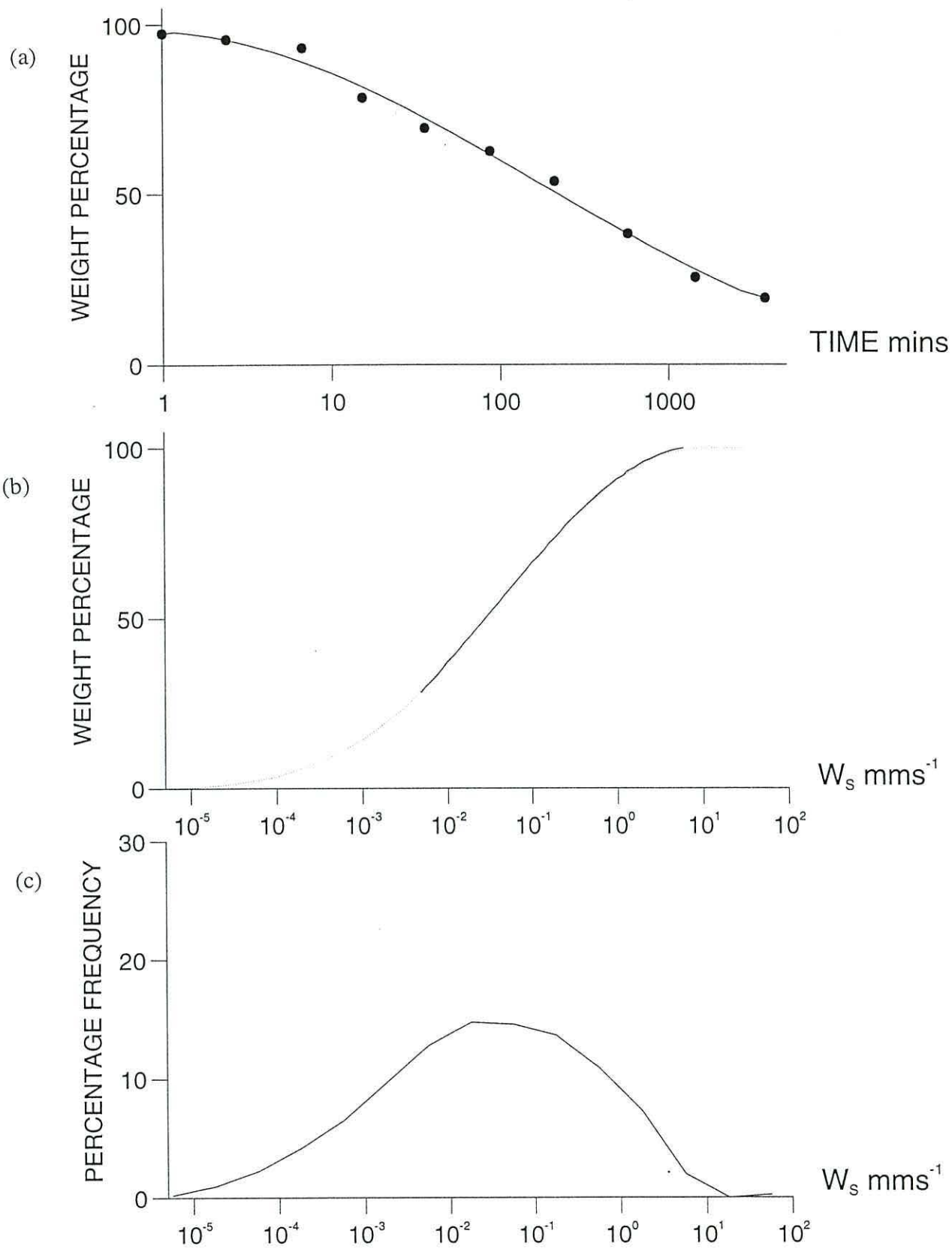
Figure 4.1: Example of the settling velocity processing program graphical output. (a) shows the weight percentage still in suspension over time. The user fits a curve through these data points. (b) shows the settling velocity curve generated from the curve fitted in (a). The solid line represents actual measurements while the faint line shows the extrapolation of that line. (c) is a histogram showing the weight percentage falling in each settling velocity class.

Median settling velocity is interpolated directly from the curve, and an estimate of mean settling velocity is obtained from percentiles using the technique of Folk and Ward (1957). Total PM or pigment concentration, and concentration within each of six settling velocity classes (partitioned on a log-scale), are also determined (Jones and Jago, 1996).

4.4 Particle size and shape

Water samples were obtained from the CTD rosette for particle size analysis. As soon as the CTD came back on board, a sample was transferred via the spigot tap of the Go-Flo bottle into a stainless steel container. The sample was gently drawn through the laser particle sizer via a peristaltic pump. In order to minimise disturbance to any flocs in the sample, the pump operated on the tubing exiting from the sample cuvette such that the sample measured in the cuvette did not come into contact with the pumping action until afterwards. Particle size data and video images were recorded on the computer disk and video tape, respectively. When the sample had run through, filtered seawater was poured into the container to flush the system through. The instrument was set to measure particles within a range of 2-600 µm.

Unfortunately, problems with the alignment of the laser beam resulted in particle size data for only two out of six cruises and video data for five out of six cruises. Continuing problems with the software package after the cruises meant that no particle shape analysis could be performed. The video data obtained allows only qualitative assessment of the particle population. However, it did provide a useful means of identifying dominant populations of phytoplankton during the spring blooms.

4.5 Correction of CTD transmissometer data

Examination of the CTD transmissometer data revealed that there were problems with several of the Sea-Tech instruments used during SES. The problems became evident when some casts at deep (1500 m) stations showed mid-water minimum beam attenuation values which were anomalously high (> 0.40 m^{-1}) and others which were too low (< 0.364 m^{-1}). In order to assess the extent of the problem, all deep

CTD casts (> 1000m) obtained during all SES cruises were examined for variability in the beam attenuation mid-water minimum (MWM). Additionally, the surface values from all CTD casts and temporally corresponding underway transmissometer data were examined for offsets, agreement in trends, and sudden jumps.

A number of problems were highlighted in this investigation: some within cruise anomalies due to changes in the CTD transmissometer, and a wider ranging problem with causes in the manufacturing stage of certain transmissometers. Transmissometer SN079D, used on CH123 and CH128 cruises, had an air value at the beginning of its use in the project that was greater than the manufacturer's air value (Table 4.3), suggesting incorrect manufacturer's calibration. The same problem was noted for the underway transmissometer used on cruise CH125 (Table 4.3).

Attempts were made to objectively improve consistency of casts within each cruise using comparisons with the underway instrument and changes in offset. The bigger problem involving incorrect manufacturer's calibration was addressed by comparison of the mid-water minimum in beam attenuation measured with a reliable instrument at the deepest stations visited in SES. These adjustments are addressed in more detail in the following cruise-by-cruise sections. Summary details of transmissometers used, offsets between instruments and the need for adjusting data are given in Table 4.3. All tables pertaining to the correction of CTD transmissometer data are located at the end of this section.

Average beam attenuation minimum values for all stations greater than 700 m depth used in this thesis are shown in Tables 4.4-4.11. There are sites listed in the tables for which no data are presented as no casts were obtained. They have not been removed from the tables in order to preserve symmetry between the transects, making it easier to compare stations on the N and S lines.

CH121 data were discarded as the CTD transmissometer (SN103D) consistently returned poor quality data. Apparent intermediate nepheloid layers present on the downcast were not present during the upcast. This instrument is known to have

47

suffered an intermittent fault. Additionally, the profiles from this cruise appeared odd in that the deep cast minimum beam attenuation occurred just below the surface layer (~100m) and beam attenuation increased again through the water column (Figure 4.2). These were not characteristic deep site beam attenuation profiles. It was concluded that the data for this cruise were too unreliable to use.

4.5.1 Cruise-by-cruise assessment

CD93A: The deep station beam attenuation profiles were fairly consistent, with mid-water minimum ~0.38 m^{-1}. Underway and CTD transmissometers agreed well at the beginning of the cruise. During the second half, there was an increased offset between the instruments. However, CTD transmissometer values at revisited sites were consistent through the cruise. Therefore it was concluded that the CTD transmissometer was functioning well and the underway instrument was erratic. This is a reasonable explanation as the underway was always greater than the CTD throughout CD93A. For the offset to increase, either the underway readings increased or the CTD readings decreased. It is more likely that the underway optics became fouled, than the CTD optics became progressively cleaner. No correction has been applied to these data. Mid-water minimum beam attenuation data are shown for 700 m to 1500 m stations on the N and S transects in Table 4.4(a) and repeat casts in Table 4.4(b).

CD93B: In general, the CTD profiles were more variable than in leg A, with beam attenuation minimum ~0.38-0.41 m^{-1}. The trend between the CTD and underway transmissometers was in good agreement but there was more variability in the offset between them. In CD93A the offset was always positive but in CD93B there were times when the offset was negative and times when it was positive. The same underway and CTD transmissometers were used on each leg. For the offset to become negative, either the underway optics became cleaner or the CTD optics became fouled, the latter being the more likely explanation. Thus, three groups of casts were identified that required adjustment in order to correct for temporary fouling on the transmissometer window. Details of MWM and adjustments made are given in Tables 4.5(a) and 4.5(b). The repeated stations show some variability in

MWM over the cruise period. However, both the N and S line repeated stations show an increase and then decrease in MWM with time. This may be due to the Spring phytoplankton bloom, known to be occurring at the time.

CH123A: The underway transmissometer recorded consistent surface beam attenuation at the same sites over legs A and B of this cruise. CTD transmissometer values were much higher for a given station in leg A than in leg B. It was concluded that CH123A readings were in error, perhaps due to lack of frequent cleaning. However, as this was a mooring leg no transects were done during this cruise, so these data have not been used.

CH123B: There was a constant offset between underway and CTD transmissometers of ~0.02 m^{-1}. CTD profiles were very consistent, bar one (cast 43), with MWM 0.341-0.347 m^{-1}. This is too low according to the SeaTech transmissometer manual, which states 0.364 m^{-1} as the attenuation of particle free water at 660 nm.

The CTD transmissometer was identified in Table 4.3 as having a cruise air value that was greater than the manufacturer's air value, suggesting that this instrument had been calibrated incorrectly at the factory. The consistency of the CTD profiles meant that a bulk correction could be applied to the whole CH123B beam attenuation dataset. This was achieved by comparing the deep water beam attenuation minimum at N2300 during CH123B and CD93B. Assuming the MWM at N2300 in CD93B was reliable, the difference between CD93B and CH123B N2300 MWM could be used to adjust the whole cruise up to more reasonable values. All casts were adjusted by adding 0.027 m^{-1}, based on the difference between N2300 average MWM of 0.368 m^{-1} (cast 133, 1500-2000 m, CD93B) and 0.341 m^{-1} (cast 44, 1600-2000 m, CH123B). This resulted in much more realistic MWM values, though they were still slightly on the low side (~0.37 m^{-1}). However, it is reasonable to assume lowest MWMs throughout SES during this cruise, as it was a very calm Autumn with little storm activity.

After global adjustment, cast 43 was still anomalously high when compared with the other casts. Examination of the underway-CTD offset showed that a change had occurred at cast 43. The average offset from casts 33-42 was +0.0197 m^{-1}, and for cast 43 was –0.002 m^{-1}. Cast 43 was adjusted back so that the offset was similar to the other casts. Details of all adjustments are given in Table 4.6 (a, b).

CH125A: Although the faulty CTD transmissometer, SN103D, was used on this cruise, it seemed to perform normally for the majority of casts. The CTD was quite consistent with minimum values 0.377-0.388 m^{-1} at stations >1000 m. There was reasonable agreement between underway and CTD values at the surface. However, a relatively low correlation coefficient was obtained due to change in the level of offset during this leg. The offset was ~0.02 m^{-1} at first, increasing to 0.05 m^{-1} for the second third, then decreasing again. This is likely to be due to the underway transmissometer windows becoming fouled and then being cleaned. Also, CTD surface values were more consistent than the underway for a given site. It was therefore concluded that no correction was required for this leg. Details of MWM are given in Table 4.7.

CH125B: The CTD transmissometer profiles showed more variability in minimum values, ranging from 0.39-0.42 m^{-1}. Most, however, were in the 0.39-0.40 m^{-1} region. There was a small, steady offset between the underway and CTD instruments, with the underway values higher than the CTD values. Pre and post-storm S line transects showed consistent deep station minima (~0.38-0.39 m^{-1}). However, post-storm N line deep water MWM were rather high.

A change in the underway-CTD offset occurred along the N line during casts 86, 88, 89, 90, and 91. The instrument appeared to be functioning normally during cast 87, with an offset of 0.036 m^{-1}. The average offset during the S line casts was also 0.036 m^{-1}. The casts where the CTD appeared to be malfunctioning were adjusted to give the same offset as when it appeared to function normally. Table 4.8 shows MWM and adjustments made.

CH126A: This cruise also used transmissometer SN103D on the CTD. Many of the casts were adjusted by BODC during quality control but the deep casts still had variable minimum values (0.38-0.41 m^{-1}). Casts were noisy with many INL type features. However, when the transmissometer was replaced in the second leg of the cruise all the profiles were very consistent with none of the apparent features seen in leg A. It was decided not to use any of the data from this leg as they appeared to be erratic and of poor quality.

CH126B: As mentioned above, SN103D was replaced during this leg with a different transmissometer. The deep station profiles were now much more consistent with MWM ~0.36-0.37 m^{-1}, though this was on the low side, especially on N line casts. There was very good agreement between the underway instrument and the CTD transmissometer. For many of the stations, surface values were essentially the same. The consistency of the profiles meant that an adjustment could be made for the whole cruise. The average MWM from N2000 during CD93B (0.369 m^{-1}, cast 135) was compared with that from CH126B (0.357 m^{-1}, cast 175) and the difference, 0.012 m^{-1}, added to all CH126B casts. This gave more realistic MWM (Table 4.9(a)). There was a marked difference between the transects, with the S line showing higher MWM than the N line. The underway and CTD data were closely examined for an indication the CTD was fouled at this time. However, this was not the case. In fact, the offset between underway and CTD increased at the time of the S line transect, indicating that the underway was becoming fouled, not the CTD. It is therefore assumed that the difference between the transects is due to the Spring bloom in some way (possibly a difference in biology or patchiness).

CH128A: The CTD was fairly consistent on this cruise with minimum values ranging between 0.36 and 0.37 m^{-1}, some of which again were too low (Table 4.11). The underway and CTD instruments agreed very well, generally. This was the same CTD transmissometer as in CH123B, with incorrect manufacturer's calibration. As the profiles were consistent during this cruise, the whole dataset could be corrected as in CH123B and CH126B by using >2000 m cast comparisons. Unfortunately, there were no 2000 m stations visited during CH128A.

N2000 was visited during CH128B, however. The MWMs from casts 122 and 124 at this station were obviously high (Table 4.10). The profiles were markedly offset from the rest of the deep station profiles, and there was a change in the offset between the underway and CTD at this time. Using the average underway-CTD offset in CH128A, these casts were adjusted, resulting in much lower and very similar MWMs (0.337 and 0.336 m^{-1}). Though these values are very low, this is to be expected since very low values were also recorded by this instrument in CH123B. They were further adjusted as in CH123B using the difference between N2000 MWM in CD93B and the new MWM in CH128B. This adjustment factor was then applied to the CH128A data.

CH128B: Unfortunately, the rest of the CH128B data could not be adjusted in this way as there was erratic behaviour by both the CTD and underway transmissometers, meaning offset adjustments were not reliable. As complete transects were available from CH128A, it was decided not to use CH128B except for the N2000 stations, which gave good results once adjusted, and compared well with casts at the same station during different cruises.

4.5.2 CTD transmissometer correction summary

In conclusion, the transmissometers used during SES appear to have performed poorly in general. One instrument (SN103D) was clearly malfunctioning, with variable offsets and suspect behaviour under pressure (CH121). Two other instruments also appear to have behaved abnormally with SN079D returning consistently low deep water minimum values during CH123B and CH128A, despite this being a new instrument with air values close to (in one case above) manufacturer's. SN125D also produced low deep water minima during CH126B. Two possible reasons for these consistently low readings include incorrect manufacturer calibration or imprecise diode specification, producing different or wider range of light source.

At least one of the underway transmissometers also indicated incorrect factory calibration, with cruise air values being higher than manufacturer's air values (cruise CH125, Table 4.3) and also underway values were less than CTD values when CTD MWMs were too low (cruise CH128A, Table 4.3). However, in the latter case this did not affect correction of the CTD data as the underway was not used in calculating the adjustment required.

These data have been examined at length and the adjustments made are supported with data from other instruments. This has resulted in an improved dataset, but there is undoubtedly a degree of error still present. Not all transects show a consistent increase in beam attenuation towards the shelf, as would be expected. However, there is an element of instrument noise included in the averaging of these data, and the discrepancy is never greater than 0.007 m^{-1} at the stations >1000 m.

N 1500 CTD 220 CH 121
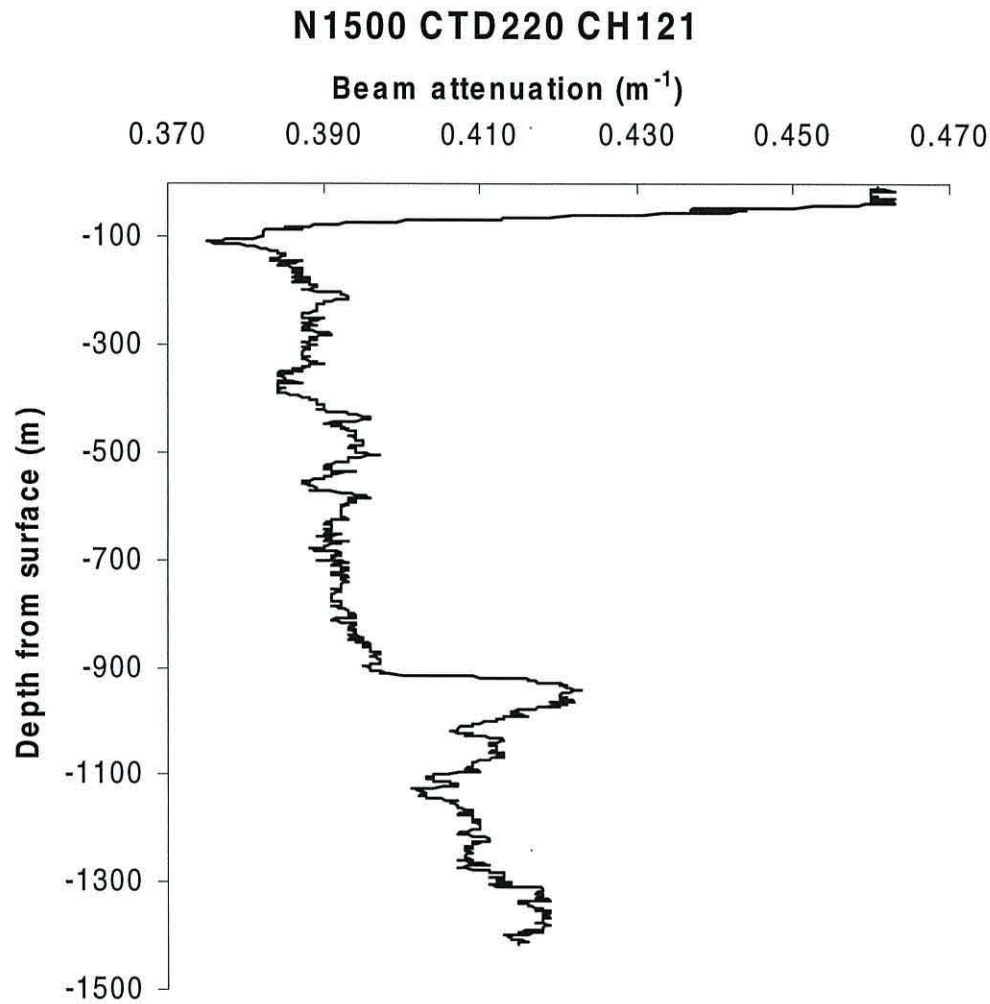
Figure 4.2: Example of a beam attenuation profile obtained from a 1500 m station during cruise CH121 in August 1995. Note the odd appearance of the profile with the beam attenuation minimum occurring at ~100 m from the surface and not in the mid-water region, and the general increase in beam attenuation with depth. This profile is characteristic of most obtained during this cruise with a malfunctioning transmissometer, SN103D.

Table 4.3: Summary details of transmissometers, offsets and adjustments made to CTD beam attenuation data in SES. Cruises shown in italics were not used due to extreme problems with the dataset or lack of CTD transects. CTD and UWAY refer to the CTD-mounted and underway tank transmissometers, respectively. SN refers to serial no. of CTD transmissometer, none were available for the UWAY. MAV and CAV are the manufacturer and cruise air values, in volts, respectively. <UWAY-CTD> is the mean offset between underway and CTD transmissometers, with pre-correction and post-correction given in the Unadjusted and Adjusted columns, respectively. A measure of the agreement between trends in CTD and UWAY is given by the correlation coefficient, r, followed by details of any adjustments made within a cruise (internal) and the number of casts involved, or cruise-wide (global). All air values and serial numbers were obtained from the BODC SES CD-ROM.

Season	Cruise	CTD SN	CTD MAV	CTD CAV	UWAY MAV	UWAY CAV	<UWAY-CTD> Unadjusted	<UWAY-CTD> Adjusted	Correlation (r)	Adjustment Internal	# Casts	Global	Value
Spring 95	CD93A	115D	4.805	4.789	4.823	4.778	0.016**	0.03**	0.84 **	No		No	
Spring 95	CD93B	115D	4.805	4.789	4.823	4.778	0.02	0.02	0.97	Yes	51	No	
Autumn 95	*CH123A*	079D	4.744	4.748*	4.823	4.753	-0.158	N/A	-0.31	N/A	N/A	N/A	N/A
Autumn 95	CH123B	079D	4.744	4.748*	4.823	4.753	0.021	-0.01	0.98	Yes	1	Yes	+0.027
Winter 95/96	CH125A	103D	4.758	4.622	4.655	4.810*	0.025		0.74	No		No	
Winter 95/96	CH125B	103D	4.758	4.622	4.655	4.800*	0.036	0.039	0.99	Yes	5	No	
Spring 96	*CH126A*	103D	4.758	4.622	4.744	4.740	0.041	N/A	0.94	N/A	N/A	N/A	N/A
Spring 96	CH126B	125D	4.789	4.690	4.744	4.740	0.015	0.003	0.95	No		Yes	+0.012
Summer 96	CH128A	079D	4.744	4.736	4.789	4.685	-0.019	-0.04	0.97	No		Yes	+0.033
Summer 96	CH128B	079D	4.744	4.736	4.789	4.685	-0.036	N/A	0.92	Yes	2	Yes	+0.033

*Cruise air values are *higher* than manufacturer's air values.

** No adjustments were made to CTD casts during CD93A. The unadjusted and adjusted <UWAY-CTD> offset refers to it being calculated over the whole cruise period and over the period before the underway became fouled. The correlation coefficient covers the whole cruise period.

Table 4.4 (a): Details of mid-water beam attenuation minimum (MWM) for stations on the N and S transects during cruise CD93A.

N Line				S Line			
Station	Cast	MWM (m^{-1})	Depth (m)	Station	Cast	MWM (m^{-1})	Depth (m)
N1500	44	0.381	650-1100	S1500			
N1400	48	0.383	500-1100	S1400			
N1300	49	0.378	500-950	S1300	24	0.382	400-1100
N1150	50	0.375	670-850	S1150	25	0.376	500-1050
N1000	43	0.38	600-800	S1000			
N800	42	0.382	400-700	S850	26	0.382	500-700
N700	41	0.389	300-500	S700	23	0.386	350-550

Table 4.4 (b): Details of mid-water beam attenuation minimum (MWM) at repeated stations during CD93A.

Station	Cast	MWM (m^{-1})	Depth (m)
N1500	44	0.381	650-1100
N1500	32	0.383	500-850
N1600	33	0.384	900-1290

Table 4.5 (a): Details of mid-water beam attenuation minimum (MWM), cast adjustments and new MWM (adj. MWM) for stations on the N and S transects during cruise CD93B.

N Line						S Line					
Station	Cast	MWM (m^{-1})	Depth (m)	Adjustment	Adj. MWM (m^{-1})	Station	Cast	MWM (m^{-1})	Depth (m)	Adjustment	Adj. MWM (m^{-1})
N2300	133	0.368	1500-2000	N/A	0.368						
N2000	135	0.369	1350-1550	N/A	0.369						
N1500	90	0.394	1340-1450	-0.015	0.379	S1500	111	0.382	700-1200	N/A	0.382
N1300	89	0.405	870-970	-0.015	0.390	S1300	112	0.385	500-1100	N/A	0.385
N1150						S1150	113	0.389	500-1000	N/A	0.389
N1000	88	0.402	810-830	-0.015	0.387	S1000	114	0.392	500-800	N/A	0.392
N850	87	0.407	150-250	-0.015	0.392	S850	115	0.395	400-600	-0.006	0.389
N700	86	0.436	200-400	-0.015	0.421	S700	116	0.396	150-330	-0.006	0.390

Table 4.5 (b): Details of mid-water beam attenuation minimum (MWM), cast adjustments and new MWM (adj. MWM) at repeated stations during CD93B.

N Line						S Line					
Station	Cast	MWM (m^{-1})	Depth (m)	Adjustment	Adj. MWM (m^{-1})	Station	Cast	MWM (m^{-1})	Depth (m)	Adjustment	Adj. MWM (m^{-1})
N1500	90	0.394	1340-1450	-0.015	0.379	S1500	111	0.382	700-1200	N/A	0.382
N1500	138	0.402	1050-1325	-0.014	0.388	S1500	140	0.401	1000-1330	-0.014	0.387
N1500	151	0.400	1000-1270	-0.014	0.386						
N1500	152	0.398	1100-1250	-0.014	0.384	S1000	114	0.392	500-800	N/A	0.392
N1500	153	0.401	1000-1300	-0.014	0.387	S1000	141	0.402	500-770	-0.014	0.388
N1500	154	0.396	1000-1300	-0.014	0.382	S1000	189	0.373	140-880	N/A	0.373
N1500	156	0.395	1000-1350	-0.014	0.381						
N1500	165	0.371	500-1400	N/A	0.371						

Table 4.6 (a): Details of mid-water beam attenuation minimum (MWM), cast adjustments and new MWM (adj. MWM) for stations on the N and S transects during cruise CH123B.

N Line						S Line					
Station	Cast	MWM (m^{-1})	Depth (m)	Adjustment	Adj. MWM (m^{-1})	Station	Cast	MWM (m^{-1})	Depth (m)	Adjustment	Adj. MWM (m^{-1})
N2300	44	0.341	1600-2000	+0.027	0.368						
N1500	39	0.343	800-1300	+0.027	0.370	S1500	21	0.347	1200-1400	+0.027	0.374
N1300	38	0.343	900-1100	+0.027	0.370	S1300	20	0.35	700-900	+0.027	0.377
N1150	37	0.343	700-950	+0.027	0.370	S1150	15	0.345	600-800	+0.027	0.372
N1000	36	0.345	650-750	+0.027	0.372	S1000	14	0.343	600-800	+0.027	0.37
N850	35	0.345	200-400	+0.027	0.372	S850	11	0.347	200-400	+0.027	0.374
N700	34	0.35	170-250	+0.027	0.377	S700	7	0.344	130-200	+0.027	0.371

Table 4.6 (b): Details of mid-water beam attenuation minimum (MWM), cast adjustments and new MWM (adj. MWM) at repeated stations during CH123B.

Station	Cast	MWM (m^{-1})	Depth (m)	Adjustment	Adj. MWM (m^{-1})
N1500	39	0.343	850-1300	+0.027	0.370
N1500	40	0.342	850-1300	+0.027	0.369
N1500	42	0.343	900-1300	+0.027	0.370
N1500	43*	0.359	850-1300	+0.027	0.368*
N1500	59	0.343	850-1300	+0.027	0.370
N1500	60	0.344	750-1200	+0.027	0.371

*Cast 43 was anomalously high and required a second adjustment to give the adj. MWM shown in the table.

Table 4.7: Details of mid-water beam attenuation minimum (MWM) for stations on the N and S transects during cruise CH125A.

N Line				S Line			
Station	Cast	MWM (m^{-1})	Depth (m)	Station	Cast	MWM (m^{-1})	Depth (m)
N1500	33	0.377	650-1000	S1500	13	0.384	650-1000
N1300	34	0.377	600-900	S1300	16	0.377	650-1000
N1150	35	0.388	500-650	S1150			
N1000	29	0.382	550-720	S1000	12	0.379	600-800
N850	28	0.386	450-650	S850	11	0.379	600-750
N700	27	0.396	560-577	S700	10	0.399	400-500

Table 4.8: Details of mid-water beam attenuation minimum (MWM), cast adjustments and new MWM (adj. MWM) for stations on the N and S transects during cruise CH125B.

N Line						S Line			
Station	Cast	MWM (m^{-1})	Depth (m)	Adjustment	Adj. MWM (m^{-1})	Station	Cast	MWM (m^{-1})	Depth (m)
N1500	86	0.404	1100-1300	-0.02	0.384	S1500			
N1400	88	0.393	650-1250	-0.01	0.383	S1400			
N1300	89	0.405	1100-1200	-0.019	0.386	S1300			
N1150	90	0.423	830-1100	-0.025	0.398	S1150	85	0.389	650-930
N1100	91	0.409	440-540	-0.007	0.402	S1100	84	0.404	360-460
N1000	92	0.407	510-610	N/A	0.407	S1000	83	0.399	315-480
N850	93	0.404	600-650	N/A	0.404	S850	82	0.396	400-430
N700	94	0.411	575-630	N/A	0.411	S700	81	0.401	350-410

Table 4.9 (a): Details of mid-water beam attenuation minimum (MWM), cast adjustments and new MWM (adj. MWM) for stations on the N and S transects during cruise CH126B.

N Line						S Line					
Station	Cast	MWM (m^{-1})	Depth (m)	Adjustment	Adj. MWM (m^{-1})	Station	Cast	MWM (m^{-1})	Depth (m)	Adjustment	Adj. MWM (m^{-1})
N1500	97	0.354	820-1310	+0.012	0.366	S1500	139	0.382	400-900	+0.012	0.394
N1300	98	0.36	200-1000	+0.012	0.372	S1300	140	0.377	400-800	+0.012	0.389
N1000	99	0.371	200-650	+0.012	0.383	S1000	135	0.376	400-700	+0.012	0.388
N850	101	0.364	400-600	+0.012	0.376	S850	134	0.377	400-700	+0.012	0.389
N700	102	0.367	400-600	+0.012	0.379	S700	133	0.378	500-550	+0.012	0.39

Table 4.9 (b): Details of mid-water beam attenuation minimum (MWM), cast adjustments and new MWM (adj. MWM) at repeated stations during CH126B.

Station	Cast	MWM (m^{-1})	Depth (m)	Adjustment	Adj. MWM (m^{-1})
N1500	87	0.359	650-1200	+0.012	0.371
N1500	88	0.357	650-1200	+0.012	0.369
N1500	90	0.356	500-1400	+0.012	0.368
N1500	92	0.357	500-1200	+0.012	0.369
N1500	94	0.356	900-1250	+0.012	0.368
N1500	97	0.356	850-1300	+0.012	0.368
N2000	175	0.357	1700-2000	+0.012	0.369
N2000	176	0.359	1300-2000	+0.012	0.371

Table 4.10: Details of mid-water beam attenuation minimum (MWM), cast adjustments and new MWM (adj. MWM) for station N2000 during cruise CH128B. Adjustment 1 refers to the dirty optics adjustment, 2 is the adjustment required due to the incorrect manufacturer's calibration.

Station	Cast	MWM (m^{-1})	Depth (m)	Adjustment 1	Adjustment 2	Adj. MWM (m^{-1})
N2000	122	0.437	1450-1950	-0.1	+0.033	0.370
N2000	124	0.416	1500-1990	-0.08	+0.033	0.369

Table 4.11: Details of mid-water beam attenuation minimum (MWM), cast adjustments and new MWM (adj. MWM) for stations on the N and S transects during cruise CH128A.

N Line						S Line					
Station	Cast	MWM (m^{-1})	Depth (m)	Adjustment	Adj. MWM (m^{-1})	Station	Cast	MWM (m^{-1})	Depth (m)	Adjustment	Adj. MWM (m^{-1})
N1500	67	0.359	700-1400	+0.033	0.392	S1500	37	0.363	500-1000	+0.033	0.396
N1300						S1300	39	0.364	500-1000	+0.033	0.397
N1150						S1150	36	0.365	500-1000	+0.033	0.398
N1000	65	0.377	400-800	+0.033	0.41	S1000	41	0.369	400-800	+0.033	0.402
N850	68	0.38	400-600	+0.033	0.413	S850	42	0.371	400-700	+0.033	0.404
N700	69	0.389	350-600	+0.033	0.422	S700					

4.6 Moored transmissometer data processing

The majority of the moored transmissometers were strapped to the CTD for an intercalibration cast prior to their deployment. Beam attenuation from the CTD transmissometer (post-correction) and raw counts from the mooring transmissometer were averaged over the time period for which they were at their calibration depth. Using the relationship in equation 3.5, in the previous chapter, where

$$c = -\frac{1}{z} \ln\left(\frac{I_{(z)}}{I_{(o)}}\right)$$

and given that

$$\frac{I_{(z)}}{I_{(o)}} = \left(\frac{\overline{count} - BP}{C_o - BP}\right) \tag{4.9}$$

then C_0 can be determined as all other variables are known. c is beam attenuation (m^{-1}), z is the pathlength of the transmissometer, 0.25 m in this case, $\overline{count}$ is the average from the mooring transmissometer during the calibration period, BP is the blocked path reading in air, C_o is the count value obtained at $I = I_{(o)}$. Once C_0 is calculated, it can be substituted into equations 3.5 and 4.9 to convert raw counts into beam attenuation for the full mooring deployment.

The above procedure was performed for each individual instrument where there was a calibration cast. As priority for berths was given to mooring personnel on the mooring legs of cruises, there was no berth available for people involved in the data collection for this particular study. Consequently, several transmissometer deployments were without calibration casts or the details had not been recorded. In order to process these data, beam attenuation values from casts at the site during the deployment period were matched with concurrent transmissometer counts, and the same procedure as described above was employed. Details of calibration data for each Sea Tech and TRB transmissometer deployment are given in Table 4.12 (a) and (b), respectively.

Three instruments had calibration casts on cruise CH121, when the CTD transmissometer was unreliable. All subsequent casts at the site during the mooring

deployment period were during CH121 and no other CTD data were available for calibration purposes. Consequently, the only way remaining to convert the instrument readings into beam attenuation was by using the air values from the manufacturer's calibration and the pre-deployment values. Unfortunately, air values were available for only one of the instruments. Calibration details for this instrument are shown in Table 4.13. Transmissometer counts were converted into volts using the relationship

$$volts = \left(\frac{FP_{(v)}}{FP_{(c)}} \right) counts \qquad (4.10)$$

Voltages were converted into % Transmission by

$$\%T = 20(volts) \qquad (4.11)$$

Beam attenuation was calculated using the relationship

$$c = -\frac{1}{z}\ln\left(\frac{\%T}{100} \right) \qquad (4.12)$$

The remaining two instruments were calibrated using the CH121 calibration cast since, although the actual values may be unreliable, the dataset is still of value when looking at relative changes. Calibration details for these instruments are given in Table 4.12 (d). Data from these instruments have not been used quantitatively in this thesis.

Several of the time series had beam attenuation values that were too low, i.e. less than 0.364 m^{-1}, the beam attenuation corresponding to particle free water at 660 nm. The whole data set from these instruments was adjusted upwards, so that the lowest beam attenuation was 0.370 m^{-1}, an arbitrarily chosen value. A beam attenuation of 0.370 m^{-1} is more typical of mid water minimum values at deep stations. One would not expect a time series from the surface or the bed, where relatively higher concentrations of particles are present, to attain a value below this, which is why this value was chosen as the lower limit.

This arbitrary adjustment may still result in an underestimation of beam attenuation in some time series, but all CTD profiles which coincided with a mooring deployment were checked, revealing that the records agreed relatively well (Table 4.13). One cannot expect the CTD transmissometer and mooring transmissometer to

give consistently similar readings, as PM is patchy in distribution and there was a spatial offset between the instruments. The CTD cannot be deployed too close to the mooring in case of entanglement, and additionally, it usually stopped 5-10 m above the bed.

The majority of near-bed transmissometers had higher beam attenuation values than the CTD transmissometer. More variability in the readings was seen in the surface instruments, but the majority of these deployments were during the 1995 and 1996 Spring bloom when one would expect the effects of patchiness in PM distribution to be greater.

Table 4.12 (a): Summary of calibration details for SeaTech transmissometers where calibrated against CTD transmissometer. SN is the instrument serial number; Rig is the POL rig identification number; Cal. Cast shows the cruise and cast # used in the calibration. Calibrations using underway data are denoted with UW and the date; Date gives the deployment duration, C_o is the count value corresponding to 5 volts, BP is the count value when the light path is blocked; Adjustment gives the offset used to adjust time series where some records were less than 0.364 m^{-1}, so that the minimum value was 0.370 m^{-1}.

SN	Rig ID	Cal. Cast	Date	C_o	BP	Site	Adjustment
080D	11817.780	128A: 4	11/07/96-28/07/96	1003.12	0	S300	
099D	09069.761	UW 17/04/96	17/04/96-28/07/96	1010.62	0	S140	
101D	00903.765	126B: 79,131	18/04/96-10/05/96	201.12	799	S300	
555	11045.667	91B: 5	29/03/95-11/05/95	1144.42	0	S700	
556	11814.745	125A: 4	01/02/96-07/04/96	1046.80	0	S140	+0.050
556	11814.733	123B: 2,45-47,93	19/11/95-23/01/95	1042.00	0	S140	
631	11820.757	125A: 18	06/02/96-21/04/96	1013.48	0	N1500	+0.029
631	11812.682	93A: 11	09/05/95-12/08/95	1075.63	0	S300	
631	11820.774	126B:87,92,94,97;128A:67	22/04/96-12/08/96	1003.75	0	N1500	+0.041
636	11816.684	93A: 27	11/05/95-04/08/95	1086.79	0	S700	+0.017
637	11817.684	93A: 27	11/05/95-04/08/95	1072.80	0	S700	+0.016
640	11820.682	93A: 5	09/05/95-12/08/95	1072.36	0	S300	

Table 4.12 (b): Summary of calibration details for TRB transmissometers where calibrated against CTD transmissometer.

SN	Rig	Cal. cast	Dates	C_o	BP	Site	Adjustment
TR001	747	CH125A: 2	01/02/96-05/03/96	725	177	S140	+0.105
TR1683	688	CD93: 56	15/05/95-23/06/95	4373	2	S140	
TR1686	763	CH126B: 128, 196	23/04/96-11/05/96	4714	4	S140	
TR1760	669	CD93A: 9, 13	17/04/95-09/05/95	4275	44	S200	+0.0855
TR1760	670	CD93: 20	10/05/95-28/05/95	4760	44	S200	
TR1761	677	CD93: 12	27/03/95-01/04/95	3362	5	S200	
TR1761	676	CD93: 23,79,116,183,188	10/05/95-04/06/95	4252	4	S700	+0.0085
TR1761	769	UW 15/04/96	15/04/96-19/05/96	4757	4	S700	

Table 4.12 (c): Calibration details where transmissometer calibrated with air values as no CTD casts were available. $MAV_{(v)}$ is the manufacturer's air value in volts, $BP_{(v)}$ is the blocked path in volts, $AV_{(c)}$ is the pre-deployment air value in counts, and $BP_{(c)}$ is the pre-deployment blocked path in counts.

SN	Rig	Date	$MAV_{(v)}$	$BP_{(v)}$	$AV_{(c)}$	$BP_{(c)}$	Site	Adjustment
637	11817.702	13/08/95-06/09/95	4.659	0.000	997	0	S700	+0.021

Table 4.12 (d): Calibration details for two transmissometers that were calibrated using CH121 CTD data.

SN	Rig	Cal. cast	Dates	C_o	BP	Site	Adjustment
TR1761	692	CH121A: 5	15/08/95-03/09/95	4144	4	S140	
638	11818.689	CH121A: 4	11/08/95-31/08/95	1120	0	S140	

Table 4.13: Comparison of beam attenuation from CTD transmissometer with moored transmissometers.

SN	Rig	Site	Depth (m)	Cruise	Cast	Date	Time (GMT)	CTD (m^{-1})	Mooring (m^{-1})	Offset
TR1683	688	S140	1	CD93A	57	15/05/95	11.17-11.35	1.583	1.488	-0.095
				CD93B	63	17/05/95	14.35-14.51	1.45	1.201	-0.249
					66	17/05/95	19.03-19.25	1.281	1.195	-0.086
					70	18/05/95	02.57-03.13	1.122	1.073	-0.049
					74	18/05/95	06.55-07.04	1.272	1.155	-0.117
					78	18/05/95	11.09-1126	1.219	1.199	-0.02
					121	21/05/95	17.40-18.03	0.685	0.602	-0.083
					193	29/05/95	10.58-11.15	0.766	0.775	0.009
556	11814.733	S140	136	CH123B	2	03/12/95	22.11-22.35	0.424	0.421	-0.003
					45	09/12/95	19.20-19.43	0.429	0.422	-0.007
					93	14/12/95	10.26-10.43	0.413	0.421	0.008
556	11814.745	S140	136	CH125A	2	01/02/96	11.10-11.30	0.44	0.422	-0.018
TR001	747	S140	1	CH125A	3	01/02/96	18.00-18.24	0.453	0.603	0.15
					4	01/02/96	18.37-18.55	0.447	0.605	0.158
					4	01/02/96	18.37-18.55	0.442	0.421	-0.021
				CH125B	50	14/02/96	10.10-10.35	0.463	0.48	0.017
					50	14/02/96	10.10-10.35	0.455	0.435	-0.02

Table 4.13 continued.

SN	Rig	Site	Depth (m)	Cruise	Cast	Date	Time (GMT)	CTD (m^{-1})	Mooring (m^{-1})	Offset
099D	9069.761	S140	131	CH126B	128	05/05/96	04.06-04.22	0.527	0.576	0.049
TR1686	763	S140	1	CH126B	128	05/05/96	04.06-04.22	0.701	0.827	0.126
					196	11/05/96	05.36-05.49	0.494	0.572	0.078
					196	11/05/96	05.36-05.49	0.629	1.022	0.393
TR1760	669	S200	1	CD93A	9	09/05/95	05.14-05.49	0.742	0.777	0.035
TR1760	670	S200	1	CD93A	22	10/05/95	16.55-17.19	0.828	0.72	-0.108
				CD93B	119	21/05/95	15.25-15.46	0.658	0.635	-0.023
					143	25/05/95	03.00-03.28	0.585	0.643	0.058
					147	25/05/95	09.19-09.45	0.642	0.684	0.042
					150	25/05/95	12.42-13.08	0.66	0.693	0.033
631	11812.682	S300	155	CD93A	55	15/05/95	04.25-04.55	0.4	0.426	0.026
640	11820.682	S300	293	CD93A	55	15/05/95	04.25-04.55	0.408	0.439	0.031
				CD93B	118	21/05/95	14.14-14.38	0.42	0.422	0.002
					166	27/05/95	15.40-16.07	0.412	0.439	0.027
					170	27/05/95	20.58-21.24	0.416	0.426	0.01
					174	28/05/95	01.07-01.31	0.407	0.422	0.015
					177	28/05/95	04.09-04.26	0.409	0.439	0.03
					180	28/05/95	07.10-07.31	0.409	0.422	0.013
101D	903.765	S300	293	CH126B	79	30/04/96	18.37-19.01	0.423	0.422	-0.001
					131	05/05/96	06.01-06.23	0.465	0.467	0.002
080D	11817.780	S300	293	CH128A	47	18/07/96	19.43-20.14	0.451	0.443	-0.008
TR1761	676	S700	1	CD93A	27	11/05/95	08.44-09.15	0.619	0.42	-0.199
					28	11/05/95	10.17-11.14	0.635	0.415	-0.22
				CD93B	79	18/05/95	14.39-14.48	0.689	0.599	-0.09
636	11816.684	S700	704	CD93B	80	18/05/95	15.17-15.58	0.409	0.382	-0.027
637	11817.684	S700	222	CD93B	80	18/05/95	15.17-15.58	0.392	0.386	-0.006
					80	18/05/95	15.17-15.58	0.725	0.599	-0.126
					116	21/05/95	11.13-11.50	0.486	0.458	-0.028

66

Table 4.13 continued.

SN	Rig	Site	Depth (m)	Cruise	Cast	Date	Time (GMT)	CTD (m^{-1})	Mooring (m^{-1})	Offset
					116	21/05/95	11.13-11.50	0.392	0.393	0.001
					116	21/05/95	11.13-11.50	0.659	0.603	-0.056
					183	28/05/95	21.49-22.29	0.5	0.473	-0.027
					183	28/05/95	21.49-22.29	0.378	0.381	0.003
					183	28/05/95	21.49-22.29	0.563	0.703	0.14
					188	29/05/95	04.05-04.37	0.44	0.47	0.03
					188	29/05/95	04.05-04.37	0.4	0.399	-0.001
					188	29/05/95	04.05-04.37	0.552	0.68	0.128
TR1761	769	S700	1	CH126B	133	05/05/96	07.49-08.34	0.917	1.067	0.15
631	11820.757	N1500	1492	CH125B	86	20/02/96	11.02-12.10	0.425	0.42	-0.005
631	11820.774	N1500	1493	CH126B	87	02/05/96	07.26-09.24	0.383	0.39	0.007
					88	02/05/96	09.59-11.19	0.381	0.405	0.024
					90	02/05/96	17.49-18.58	0.38	0.382	0.002
					92	02/05/96	22.32-00.10	0.382	0.42	0.038
					97	03/05/96	06.02-07.27	0.381	0.389	0.008

4.6 Current meter data processing

The current meter data were processed and quality controlled at BODC before being made available to this project. All of the current meters interfaced with transmissometers that were deployed before August 1995 returned erroneous current data as the directional vanes were not correctly balanced. In these cases, the nearest RCM on the same rig was used to infer conditions at the location of the transmissometer. The majority of these substitute current meters were within 30 m of the region of interest. Temperature time series from the interfaced RCMs were compared with the substitute RCM data. The data from the instruments agreed well and are deemed to represent similar conditions at both instrument locations.

Speed and direction data were processed into u and v velocity components. Because of the tendency for the flow to follow the isobaths, the components were rotated so that v was along the shelf (positive to the north) and u was cross-shelf (positive on-shore).

Summary

Water samples were filtered to provide data on PMC. SVT deployments provided information on the settling velocity distribution of total PM and chlorophyll related particles, while the Galai Cis-100 laser particle sizer provided information on particle size and shape. Problems came to light with the CTD beam transmissometers used on several of the cruises and required corrections to be made. Moored transmissometers were calibrated using corrected CTD data, where a calibration cast was carried out. In the absence of calibration casts, CTD casts at the site during the deployment were used. Current meter data were processed to give u and v velocity components rotated to cross-shelf and along-shelf directions, respectively.

68

CHAPTER 5

Calibration of the beam transmissometer for prediction of PM mass concentration

5.1 Introduction

In situ observations of beam attenuation are routinely used as a substitute for direct measurements of particle mass. As the most popular optical instrument for making these measurements, the beam transmissometer has been widely deployed in estuaries (Campbell and Spinrad, 1987), in coastal waters and the continental shelf (Moody *et al*, 1987), and in the deep sea (McCave, 1983; Gardner *et al*, 1985). The appeal of transmissometers is in their speed, simplicity, low cost, and general availability. However, the use of beam attenuation as an indirect measure of PMC requires that a valid calibration between these variables be first established through regression analysis.

Laboratory studies by Baker and Lavelle (1984) concluded that PMC could be accurately determined from optical data, but only when sufficient samples for calibration have been obtained for each environment studied. The properties of particles that affect beam attenuation are their concentration, size distribution, index of refraction and shape, with the first two being most important. If the size distribution, index of refraction, and shape of particles are constant, beam attenuation is linearly related to particle concentration (Spinrad *et al*, 1983; Baker and Lavelle, 1984; Moody *et al*, 1987). Although characteristics of particles in the ocean are very diverse, empirical studies have shown that in the open ocean beam attenuation is linearly correlated with filtered mass concentrations below the surface 100 m (Spinrad *et al*, 1983; Gardner *et al*, 1985).

5.2 Particulate matter calibration of SES transmissometer data.

CTD water samples were filtered and gravimetrically analysed for determination of PMC over six SES cruises, as described in Chapter 4. CTD stations ranged from 60 m on the shelf to 2000 m across the shelf edge. However, data were used from only

five cruises as both beam attenuation and PMC data were unreliable for cruise CH121B and have been omitted.

Scatter plots of PMC and concurrent beam attenuation for the remaining five cruises revealed a substantial amount of scatter present (Figure 5.1(a)). Much of the scatter was in the data from CD93B. It was decided to omit CD93B data as the samples were collected and filtered by a different operator, smaller volumes were filtered as a result of competition for the CTD water, and the location of the filtering apparatus was more exposed to contamination on this cruise (*RRS Charles Darwin*) than on the other cruises (*RRS Challenger*). The *Charles Darwin* wetlab is a main route between deck and laboratory, and some of the filters from CD93B appeared to be contaminated by clothing fibres (S.E. Jones, pers. comm.). Omission of these data resulted in some improvement in the scatter observed (Figure 5.1(b)).

Much of the scatter can be attributed to samples from the surface water due to the presence of biogenic particles. Particles of this type are hydrated in the water column and, therefore, present a bigger area for attenuation of a beam. This results in high beam attenuation in association with relatively low dry mass concentration. Also, phytoplankton cells have a secondary absorption maximum of chlorophyll at 685 nm (Sathyendranath and Platt, 1990) close to the 660 nm wavelength used in the transmissometer beam, introducing an additional source of beam attenuation. In order to reduce scatter of this nature, samples from the surface layer were excluded.

Exclusion of the surface samples greatly improved the relationship (Figure 5.2, $R^2 =$ 0.73). Seven data points, clearly marked on the graph, were excluded from the regression analysis, as the mass concentrations were clearly erroneous. Other calibrations from the North Atlantic are plotted for comparison. The regression details are given in Table 5.1.

There are two SES equations because regression analysis was carried out with PMC as the dependent and beam attenuation as the independent variable, SES (1), and vice versa, SES (2). Although changing of the dependent and independent variables has no effect on the R^2 value, it does affect the prediction of PMC.

The majority of regressions of this nature in the literature used PMC as the independent variable and beam attenuation as the dependent variable. This is based on the fact that beam attenuation is a function of PMC. However, in regression analysis, the choice of dependent and independent variables should be based on statistical criteria, rather than physical. Since we are trying to predict PMC from beam attenuation, there is some justification that the former should be the dependent variable. Additionally, as beam attenuation is measured with less error than PMC, it should constitute the independent variable.

Table 5.1: Details of regression equations obtained in SES and by other workers in the North Atlantic. PMC refers to particulate matter concentration (mg dm^{-3}), c is beam attenuation (m^{-1}), n is the number of samples in the regression, and c_w is the clear water intercept, i.e. the beam attenuation when PMC is zero.

Author	Location	Equation	R^2	n	c_w
SES (1)	Hebridean margin	PMC = (2.427c) – 0.891	0.73	251	0.367
SES (2)	Hebridean margin	PMC = 3.331(c – 0.399)	0.73	251	0.399
Gardner et al (1985)	NW Atlantic	PMC = (1.208c) – 0.496	0.97		0.411
Bishop (1986)	NW Atlantic	PMC = 1.150(c – 0.358)			0.358
Bishop et al (1992)	NW Atlantic	PMC = 1.250(c – 0.367)	0.90	20	0.367
Antia et al (1999)	Goban Spur	PMC = 2.967(c – 0.352)	0.70	42	0.352
Hall et al (2000)	N. Iberian margin	PMC = (1.596c) – 0.573	0.96	43	0.359
McCave et al (subm.)	Goban Spur	PMC = (0.977c) – 0.357	0.95	35	0.365

From Figure 5.2, it can be seen that the slope of the SES (1) regression line is significantly higher than the slopes of all other workers, except Antia *et al*. The SES (2) slope is the highest of all, and the clear water intercept is too high. The SES (1) clear water intercept (c_w = 0.367) is reasonable when compared with the Sea Tech c_w value of 0.364 m^{-1}. It also compares well to the c_w intercept of McCave *et al* at Goban Spur, south of the SES area. There are several possible explanations for the relatively high slope found in the SES data, including filtration method used, filter type, and rinsing of the filters to remove salt.

Differences in methodology may account for the differences in the regression lines. SES and Antia *et al* used GF/C and GF/F filters, respectively, in the determination of PMC. Bishop (1986) and Bishop *et al* (1992) used large volume in situ filtration techniques; Gardner *et al* (1985), Hall *et al* (2000) and McCave *et al* (subm.) used etched polycarbonate membrane filters. They all achieved similar slopes and high R^2 values despite the relatively low number of samples obtained, when compared with SES.

Since the data of Antia *et al* and McCave *et al* were collected at the Goban Spur, one would expect them to yield similar slopes. McCave *et al* achieved a much higher R^2 value than Antia *et al*, with a similar number of samples, suggesting that his methodology is less prone to error. It is more likely that errors introduced due to the method used cause an overestimation of material present than an underestimation, i.e. are contamination related.

Durrieu de Madron (1995) compared PMC obtained using three different filters: Nuclepore, Millipore and GF/F. There was a considerable degree of variability in concentrations obtained between the different filter types, in particular, the concentration of material from GF/F filters was always higher than from Nuclepores. This could be due to trapping of more material by the GF/Fs, with their greater surface area, but is more likely to be due to contamination with residual salt (I.N. McCave, pers. comm.).

Incomplete rinsing of salt from the GF/C and GF/F filters may be an explanation for the differences in regression lines observed in Figure 5.2. In SES, rinsing was performed with one large aliquot of distilled water, while Gardner *et al*, Hall *et al* and McCave *et al* used several small aliquots. However, if incomplete rinsing of salt is the explanation for the higher slope observed in the SES work, then this would be a fairly constant error as the majority of SES samples filtered were 10 dm^3. One would expect this to affect the intercept rather than the slope. Additionally, the blank filters presumably include a correction factor for incomplete rinsing of salt since they are present beneath the top filter through the entire filtration and rinsing process. If filters with a greater particle load are more efficient at retaining salt, then this might explain the higher slope observed, but this is unlikely in this case since none of the filters in SES were heavily loaded with material.

There is a case for accepting the SES (1) regression line, in light of the c_w value and the consistency of the blanks (Table 4.1, Chapter 4), and for rejecting it, in light of the much higher slope and greater degree of scatter obtained when compared with most other workers in North Atlantic waters. The SES regression predicts concentrations of similar magnitude to those of Hall *et al* and McCave *et al* at the

lower end of the beam attenuation spectrum as shown in Table 5.2. It is at higher beam attenuation that the greatest differences arise.

Table 5.2: Comparison of PMC predicted from beam attenuation, c, using equations for north eastern Atlantic waters.

	$c = 0.38$ m^{-1}	$c = 0.40$ m^{-1}	$c = 0.50$ m^{-1}	$c = 0.60$ m^{-1}
SES (1)	30 mg m^{-3}	79 mg m^{-3}	322 mg m^{-3}	565 mg m^{-3}
SES (2)	-63 mg m^{-3}	3 mg m^{-3}	336 mg m^{-3}	869 mg m^{-3}
McCave et al	14 mg m^{-3}	34 mg m^{-3}	132 mg m^{-3}	229 mg m^{-3}
Hall et al	34 mg m^{-3}	65 mg m^{-3}	225 mg m^{-3}	385 mg m^{-3}

In SES, the majority of PMCs measured were less than 500 mg m^{-3}, but a significant proportion were greater than this. All of the concentrations greater than 1000 mg m^{-3} (excluding those encircled in Fig. 5.2) were measured during the February cruise, a cruise characterised by poor weather conditions and rough seas. It is possible that the slope of the SES regression lines are greater than those obtained by the other workers due to domination of the data by high concentration samples following storm resuspension. If this is the case, then the equations might over-estimate PMC at times and locations where resuspension is at a minimum.

The extreme difference between the Antia et al regression and that of McCave et al highlights the need to reduce the error as much as possible when measuring the relatively low concentrations found at the shelf break. In determining PM concentration Antia et al filtered 1-12 dm^3, SES filtered 5-10 dm^3, McCave et al filtered usually 20 dm^3, and Bishop filtered very large volumes in situ, removing many of the filter-handling steps present in on-board filtration methods.

The data from SES and Antia et al may be less reliable due to the smaller volumes filtered and the type of filter used. The overall consistency of the cruise blanks (Table 4.1, Chapter 4) adds some confidence to the SES measurements, but the values are large (~300 μg l^{-1}) when compared with typical concentrations obtained in the ocean: PMC in particle depleted areas is generally in the range of 10-20 mg m^{-3} and 100s of mg m^{-3} in particle rich layers (Brewer, 1976).

Since the majority of regression lines in the North Atlantic have similar slopes, it was decided to reject the SES regression and opt for the estimate of PMC offered by the Goban Spur equation derived by McCave *et al*. This equation was chosen as it was derived from data obtained in the north-east Atlantic and is closer to the SES site than the Iberian margin where the data of Hall *et al* were obtained. All PMC estimated from beam attenuation in this thesis is calculated by:

PMC (mg m^{-3})= 977c – 357 (from McCave *et al*, subm.)
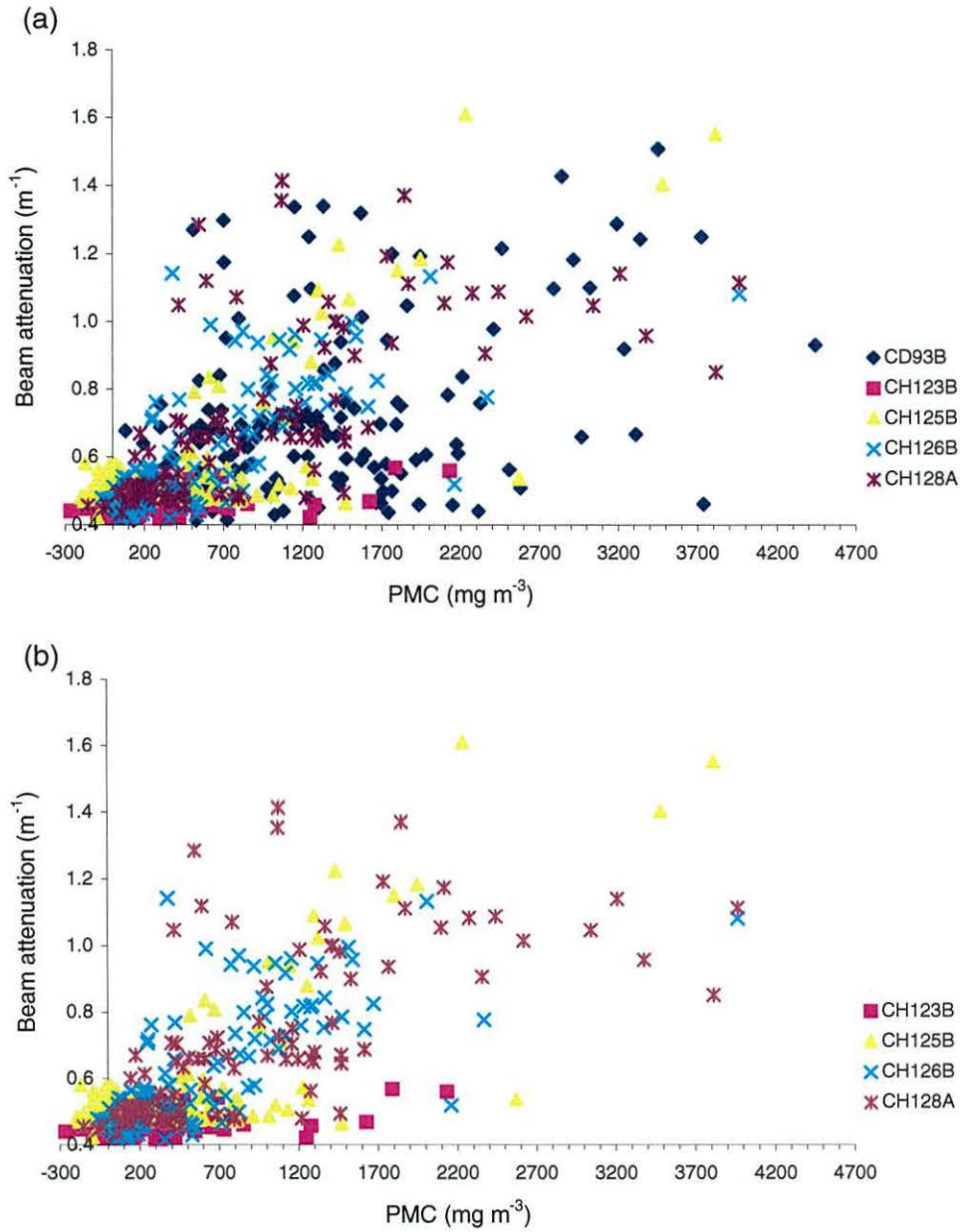
Figure 5.1: (a) Scatter plot of particulate matter concentration and concurrent beam attenuation from five SES cruises in 1995 and 1996. Data are from surface middle and bottom of the water column. In plot (b) data from CD93B are excluded.
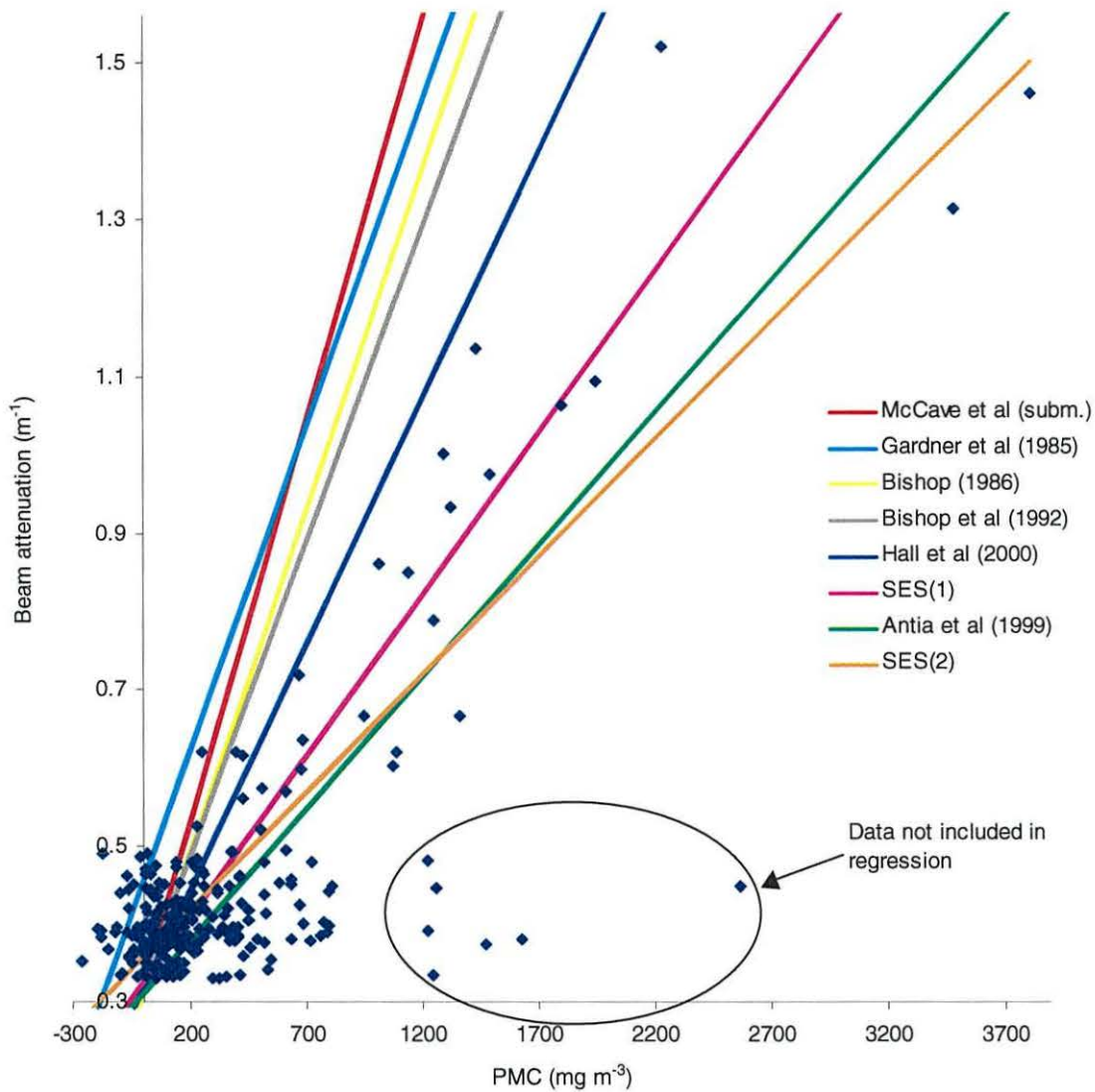
Figure 5.2: Scatter plot of particulate matter concentration and beam attenuation from four SES cruises, excluding surface samples. Regression lines for SES data are shown with regression lines by other workers in N. Atlantic waters.

CHAPTER 6

Results

6.1 Introduction

In this chapter, the results obtained for this project during the SES campaign are presented. The shipboard CTD surveys are presented as cross-shelf contour plot sections. Data from the moored instrumentation are presented as time series. PM characteristics are presented in terms of particle settling velocity and size distributions.

6.2 Water column survey results

CTD casts throughout the cruises provided information on the vertical and horizontal variation in several hydrographic properties. Beam attenuation was converted into PMC using the calibration equation shown and discussed in the previous chapter. Details of the transects surveyed with the profiling CTD during the different cruises and cruise legs were given in Table 3.2 in Chapter 3. The CTD set-up included a transmissometer and a fluorometer attached to the same frame. The whole instrument package will be referred to as the CTD throughout the remainder of the thesis.

The calibrated CTD data from the downcasts have been interpolated and are presented in the form of contour plots, created using the UNIMAP graphics package. Contour plots of PMC and chlorophyll concentration, temperature and salinity have been generated for across-slope sections of the SES box. Sections of the N line transect obtained throughout the study have been presented in Figures 6.1-6.4. The positions of the individual CTD casts are shown in the contour plots of PMC and are the same, but not shown, for the plots of chlorophyll concentration, salinity and temperature. Although there was variation in detail between transects measured on the same cruise, the main features were the same and the N line can be considered a representative cross-slope section within the SES box. PMC sections from the S line are shown in Appendix 1.

A well-defined seasonal cycle in PM distribution was observed across the shelf edge (Fig. 6.1). Spring and Summer in 1995 and 1996 were characterised by a high PMC surface layer. The particle population in this layer was dominated by phytoplankton and biological material as seen in the chlorophyll concentration distribution (Fig 6.2). PMC was at a minimum throughout the water column in December 1995. In February 1996 two-fold increases in PMC on the shelf were observed. A storm occurred between observations made during CH125A and CH125B and there was a marked contrast between the pre-storm and post-storm PMC distribution. Leg A was characterised by relatively low PMC on the shelf. In leg B, concentrations were observed to be up to two times higher over the shelf. This storm event will be described in greater detail in section 6.3.

The temperature and salinity sections (Figs 6.3 and 6.4, respectively) show a common feature near the slope around the 250 m to 500 m isobaths. There was a downward tilting of the 9.6 °C isotherm and a core of higher salinity (35.38) than the surrounding waters. The PMC sections show an area of higher PMC associated with this warm, salty water. The temperature and especially salinity contours in December 95 show a distinct front at the edge of the shelf. This can be seen in the PMC section with concentrations increasing at the surface and shorewards. The higher concentration of material occurred in the less saline shelf water.

Most of the cross-slope surveys revealed an increase in PMC near the slope bed producing a benthic nepheloid layer, which was especially marked during Spring and Winter. These can be seen more clearly in Appendix 1 Figure A.2, where each contour plot has its own scaling. The material in Spring appeared to be biological in origin as there were increased levels of chlorophyll present in this layer when compared with the overlying water column. Both a benthic and an intermediate nepheloid layer were observed during the February storm.
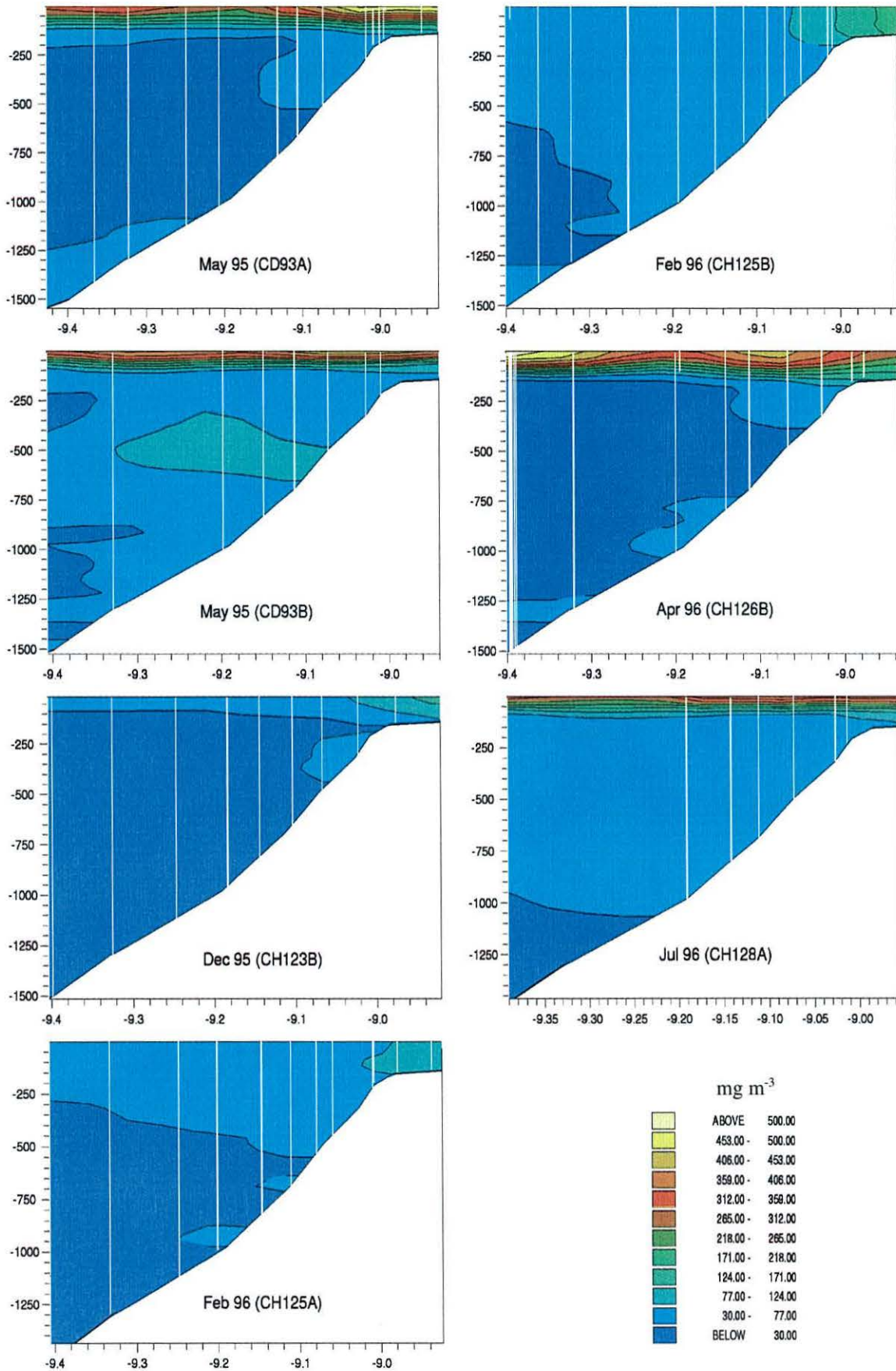
Figure 6.1: Particulate matter concentration sections along the N line across the shelf edge during SES. The vertical white lines represent individual CTD casts.
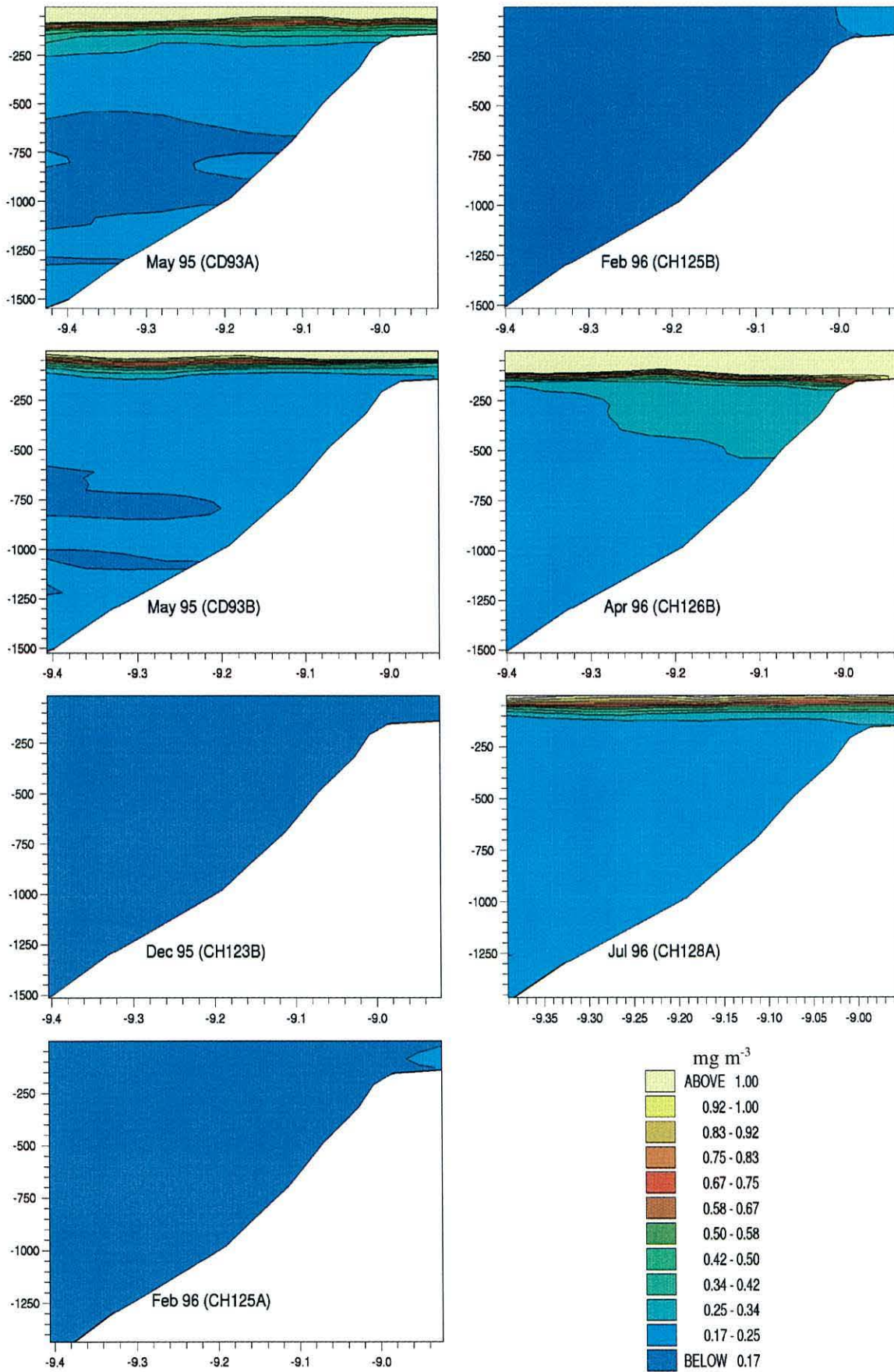
Figure 6.2: Chlorophyll concentration sections along the N line across the shelf edge during SES.
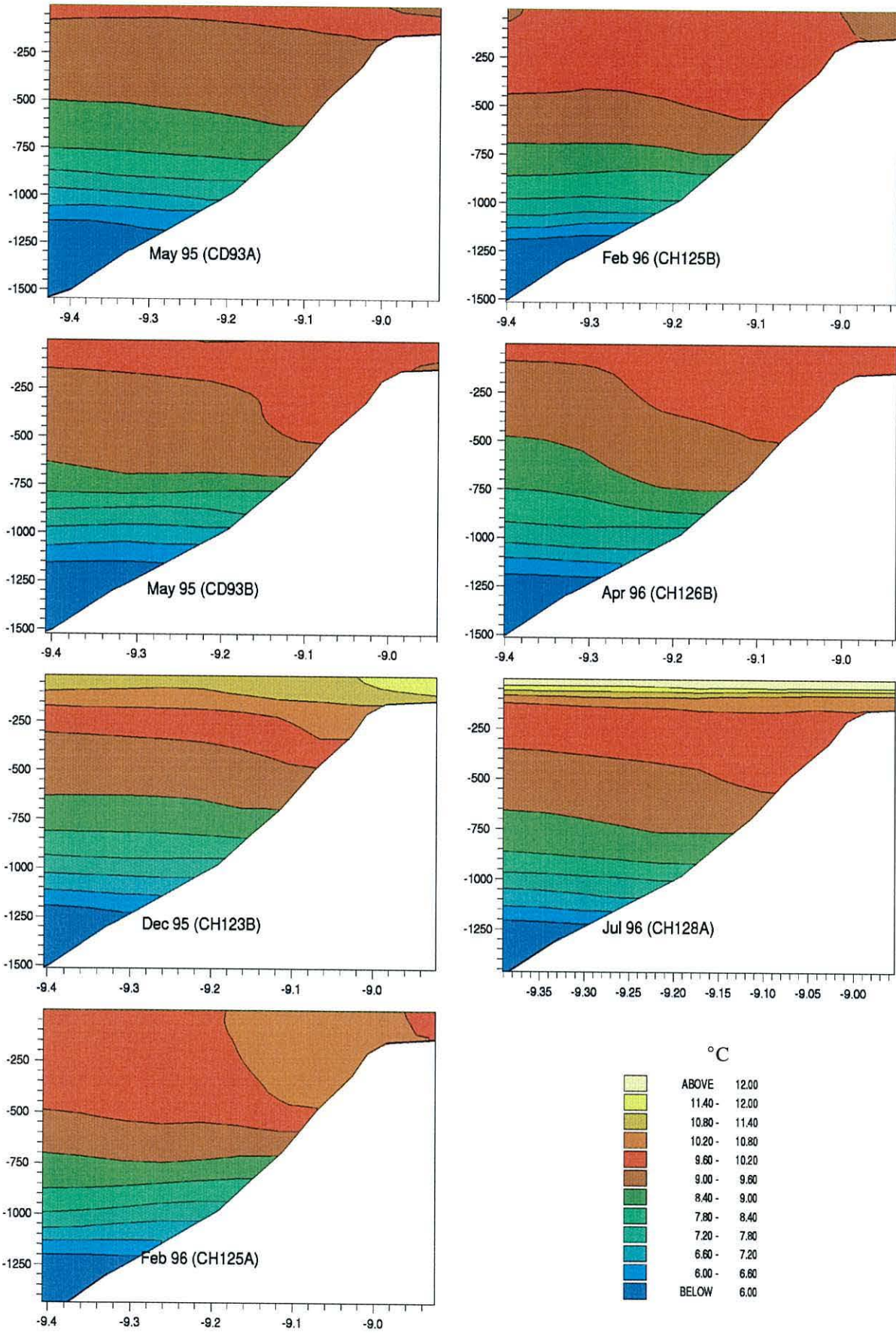
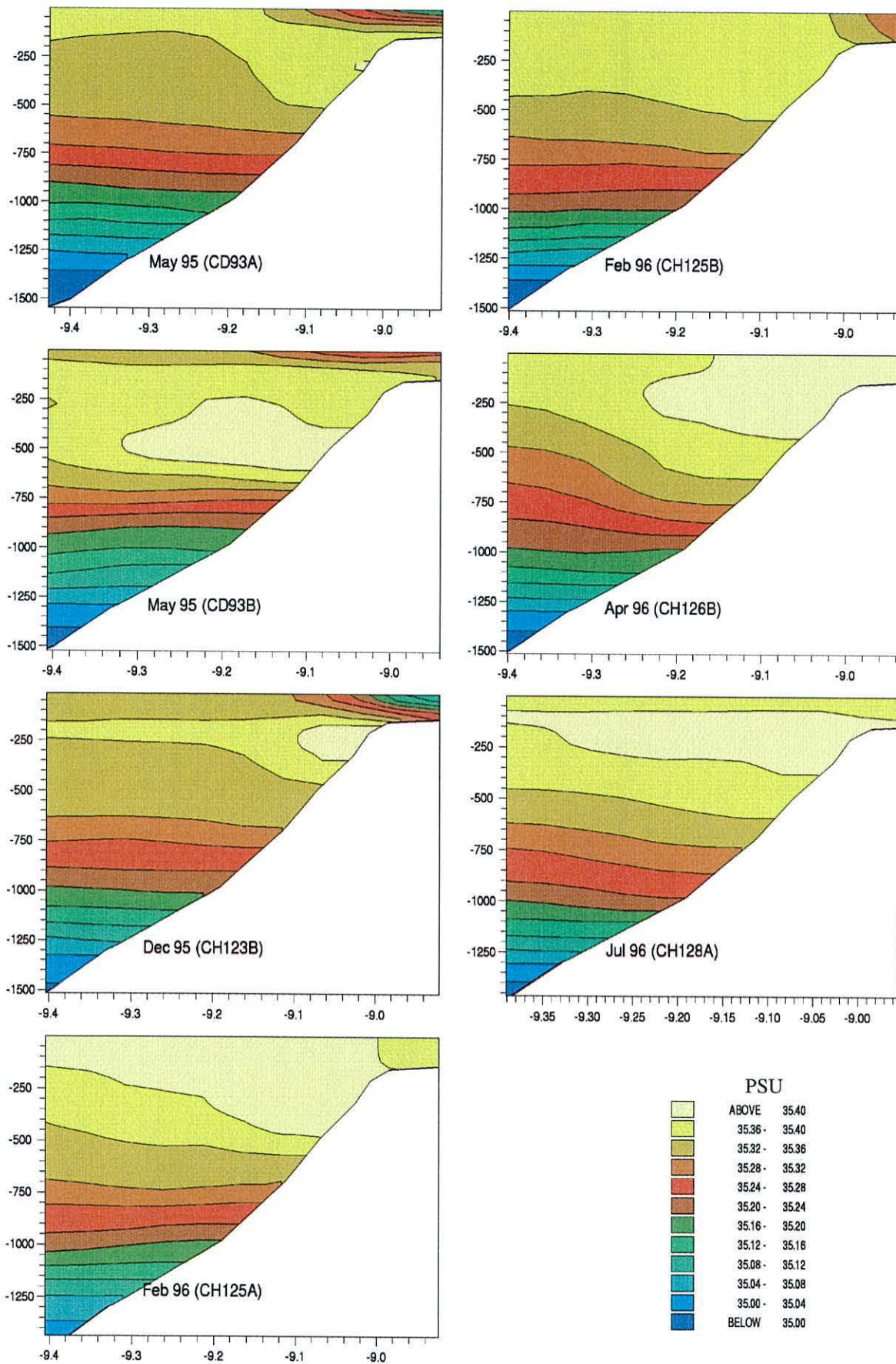Figure 6.3: Temperature sections along the N line across the shelf edge during SES.

Figure 6.4: Salinity sections along the N line across the shelf edge during SES.

6.3 Time series observations

Time series of PMC, made by transmissometers deployed in a cross-shelf array, were examined together with data from companion sensors. Near surface measurements were made using TRB transmissometers built at UWB. Mid-water and near-bed measurements were made with Sea Tech transmissometers, which were interfaced with Aanderaa Type 7 Recording Current Meters (RCMs) to provide current speed and direction information. A summary of the data return from the moored instruments is given in Table 6.1.

Table 6.1: Details of moored instruments that returned data. Note the record length specifies good data and does not necessarily represent the whole deployment period. TRB refers to the UWB transmissometers, primarily located at the surface. ST/RCM refers to Sea-Tech transmissometers integrated with Aanderaa current meters. In the data type column, A refers to beam attenuation, T is temperature, S is salinity, and C is current speed and direction.

Site	Rig	Instrument Depth (m)	Deployment From	dates To	Record length (days)	Instrument	Data type
S140	688	1	15/05/95	23/06/95	71	TRB	A, T
S140	689	140	11/08/95	31/08/95	21	ST/RCM	A,C,T,S
S140	692	1	15/08/95	03/09/95	20	TRB	A,T
S140	733	136	19/11/95	23/01/96	66	ST/RCM	A,C,T,S
S140	747	1	01/02/96	16/03/96	44	TRB	A
S140	745	136	01/02/96	17/04/96	76	ST/RCM	A,C,T,S
S140	761	131	17/04/96	28/07/96	78	ST/RCM	A,C,T,S
S140	763	1	23/04/96	11/05/96	19	TRB	A, T
S200	677	1	27/03/95	01/04/95	6	TRB	A, T
S200	669	1	17/04/95	09/05/95	23	TRB	A, T
S200	670	1	10/05/95	28/05/95	19	TRB	A, T
S300	682	155	09/05/95	02/08/95	9	ST/RCM	A,C,T
S300	682	293	09/05/95	02/08/95	67	ST/RCM	A,C,T
S300	765	293	19/04/96	10/05/96	22	ST/RCM	A,T,S,C
S300	780	293	11/07/96	28/07/96	18	ST/RCM	A,C,T
S700	676	1	10/05/95	04/06/95	26	TRB	A, T
S700	684	222	11/05/95	04/08/95	86	ST/RCM	A,C,T
S700	684	704	11/05/95	04/08/95	86	ST/RCM	A,C,T
S700	702	211	13/08/95	06/09/95	25	ST/RCM	A,C,T
S700	769	1	15/04/96	19/05/96	35	TRB	A, T
N1500	757	1493	06/02/96	21/04/96	75	ST/RCM	A,T,S,C
N1500	774	1492	22/04/96	02/08/96	103	ST/RCM	A,T,S,C

Thirteen datasets emerged from the Sea Tech transmissometers, mainly from instruments on the S line. The N line instruments suffered heavy losses through intensive trawling activity in the area during the deployment periods. Fouling reduced other datasets and some were lost through poor instrument performance. Nine datasets were obtained from the near-surface TRB transmissometers.

The extensive loss of instruments at different sites during the SES campaign has resulted in patchy time series data, which makes it difficult to present each site as a complete 15 month time series. The most coherent way of presenting all the time series is by approximate seasonal divisions, comparing the records across the slope where appropriate. Thus, the time series from the moored instruments are presented chronologically, split approximately into seasons, from on-shelf to off-shelf. The slope is nominally divided into shelf 140-300 m, upper slope 300-500 m, mid-slope 500-850 m and lower slope 850-1500 m regions.

The periods of good data vary between the instruments and some records are much shorter than others are. Where obvious fouling or deterioration in the quality of the signal occurred, the data set has been cut at that point. The main trends will be described and major events in the records identified. The current vector components were computed for a rotated co-ordinate system, such that the y-axis is along-slope, positive northward, and the x-axis is cross-slope, positive eastwards. Summary statistics for the moored instruments are given in Table 6.2. The data sets have been split into approximate one-month periods and the statistics calculated for this duration.

The time series data show both temporal and spatial changes in currents and particle concentrations across the continental slope. The mid-water transmissometers showed the lowest concentrations with the lowest standard deviation. The greatest near-bed concentrations occurred during Winter at the upper slope and in late Spring/early Summer at the upper slope, mid-slope and deep sites. Mean current speeds and maxima in currents decreased down the slope. Cross-slope currents were predominately off-shelf in direction, and along-slope currents flowed northwards in the majority of cases.

The following section presents the time series records in more detail, with particular attention to events in the PMC record and corresponding events in records of the other variables measured.

Table 6.2: Summary details of data from moored instruments in the SES box. St. dev. refers to the standard deviation of PMC. N/A denotes that there were no current meter data.

Site	Depth	Date from	Date to	Mean speed (cm s⁻¹)	Maximum speed (cm s⁻¹)	Cross-slope mean (cm s⁻¹)	Along-slope mean (cm s⁻¹)	Mean PMC (mg m⁻³)	St. dev .PMC (mg m⁻³)
S140	1	15/05/95	23/06/95	N/A	N/A	N/A	N/A	693	224
S140	140	11/08/95	31/08/95	16.9	46.1	1.27	-1.64		
S140	136	19/11/95	21/12/95	18.8	41.5	-3.67	7.56	78	37
S140	136	01/02/96	13/03/96	18.5	52.5	0.06	3.99	156	64
S140	1	01/02/96	16/03/96	N/A	N/A	N/A	N/A	98	65
S140	131	17/04/96	11/05/96	12.5	29.9	-1.36	2.34	99	61
S140	1	23/04/96	11/05/96	N/A	N/A	N/A	N/A	474	177
S140	131	12/05/96	03/06/96	12.6	32.2	-2.40	3.71	233	128
S200	1	27/03/95	01/04/95	N/A	N/A	N/A	N/A	175	33
S200	1	17/04/95	09/05/95	N/A	N/A	N/A	N/A	184	127
S200	1	10/05/95	28/05/95	N/A	N/A	N/A	N/A	422	153
S300	155	09/05/95	17/05/95	11.5	27.0	0.07	8.76	64	14
S300	293	09/05/95	10/06/95	18.2	46.4	-5.09	14.69	74	18
S300	293	11/06/95	13/07/95	18.7	53.7	-5.37	14.73	108	38
S300	293	19/04/96	10/05/96	18.3	45.3	-5.77	14.33	63	32
S300	293	11/07/96	28/07/96	15.3	44.7	-3.50	12.76	84	14
S700	1	10/05/95	04/06/95	N/A	N/A	N/A	N/A	264	126
S700	222	11/05/95	08/06/95	14.8	38.6	-4.55	12.43	26	11
S700	704	11/05/95	13/06/95	13.28	34.8	-3.50	6.44	64	41
S700	222	09/06/95	08/07/95	13.45	34.2	-4.97	16.00	11	6
S700	704	14/06/95	18/07/95	11.76	32.8	-2.82	5.90	77	28
S700	222	09/07/95	04/08/95	13.4	34.2	-4.27	11.15	20	25
S700	211	14/08/95	07/09/95	16.31	38.3	-4.41	14.93	19	7
S700	1	15/04/96	19/05/96	N/A	N/A	N/A	N/A	572	153

Table 6.2 continued.

Site	Depth	Date from	Date to	Mean speed (cm s^{-1})	Maximum speed (cm s^{-1})	Cross-slope mean (cm s^{-1})	Along-slope mean (cm s^{-1})	Mean PMC (mg m^{-3})	St. dev .PMC (mg m^{-3})
N1500	1493	06/02/96	07/03/96	12.50	33.4	-0.76	-0.78	68	45
N1500	1493	08/03/96	01/04/96	12.92	32.8	-0.58	1.19	89	28
N1500	1493	02/04/96	21/04/96	11.53	27.0	-0.98	-1.72	155	32
N1500	1492	22/04/96	25/05/96	13.60	33.4	-1.67	3.08	38	15
N1500	1492	26/05/96	28/06/96	11.46	32.2	-0.71	1.19	329	158
N1500	1492	29/06/96	02/08/96	13.08	27.8	-1.59	-0.41	305	44

6.3.1 Spring/Summer 95

Four Sea-Tech/RCM instruments were deployed between May and August 1995. Two were located at mid-water and two near-bed at S300 and S700. Near surface particulate measurements were made with three TRB transmissometers, deployed at S140, S200 and S700, between April and July.

The surface transmissometers showed similar trends in particle concentration (Fig. 6.5). There was a five-fold decrease in PMC, from 1000 mg m^{-3} to 200 mg m^{-3}, over a 7 day period from May 15-22. These records correlate well (r = 0.8) in the period where they overlap indicating a spatially coherent process in the surface waters. PM concentration gradually increased again in June.

Mean near-bed current speeds were 33% weaker at the mid-slope than at the upper slope station. Near bed PMC at the upper slope (S300, Fig 6.6) was greater but less variable than at mid-slope (S700, Fig 6.7). Strong flows exceeding 40 cm s^{-1} at times occurred with no apparent response in the PMC signal.

At the mid-slope station (S700), the mean concentration of PM was ~60 mg m^{-3}, but the record was more variable than at the upper slope, with fluctuations (15 May-04 June) which were reflected in the temperature time series. Temperature and PMC increased when the cross-slope flow was in the off-shelf direction. Mean PMC was greater near the bed than at mid-water during Spring 1995. The mid-water particle concentration was greater at the upper slope (Fig. 6.8) than at the mid-slope (Fig. 6.9) and both records showed little variability (Table 6.2).

At both sites, current speed did not appear to be the main influence on near-bed PMC, rather the main responses seemed to be related to current direction. Off-shelf currents were associated with an increase in both PMC and temperature. Strong flows in excess of 40 cm $^{-1}$ invoked no signs of resuspension in the PMC signal at S300. However, there was a significant increase in concentration at the end of the record when the flow was predominantly off-shelf in direction.
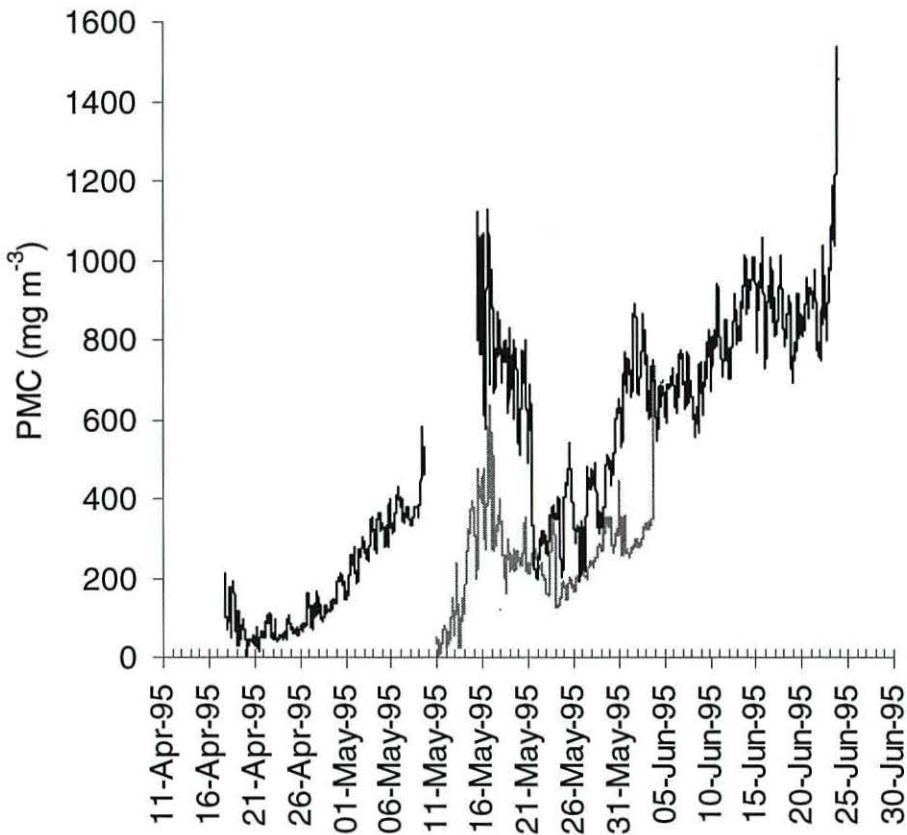
Figure 6.5: Near surface particulate matter concentration from calibrated moored transmissometers at S140 and S200 (black line) and S700 (grey line) in Spring 1995.
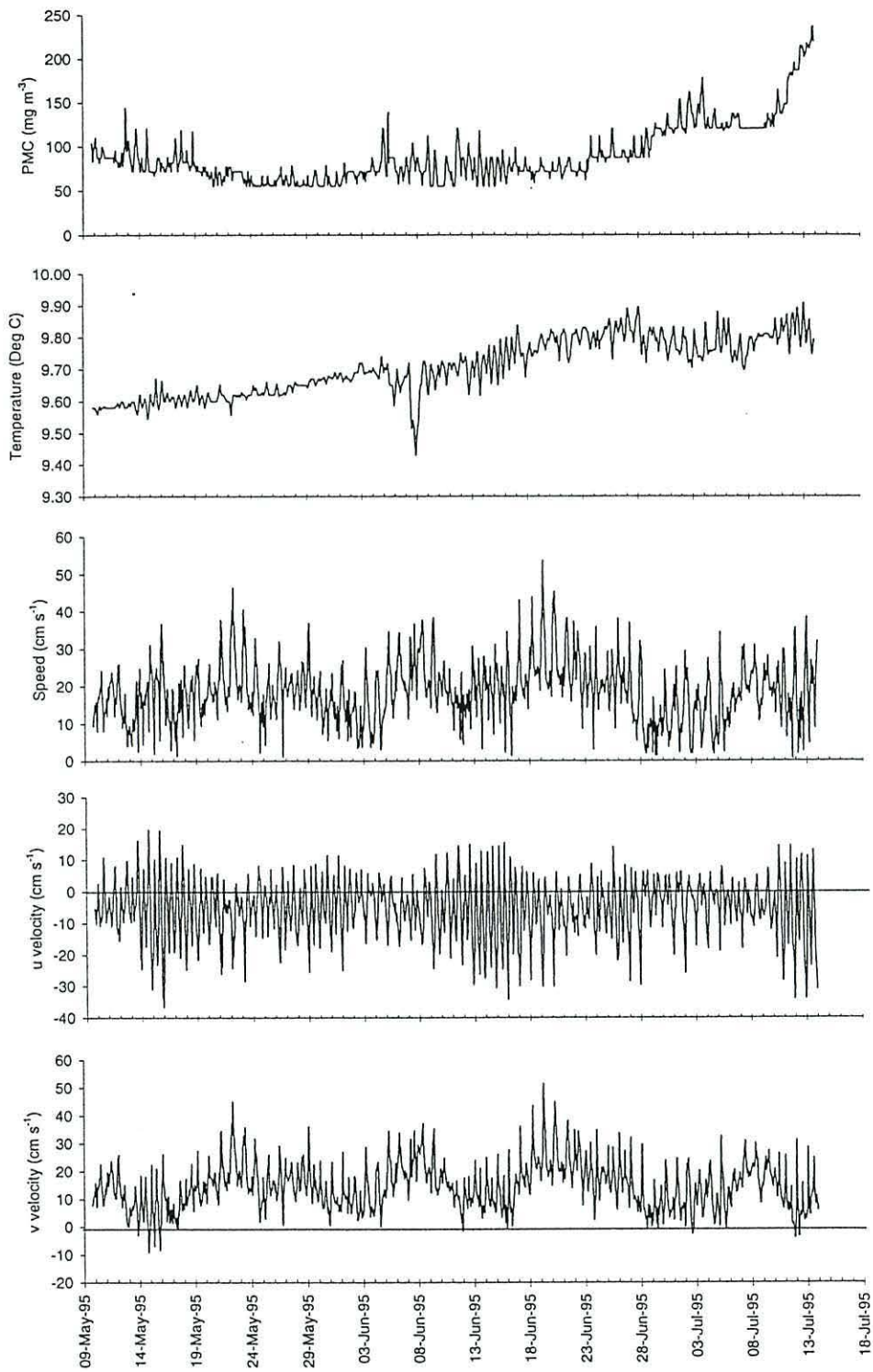
Figure 6.6: Near-bed particulate matter concentration, temperature, current speed, cross-slope velocity and along-slope velocity from moored instruments at S300 in Spring/Summer 1995.
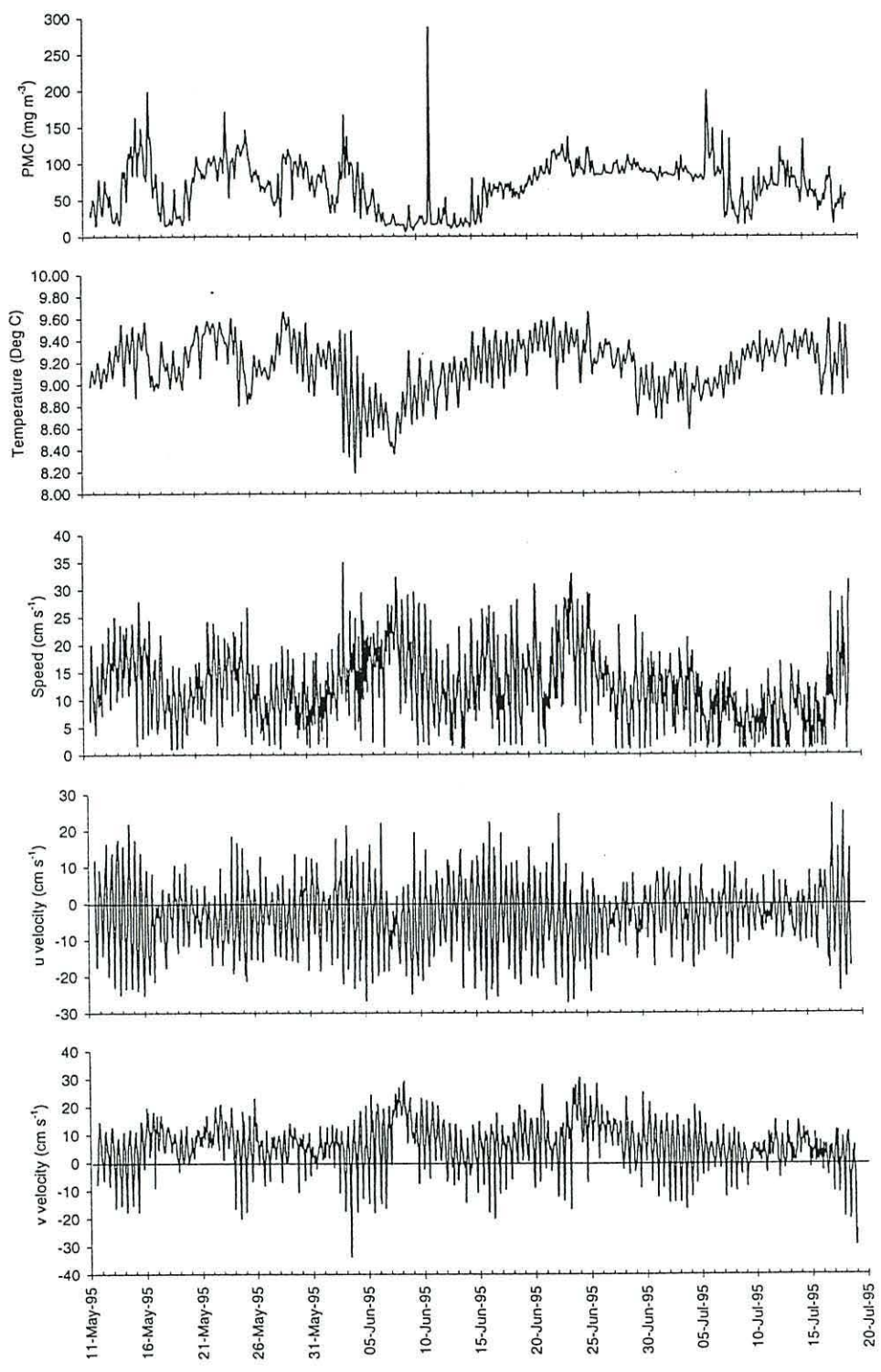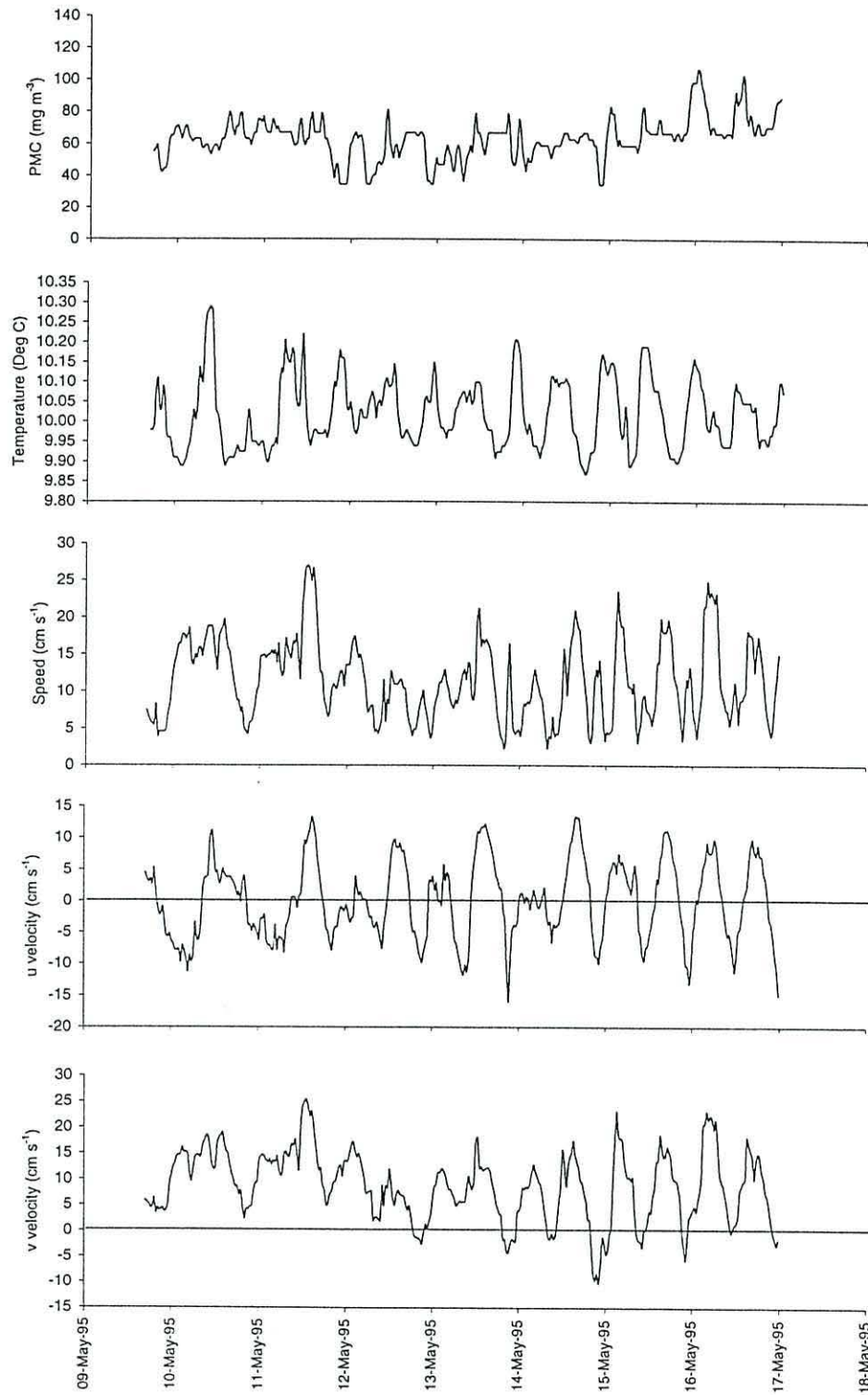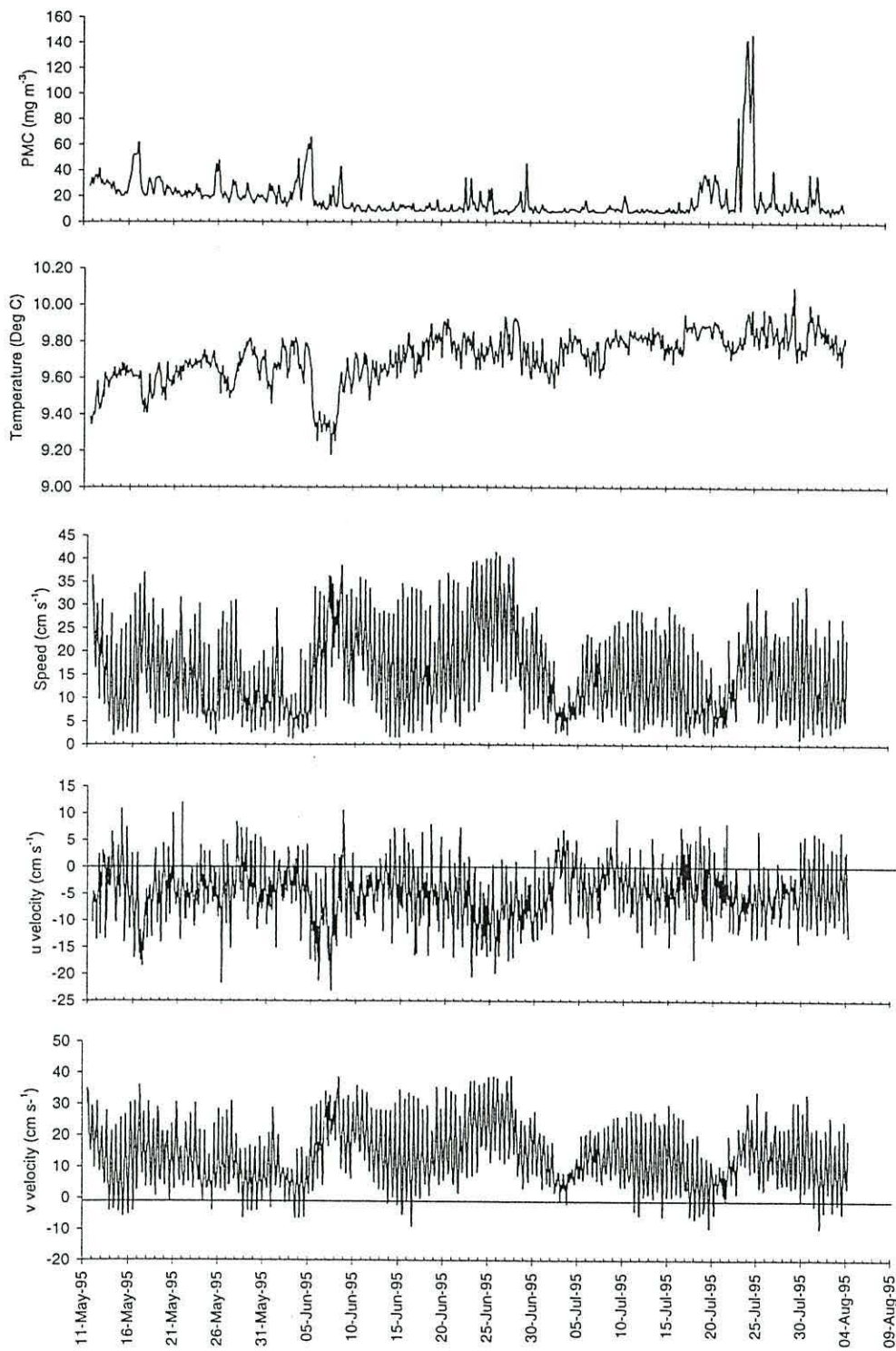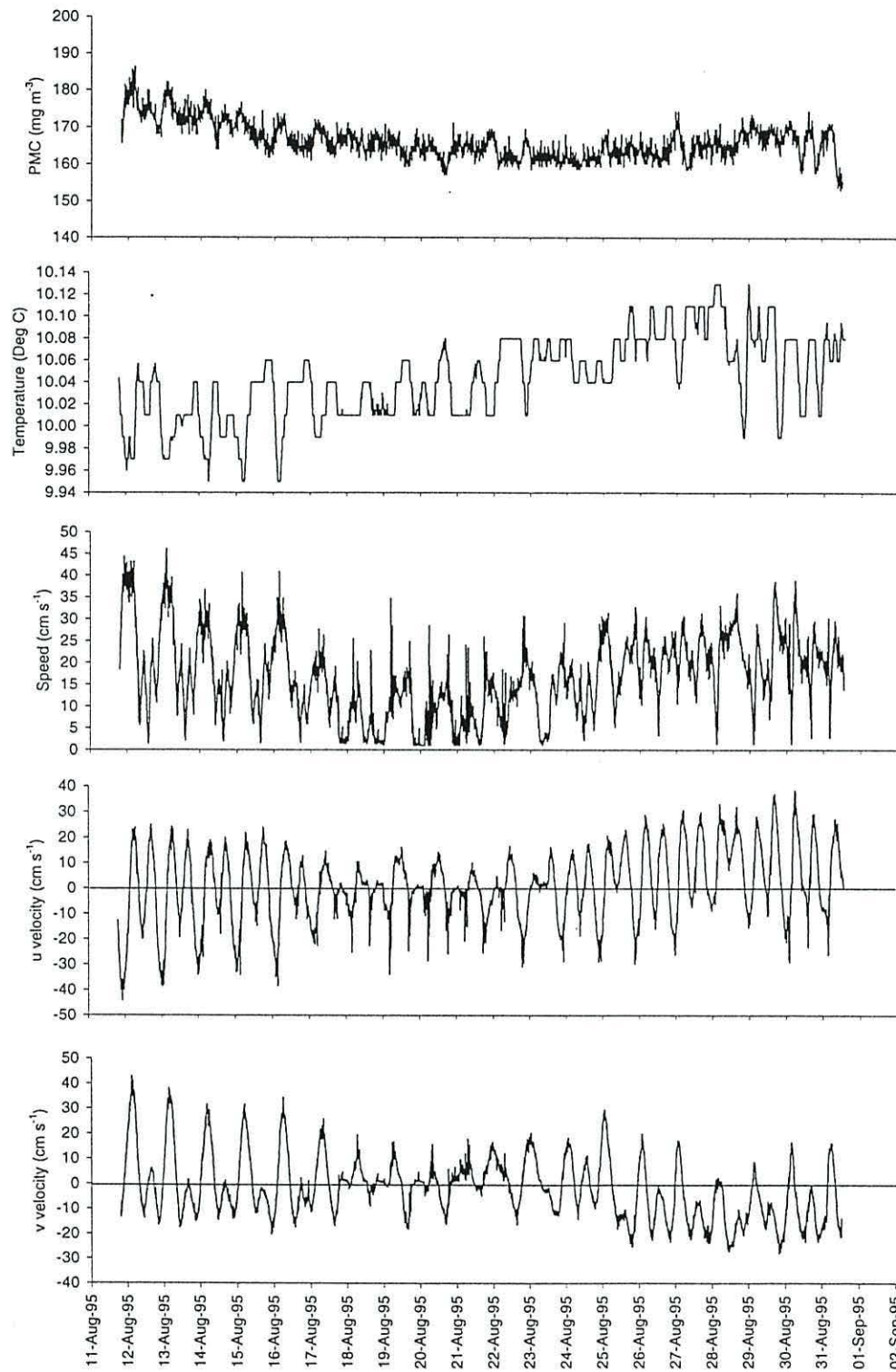
Figure 6.7: Near-bed particulate matter concentration, temperature, current speed, cross-slope velocity and along-slope velocity from moored instruments at S700 in Spring/Summer 1995.

Figure 6.8: Mid-water (155 m) particulate matter concentration, temperature, current speed, cross-slope velocity and along-slope velocity from moored instruments at S300 in Spring/Summer 1995.

Figure 6.9: Mid-water (211 m) particulate matter concentration, temperature, current speed, cross-slope velocity and along-slope velocity from moored instruments at S700 in Spring/Summer 1995.

6.3.2 Summer 95

Three datasets emerged from the Summer 95 deployment period: two at S140 (near-bed and surface) and one at S700 (mid-water). The PMC record from the near-bed transmissometer at S140 (Fig. 6.10) showed little variability throughout the time series. There was a weak response in the PMC signal at the beginning of the record when current speeds were strongest, in excess of 40 cm s^{-1}. Internal waves are known to have traversed this mooring site between August 18 and 24 (Inall & Sherwin, 1996). Their signal in the current speed record was characterised by short spikes in the record between these days. It is difficult to distinguish whether there was a change in PMC in response to internal wave activity over the noise in the record. At the surface, PMC time series was much more variable (Fig. 6.11). Both of these instruments lack reliable calibration information so the PM data must only be regarded qualitatively. PMC at the S700 mid-water transmissometer ranged between 10 and 50 mg m^{-3}, with relatively little variability in the record (Fig. 6.12).

Figure 6.10: Near-bed particulate matter concentration, temperature, current speed, cross-slope velocity and along-slope velocity from moored instruments at S140 in Summer 1995.
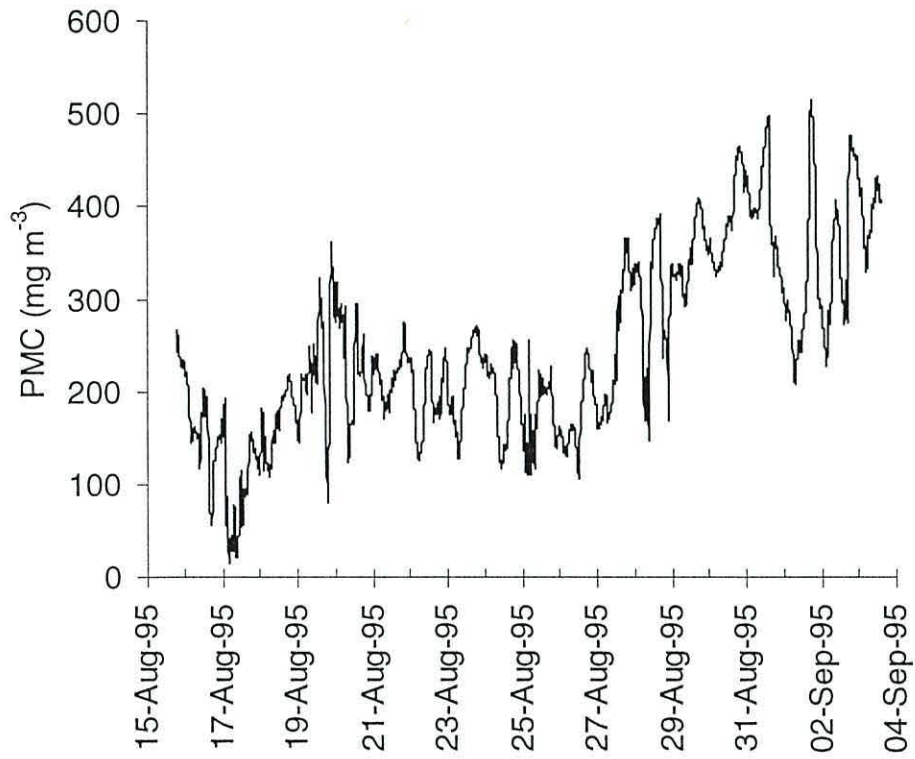
Figure 6.11: Near-surface particulate matter concentration from a moored transmissometer at S140 in Summer 1995.
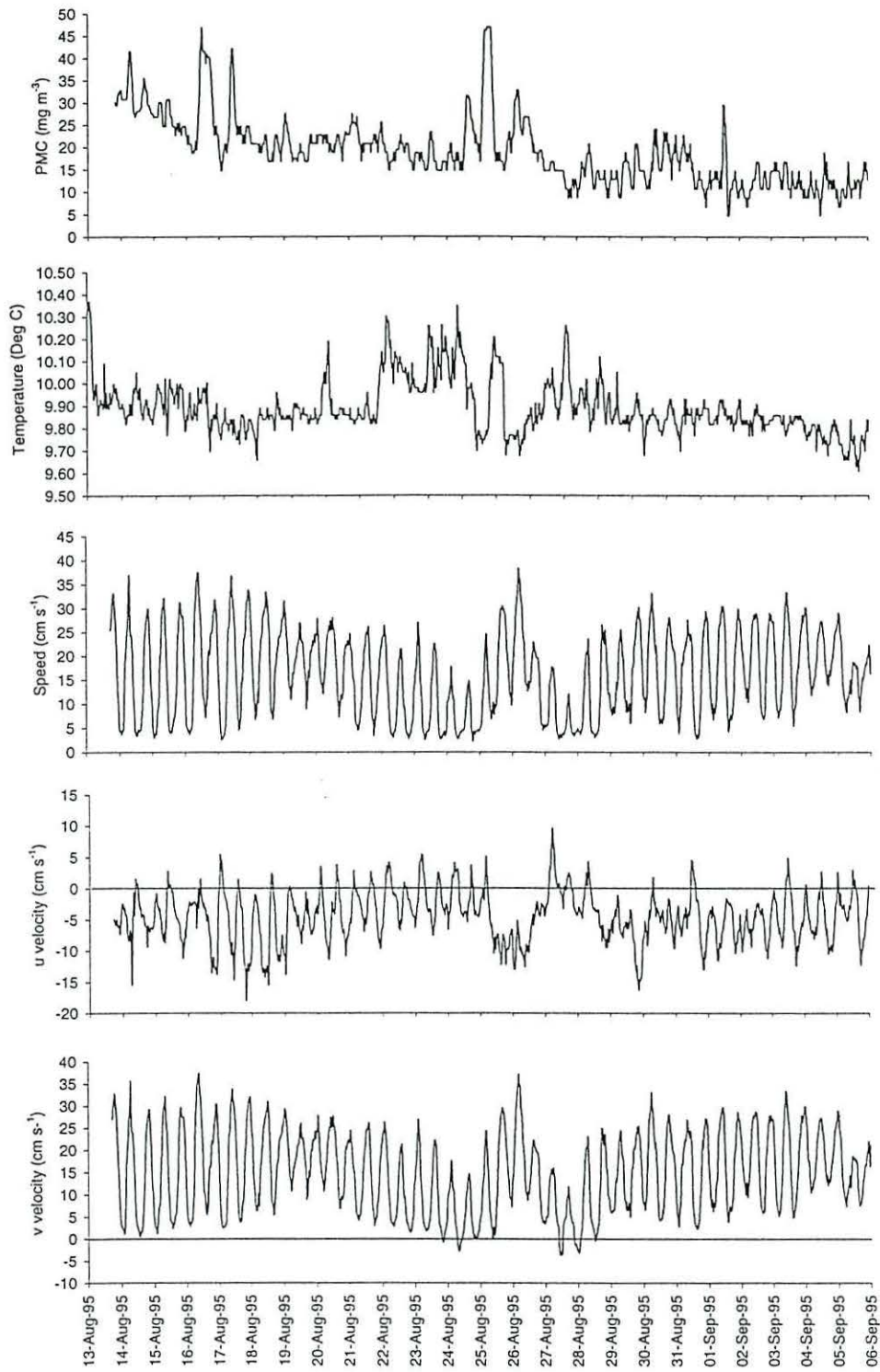
Figure 6.12: Mid-water (211 m) particulate matter concentration, temperature, current speed, cross-slope velocity and along-slope velocity from moored instruments at S700 in Summer 1995.

6.3.3 Winter 95/96

The Winter deployment period ranged from the end of November 1995 to the beginning of April 1996. Four datasets were obtained during this time period: two from near-bed instruments at S140, one from S140 near-surface, and one from a near-bed mooring at N1500.

At S140 a near-bed transmissometer and current meter were located from late November to early January. PMC was relatively uniform throughout late November and December 1995 (Fig. 6.13). Near-bed temperature increased gradually from just over 10.5 °C to 11 °C between late November and mid December. In late December, temperature decreased again, to ~10.5 °C.

The next near-bed deployment at S140 was from early February until early March (Fig. 6.14). The surface times series covered the same period (Fig. 6.15). The surface instrument recorded generally low concentrations when compared with the levels observed in Spring 1995, mean concentration was of the order of 100 mg m^{-3}. The near bed transmissometer showed a gradual increase in PM concentration throughout the time series. The near bed current meter record showed high speed events, especially between February 19-21, where they exceeded 50 cm s^{-1}. There was an increase in PMC both at the bed and at the surface at this time.

At the deep site (N1500 Fig. 6.16) there was a gradual increase in PMC throughout the deployment period from ~10 mg m^{-3} to >100 mg m^{-3}. Three events where PMC suddenly increased are evident in the record. The first was the largest and coincided with strong currents of the order of 40 cm s^{-1}. PMC increased five-fold for a period of 18 hours to ~400 mg m^{-3}. The abrupt subsequent decrease in concentration and rapid change in temperature indicate that this event was more likely to be advection of material resuspended elsewhere. The second event was less intense and coincided with relatively vigorous currents. Again, there was an associated decrease in temperature, related to up-slope flow. The third event does not appear to be related to current speed and, once again was associated with a decrease in temperature.

In summary, strong flows occurred at the shelf and lower slope site during February. The currents on the shelf were almost twice as strong as those at the lower slope site, reaching speeds in excess of 50 cm s^{-1}. There was a response in PMC record near the bed and at the surface at S140. The lower slope site showed the greatest response to a strong flow event a few days after the one observed on the shelf.
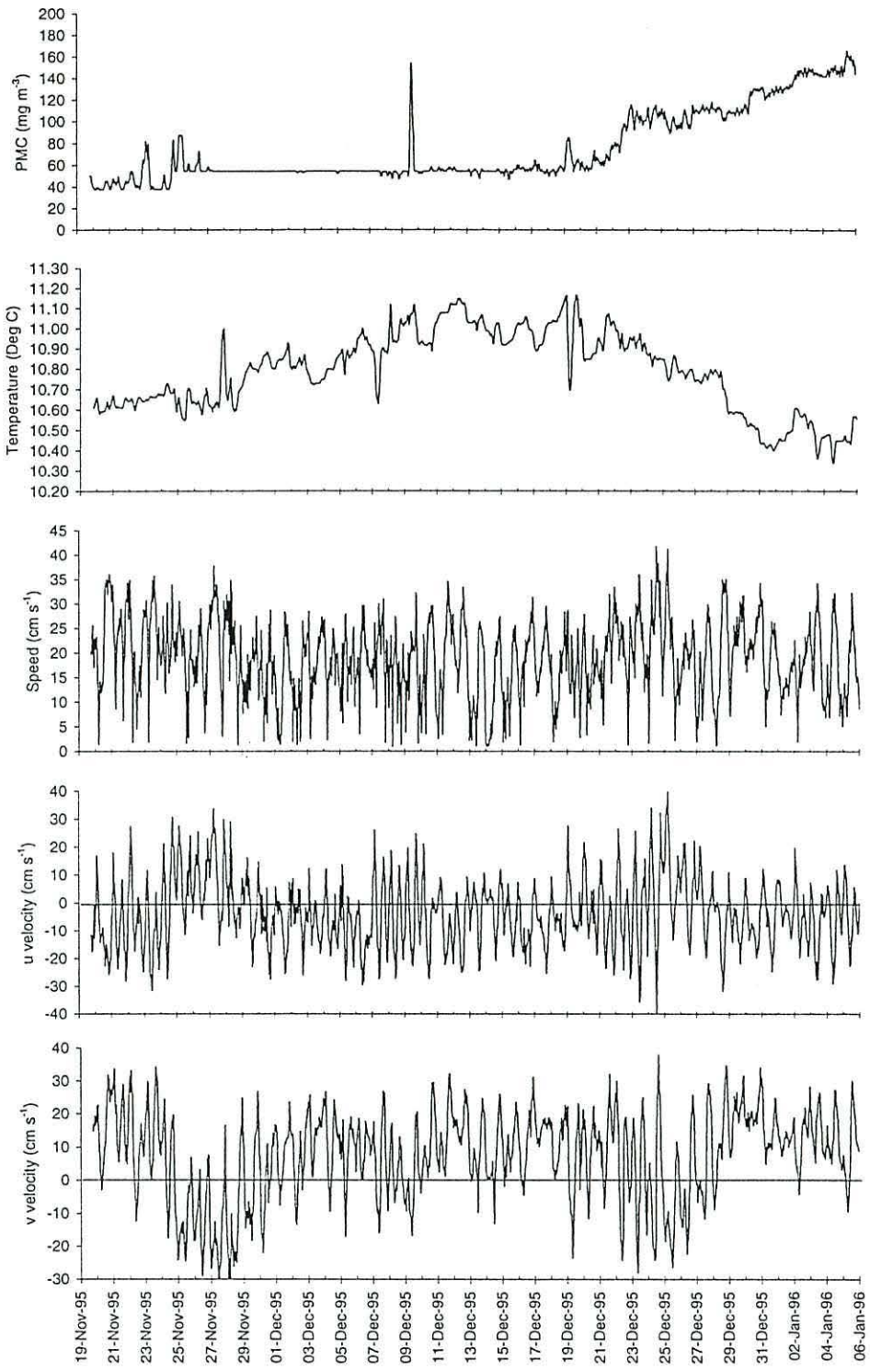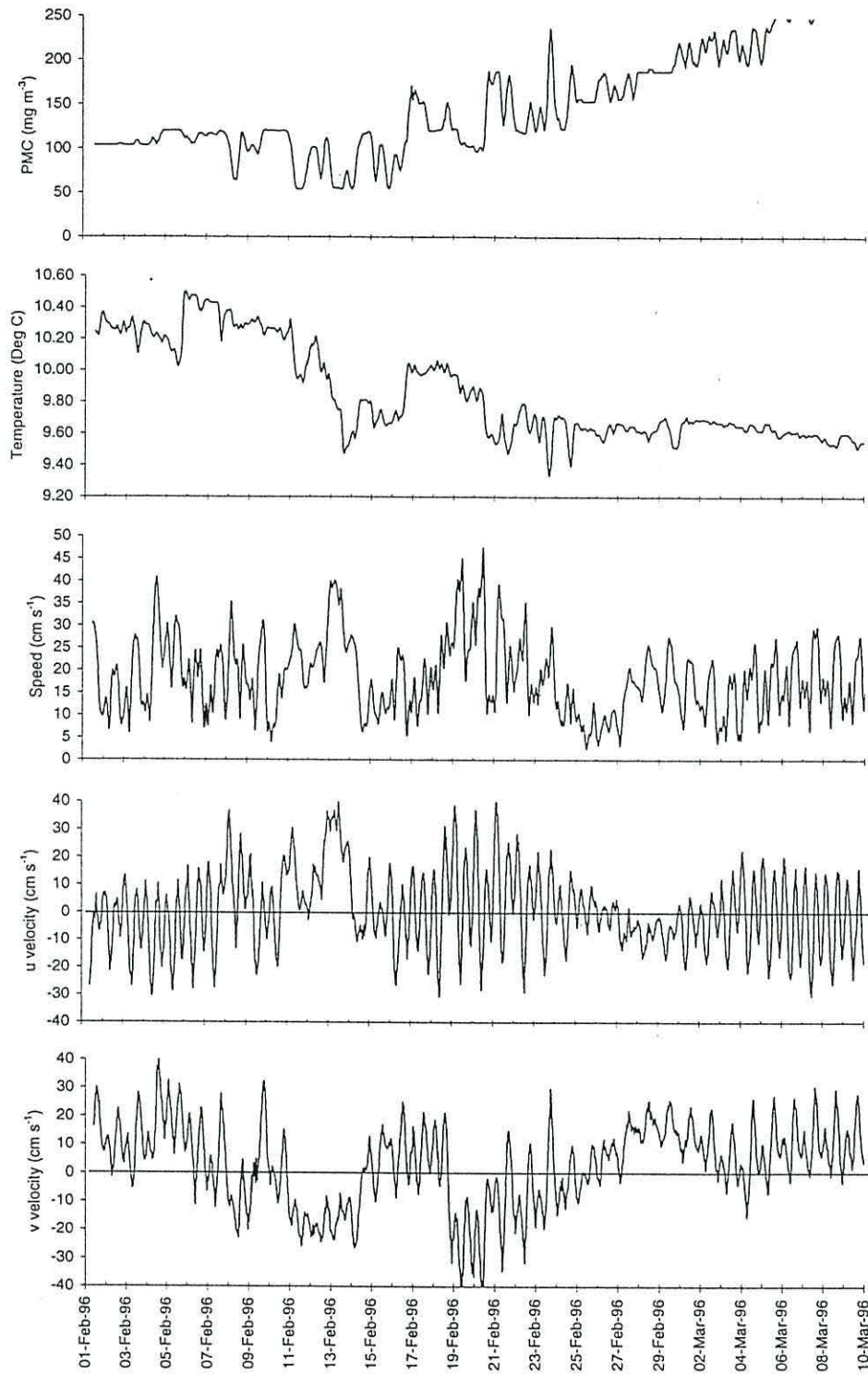
Figure 6.13: Near-bed particulate matter concentration, temperature, current speed, cross-slope velocity and along-slope velocity from moored instruments at S140 in Winter 95/96.
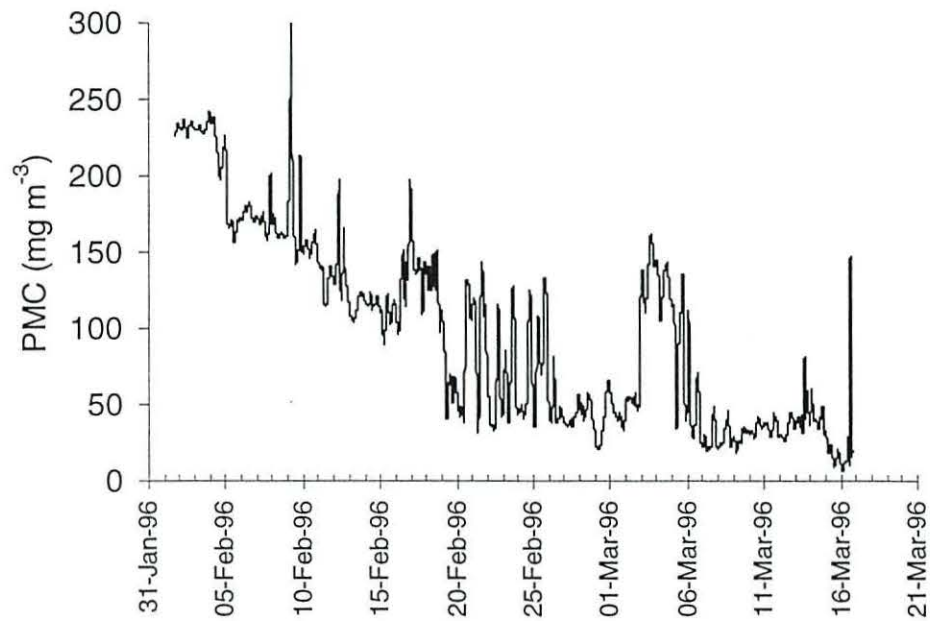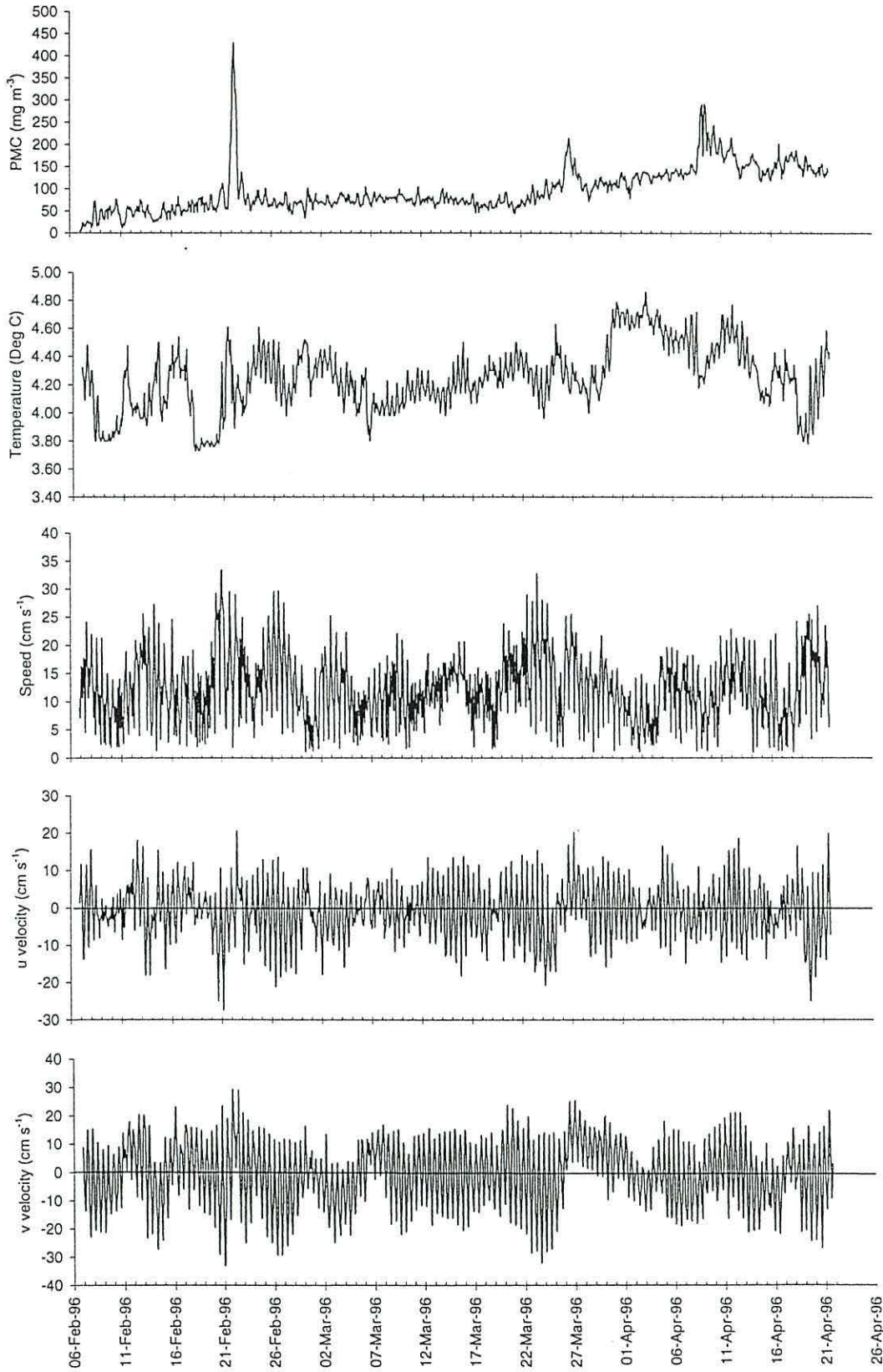
Figure 6.14: Near-bed particulate matter concentration, temperature, current speed, cross-slope velocity and along-slope velocity from moored instruments at S140 in Winter 95/96.

Figure 6.15: Near-surface particulate matter concentration from a calibrated moored transmissometer at S140 in Winter 95/96.

Figure 6.16: Near-bed particulate matter concentration, temperature, current speed, cross-slope velocity and along-slope velocity from moored instruments at N1500 in Winter 95/96.

6.3.4 Spring/Summer 1996

Five transmissometers were deployed between April and August 1996, two TRBs moored at the surface at S140 and S700, and three near-bed ST/RCMs at S140, S300, and N1500.

The surface instruments (Fig. 6.17) both showed very similar trends, with an increase in PMC from 22 April reaching a peak at ~600 mg m^{-3} on May 3. PM concentration then decreased in both records to ~400 mg m^{-3}, before increasing sharply again. The near-bed record at S140 showed mean concentration levels of the order of 50 mg m^{-3} until May 3 when concentration increased steadily to a peak of ~450 mg m^{-3} around 18 May after which concentration decreased again (Fig. 6.18). The S300 near-bed transmissometer record (Fig. 6.19) covered a much shorter period, though it shows an increase in concentration around May 3, the same time near-bed concentration increased at S140. The deep site (N1500) time series was characterised by relatively low concentrations (~50 mg m^{-3}) for the first part of the record but from the end of May to the end of June there was a steady increase to ~600 mg m^{-3} (Fig. 6.20).

Data from the current meters at the upper slope sites show that relatively strong flows exceeding 30 cm s^{-1} occurred at times, though this was not reflected in the concentration time series. None of the records showed an increase in PMC directly related to increases in current speed.

In summary, surface particle concentration increased in April and then decreased at the beginning of May, before increasing again. The near bed instruments at the upper slope showed a significant increase in PMC around the beginning of May, especially at S140. Three weeks after the peak occurred on the shelf there was an increase in concentration at the deep station N1500. These increases were not related to strong flow conditions.
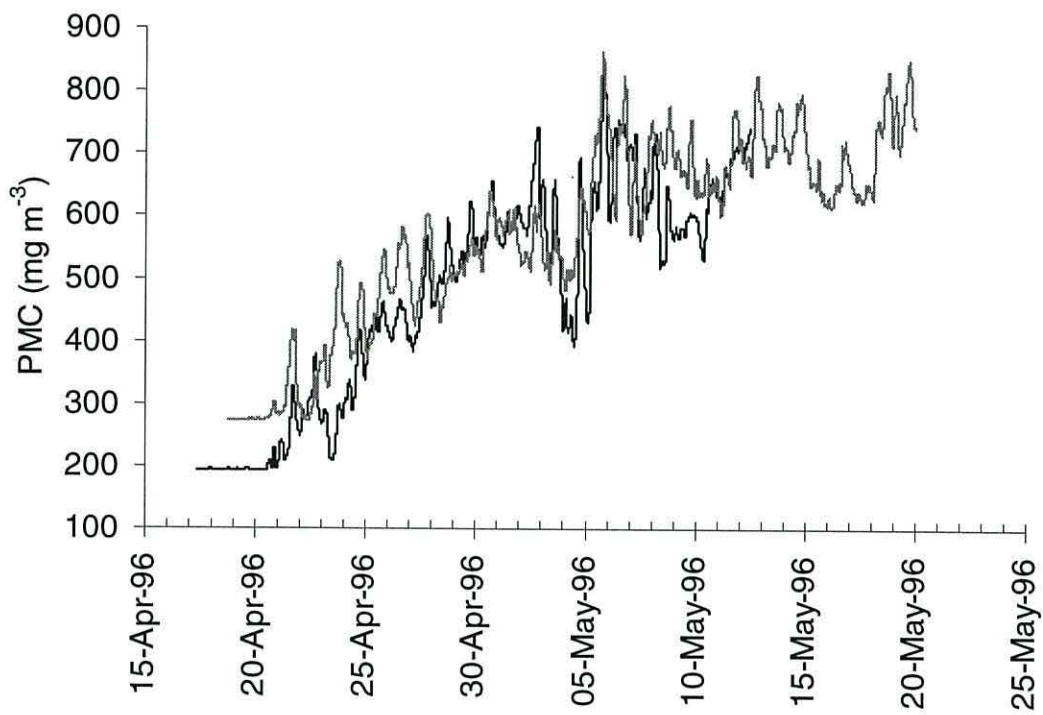
Figure 6.17: Near-surface particulate matter concentration from calibrated moored transmissometers at S140 (black line) and S700 (grey line) in Spring 1996.
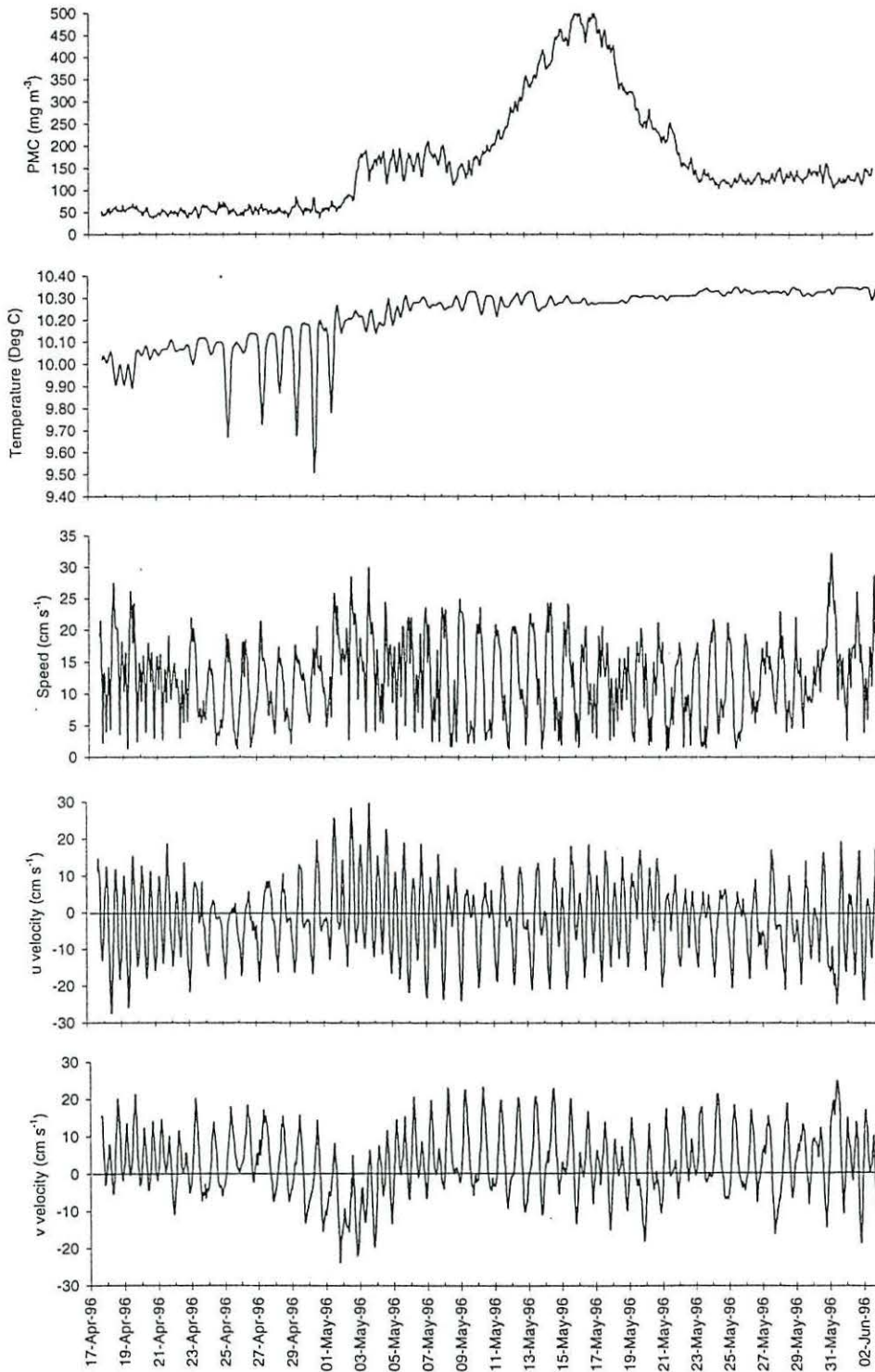
Figure 6.18: Near-bed particulate matter concentration, temperature, current speed, cross-slope velocity and along-slope velocity from moored instruments at S140 in Spring 1996.
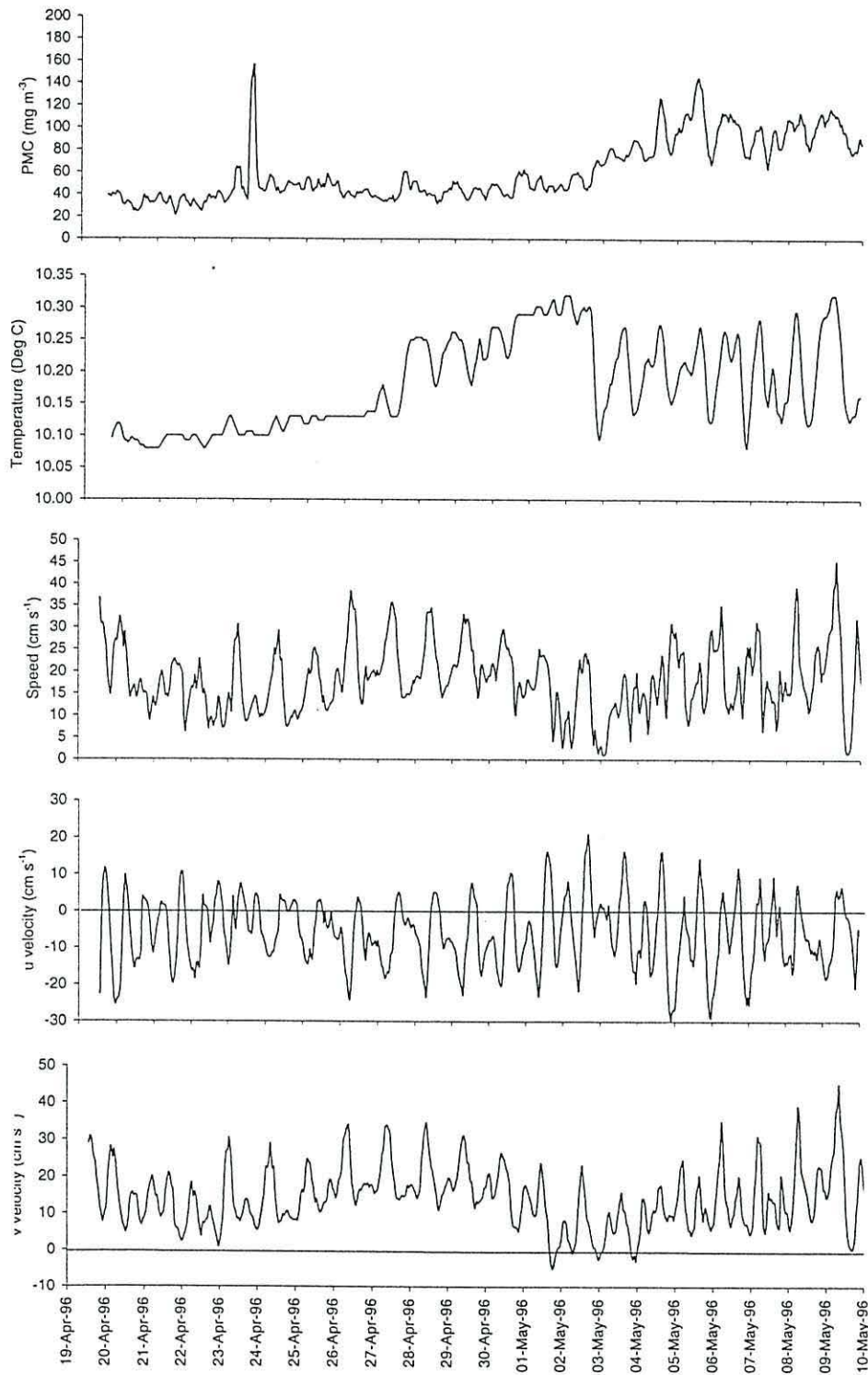
Figure 6.19: Near-bed particulate matter concentration, temperature, current speed, cross-slope velocity and along-slope velocity from moored instruments at S300 in Spring 1996.
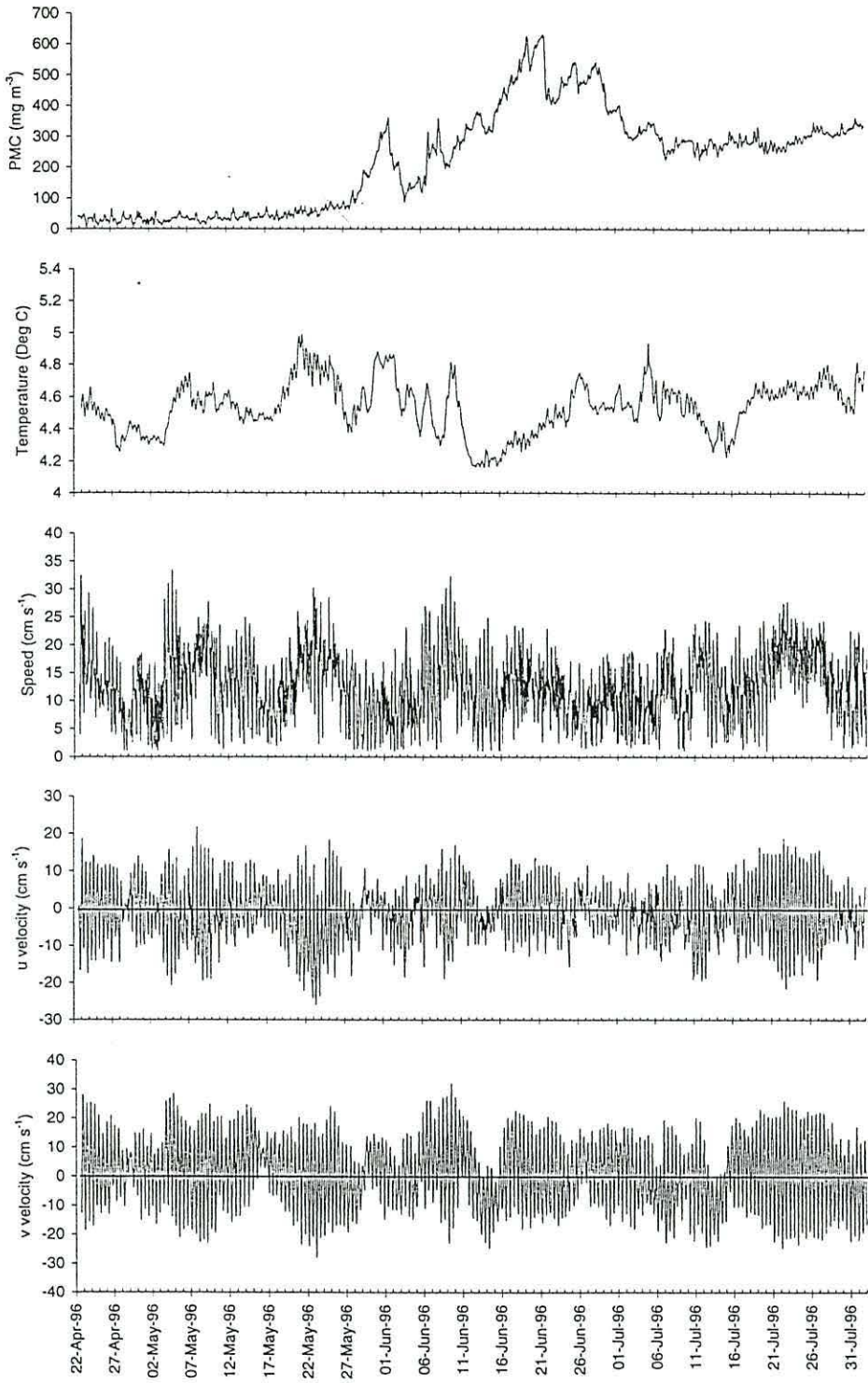
Figure 6.20: Near-bed particulate matter concentration, temperature, current speed, cross-slope velocity and along-slope velocity from moored instruments at N1500 in Spring/Summer 1996.

6.4 Settling velocity distributions

Nineteen successful deployments of the settling velocity tubes were made during the SES campaign over 5 cruises. Settling velocity distributions were calculated for the total PM population and chlorophyll. Sample identification, station, date, total PM or chlorophyll concentration and median settling velocity (W_s) have been listed in Tables 6.3 (a) and (b), respectively. Samples were processed for total PM in Spring and Summer 1996 as well as chlorophyll but contamination of the filters rendered the data unreliable and they have been excluded.

Table 6.3 (a): Sampling details and summary statistics for SVT total PM samples.

Cruise sample	Date	Site	Depth (m)	Total PM (mg m^{-3})	Median W_s (m day^{-1})
CH123B 1	11/12/95	N1500	30	1080	1.53
CH125B 1	14/02//96	S140	60	460	0.05
CH125B 2	20/02/96	N1500	60	390	3.27
CH125B 3	20/02/96	N1150	770	1390	0.83
CH125B 4	22/02/96	R1000	100	1080	0.26
CH125B 5	27/02/96	UB300	60	550	11.04

Table 6.3 (b): Sampling details and summary statistics for SVT chlorophyll samples. Samples with suffixes a, b and c are replicates from the same tube.

Cruise sample	Date	Site	Depth (m)	Chlorophyll (mg m^{-3})	Median W_s (m day^{-1})
CD93B 1	18/05/95	S140	5	5.4	0.02
CD93B 2	22/05/95	R1000	2	0.74	0.02
CD93B 3	25/05/95	S200	2	0.93	0.02
CD93B 4$_a$	26/05/95	N1500	5	0.54	0.04
CD93B 4$_b$	26/05/95	N1500	5	0.54	0.05
CD93B 4$_c$	26/05/95	N1500	5	0.55	0.04
CD93B 5	27/05/95	S300	5	0.69	0.09
CD93B 6	28/05/95	S700	2	0.69	0.07
CH126B 1$_a$	28/04/96	S140	7	3.34	0.07
CH126B 1$_b$	28/04/96	S140	7	3.33	0.05
CH126B 2	30/04/96	S700	7	2.67	0.04
CH126B 3$_a$	02/05/96	N1500	7	2.37	0.05
CH126B 3$_b$	02/05/96	N1500	7	2.27	0.07
CH126B 4$_a$	06/05/96	S1300	5	1.71	0.16
CH126B 4$_b$	06/05/96	S1300	5	1.96	0.17
CH128A 1$_a$	14/07/96	S140	12	1.87	0.03
CH128A 1$_b$	14/07/96	S140	12	1.74	0.03
CH128A 1$_c$	14/07/96	S140	12	1.85	0.02
CH128A 2$_a$	18/07/96	S1300	10	1.09	0.03
CH128A 2$_b$	18/07/96	S1300	10	1.14	0.04
CH128A 2$_c$	18/07/96	S1300	10	1.12	0.04
CH128A 3$_a$	18/07/96	S300	15	1.42	0.03
CH128A 3$_b$	18/07/96	S300	15	1.43	0.03
CH128A 3$_b$	18/07/96	S300	15	1.43	0.03

For many of these samples the median had to be estimated by extrapolation, assuming a log-normal fine tail-end distribution for the PM population (Jones and Jago, 1996). This extrapolated population settles very slowly and so is representative of a background component, permanently in suspension. Overall, slow settling sub-populations, especially in the chlorophyll samples dominated the settling velocity distributions observed from samples in the SES box. Very good replication was achieved in the chlorophyll samples (Table 6.3 (b)).

6.4.1 Total PM settling rates

As shown in Table 6.3(a), there were relatively few total PM SVTs that yielded reliable data, and there are no replicates so there may be a high degree of error. Figure 6.21 shows histograms of the settling velocity distribution calculated from samples obtained during CH123B and CH125B, December 95 and February 96, respectively. In December, two distinct modes can be seen, centred on 5.7×10^{-3} and 18 mm s^{-1}.

The cruise in February yielded five SVT samples. The first was obtained on the shelf prior to a storm. The total concentration was relatively low and dominated by slowly settling material. The second deployment, at N1500, was immediately after the passage of the storm referred to in the CTD and time series results. Although the total concentration is similar to that on the shelf before the storm, there was an increase in a faster settling sub-population. Nearby, but at a much greater depth (770 m), another tube was deployed in an intermediate nepheloid layer that was detected during a CTD cast. This was the deepest sample ever obtained with the SVTs, enabled by the novel acoustic release system. There was a marked difference in the particle population at this depth. A high proportion of the particles in this sample had settling rates of the order of $5 \times 10^{-3} \text{ mm s}^{-1}$. There was also a second mode present showing faster settling rates of $\sim 18 \text{ mm s}^{-1}$, representing a coarser fraction which was also observed in the sample at 100 m at R1000, two days later.

The sample obtained at UB300, upstream of the SES Box, was at the site of the Malin density cascade event (Hill *et al*, 1998). There was a prominent peak in the settling velocity spectrum at 0.18 mm s^{-1} ($\sim 15 \text{ m day}^{-1}$). Although the sample was not

obtained close to the bed, due to time constraints, the location at 60 m was within a region of high beam attenuation and relatively high chlorophyll concentration.

Despite the low number of samples and lack of replication, the data show consistency in the modes observed.

6.4.2 Chlorophyll settling rates

Six samples provided settling velocity spectra during Spring 1995 (Fig. 6.22). The most striking feature was the marked reduction in total concentration between the first sample and subsequent samples. Total chlorophyll concentration was more than eight times greater on the shelf on 22/05/95 than observed in the other samples (Table 6.3 (b)). On 22/05/95 the distribution was very similar for surface waters of the shelf and deep station but the shelf showed a higher total concentration. Three days later, the total concentration on the shelf (S200) had decreased significantly, to levels similar to those observed at the deep station (R1000) on 22/05/95. The settling velocity spectra were very similar. At a deep station (N1500) the next day, the SVT sample showed a further decrease in total concentration, but there was a shift in the distribution towards a more rapidly settling sub-population. Samples at S300 and S700 on 27/05/95 and 28/05/95, respectively, also showed an increase in the more rapidly settling proportion.

During the cruise in Spring 1996 there was a gradual decrease in total chlorophyll concentration with time (Table 6.3 (b)). Similar settling distributions were observed at S140, S700 and N1500 between 28/04/96 and 02/05/96 (Fig. 6.23). The lowest total concentration was at S1300 on 06/05/96 and there was a shift in the distribution towards the more rapidly settling classes.

In Summer 1996, total concentrations were very similar to those observed at the end of the Spring 1996 cruise (Table 6.3 (b)). The total chlorophyll concentration was slightly lower at the deep station (S1300) than at the shelf. Settling velocity distributions were all similar, dominated by the slower settling classes (Fig. 6.24).
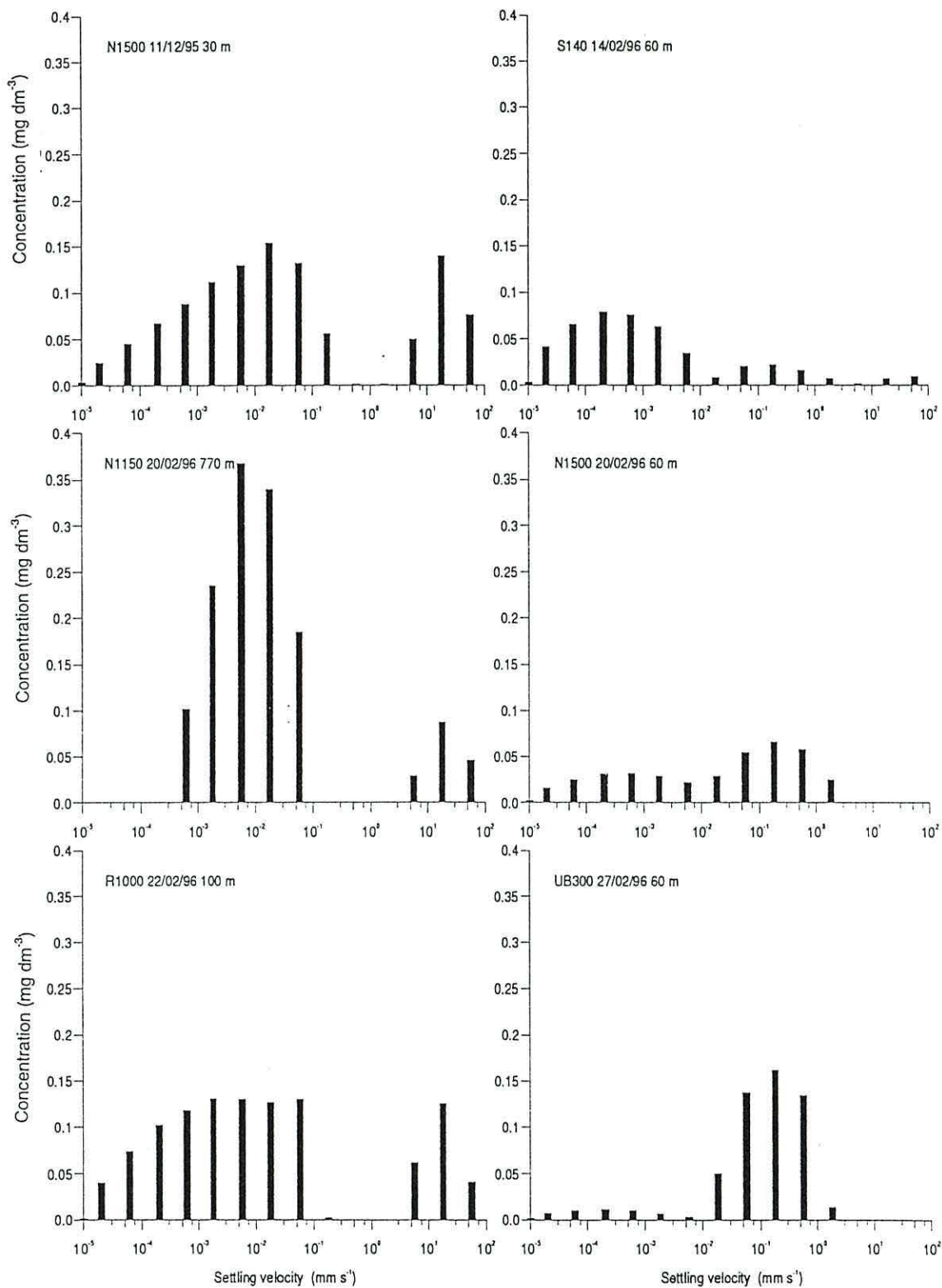
Figure 6.21: Total particulate matter settling velocity spectra for samples taken in the SES box in December 1995 (top left graph) and February 1996 (remaining graphs).
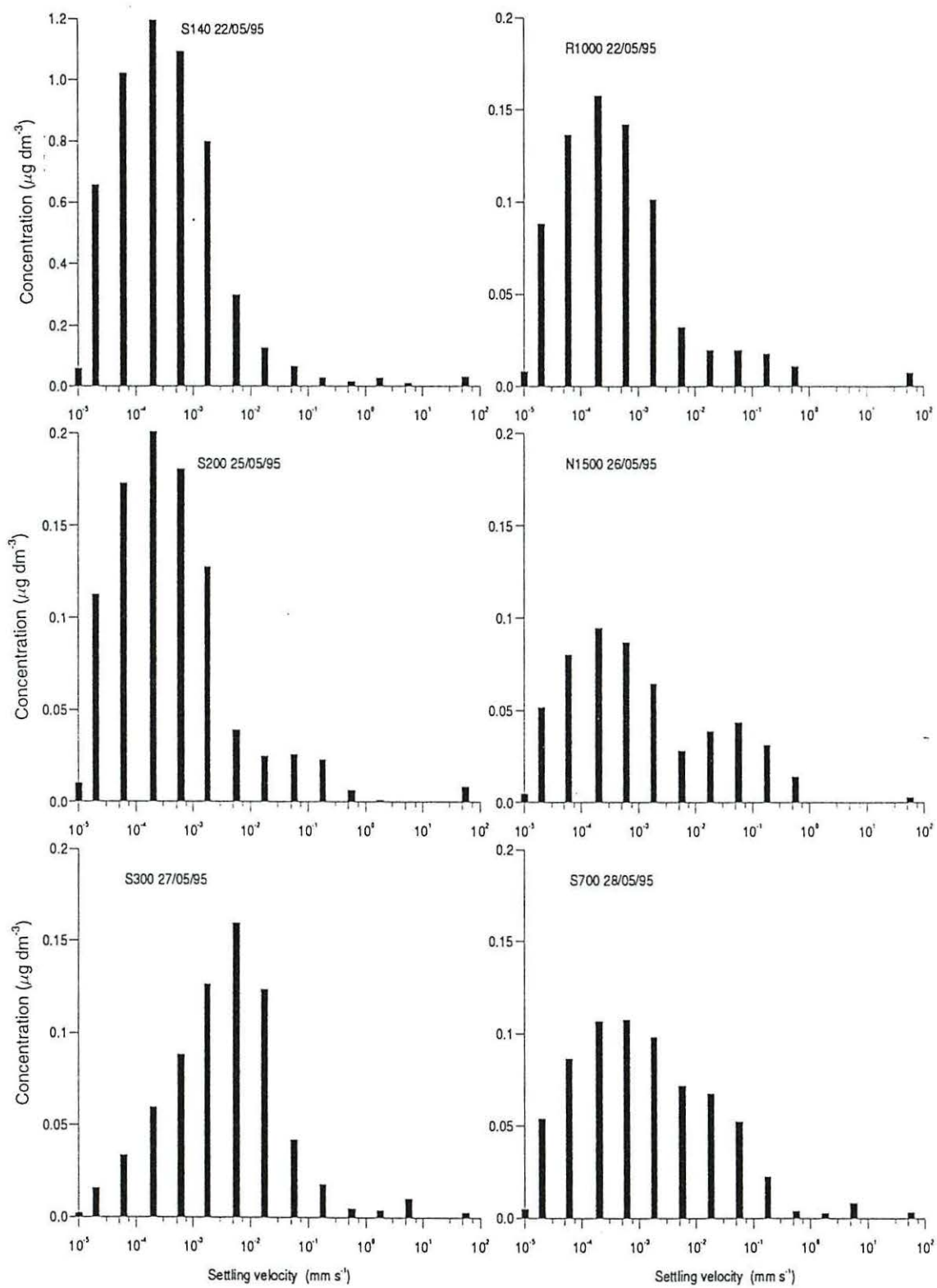
Figure 6.22: Chlorophyll settling velocity spectra for samples taken in the SES box in Spring 1995. Note the vertical scale on the top left graph is different to the vertical scale on the remaining graphs.
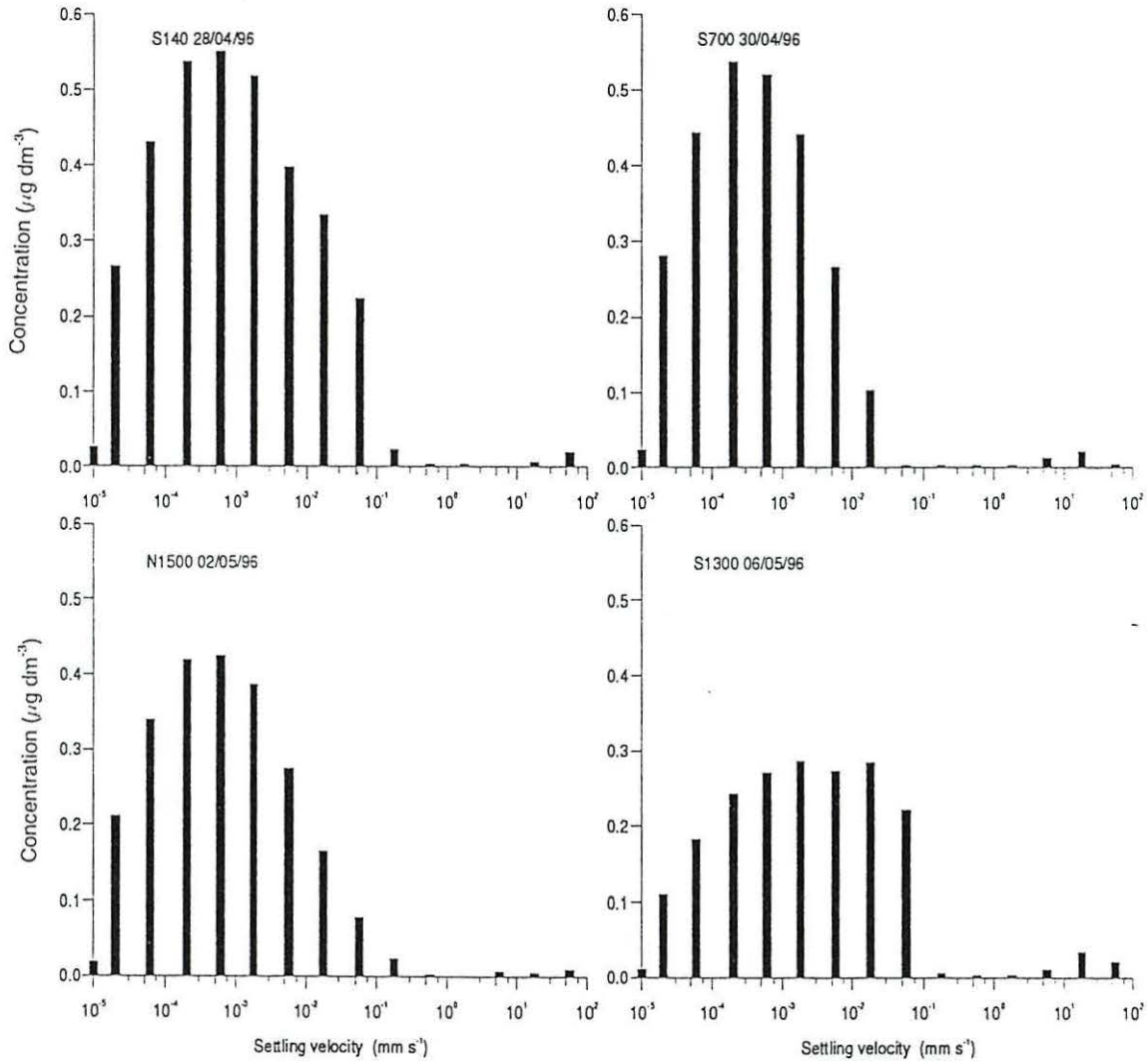
Figure 6.23: Chlorophyll settling velocity spectra for samples taken in the SES box in Spring 1996.
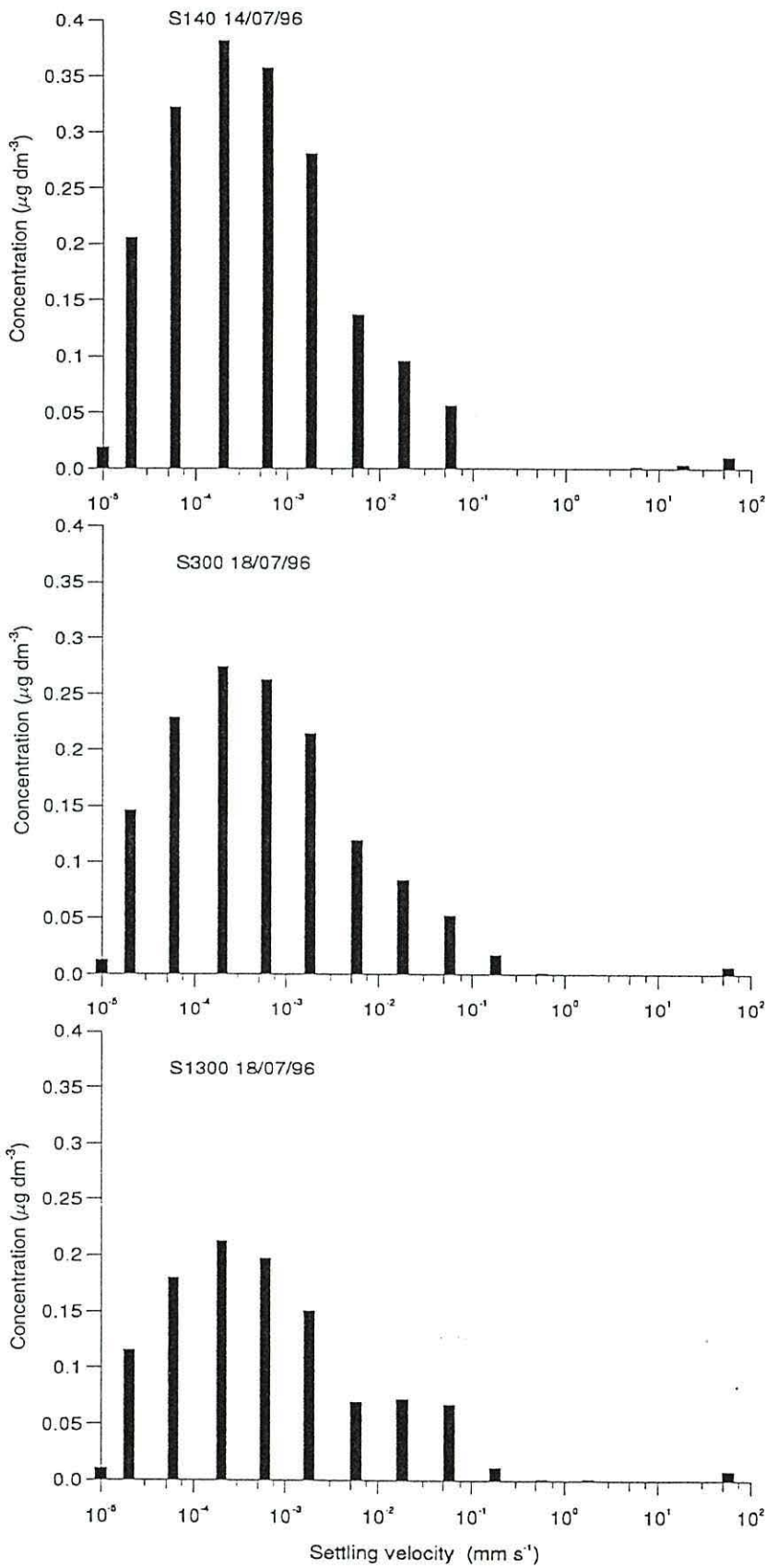
Figure 6.24: Chlorophyll settling velocity spectra for samples taken in the SES box in Summer 1996.

6.5 Particle size distribution

Persistent problems with the Galai Laser Particle Sizer resulted in particle size data being obtained for only two of the SES cruises, CD93B and CH121B, in Spring and Summer 1995 respectively. In Spring 1995, a total of 189 samples was processed through the instrument. In Summer 1995, only 21 samples were successfully measured, though many more were attempted. Many of the samples were not measurable because of the low concentration of particles. All of the samples were measured with the instrument set to a range of 2 to 600 μm.

6.5.1 Spring 1995

The surface layer in Spring 1995 was dominated by phytoplankton, as seen in the chlorophyll contour plots (Fig. 6.2). Throughout the cruise, low particle concentrations were observed at mid-depth. Figure 6.25 (a) shows the change in mean particle size with time for samples obtained at the surface. There was a steady decrease in mean particle size from > 100 μm on 17-18 May to 20-40 μm from the 22 May onwards. Video-microscope observations showed that diatoms, mainly *Chaetoceros* (Fig. 6.26) and *Rhizosolenia* species, were dominant at the beginning of the cruise leg. Towards the end of the cruise, their abundance declined and smaller dinoflagellate species were becoming more evident. Near-bed mean size also decreased over time. In mid May, mean size from bottom samples on the shelf was greater than 100 μm but this decreased to less than 50 μm by the end of May (Fig. 6.25 (b)).

Two complete transects of the S line were completed during CD93B. Surface and near-bed particle size distributions along the S line are presented. The distribution for the first transect, on 21 May (Fig. 6.27) shows that larger particles were more common at the deep stations than at the upper slope both at the surface and near the bed. The upper slope and mid-slope stations had a peak at the finer end of the spectrum (~10 μm) while the deep stations were more bimodal with peaks at ~20 μm and > 100 μm. By the end of May (Fig. 6.28), the larger particles were absent, and the distribution was similar to that of the upper slope stations, with 10-20 μm being the dominant mode.

Water samples were taken at S140 several times throughout the cruise, resulting in a time series of size distribution data for this site (Fig. 6.29). The most obvious feature is the reduction in large particles as time progressed, both at the surface and at the bed. On 17 and 18 May, the surface distribution was multimodal. At the bed, the distribution was dominated by particles in the 60-100 μm and 100-200 μm size classes, especially on 17 May. A few days later, on 21 May, there was an absence of >30 μm particles in the distribution. This remained the case at the end of May, both at the surface and at the bed.

A multicorer was deployed at S700 on 18 May. On recovery, it was found that one of the samples had been obtained from a depression in the sea bed and a layer of fluff was visible at the sediment-water interface. The water above the surface of the core was siphoned off carefully and passed through the Galai particle sizer. The particle size distribution for this sample is shown in Figure 6.30 (a). The size distribution at the surface of the core was markedly different to those of near-bed water samples obtained from the CTD. The particle population in the fluff layer was dominated by particles between 100 and 600 μm, with a mean size of 223 μm. The upper size limit for the Galai particle sizer is 600 μm, so any larger particles present were not represented. There were much larger particles present at the bed-water interface than seen in the conventional CTD water samples. Sediment from the surface of the core was passed through the Galai particle sizer also (Fig. 6.30 (b)). There was a greater proportion of finer material (10-20 μm) present than was seen in the fluff layer. Although there were large particles (> 400 μm) present in the sample, they were not as dominant in the distribution as in the fluff layer. A video-microscope image obtained from the core water sample showed aggregates and fragments of diatom chains present (Fig. 6.31).

A profile of the particle size distribution at several depths in the water column was obtained at N1500 (Fig. 6.32). Water samples were taken from the CTD where bottles were fired at 5 m, 100 m, 200 m, 350 m, and near-bed on 24 May 1995. At 5 m, the distribution was dominated by particles in the 10-20 μm size classes. Fewer large (> 50 μm) particles were present than had been seen previously. At 100 m there was a greater proportion of particles larger than 20 μm present. The distribution was

more strongly bimodal than at the surface, with peaks at ~15 and 40 μm. At 200 m mean size was 16μm with a standard deviation of only 5 μm. A marked change in the distribution was seen at 350 m with a decrease in mean particle size to 7 μm, one third of the upper water column values. The standard deviation for this sample was only 1.8 μm, indicating a uniform population of fine particles. Near the bed, there was a peak at 10-20 μm and there were large particles present (>100 μm). A video-microscope image from near-bed water sample shows that fragments of diatom chains were present (Fig. 6.33)

6.5.2 Summer 95

Far fewer samples were obtained in the Summer cruise than in Spring due to concentrations of PM being too low for the particle sizer to analyse. Surface and near-bed particle size distributions for upper slope, mid-slope and lower slope locations are shown in Figure 6.34. The surface and bed distribution at the upper slope was dominated by the larger size classes. At the mid-slope, fewer larger particles were present at the surface but there was a peak in the near-bed distribution at ~100 μm. There was an absence of particles >30 μm near-bed at the deep site.
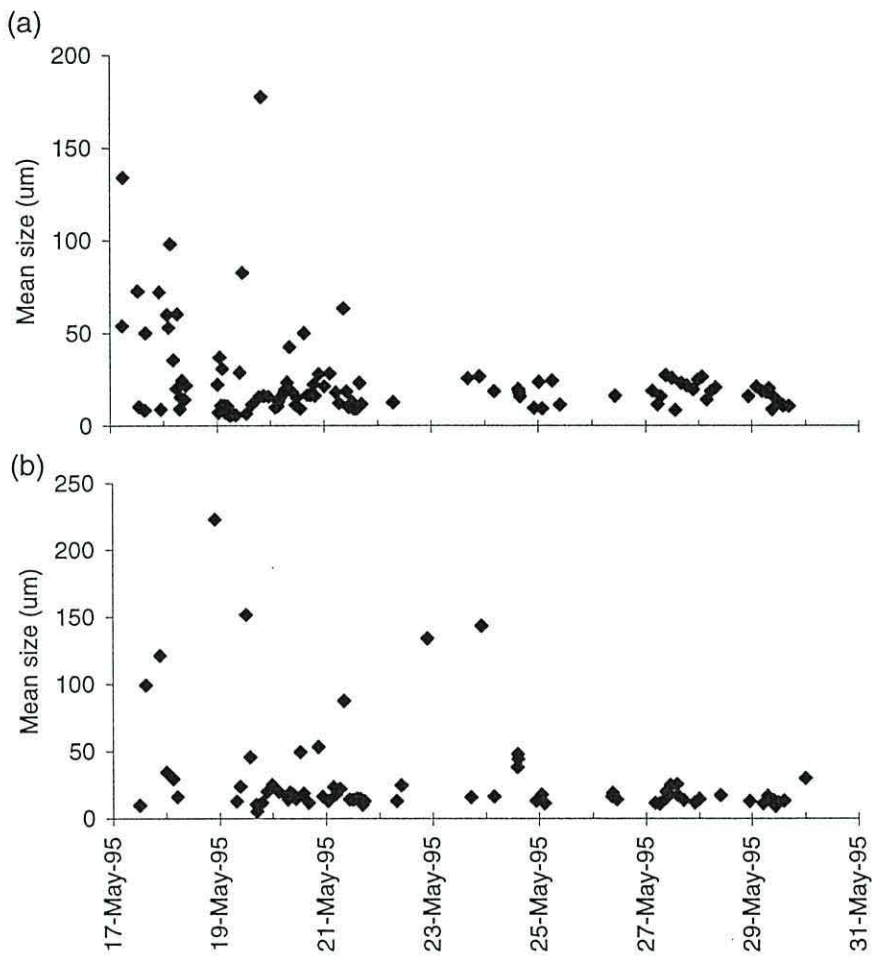
Figure 6.25: Variation in mean particle size at (a) surface and (b) near-bed in the SES box during May 1995.

Scale: ⟵——————⟶
           140 μm

Figure 6.26: Typical video-microscope image from surface water during May 1995 showing the diatom *Chaetoceros socialis*.
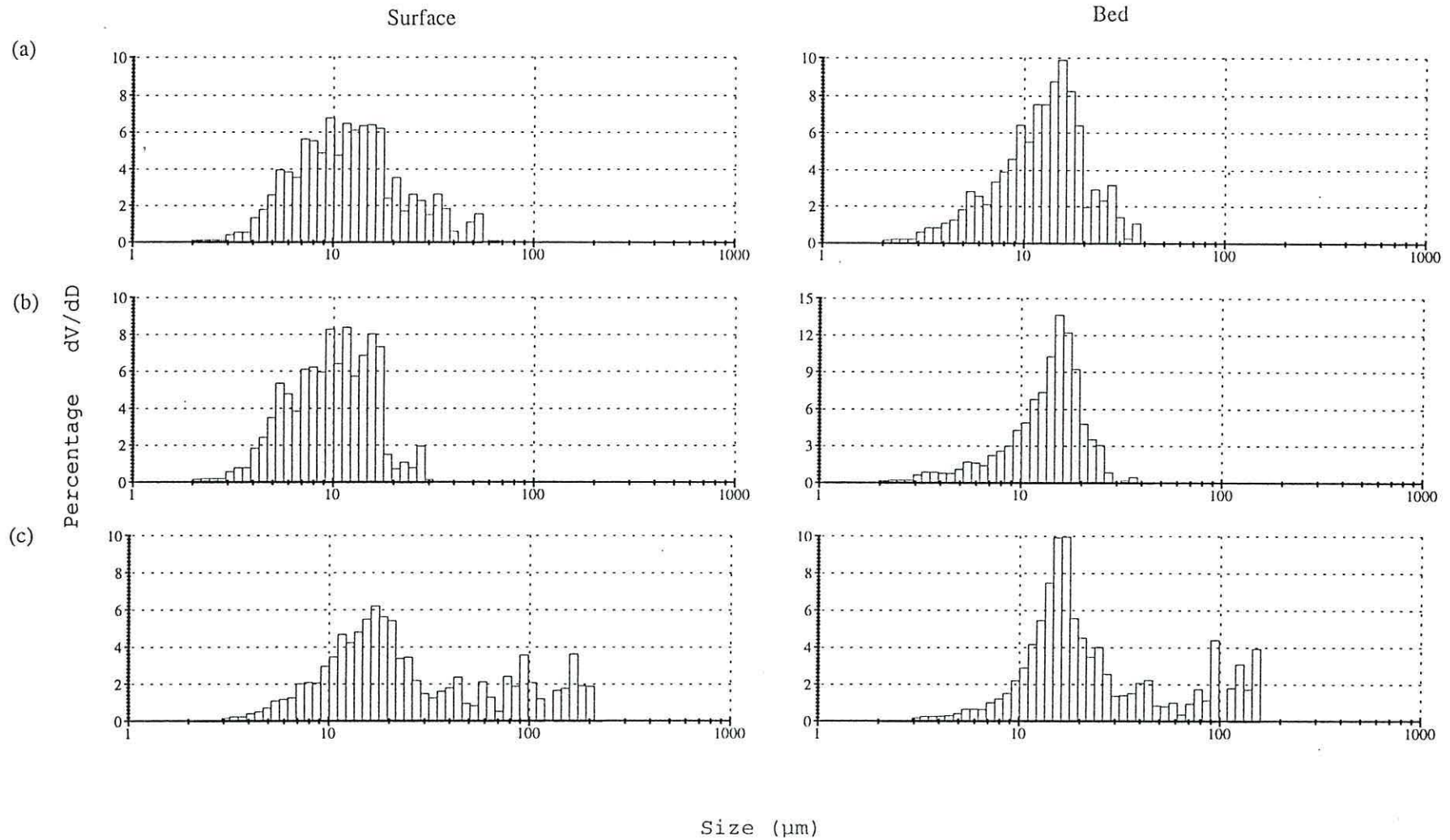
Figure 6.27: Cross-slope particle size distribution spectra along the S₁line on May 21 1995. Upper slope, mid-slope and lower slope spectra are shown in (a), (b) and (c), respectively. Graphs on the left of the page are surface spectra and on the right of the page are near-bed.
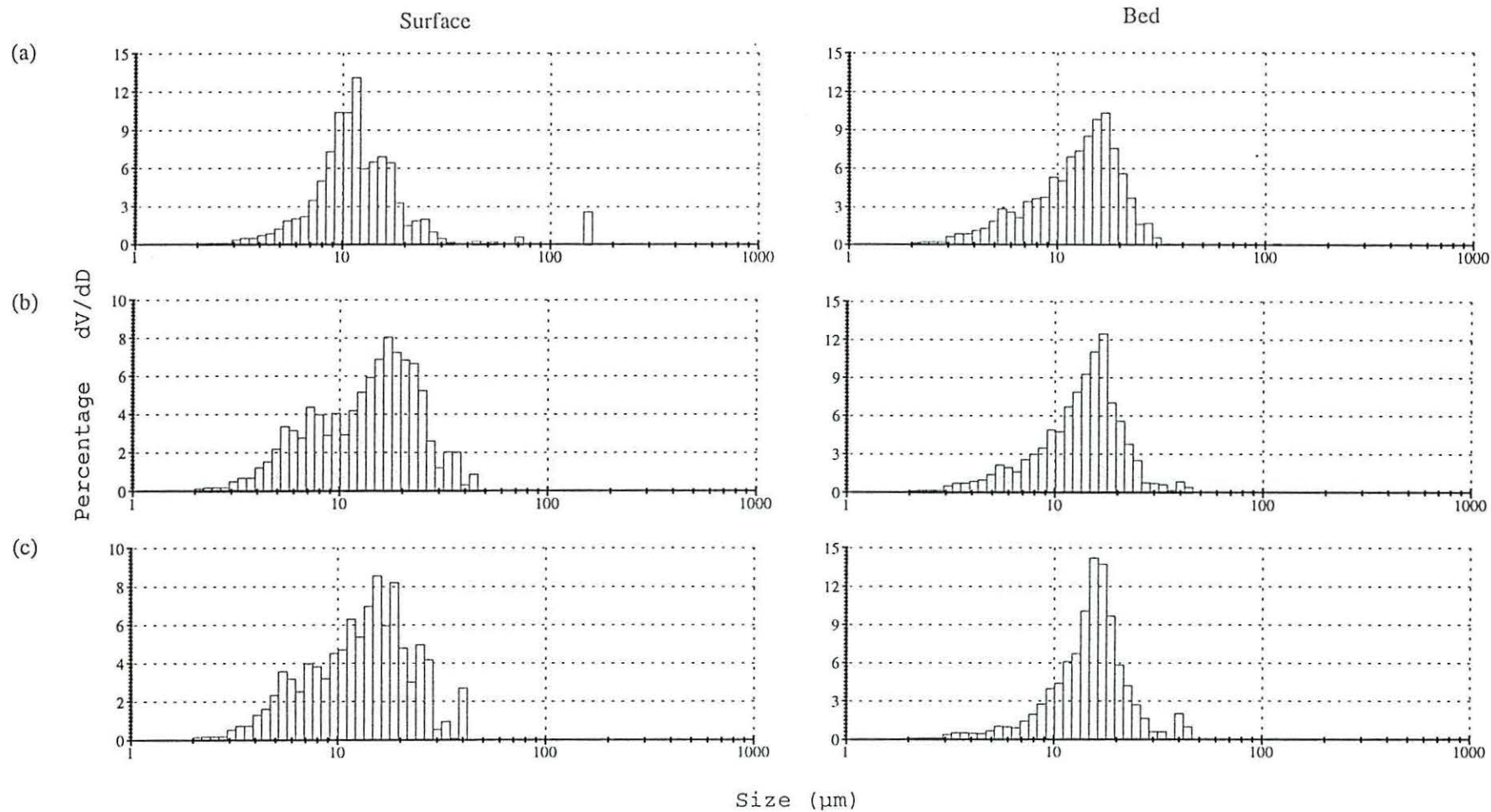
Figure 6.28: Cross-slope particle size distribution spectra along the S line on May 25-29 1995. Upper slope, mid-slope and lower slope spectra are shown in (a), (b) and (c), respectively. Graphs on the left of the page are surface spectra and on the right of the page are near-bed.
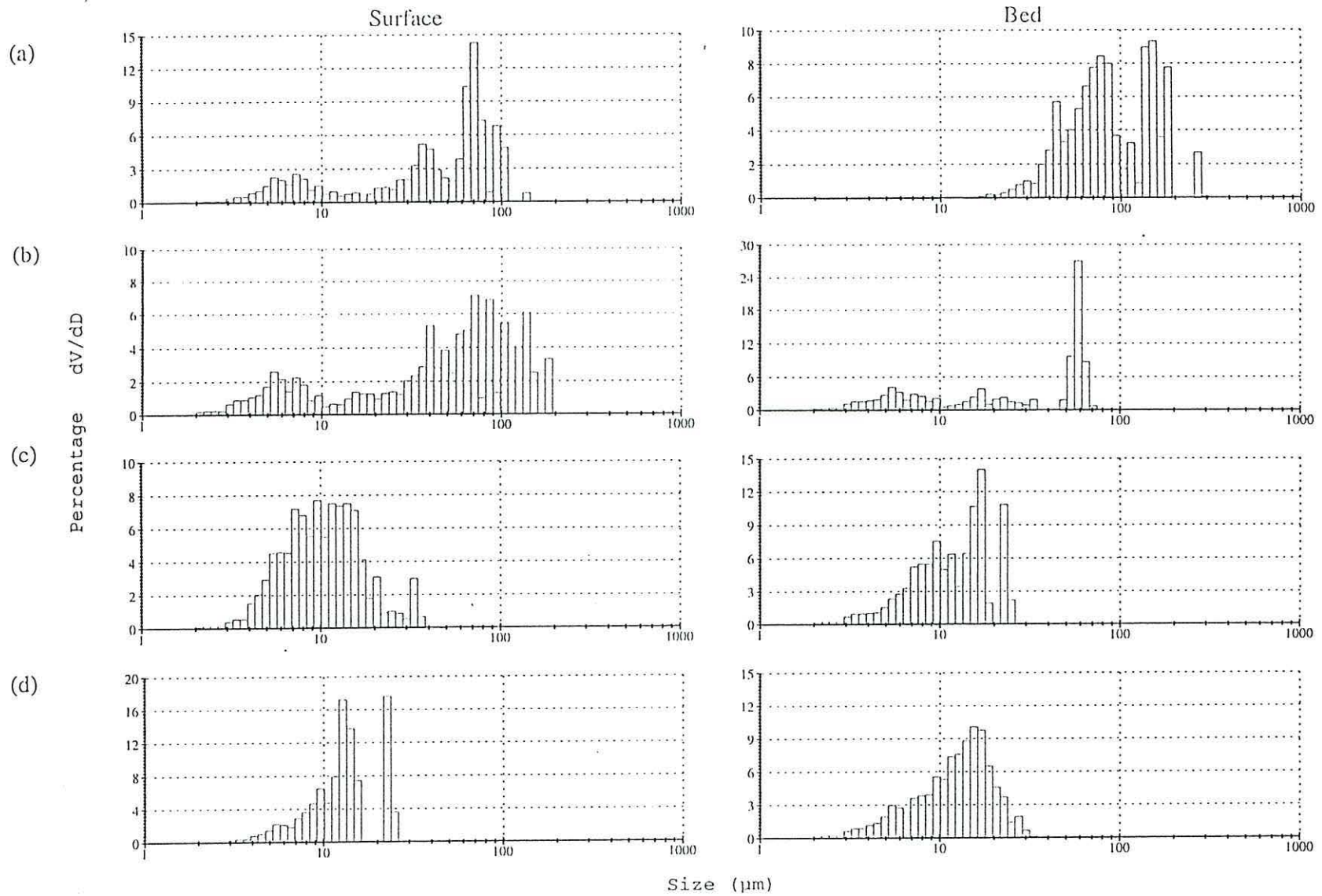
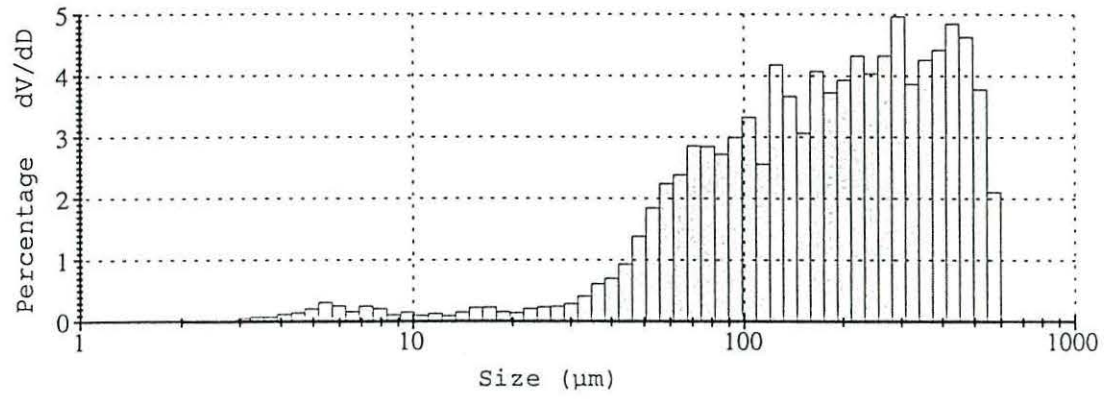Figure 6.29: Surface (left of page) and near-bed (right of page) particle size distribution spectra at S140 on (a) 17/05/95, (b) 18/05/95, (c) 21/05/95 and (d) 29/05/95.

(a)

(b)
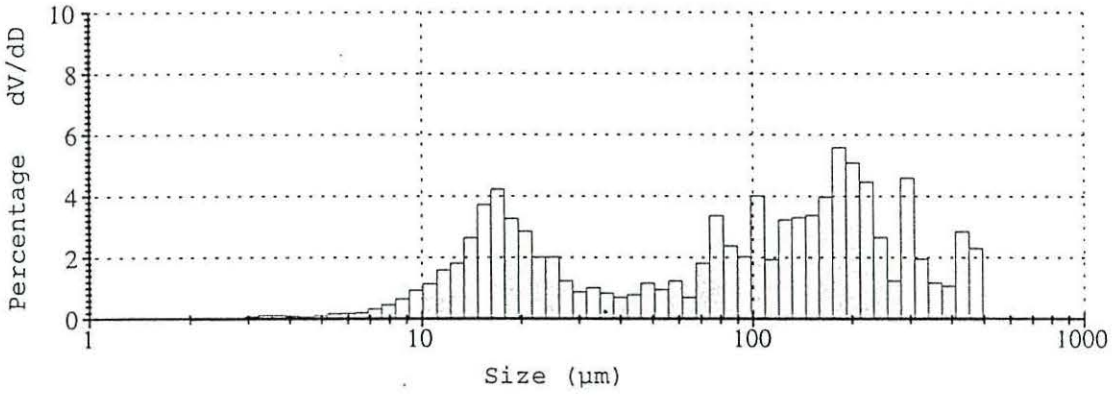
Figure 6.30: Particle size distribution spectra of (a) water siphoned from the surface of a core and (b) sediment from the surface of the core. These samples were obtained from a multicorer deployed at S700 on May 18 1995.
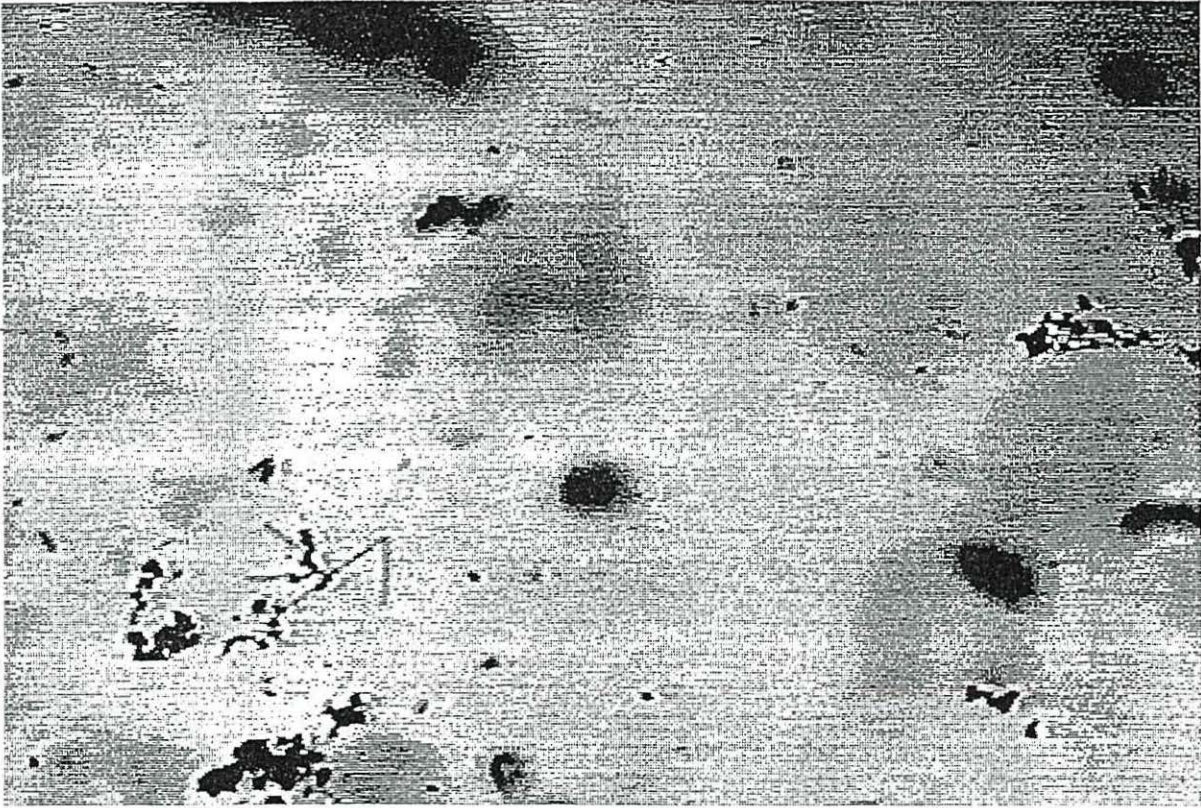
Scale: ←——————→
140 μm

Figure 6.31: Video-microscope image from a water sample containing benthic fluff found at the surface of a multicorer sample at S700 in May 1995.
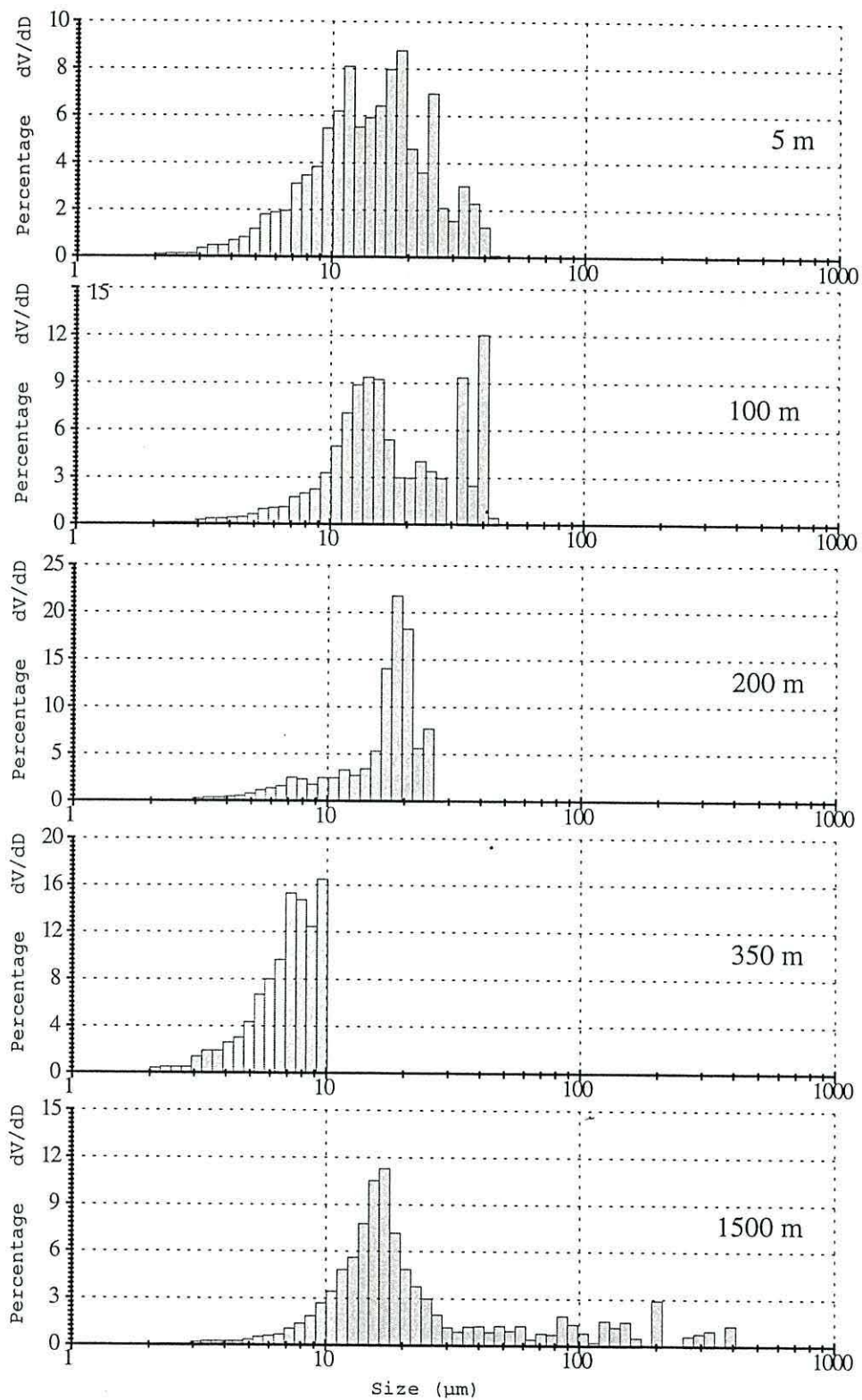
Figure 6.32: Particle size distribution spectra from samples taken at various depths in the water column at N1500 in May 1995.
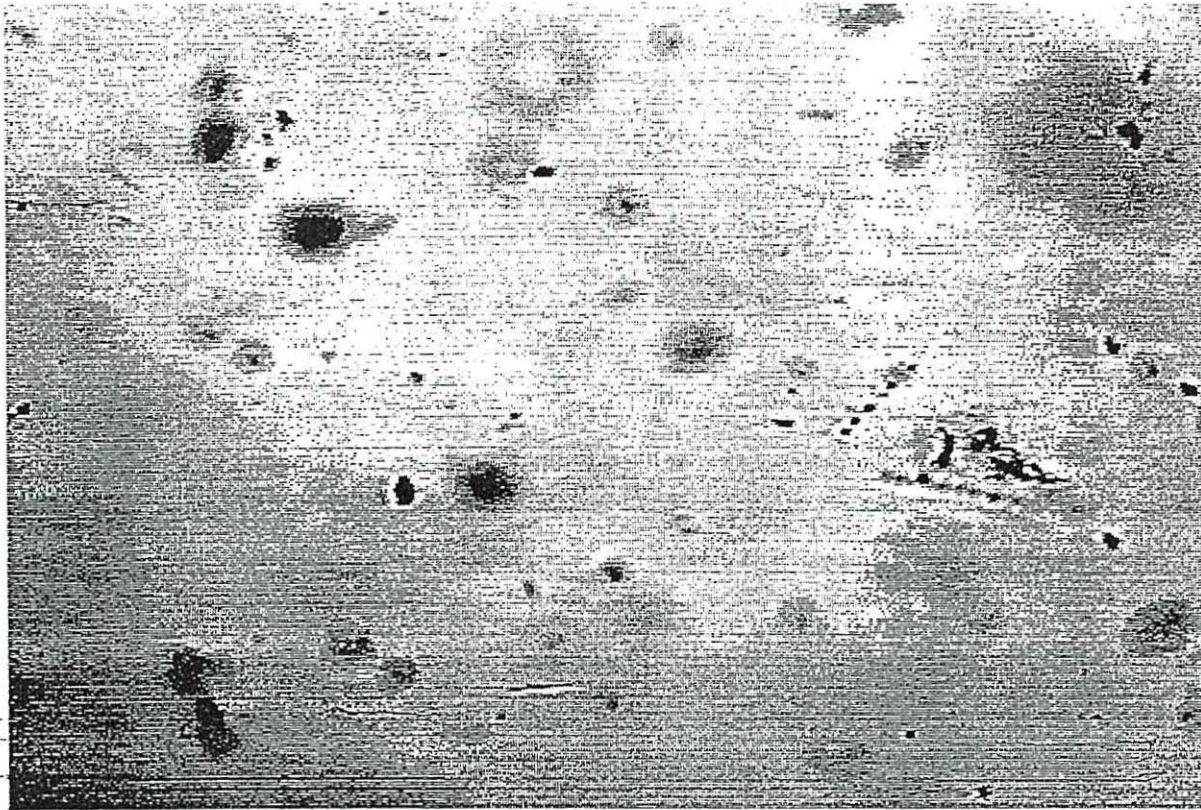
Scale: $\longleftrightarrow$

140 μm

Figure 6.33: Video-microscope image from a near-bed water sample taken at N1500 on 24 May 1995. Diatom chain fragments are visible in the centre-right area of the image.
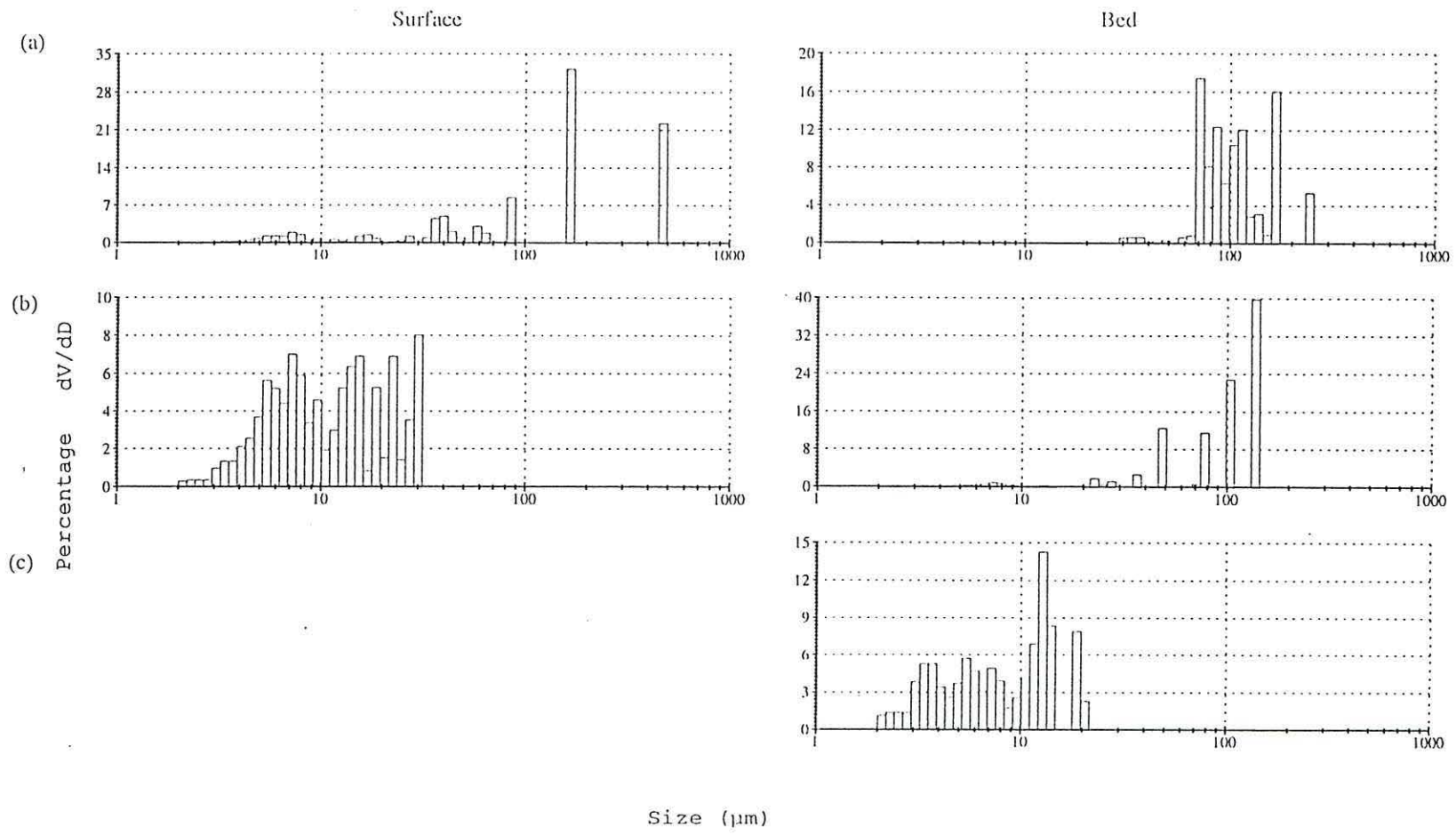
Figure 6.34: Surface (left of page) and near-bed (right of page) particle size spectra of samples taken at (a) upper slope, (b) mid-slope and (c) lower slope stations in August 1995. No surface lower slope samples were obtained.

6.6 Results summary

There was marked seasonal variation in the distribution of PM across the Hebridean shelf edge. Spring and summer were characterised by a relatively high concentration surface layer, dominated by phytoplankton. PMC was lowest throughout the water column in late Autumn. Under stormy Winter conditions, increased PMC was observed on the shelf and slope. These main features are characteristic of all four transect lines.

Maximum PMC occurred on the shelf in Winter and in late Spring/early Summer in surface and near bed layers. The predominant direction of cross-shelf residual current was off-shelf, which has implications for sediment transport. PMC increased when cross-slope currents were off-shelf, and showed little correlation with current speed. However, all of the moored transmissometers were several meters above the bed, and there may have been resuspension occurring that was not detected by the instruments.

The majority of the particle population was dominated by slowly settling material in Spring and Summer. This mode was remarkably persistent for both 1995 and 1996 samples except at S300 in 1995 and S1300 in 1996, where the mode was nine times greater. Both Spring cruises showed an increase in the more rapidly settling sub-population in samples taken towards the end of the cruises.

Despite problems with the particle sizer, especially during the summer cruise and subsequent cruises, we gained a valuable insight into the variability of particle size distributions at the shelf-break. In Spring, mean particle size decreased as the cruise progressed. Distributions in mid-May showed peaks at 10-20 μm and ~100 μm both at the surface and at the bed. At the end of the cruise, there were fewer large particles present, in general. A profile of size distribution at N1500 showed larger particles present at the surface and at the bed, and an absence of larger size classes in the mid water column region. Diatom fragments were visible in the near-bed sample. The largest particles were sampled in the fluff overlying the surface of a core. Particles up to 600 μm were measured, and fragments of phytodetritus were seen in video images obtained of this sample.

CHAPTER 7

Lateral flux calculations and harmonic analysis of PMC time series

7.1 Introduction

In Chapter 6, results from the CTD survey, moored instrument time series, and particle size and settling velocity distributions were presented. A persistent near-bed layer of PM was observed across the shelf edge. Cross-slope residual flows were predominately off-shelf, implying transport of PM down the slope. The time series of PMC and concurrent current velocity enable estimates of lateral fluxes to be made. Two methods for calculating fluxes have been compared and flux estimates are presented in section 7.2. One of the objectives of this study was to investigate the impact of tides on resuspension of PM in the SES box. Harmonic analysis was used to examine PMC time series for tidal variability. The results of this analysis are presented in section 7.3.

7.2 Calculation of lateral fluxes of PM

Simple point flux calculations were made using time series of PMC and current velocity data. If a linear relationship exists between the concentration of suspended particles and the light attenuation coefficient c, then a transmissometer integrated into a current meter is a suitable device for providing long time series of material fluxes (Krause & Ohm, 1984).

The instantaneous particle flux is related to the instantaneous values of the horizontal current velocity components ($u_{(t)}$ and $v_{(t)}$) and particle concentration ($C_{(t)}$). The instantaneous velocities and concentrations can be broken down into the mean ($\langle \ \rangle$) and fluctuating (') components (Puig et al, 2000)

$$u_{(t)} = \langle u \rangle + u' \tag{7.1a}$$

$$v_{(t)} = \langle v \rangle + v' \tag{7.1b}$$

$$C_{(t)} = \langle C \rangle + C' \tag{7.1c}$$

The instantaneous particle flux ($qu_{(t)}$ and $qv_{(t)}$) results from the product of the instantaneous concentration and instantaneous velocity. Averaging the instantaneous particle fluxes over time produces mean cross and along-slope particle fluxes given by

$$\langle q_u \rangle = \langle u_{(t)} C_{(t)} \rangle = \langle u \rangle \langle C \rangle + \langle u'C' \rangle \qquad (7.2a)$$

$$\langle q_v \rangle = \langle v_{(t)} C_{(t)} \rangle = \langle v \rangle \langle C \rangle + \langle v'C' \rangle \qquad (7.2b)$$

which have contributions from the advective ($\langle u \rangle \langle C \rangle, \langle v \rangle \langle C \rangle$) and fluctuating ($\langle u'C' \rangle, \langle v'C' \rangle$) components of the suspended particle flux (Van Rijn, 1993). Where transmissometer and current velocity measurements were available, fluxes of PM were calculated in the cross-slope and along-slope directions. PMC ($g\ m^{-3}$) was multiplied by the concurrent velocity ($m\ s^{-1}$) to give an instantaneous point flux of material ($g\ m^{-2}\ s^{-1}$).

Large gaps were present in the moored transmissometer dataset due to instrument failure or loss. However, near-bed current measurements were available, especially on the shelf, for much of the SES period. This meant that fluxes could be estimated using mean near-bed current data and mean near-bed PMC estimated from the cruises, allowing some of the gaps in the flux calculations from the mooring dataset to be filled. This would represent the advective, but not the fluctuating, particle flux. Lateral fluxes have been estimated in this way in other studies (e.g. Thomsen & van Weering, 1998).

The importance of the fluctuating flux in the SES area, across and along-slope, was investigated by plotting $\langle u_{(t)} C_{(t)} \rangle$ against $\langle u \rangle \langle C \rangle$ (Figure 7.1a), and $\langle v_{(t)} C_{(t)} \rangle$ against $\langle v \rangle \langle C \rangle$ (Figure 7.1b), respectively. There is one clear example of high fluctuating flux contribution to the mean flux, in both the along-slope and cross-slope plots: S140 in February 1996. This is explained by resuspension on the shelf in Winter, when high current velocities coincide with increased PMC. The majority of points on the graphs come from deployments in Spring and Summer, when storm resuspension is rare, so firm conclusions about the importance of the fluctuating flux at other locations on the slope cannot be drawn. It is likely that any fluxes calculated using

mean currents and mean concentrations in Winter will be underestimated. Additionally, it is possible that they will be in the wrong direction: $\langle u_{(t)} C_{(t)} \rangle$ is offshelf but $\langle u \rangle \langle C \rangle$ is onshelf for S140 in February 1996.

Near-bed mean PMC for each season was estimated from the bottom 15 m of CTD casts that went to within 10 m of the bed. The CTDs were divided into shelf (140-200 m), upper slope (300-500 m), mid-slope (700-850 m) and lower slope (1000-1500 m). CTD casts from all transects were included. Table 7.1 gives mean near-bed PMC, with standard deviation in brackets, for the seasons during the SES campaign.

Table 7.1: Mean and (standard deviation) of near-bed PM mass concentration (mg m^{-3}) estimated from CTD casts during cruises.

Season	Shelf	Upper slope	Mid slope	Lower slope
Spring 95	67.52 (30.95)	66.51 (29.70)	79.85 (39.16)	123.98 (96.84)
Autumn 95	50.94 (10.33)	50.62 (8.88)	20.06 (9.55)	21.47 (13.45)
Winter 95/96	91.28 (36.65)	67.20 (23.26)	52.55 (11.83)	55.27 (26.90)
Spring 96	115.66 (38.99)	69.63 (19.69)	69.55 (16.77)	44.99 (35.65)
Summer 96	91.37 (15.20)	78.49 (10.05)	53.88 (4.90)	65.60 (22.82)

As well as the absence of the fluctuating flux component in this method, another source of uncertainty is in the mean concentration value used in calculating the flux. Estimating mean near-bed PMC from cruises may not reflect the full situation. During Spring, for example, if near-bed PMC is estimated on the shelf before the settling of phytodetritus, an underestimation of the flux for moored instruments deployed over the full bloom period will result, since PMC will increase with input of phytodetritus to the near-bed layer.

This type of discrepancy is seen in Figure 7.2, which shows fluxes estimated from mean PMC from mooring data versus fluxes estimated using mean PMC from CTD casts. All of the points along the 1:1 line are fluxes over periods when cruises and moorings coincided. This meant that a reasonable CTD estimate of PMC was obtained, and the fluxes were similar. At times when cruises were not occurring, the CTD method significantly underestimates the flux (by as much as five-fold at N1500 in Summer 1996). What is encouraging, however, is the reasonably good agreement between the CTD and mooring fluxes where they coincide in time. This lends

confidence to the calibration of moored transmissometers into beam attenuation, described in Chapter 4. There were occasions when there were relatively large offsets between CTD and mooring beam attenuation (Chapter 4, Table 4.13). It is likely that this was due to PMC patchiness in space rather than inaccurate calibration.

While the 'CTD' flux may generally be an underestimate, it nonetheless is useful for filling in the gaps that exist where no moored transmissometer measurements are available. However, there remains a strong case for deploying transmissometers with current meters when accurate flux estimates are required. For the purposes of this study, where near-bed current velocity measurements were available, fluxes were therefore estimated from the product of mean velocity and mean PMC from the cruises, in order to complement the moored transmissometer and current meter flux measurements. It is clearly shown in the graphs (Figs. 7.3 and 7.4) which calculation method was applied.

Fluxes in the along-slope direction (Fig. 7.4) were generally 2 to 3 times greater than in the cross-slope direction (Fig. 7.3). Most of the time, the flux along-slope was towards the north, and the cross-slope component was usually off-shelf, except in Summer on the shelf and in Winter at the upper slope. Cross-shelf fluxes were greatest in Winter and Spring 1996 on the shelf, similar in Spring and Winter at the upper slope, and greater in Summer than Winter or Spring at the lower slope. Although there were large gaps in the mid and lower slope flux estimates, it seems that the greatest cross-slope fluxes occurred on the shelf and at the upper slope, decreasing in magnitude down the slope. Along-slope fluxes were similar in that the greatest fluxes on the shelf occurred in Winter and Spring, and at the upper slope in Spring. It should be noted that fluxes calculated from current velocity and mean PMC may be underestimated, especially in Winter and Spring conditions.
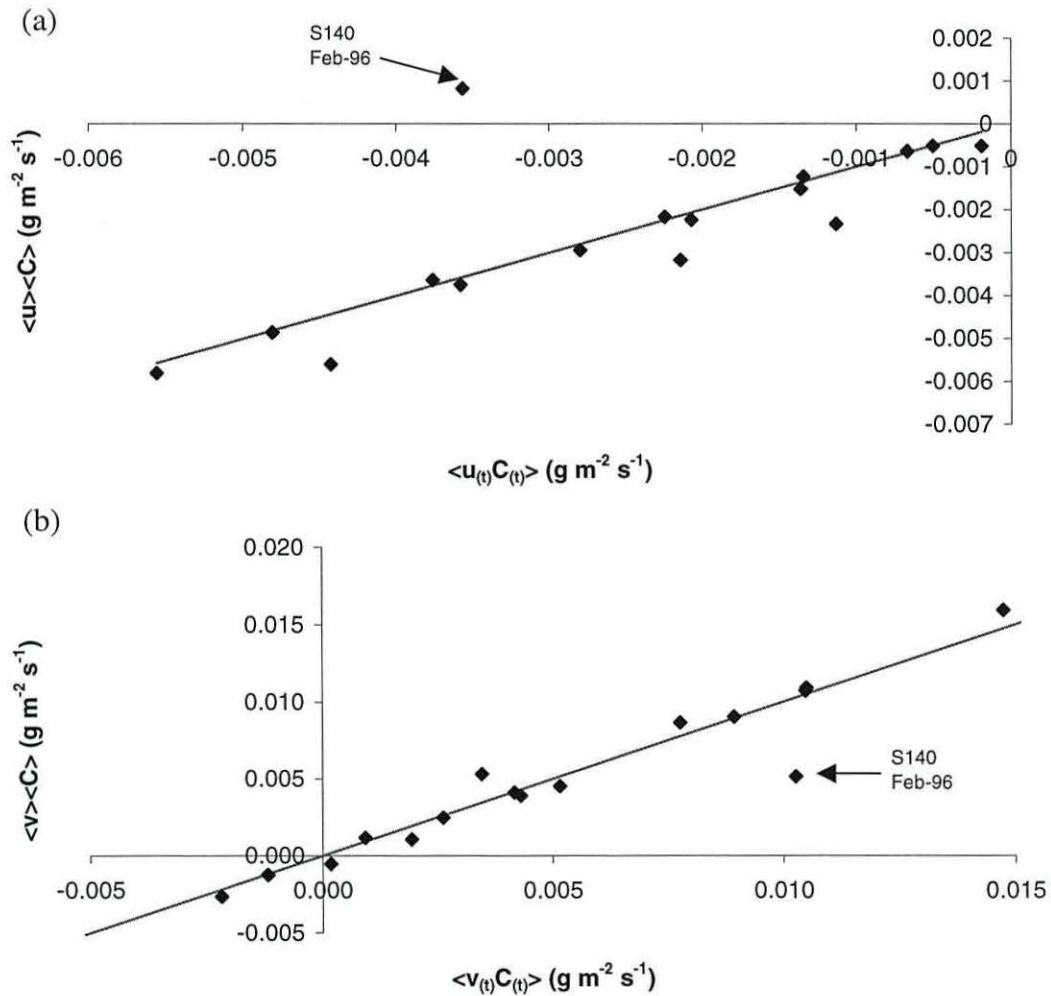
Figure 7.1: Scatter plot of mean instantaneous particle flux versus advective flux (a) across-slope and (b) along-slope. Negative fluxes indicate off-shelf and southward directions, respectively. The straight line shows a 1:1 relationship.
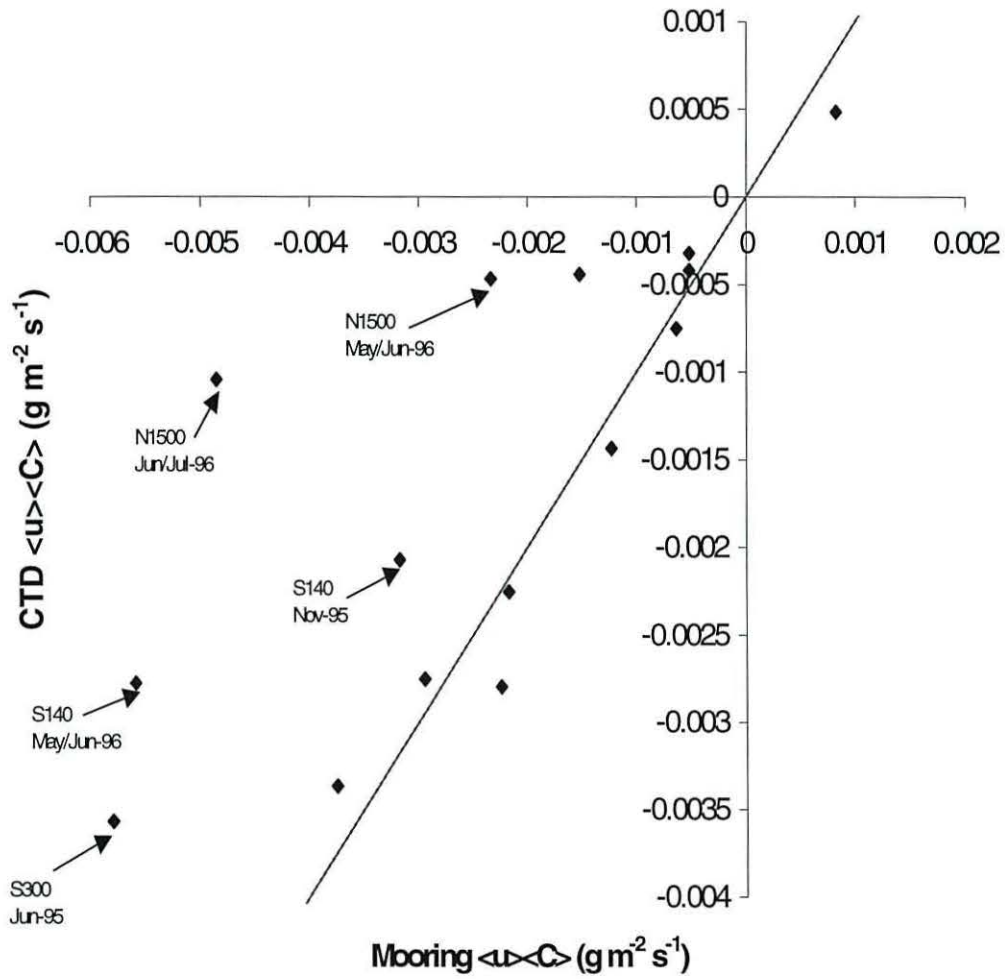
Figure 7.2: Comparison of fluxes calculated with mean PMC from moorings and mean PMC from CTD casts. The straight line shows a 1:1 relationship. Arrows point to fluxes calculated over a time period in which there were no cruises.
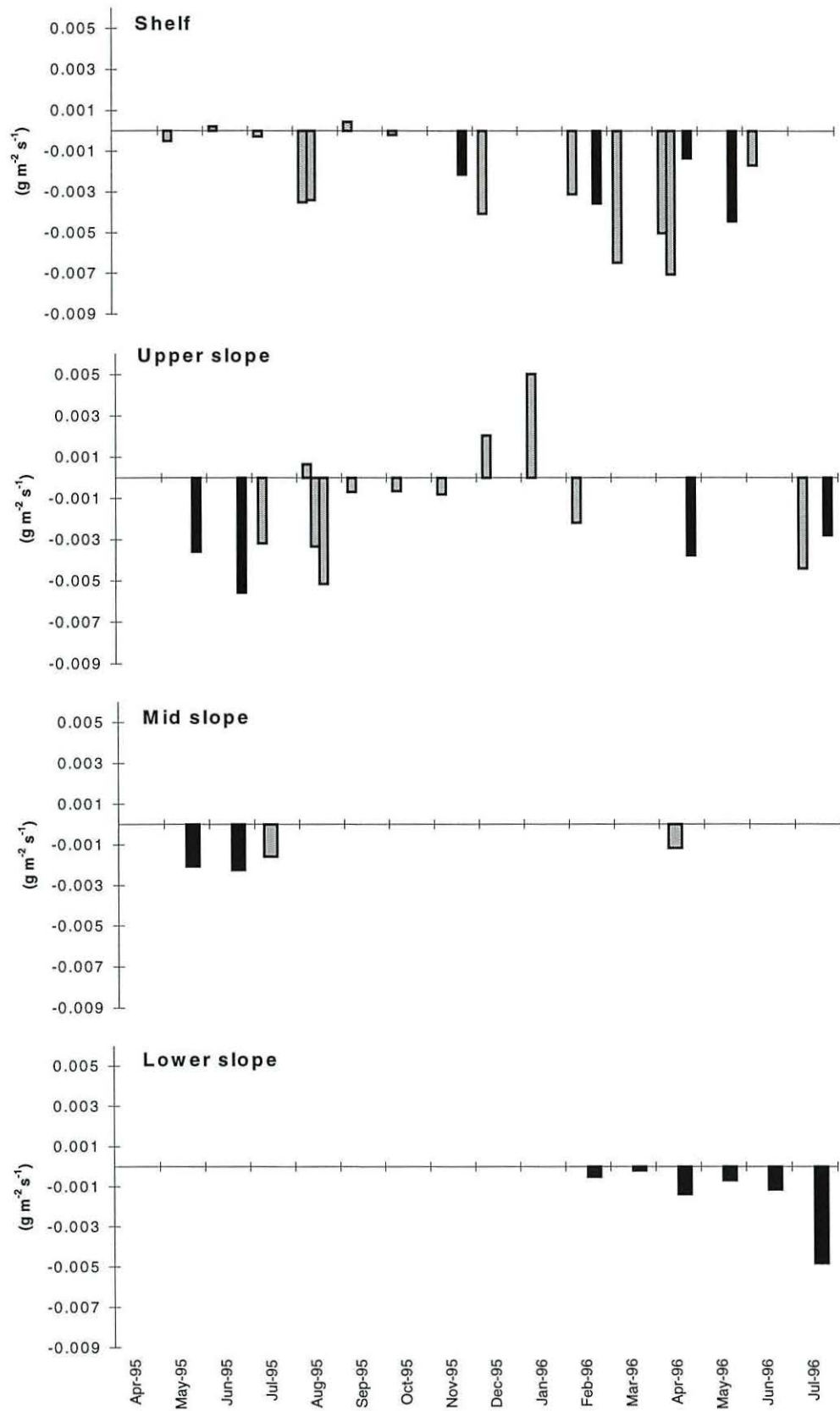
Figure 7.3: Near-bed cross-slope fluxes estimated using the 'Mooring' method (black bars), supplemented with fluxes using the 'CTD' method (grey bars) where current velocity, but not PMC, data are available. Negative values indicate off-shelf direction.
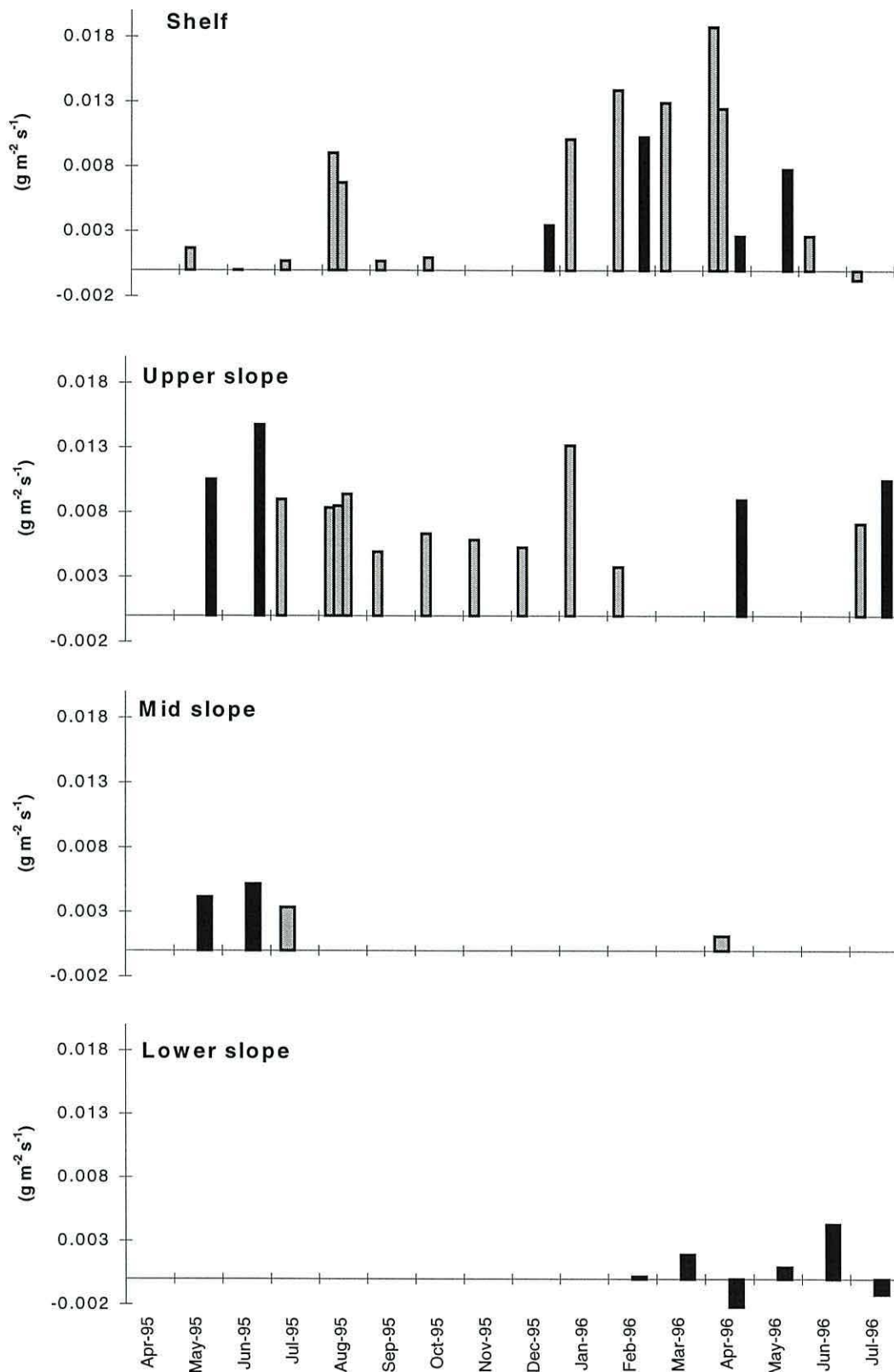
Figure 7.4: Near-bed along-slope fluxes estimated using the 'Mooring' method (black bars), supplemented with fluxes using the 'CTD' method (grey bars) where current velocity, but not PMC, data are available. Negative values indicate southward direction.

7.3 Harmonic analysis of PMC signal

Maximum currents occur during the flood and ebb phase of the tide and can induce a quarter-daily signal in PMC time series if the current maxima are causing local resuspension (Campbell, 1996). Increases in PMC at a semi-diurnal frequency indicate advection of a horizontal background sediment concentration gradient. Sediment signals with strong variation at both semi- and quarter-diurnal frequencies are termed the 'twin peaks' signal (Weeks, 1989; Campbell, 1996). A method for detecting tidal variability in PMC is harmonic analysis of the concentration time-series signal (Campbell, 1996).

A. Souza and M. Harikrishnan (University of Wales, Bangor) kindly provided the tidal analysis program used in analysis of the currents in another SES project for the harmonic analysis of PMC time-series. Pugh (1987) gives a more detailed description of harmonic analysis than is presented here. The resultant time variation of a scalar tidal parameter (e.g. surface elevation or tidal current component, Z_{tidal}) due to N constituents is expressible as (Pugh, 1987):

$$Z_{tidal}(t_i) = Z_o + \sum_{n=1}^{N} H_n f_n \cos\left[\omega_n t_i - g_n + \left(V_n + u_n\right)\right] \tag{7.3}$$

where:

Z_o	= mean value
H_n	= amplitude of the nth constituent
g_n	= phase lag of the nth constituent
N	= number of tidal constituents
ω_n	= frequency of the nth tidal constituent
t_i	= time at the ith time step
f_n	= nodal amplitude modulation of the nth constituent
u_n	= nodal phase modulation of the nth constituent
V_n	= equilibrium phase angle of the nth constituent

Given a set of M observations of the parameter Z, estimates of Z_o and the set of (H_n, g_n) may be made by fitting equation 8.1 to the observations. The fit is made by least squares such that the sum of the squares of the residuals, χ^2, is minimised:

$$\chi^2 = \sum \varepsilon^2 = \sum_{i=1}^{M} \left[Z(t_i) - Z_{tidal}(t_i) \right]^2 \qquad (7.4)$$

Six constituents were used in the harmonic analysis (Table 7.2).

Table 7.2: Tidal constituents used in harmonic analysis of the PMC time series.

Constituent	Period (hours)	Frequency ω (°/hour)
O1	25.819	13.946
K1	23.934	15.040
N2	12.658	28.442
M2	12.421	28.985
S2	12.000	30.000
M4	6.210	57.972

Harmonic analysis was carried out on all the PMC time series data during the SES campaign. The results of this analysis are shown in Table 7.3.

Table 7.3: Results of harmonic analysis of the PMC records. All records are near the bed except those with an asterisk which are located at mid-water depth. Values shown are the percentage of variance in the PMC record explained by the tidal harmonic shown in the column heading.

Site	Deployment period	M2, S2	M4	M2, S2, N2, O1, K1, M4
N1500	06/02/96-21/04/96	0.65	0.81	2.07
N1500	22/04/96-02/08/96	0.35	0.09	0.75
S140	11/08/95-31/08/95	0.16	0.14	0.70
S140	19/11/95-23/01/96	0.16	0.18	0.69
S140	01/02/96-12/03/96	0.11	0.02	0.50
S140	17/04/96-23/06/96	0.39	0.16	0.63
S300	09/05/95-17/05/95	12.35	N/A	18.66
S300	09/05/95-14/07/95	1.54	0.01	3.57
S300	19/04/96-10/05/96	0.83	0.01	2.14
S300	11/07/96-28/07/96	1.81	0.08	8.75
S700	29/03/95-28/04/95	0.02	0.01	0.40
S700	11/05/95-04/08/95	1.32	0.22	2.00
S700	13/08/95-06/09/95	0.61	N/A	1.75
S700	18/04/96-09/05/96	1.42	0.04	4.04
S140	01/02/96-16/03/96	0.55	N/A	1.15
S140	23/04/96-11/05/96	0.94	N/A	5.58
S200	17/04/95-09/05/95	0.06	N/A	0.74
S200	10/05/95-28/05/95	4.88	N/A	6.83
S140	15/05/95-24/07/95	0.32	N/A	1.88
S700	15/04/96-19/05/96	0.14	N/A	2.40

The shelf station (S140) showed very little evidence of tidal effects in the signal near the bed, possibly because this is a region of consistently strong currents and there is evidence from photographs of armouring at the sea-bed (J. Humphery, 1998). The

upper-slope station (S300) showed the greatest association with tidal signals, especially at the mid-water transmissometer at S300 in Spring 1995. The other records at this station showed much lower degrees of association but these were still greater than at the other sites.

There was a decrease down the slope in the variability explained by tidal harmonics, with the maximum occurring at the upper slope and the minimum occurring on the shelf. In all records, very little (< 1%) of the variation in the concentration signal was due to the M4 harmonic.

7.4 Summary

PM flux calculations have shown that there was a significant proportion of material exported across the shelf break down the slope. The along-slope flux was 2-3 times greater than the cross-slope flux due to the strong residual northward flow in the slope current. Greatest fluxes occurred during Winter and Spring on the shelf and upper slope.

Harmonic analysis has shown that tidal resuspension in the SES box was negligible, with less than 1% of the variability in the concentration time series signal being explained in this way. However, as previously mentioned, the transmissometers were located at least seven metres away from the bed so it is possible that some resuspension was occurring below them that has not been detected. There was also little variation in the near-bed signal at the M2 frequency, indicating horizontal uniformity in the near bed concentration distribution.

CHAPTER 8

Discussion

8.1 Introduction

In the last decade, awareness has emerged of the importance of continental margins in the exchange of water and particulate matter between shelf sea and oceanic regimes. There is a strong need to study continental margins as they are domains highly active in the carbon cycle, whether in terms of production or storage (Walsh, 1988), and play an important role in the cycling of many other elements or compounds (Walsh, 1988). The increasingly important role of PM in the determination of water quality and the fate of pollutants has been recognised in recent years (Tett *et al*, 1993; Eisma and Irion, 1988), and has been a prime motivation for scientists seeking to understand the processes responsible for the spatial and temporal distribution of PM at the continental shelf. The Shelf Edge Study of LOIS has been concerned with understanding the processes operating in the critical boundary region between the deep ocean and shelf sea regimes. This thesis is more specifically aimed at examining the distribution and transport paths of particulate material at the shelf edge.

In Chapter 6, all the results obtained during the SES campaign in relation to this project were presented in the form of spatial distribution plots of PMC, time series of PMC and currents, and PM characterisation by size and settling velocity. Chapter 7 presented the results of point flux calculations, in order to estimate the magnitude of lateral transport of material, and harmonic analysis of the time series that showed resuspension due to tidal currents was negligible at the location of the moored transmissometers (7 metres above the bed) at the Hebridean slope. This chapter draws together the main results and discusses them in an attempt to present a coherent view of PM distribution and dynamics at this shelf break system.

8.2 Variability in PM distribution

Evidence of variability in PMC and distribution, both in space (horizontal and vertical) and time, emerged from the water column survey results. The vertical distribution of PM at the Hebridean shelf edge is characterised by a three-layered system, with relatively high suspended matter concentrations in the surface and bottom waters and less turbid water in between. Particle concentrations increase shelf-wards. This is typical of many shelf breaks (Baker & Hickey, 1986; Dickson & McCave, 1986; Churchill *et al*, 1988; Monaco *et al*, 1990a; Churchill *et al*, 1994; Trowbridge *et al*, 1994).

High concentrations in the surface waters, when not caused by advection from a shoreward source, are caused by phytoplankton growth once increased solar heating in the Spring allows stratification to develop. Within the surface layer nutrients are rapidly depleted by growing plankton, and a deeper layer is formed where organic particles settle downwards and carpet the sea bed with a fluffy layer. The layer at the bed is kept in intermittent suspension by the relatively strong currents and is transported down the slope by residual cross-slope currents. Lampitt (1985) observed that currents as weak as 7 cm s^{-1} were sufficient to keep the fluffy organic material in suspension, i.e. keep it from being deposited and consolidated into the sediment.

The cross-slope contour plots of PMC and chlorophyll concentration (Chapter 6, Figs. 6.1 and 6.2) showed that in Spring and Summer, the particle population was dominated by biogenic material. This was evident in the surface layer, and at times, near the bed down the slope. The presence of a near-bed tongue of high concentration suggests there is downslope seaward transport of particles that have settled through the water column on the shelf and not been incorporated into the sediments. The persistent off-shelf residual flow, observed in the moored velocity measurements, supports this explanation. An additional source of PM to the near-bed layer is the resuspension of bed material under strong flow conditions. On the outer shelf, episodic periods of high bottom stress caused by storms can lead to resuspension of bed material. The resuspended material can move farther off-shore along the density surfaces in an intermediate nepheloid layer, as well as down the slope in a benthic nepheloid layer. This has been observed on the western Atlantic shelf, off Cape Cod

(Churchill *et al*, 1988) and along the margin at the Gulf of Lions in the north western Mediterranean (Durrieu de Madron *et al*, 1990).

There was evidence that shelf-wide resuspension in the SES region occurred after the February 1996 storm (Chapter 6, Fig. 6.1 CH125 sections). This is discussed in more detail in section 8.3. Particle concentration over the shelf increased between legs A and B of the cruise, with PMC increasing shorewards. A plume of more turbid water extended out over the shelf break in a surface layer approximately 100-150 m deep. A likely explanation for this is advection of water, containing resuspended matter from the shelf, out over the slope.

A feature in the concentration distribution not common to all shelf breaks was the core of higher concentration water located close to the 400 m isobath, adjacent to the slope. The maximum in PMC was associated with the slope current and coincided spatially with the salinity maximum (Chapter 6, Fig. 6.4) but not with the velocity maximum reported by Harikrishnan (1998) (Figure 8.1). He reported the velocity maximum to occur further away from the slope. The reason for this is that the slope bed effectively acts as a sink for velocity as it will lose energy through friction and thus the velocity maximum will be displaced away from the slope bed. Properties such as PM and salinity are not dissipated in this manner and therefore attain maxima at the boundary, provided PM is not deposited on the bed.
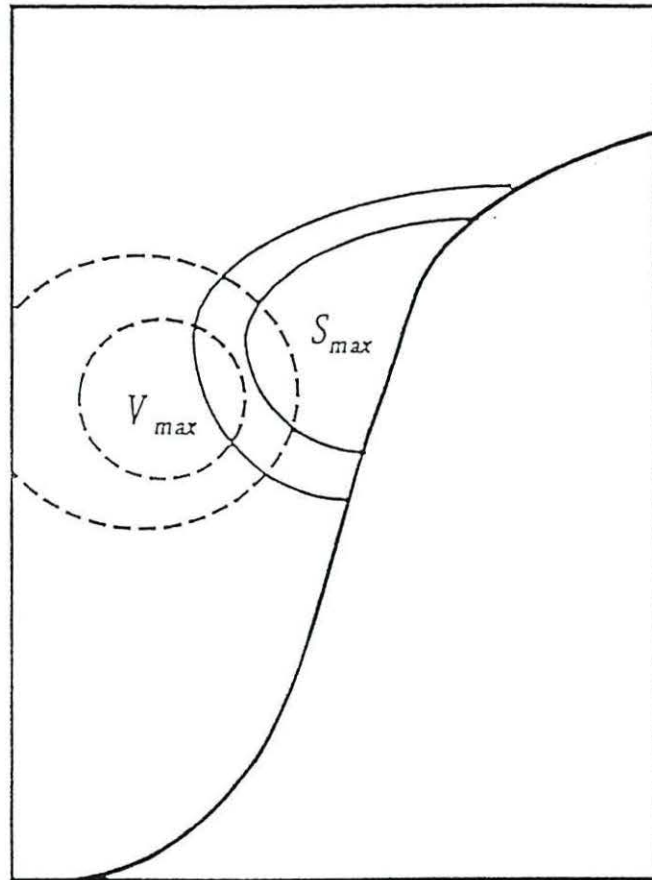
Figure 8.1: Schematic of slope current and salinity anomaly showing the different positions of velocity (V) and salinity (S) maxima across the slope (from Harikrishnan, 1998).

8.3 Resuspension of sediment

Examination of transmissometer and current meter time series revealed no significant correlation between PMC and current speed. Indeed, some of the highest concentrations occurred while speeds were low, and vice versa. Harmonic analysis of PMC time series was also performed and this confirmed that local resuspension due to tidal currents was negligible at the Hebridean slope. There was also no evidence of significant resuspension in response to internal waves propagating onto the shelf, although mooring data were sparse for the summer period when internal wave activity was strongest. The presence of a diverse benthic community on the slope in Spring and Summer (Humphery *et al*, 1998) may alter recently arrived sediment and make it less resuspendable.

However, there was strong evidence that energetic Winter weather conditions induced resuspension. Atlantic low pressure systems frequently cross the SES area in Winter. The cruise in February 1996 highlighted the contrast between Autumn conditions, where the lack of stormy weather resulted in a very clear water column with low concentrations of material present, and the Winter scenario, where more energetic conditions induced resuspension on the shelf and over the slope. The ship-board survey in February obtained pre and post-storm water column data. Heavy swell conditions made it impossible to deploy instruments for direct measurements during the event. Moored instruments, however, are ideally suited to observe the response of variables at the height of the forcing. The ship-board survey complemented moored instrument data obtained during a storm event in February 1996. The Proudman Oceanographic Laboratory Sediment Transport and Boundary Layer Equipment (STABLE) was also in the SES box during this time at S200, providing shear velocity and acoustic backscatter data for another SES project.

Meteorological data were obtained from a buoy located at 57 ° N 10 ° W. Figure 8.2 shows the wind, wave height and atmospheric pressure time series for the months of January and February 1996. January was a month dominated by moderate gales but February is more notable as much larger swell conditions occurred in response to strong winds. The particular storm that will be discussed occurred between 14 and 20 February. During the event, atmospheric pressure dropped by 40 mb and wind speed

increased to 18 m s^{-1} until it ceased to record on 16 February. The assumption has been made that wind speed reached storm force (28-33 m s^{-1}) as the maximum wave height (approximately 14 m) corresponds with winds of this magnitude, according to the Beaufort scale (Harvey 1982). This was the biggest storm during the SES campaign, and one for which we obtained moored instrument data along with pre and post-storm CTD surveys.

Individual CTD profiles of PMC at stations (N140 to N1500) along the N line before and after the storm are shown in Figure 8.3. The water column on the shelf was fully mixed and had higher concentrations of material than the adjacent slope water. A CTD section taken after the storm showed much higher concentrations present on the shelf and there appeared to be advection of material seaward out over the slope.

There was a well developed benthic nepheloid layer from N700 to N1500, with a local concentration maximum at N1150. This layer was approximately 100 m thick at N700, and 200 m thick at N1500. An intermediate nepheloid layer (INL), located around the 750 m isobath, was present at the 1000 m and 1150 m stations. It appeared to originate in the bottom nepheloid layer further upslope and spread along the constant density surfaces over the slope. The offshore INL at 1000 m and 1150 m stations is shown to lie along the same density surface (σ_t = 27.39-27.44 kg m^{-3}) as the bottom layer further inshore (Figure 8.4). Steps in the density profiles corresponded with PMC inversions (Figure 8.5). Concentrations of material in the intermediate layer were similar to the benthic layer, indicating that this was recently resuspended material. The nepheloid layers in the pre-storm survey were less prominent, but indicate that resuspension and advection of resuspended material was occurring before this storm.

Intermediate nepheloid layers have been observed previously at the north-west European continental slope. Dickson and McCave (1986) reported INLs in the Summer centred around 600 m which appeared to originate from bottom layers closer inshore at the west slope of Porcupine Bank. The conditions supporting genesis of INLs off Porcupine Bank are northerly winds which drive the integrated Ekman transport offshore and cause colder water from the deeper levels on the slope to rise

to replace it (Dickson and McCave, 1986). Resuspended material flows out along the density surface to form INLs further offshore. There may have been a period of northerly winds as the depression moved away from the SES box but the malfunction of the wind instrument on the meteorological buoy resulted in a lack of wind data for this time period. The temperature sections during CH125B showed no evidence of an uptilt of isotherms at the slope.

The formation of intermediate nepheloid layers in response to storms is well documented. On the Washington shelf, surface wave and current stresses resuspend sediment that is then advected along shelf as a bottom nepheloid layer (Hickey *et al*, 1986). This layer becomes an intermediate depth nepheloid layer where it passes over the heads of submarine canyons or where it diffuses seaward over the continental slope (Baker & Hickey, 1986).

In addition to pre and post-storm CTD surveys, moored instruments provided data during the storm itself and indicated that even more dramatic changes occurred over shorter timescales. Three transmissometers, one surface (S140) and two near-bed with integrated current meters (S140, N1500), were moored in the SES box during the storm. Time series of PMC and current velocity at S140 are shown in Figure 8.6. There was a similar pattern in surface and near-bed PMC, showing an increase between February 16 and 19. Near-bed concentrations were slightly higher than at the surface, reaching a maximum of approximately 250 mg m^{-3} on 16-17 February. This coincided with a maximum in shear velocity (0.05 m s^{-1}) and acoustic backscatter measured by STABLE (Gatehouse and Huthnance, 1997)). This was also when surface wave height was at a maximum. Current speeds reached 30 cm s^{-1} during the increase in PMC but reached 50 cm s^{-1} a few days later, with no apparent increase in particle concentration, however the source of resuspendable material may have been limited.

A significant increase in PMC occurred at N1500 on 21 and 22 February, from approximately 50 mg m^{-3} to 450 mg m^{-3} (Figure 8.7). The event lasted for 18 hours after which concentration decreased as rapidly as it had increased. The temperature record was very variable at this time. When flow was from the north, there were

sharp drops in temperature by 0.5 °C. Current speeds at N1500 were of the order of 35 cm s^{-1} before the event. The increase in concentration occurred while current speed decreased to approximately 2 cm s^{-1} and temperature dropped by 0.75 °C.

Richardson *et* al (1993) observed increases in concentration that occurred with decreases in speed in the Argentine Basin. They postulated that the relationship between particle concentration and velocity could be explained by rapid local changes in the mixed layer height. Specifically, the proposed mechanism requires the mixed layer height to increase rather rapidly just as the maximum velocity is approached, then for the mixed layer height to decrease rapidly just after the maximum velocity is reached and begins to decrease. As maximum velocity is approached, the load of resuspended sediment must be distributed throughout a thicker layer yielding a lower average concentration for the mixed layer. When the current decelerates, the mixed layer thickness decreases, isolating particles above the mixed layer. Because of reduced turbulence, the resuspended particles settle into a thinner mixed layer yielding a higher average concentration for the mixed layer. The rate at which this happens is a function of particle settling velocity and mixed layer thickness. With this mechanism, one would expect to see a decrease in concentration with maximum velocity and an increase with minimum velocity. In this case we see the latter but not the former, indicating some other process was responsible.

The fact that the increase in PMC corresponded with a sharp reduction in current speed, combined with its abrupt subsequent decrease, indicates that the signal could not have been caused by local resuspension followed by gradual settling. Asymmetry in the peak, i.e. rapid increase followed by a gradual decrease as particles settle out of the water column, is indicative of local resuspension (Gross & Williams, 1991). The sudden decrease in concentration indicates that this was an advection event and not local resuspension. The change in temperature associated with the change in concentration also indicates advective processes.

Concentrations observed at the N1500 mooring on February 20 were similar to those measured in the benthic nepheloid layer during the CTD casts. Clearly, there was a flow event that occurred after the CTD casts, which caused resuspension of material

that was advected past the mooring at N1500. An ADCP at S400 recorded a sudden sharp pulse in velocity from 10 to 50 cm s^{-1}, with a duration of 5 hours. It may have caused resuspension of material on the slope. This material could then be advected down the slope past the N1500 mooring. Residual cross-slope velocities from the current meter at the N1500 mooring were of the order of 5 km day^{-1} at this time and were sufficient to explain the event

It is clear from the CTD casts that energetic near-bed events on the slope cause resuspension of material in winter. This was evident from the CTD profiles with weak nepheloid layers before the main storm. The layers had higher concentrations after the storm. However, the CTD survey must have narrowly missed a high concentration layer, which was generated by a sudden surge in current speed on the slope. This caused resuspension of material giving concentrations nearly five times greater than those observed immediately after the storm.

In summary, storms causing shelf-wide resuspension occur intermittently on the Hebridean shelf in Winter. This resuspended material may be advected out over the slope where some will settle out and some will be transported down the slope and out of the SES box. Storms are the major agent influencing off shelf export of material in winter. The effect of storms decreases with depth across the slope. The greatest effect was observed at S140, where fluxes were of the same magnitude as those observed post-bloom in Spring. However, fluxes due to storms are of shorter duration, i.e. of the order of days compared with those enhanced by bloom detritus, which are of the order of weeks.
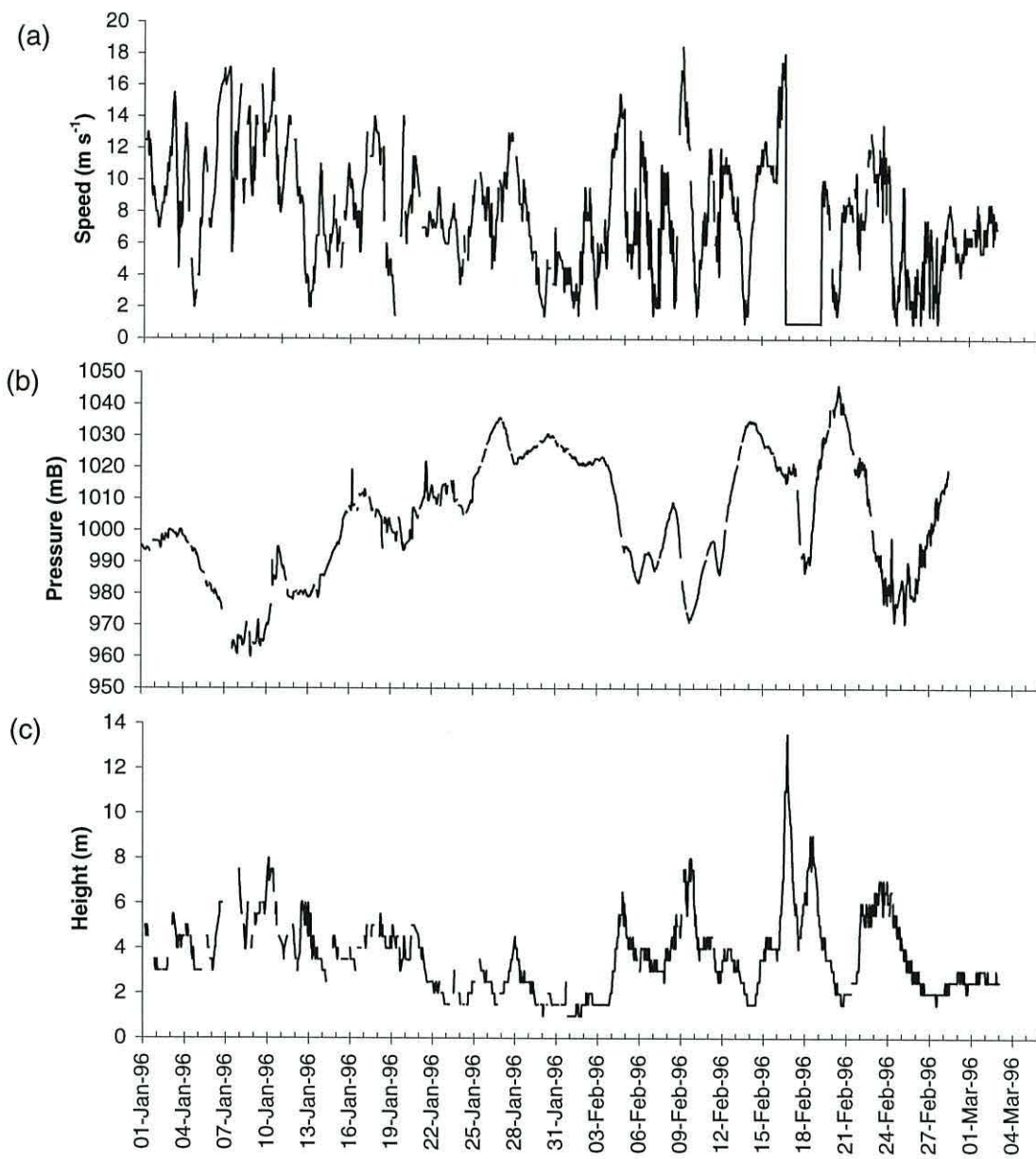
Figure 8.2: Time series of (a) wind speed, (b) atmospheric pressure and (c) surface wave height measured by a meteorological buoy located close to the SES box at 57° N, 10° W in January and February 1996.
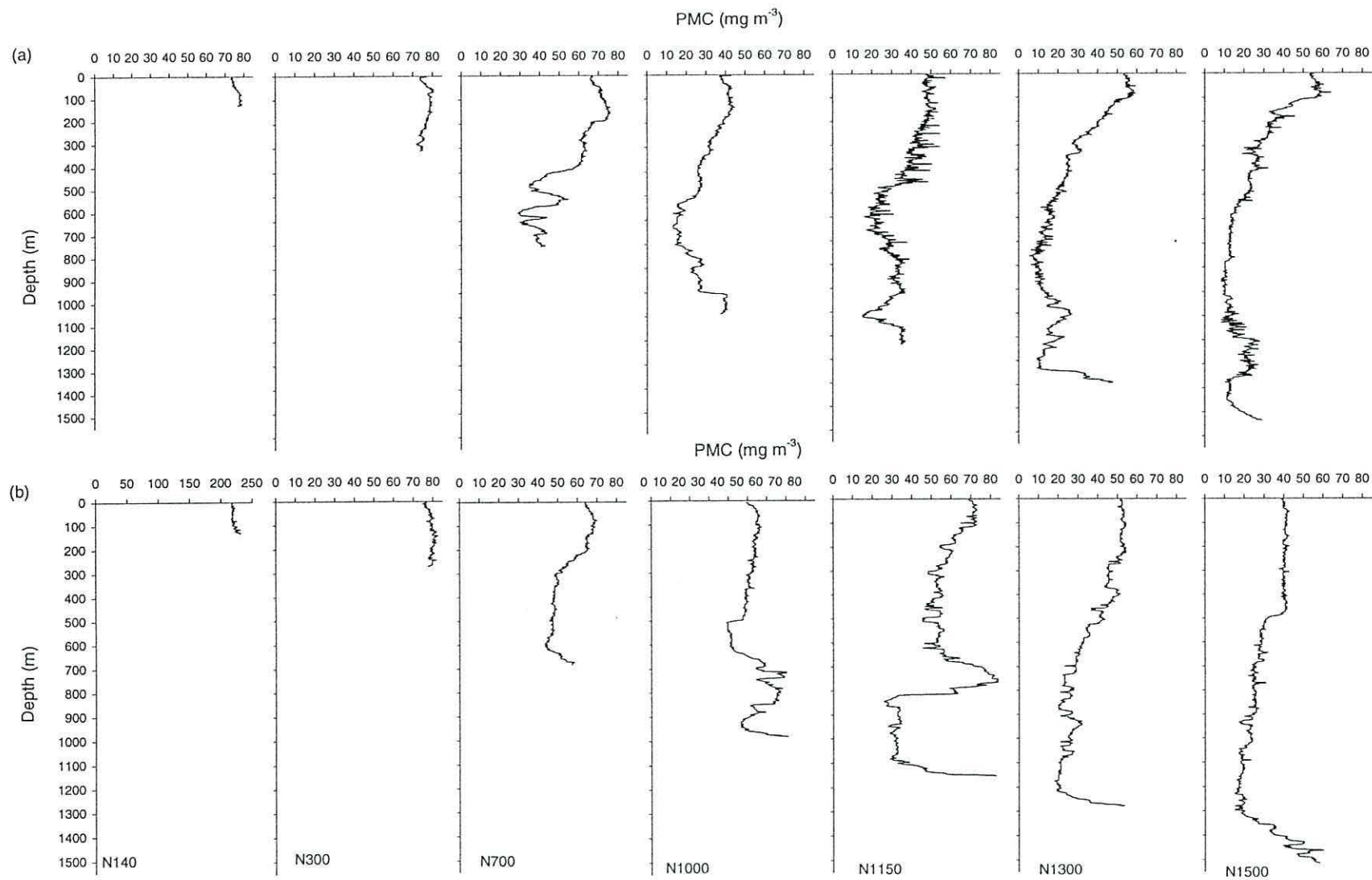
Figure 8.3: Profiles of particulate matter concentration along the N line in February 1996. Graphs in groups (a) and (b) show concentrations across the slope before and after the storm, respectively. Note the x-axis scale on the N140 graph in group (b) is different to the rest of the graphs. There is an intermediate nepheloid layer visible at 600-800 m at N100 and N1150.
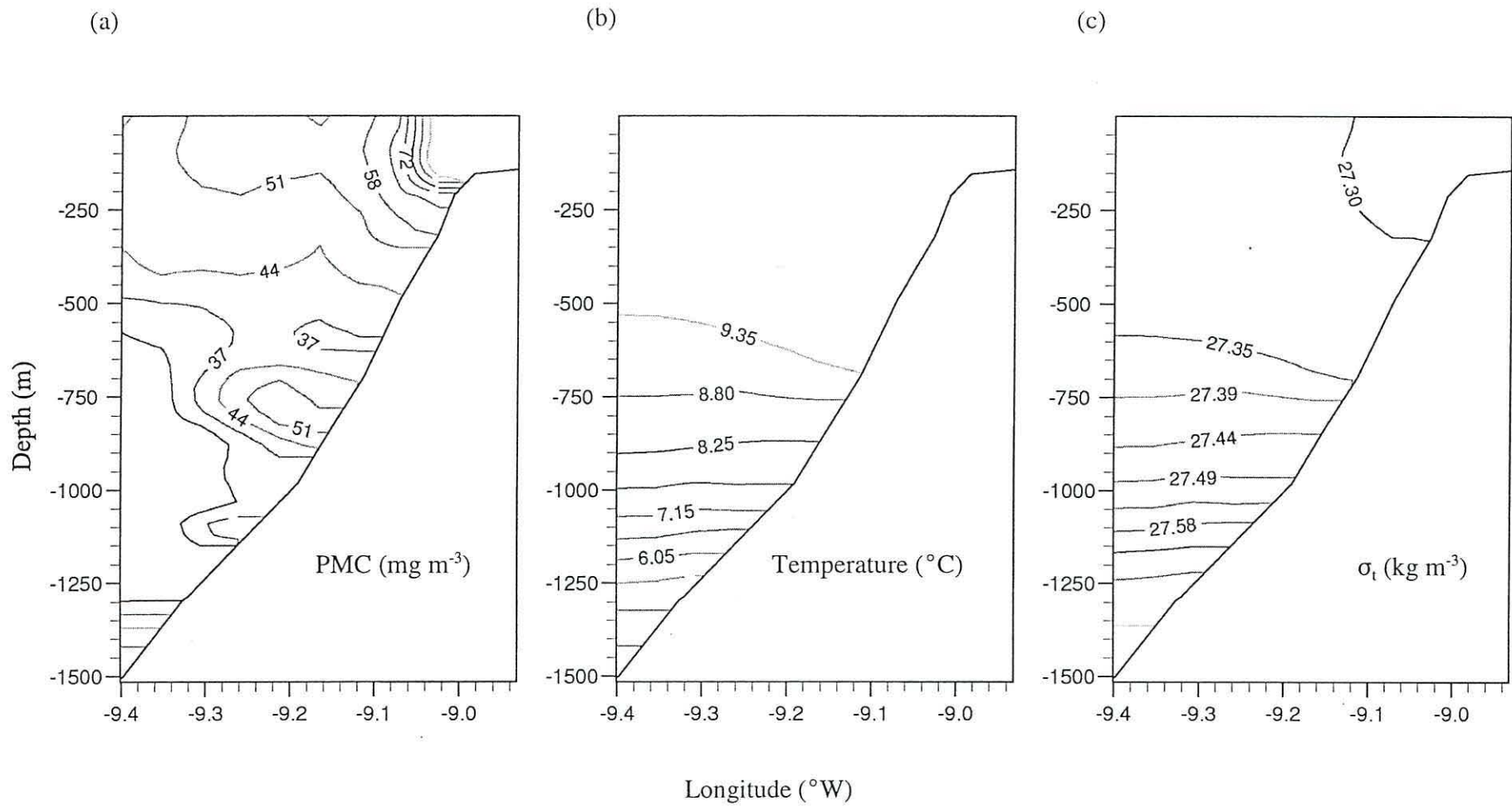
Figure 8.4: Contour plots of (a) particulate matter concentration, (b) temperature and (c) σ_t along the N line during cruise CH125B, after the storm.
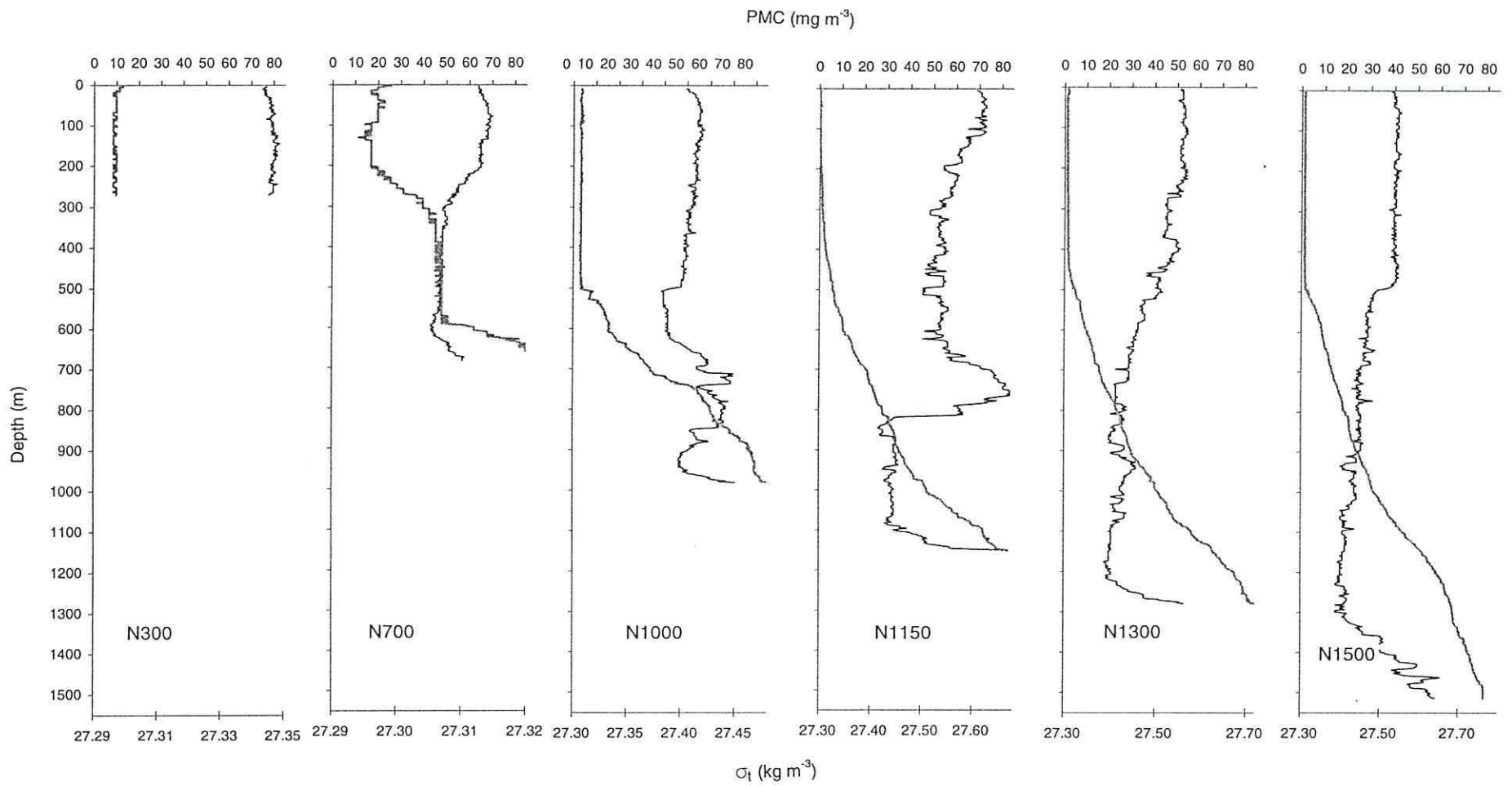
Figure 8.5: Profiles of particulate matter concentration (black line) and σ_t (grey line) at stations along the N line after the storm in February 1996.

Figure 8.6: Time series of PMC (a) near-surface, (b) near-bed, and (c) current speed from moored instruments at S140 in February 1996.

Figure 8.7: Time series of particulate matter concentration, temperature, current speed, cross-slope and along-slope velocities from near-bed moored instruments at N1500 in February 1996.

8.4 Fate of phytodetritus

Another major influence on the concentration distribution of PM at the shelf break was the occurrence of planktonic blooms. Although the cr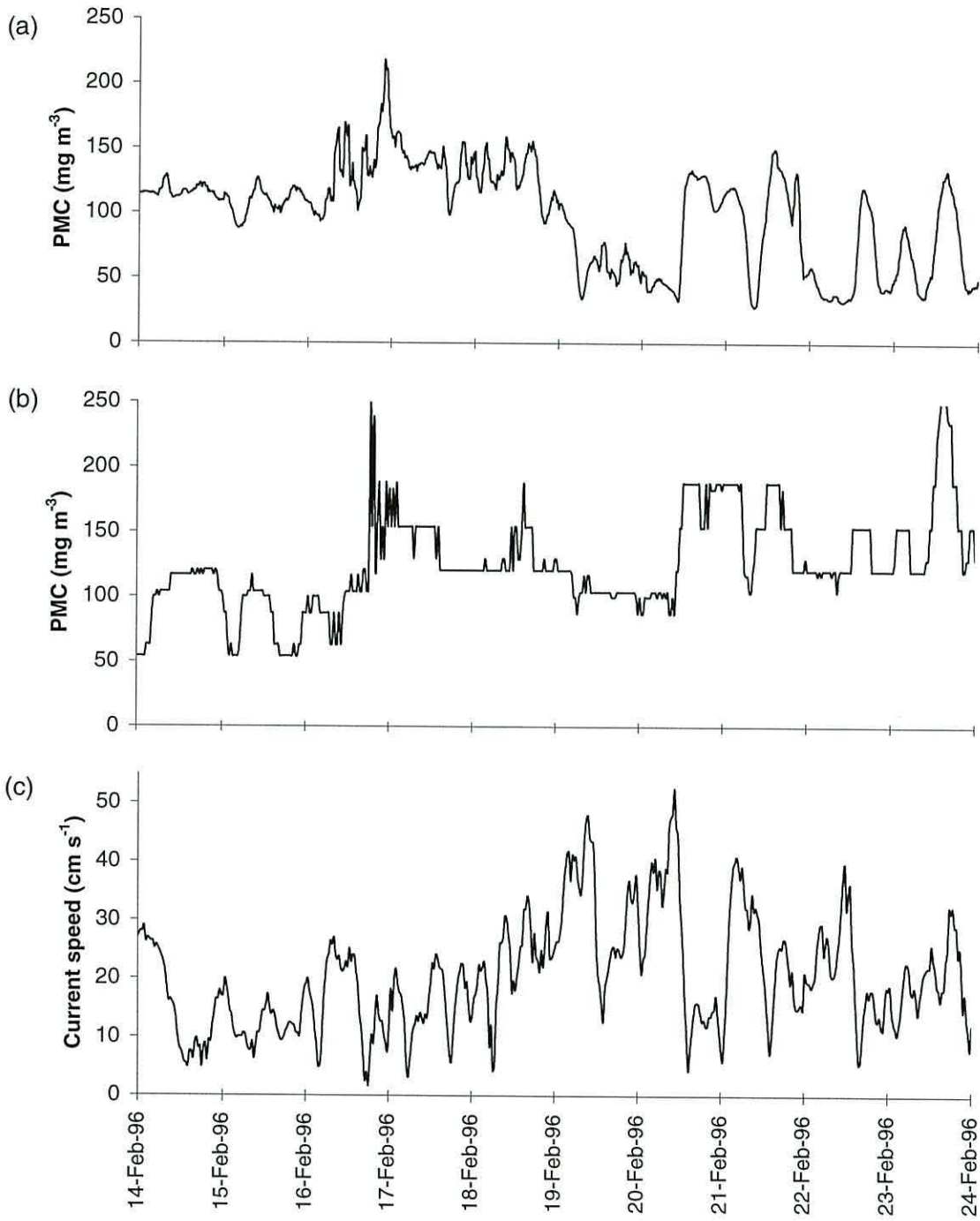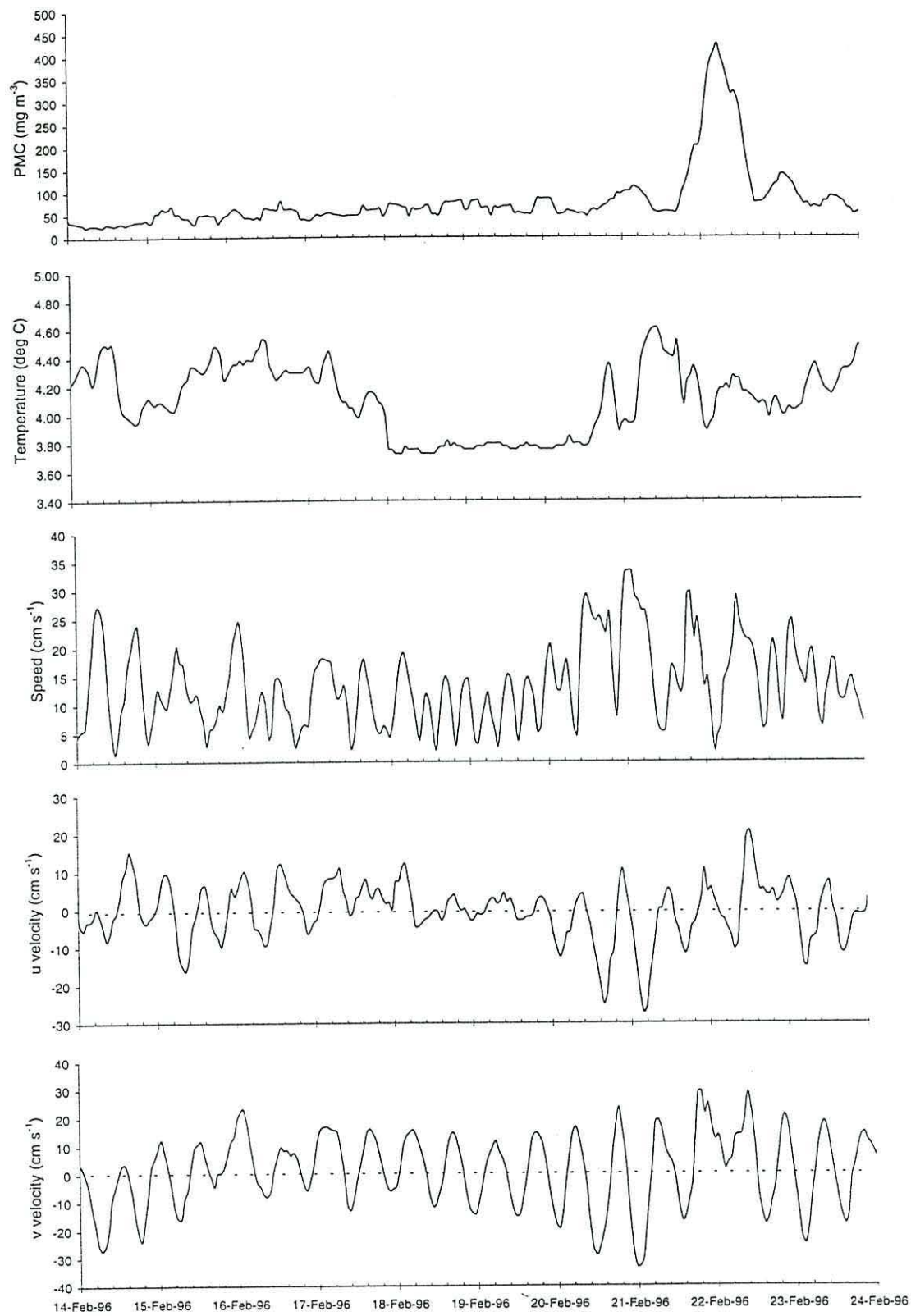uise in May 1995 and the deployment of the moored instruments were too late to observe the onset and peak of the 1995 Spring bloom, some interesting trends were observed. The PMC spatial distribution plots in Chapter 6 indicated that there was a layer of higher concentration material present near the bed down the slope, particularly below the 1000 m isobath. Mean particle size, both at the surface and at the bed, decreased as the end of May approached, indicating a change in the particle population (Chapter 6, Figs. 6.25, 6.29). A layer of fluff was observed on the bed at the mid-slope in mid May (Fig. 6.31). This was made up of bloom detritus that either settled vertically from the surface or was carried laterally from elsewhere. The fluff layer was dominated by particles in the larger size classes (Chapter 6, Fig. 6.30a). Since the upper limit to the size range that the Galai Cis-100 measures is 600 μm, there may have been particles larger than 600 μm present that were not represented in the size distributions. Thomsen (1999) found maximum aggregate sizes of up to 1400 μm at 670 m water depth and 2000 μm at 2800 m water depth at the Celtic Sea continental slope and the Rockall Trough, respectively. There were fewer large particles measured from conventional CTD near-bed water samples but this may be due to the fact that the CTD casts ended approximately 8-10 m above the bed, too high to sample the fluff layer.

Two independent measurements from a CTD cast showed phytoplankton detritus was present at the bed at N1500: a profile of chlorophyll and PM concentration with depth (Figure 8.8), and an image from the Galai video-microscope (Chapter 6, Fig. 6.33). All the deep stations showed similar vertical PMC distributions, with a high concentration surface layer extending 80-100 m deep, decreasing to a minimum throughout the middle of the water column until 50 metres above the bed where PMC increased sharply to levels of similar magnitude as at the surface. The chlorophyll profile in Fig. 8.8 also showed an increase in concentration at the sea floor, from ~0.2 to 0.35 mg m^{-3}. The increase in chlorophyll concentration coincided directly with the increase in PMC, indicating the presence of a near-bed layer with a high concentration of particulate matter, containing phytoplankton detritus. While the

chlorophyll signal was relatively faint at these depths, it nonetheless suggests that the material here had arrived somewhat rapidly from the surface.

In addition to the increase in chlorophyll concentration near-bed, the video-microscope image from near-bed water from the same cast showed clear fragments of diatom chains, indicating that the material was relatively fresh (Chapter 6, Fig. 6.33). The particle size distribution at the bed was dominated by large (> 100 μm) particles but these were absent from the mid-water distribution. The presence of fresh phytodetritus at the bed, combined with a complete absence of larger size classes in the mid-water distribution (Chapter 6, Fig. 6.32) suggests that the bloom detritus at the bed did not settle vertically through the water column from the surface, but was more likely to have been transported laterally from another source.

Settling velocity measurements showed that most of the phytoplankton population in Spring 1995 was settling at rates less than 1-10 m per day. Even if the majority settled from the surface at 10 m per day, it would take 150 days for the material to reach the sea floor at 1500 m. It is unlikely that there would still be even a faint fluorescence signature due to chlorophyll degradation.

Current velocity measurements by moored instruments further up the slope and on the shelf show that the residual cross-shelf flow was in the off-shelf direction and of the order of 3-5 cm s^{-1}. Taking N1500 as an example, the distance between the 140 m and 1500 m isobaths is approximately 30 km. Residual downslope currents could transport material over this distance in approximately 6 to 8 days. This provides a much faster method of transferring material than the vertical settling route, assuming a median settling velocity of the order of 10 m day^{-1}.

Further evidence for the downslope movement of bloom detritus emerged from the 1996 Spring bloom data. Independent measurements from moored and CTD-mounted transmissometers and fluorometers clearly show an event in the bloom, commencing on 02 May. Surface PMC at S140 increased during the latter half of April, while the near-bed concentration remained relatively stable (Figure 8.9(a)). This increase in surface PMC was due to phytoplankton production as CTD profiles

during cruise CH126 in April and May 1996 showed an increase in chlorophyll concentration at this time, reaching a peak around 30/04/96-01/05/96. The CTD beam attenuation signal was closely correlated with chlorophyll concentration (r = 0.92), indicating that the dominant particle population at the surface was biogenic. On 02-03 May, there was a sudden decrease in surface PMC, which coincided with an increase in near-bed PMC (Figure 8.9(a)). The decrease in surface PMC was probably due to the decline of a particular phytoplankton species at that stage of the bloom. Surface PMC did increase again, probably due to succession of other phytoplankton species. For the purposes of this discussion, the subject will be confined to the PMC decrease that occurred on 02-03 May.

Along with the increase in near-bed PMC, an increase in near-bed chlorophyll concentration was observed. Low levels of chlorophyll concentration were observed near the bed (<0.4 mg m^{-3}) for the first two weeks of the cruise (Figure 8.9(b)). However, a sudden increase occurred on 03 May, with near-bed chlorophyll concentration reaching in excess of 1 mg m^{-3}. The CTD beam attenuation record reflected the sudden increase, indicating that the near-bed particle population at this time was dominated by material that had originated at the surface. Near-bed beam attenuation and chlorophyll concentration were highly correlated (r = 0.84) for all shelf and upper slope casts but this correlation improved significantly (r = 0.94) when casts prior to the settling event were excluded. This event was also seen in a moored fluorometer record (data obtained from BODC SES CD-ROM). The time series shows a steady level of chlorophyll concentration near-bed at ~0.4 mg m^{-3} until 03 May, when the concentration increased sharply to ~ 1.4 mg m^{-3} (Figure 8.9(c)).

All of this evidence suggests that biogenic material from the shelf and upper slope surface layer settled rapidly to the bed. The decrease in surface PMC began on 02 May, while the near-bed increase was observed on 03 May, suggesting that material settling from the surface was reaching the bed in approximately one day. Estimates for the height of the surface and bottom mixed layers for the shelf on 03 May were obtained from a temperature profile at N140 on 03 May. Figure 8.10 is a schematic showing the heights of the mixed layers and thermocline, and an upper and lower estimate of the distance that PM could settle through. If it is assumed that there is a

particle population centred on the middle of the surface mixed layer (SML) then this population is required to settle at a rate of 70 m day^{-1} (0.81 mm s^{-1}) to reach the middle of the bottom mixed layer (BML) in one day, representing the upper settling velocity estimate on the shelf. The lower estimate assumes that the particles settle from the bottom of the SML, through the thermocline into the top of the bottom mixed layer where turbulence mixes them through the BML. This gives an estimate of 7 m day^{-1} (0.081 mm s^{-1}), ten times less than the upper estimate.

The settling velocity distribution spectra for Spring 1996 (Chapter 6, Fig. 6.23) showed the majority of chlorophyll-related particulate matter was concentrated in the slower settling classes (< 0.01 mm s^{-1}) for the samples obtained before 03 May. However, in the single sample obtained after this date, there was a shift in the distribution, with an increase in the proportion occupying the 0.02 and 0.06 mm s^{-1} modes. The SVT samples taken during Spring 1996 may have missed a time window during which aggregation was taking place. There is strong evidence to suggest that the main settling event occurred within a time period of a couple of days. The SVTs may have been deployed before and after, but not during the settling event, which could explain the absence in the settling velocity distribution of the modes closer to the upper estimate in the previous paragraph. The increase in the 0.06 mm s^{-1} (5 m day^{-1}) settling class suggests that the lower estimate (7 m day^{-1}) in the previous paragraph may be the more appropriate one for this event.

There was also a marked reduction in the proportion of fine, slowly settling material between the end of April and 06 May (Figure 8.11). A possible explanation for the reduction in the slower settling modes is the occurrence of 'scavenging' by large sticky aggregates formed by phytoplankton. A number of authors (Honjo et al, 1982; Asper, 1987; Alldredge & Silver, 1988) have assumed or demonstrated that large particles of biogenic origin are adhered to by fine particles (< 20 μm) which form the standing stock of particulate matter in the ocean (McCave, 1975; Bishop et al, 1977). Such mechanisms are favoured during periods of phytoplankton blooms (Monaco et al, 1990a). Phytoplankton in shelf seas have been observed to actively secrete sticky substances which enhance aggregation and cause more rapid settling to the bed (Jago et al, 1998). Jones et al (1998) reported 'scavenging' of fine (7 μm) inorganic

particles from the surface layer by large phytodetrital aggregates at the end of a diatom bloom in the North Sea.

Although large phytodetrital aggregates were settling to the bed, there was sufficient energy in the flow to resuspend them. Lampitt (1985) observed resuspension of benthic fluff in currents as weak as 7 cm s^{-1}. Even at the lower slope mean flows were greater than 7 cm s^{-1}, the lowest mean current speed from all of the current meter time series was 11.5 cm s^{-1} (Chapter 6, Table 6.2). Recent experiments using erosion chambers in a BBL show that under critical shear velocities of 0.004-0.009 m s^{-1} aggregates on the surface of the sea bed are resuspended and 0.009-0.012 m s^{-1} have been quoted for phytodetrital fluff (Thomsen, 1999). Gatehouse and Huthnance (1997) estimated the average shear velocity at the upper slope of the SES box as 0.01 m s^{-1}, based on two STABLE deployments for a period of two weeks in August 1995 and February 1996. This is sufficient to resuspend phytodetrital fluff based on the critical shear velocities quoted above, assuming shear velocities in Spring were similar.

CTD casts at mid-slope and lower slope stations showed no evidence of an increase in near-bed chlorophyll concentration by the end of the cruise in mid-May 1996. However, near-bed data from a transmissometer at N1500 and two moored fluorometers at N1500 and P1500 showed that phytoplankton detritus was arriving at the lower slope by the end of May (Figure 8.12).

At N1500, near-bed chlorophyll concentration increased from a consistent background level of ~0.01 mg m^{-3} to 0.03 mg m^{-3} between 20 and 29 May (Fig. 8.12b). During this time, daily mean PMC steadily increased from 40 mg m^{-3} to 150 mg m^{-3} (Fig. 8.12a). A progressive vector plot of currents near-bed at N1500 shows flow was directly offshelf between 19 and 29 May (Figure 8.13). This offshelf flow was transporting material down the slope that probably originated in the surface waters on the shelf.

On 29 May, however, PMC increased sharply from 150 mg m^{-3} to ~320 mg m^{-3} on 01 June. There was no corresponding increase in the chlorophyll record. The progressive

vector plot shows that the current had switched direction between 29 May and 01 June, so that the flow was now upslope, with a slight southerly component. The upslope flow transported material from further down the slope, which was probably older than the relatively fresh material previously transported from upslope. The peak in PMC decreased sharply on 02 June, coinciding with a change in current direction from upslope to downslope.

From 04 June, there was a steady, rapid increase in PMC from ~120 mg m^{-3} to a maximum of ~600 mg m^{-3} on 20 June. One peak in the PMC record coincided exactly with a prominent peak in the chlorophyll signal. Chlorophyll concentration increased on 06 June from 0.02 to 0.04 mg m^{-3} on 07 June. This was reflected in the PMC record with an increase from 165 to 260 mg m^{-3}. Clearly, a pulse of relatively chlorophyll-rich phytodetritus arrived at N1500 during this time. The progressive vector plot shows flow was from the south, along the slope between 05 and 08 June. This pulse may have been related to bloom material from further south which settled on the shelf and was transported down and along-slope to N1500. The timing between the onsets and peaks of the near-bed bloom detritus at S140 and N1500 is very similar (Figure 8.14), strongly implying that the same process is responsible at both sites, i.e. the Spring bloom.

We have evidence that phytoplankton settled to the bed on the shelf on 03 May and bloom-related material started arriving at N1500 near-bed on 25 May, a period of 22 days. The near-bed current meter record at S140 measured a residual off-shelf flow of 1.8 cm s^{-1} (1.6 km day^{-1}) between the time material arrived at the bed at S140 and the increase in chlorophyll and particle concentration at N1500 in late May. The cross-shelf velocity component at the deep site was ~1 km day^{-1}. The distance between the 140 m and 1500 m isobaths is approximately 30 km. A residual off-shelf flow of 1-1.6 km day^{-1} could transport material over this distance in 20-30 days. Thus, one reasonable explanation for the increase in PMC at N1500 is the downslope transport of bloom detritus, which settled to the bed at the shelf and upper slope.

Vertical settling provides an alternative mechanism for the transfer of bloom detritus to the bed at N1500. Using the upper settling rate estimate of 70 m day^{-1} for bloom

material, it would take ~22 days to settle from the surface to the bed at N1500, which is of the right timescale. However, independent settling rates of 2 m day^{-1} (0.02 mm s^{-1}) in Spring 1996 (Perez-Castillo, 1999) were calculated in a parallel study using sediment traps, and are similar to the lower limit estimated in this discussion (7 m day^{-1}). Vertical transfer of material from surface to bed through 1500 m of water at 2-7 m day^{-1} would take ~200-700 days. It is unlikely that after this length of time bloom detritus would invoke a fluorescence signal or retain recognisable structure as seen in the near-bed image (Chapter 6, Fig. 6.33). There was, undoubtably, a proportion of the bloom in the surface waters over the slope that formed large aggregates and settled rapidly to the bed. Vertical settling may also have contributed to the continuing high levels at N1500 after the maximum peak. Therefore, a combination of vertical settling and horizontal down-slope transport of a near-bed layer of detritus that originated on the shelf, is the most likely explanation for the observed increase in PMC at N1500 in June 1996.

The trap data provided additional evidence that a substantial proportion of material arriving at the bed at N1500 did not settle vertically from the surface. On average, throughout the SES campaign, a near-bed sediment trap at 1500 m collected 50% more material than the trap 500 m above the bed at 1000m (Perez-Castillo, 1999), implying that lateral transport of material in a near-bed layer was occurring. Another SES project yielded measurements of slope sediments oxygen consumption rates which indicated that remineralisation of organic carbon was an order of magnitude greater than the vertical supply as measured by the sediment traps (J.Gage, pers. comm.; Perez-Castillo, 1999).

This variety of circumstantial evidence provides support for lateral transport, as opposed to vertical settling, as the dominant mechanism for particle transfer to the lower slope near-bed region, in common with previous margin studies.

The sudden increase in near-bed particle concentration on continental slopes following phytoplankton blooms has been reported by other workers. Photographs of the sea bed on the continental slope south-east of George's Bank in water depths of 450-2400 m showed substantially more flocculent detrital material present on the sea

floor 5 days after the first photographs were taken (Hecker, 1990). This material had a distinctly green hue and it was assumed that the source of this material was surface phytoplankton production during the Spring bloom. Differences in the amount of material at different parts of the slope suggested that the material was not just settling vertically as one would expect the coverage to be fairly uniform down the slope. It was concluded that a rapid settling event had occurred combined with lateral transport of the bloom detritus down the slope.

The OMEX I study reported pulse-like vertical fluxes of fresh phytodetritus into the benthic boundary layer from the euphotic zone (Thomsen & van Weering, 1998). Settling velocities of the order of 150 m day^{-1} were quoted for phytodetrital aggregates. However, they concluded that down slope transport dominates close to the sea bed and quote a transport time of within 21 days for fresh phytodetritus from near-bed shelf waters to 1500 m, similar to the time estimated for the same process to occur in the SES box.

Biological mediation of aggregates during bloom conditions has been shown to occur in the Irish Sea (Jago *et al*, 1998). It is therefore not unreasonable to assume that a population of phytoplankton at the Hebridean slope underwent biologically mediated aggregation, settled rapidly to the bed, especially at the shelf and upper slope where depths are shallower, and the residual off-shelf flow transported this material down the slope and out of the SES box. Of course a larger proportion of material at the upper and mid-slope will be transported along the slope, under the influence of the slope current, than will go off-shelf. Nevertheless, this represents an important transfer of organic material to the lower slope, and potentially the deep ocean. Future studies should extend the mooring array further down the slope in order to better quantify the currents at the lower slope as we have very limited data at this depth in this study.
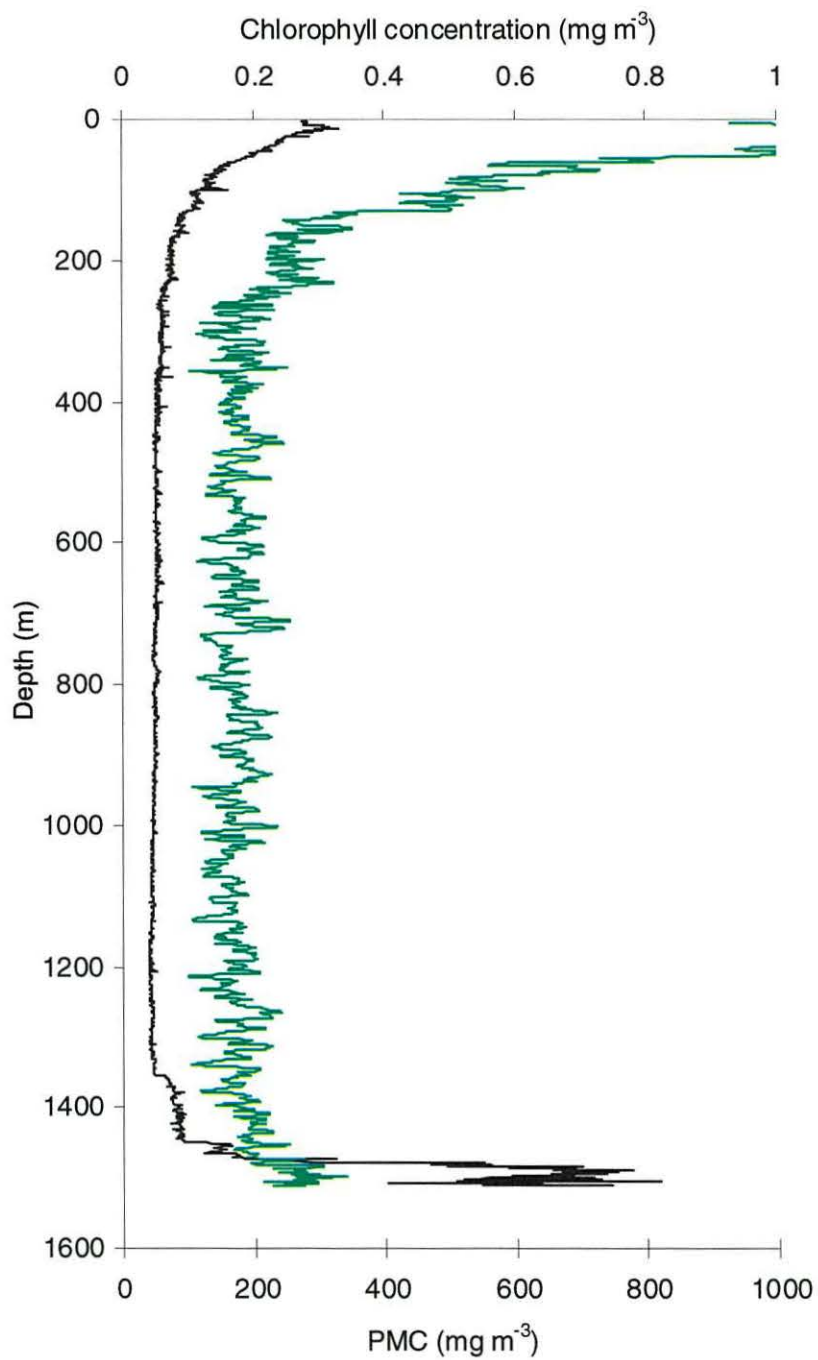
Figure 8.8: Profiles of PMC (black line) and chlorophyll concentration (green line) at N1500, 24 May 1995.
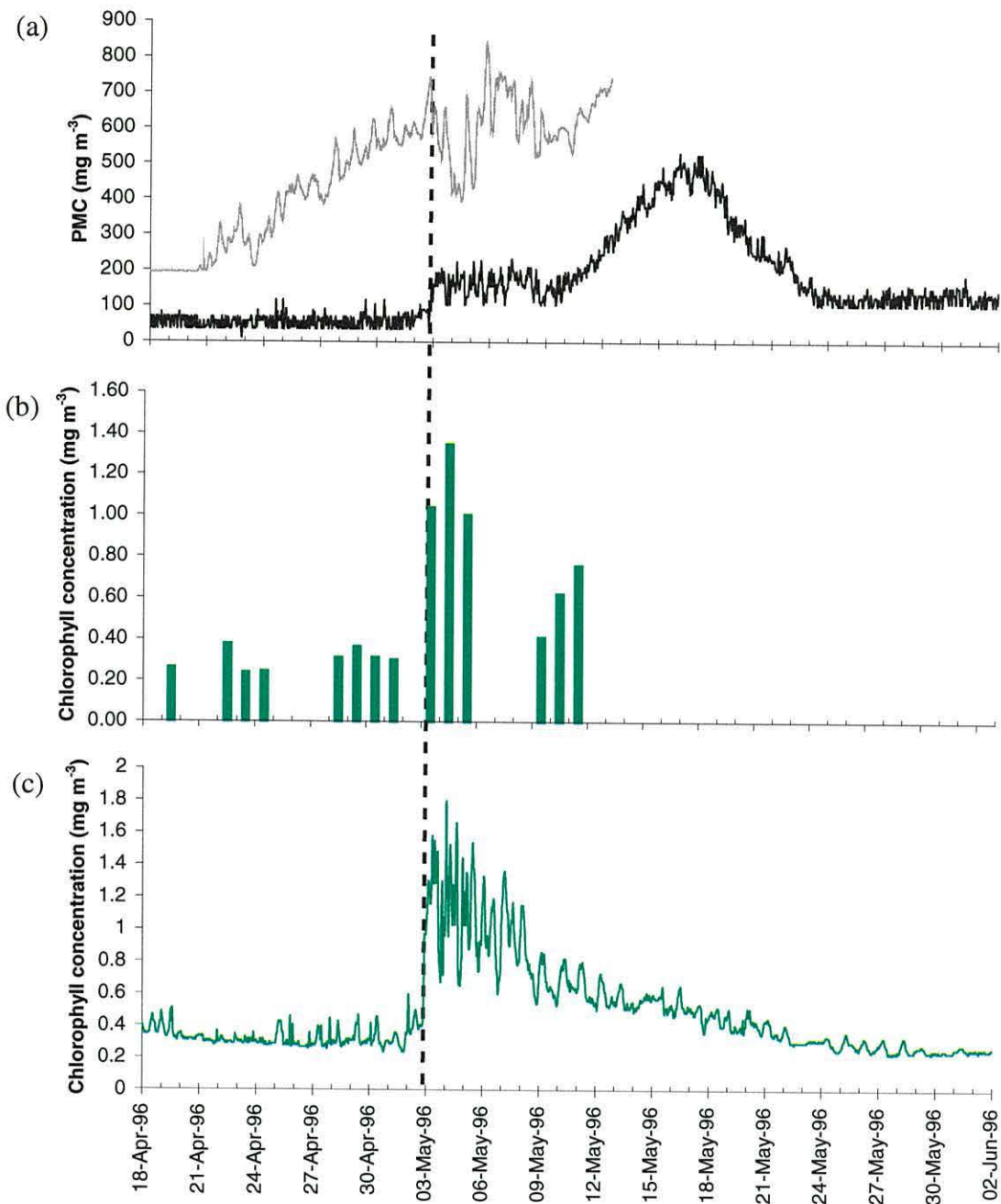
Figure 8.9: (a) Time series of particulate matter concentration at S140 from near-surface (grey line) and near-bed (black line) moored tranmissometers; (b) Near-bed chlorophyll concentration at 140-300 m stations from CTD casts; (c) Time series of chlorophyll concentration at S140 from a near-bed moored fluorometer. The dashed line marks an event which started on 03 May where surface PMC decreased, whilst near-bed PMC and chlorophyll concentration increased.
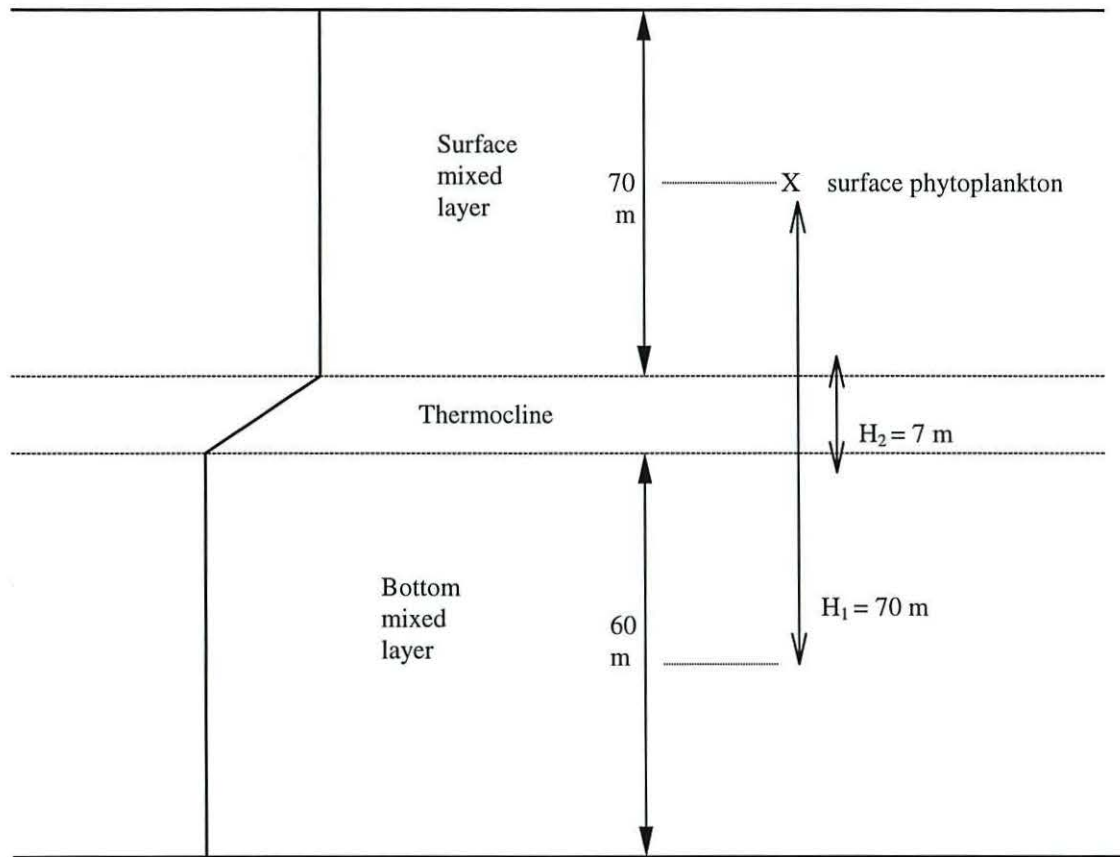
Figure 8.10: Schematic representation of phytoplankton settling from the surface mixed layer to the bottom mixed layer on the shelf in the SES box. Mixed layer heights and thermocline thickness are based on a temperature profile at N140 on 03 May 1996. H_1 represents an upper estimate and H_2 a lower estimate for the distance the particles are settling through.
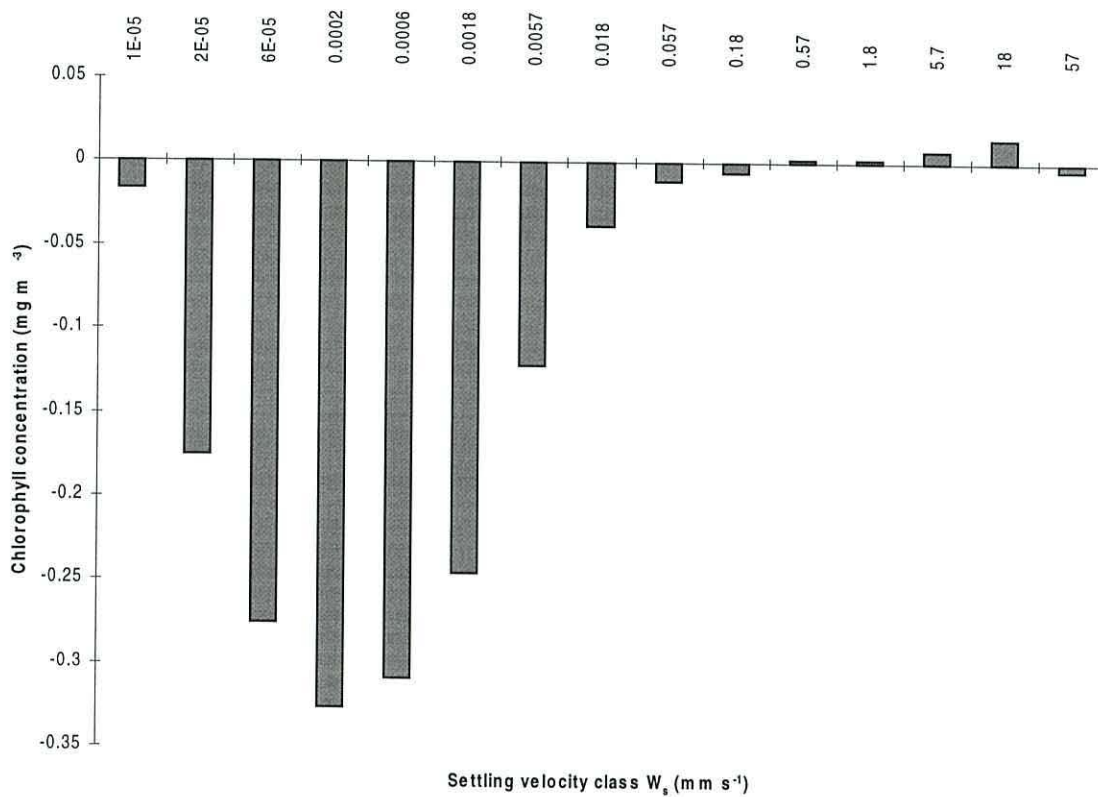
Figure 8.11: Graph showing the difference between chlorophyll settling velocity distributions on 28/04/96 (S140) and 06/05/96 (S1300). A negative value means that there has been a reduction in chlorophyll concentration in that particular settling class with time.
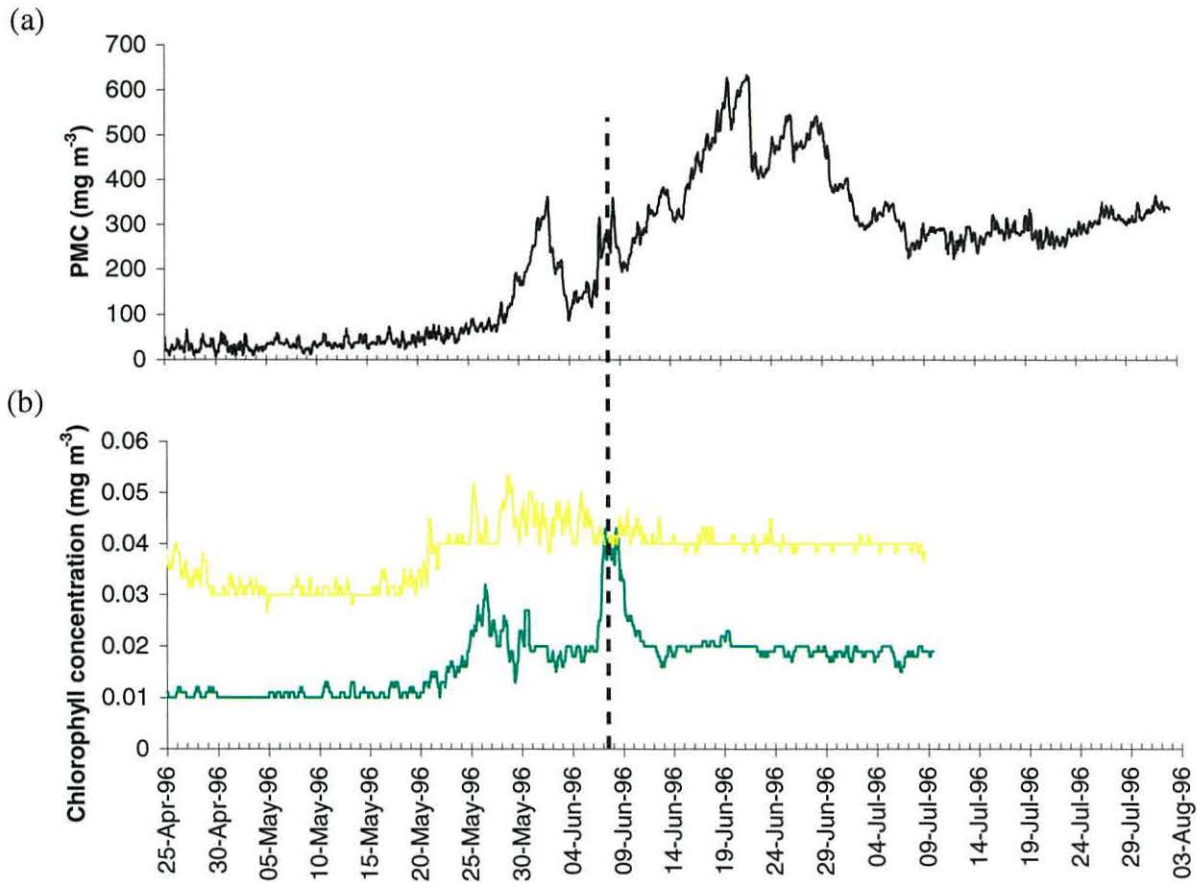
Figure 8.12: Time series of (a) near-bed PMC at N1500 and (b) near-bed chlorophyll concentration at P1500 (yellow line) and N1500 (green line). The dashed line shows an increase in PMC coinciding with an increase in chlorophyll concentration at N1500.
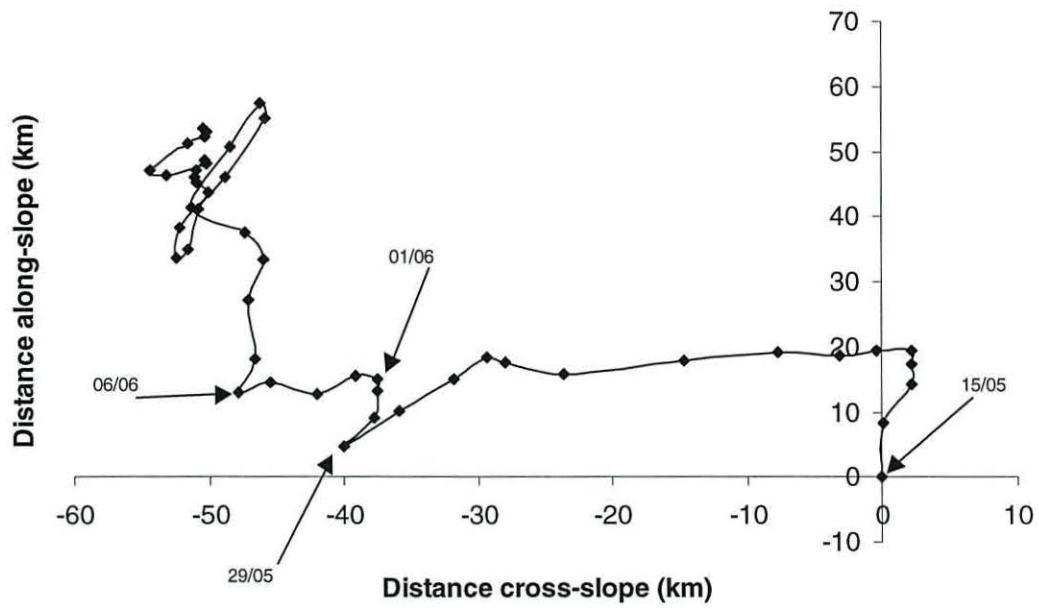
Figure 8.13: Progressive vector plot from near-bed velocity measurements at N1500 in Spring 1996. Dates of specific points are indicated with arrows.

Figure 8.14: Time series of particulate matter concentration at S140 (black line) and N1500 (grey line) in Spring and Summer 1996. The arrows point to the onsets and peaks of the Spring bloom event in both records.

8.5 The importance of lateral fluxes

The two major contributors to near-bed PMC have been identified as resuspension due to storms, and detritus settling in the aftermath of phytoplankton blooms. Once PM has reached the benthic boundary layer (BBL) it must be transported by a physical process pro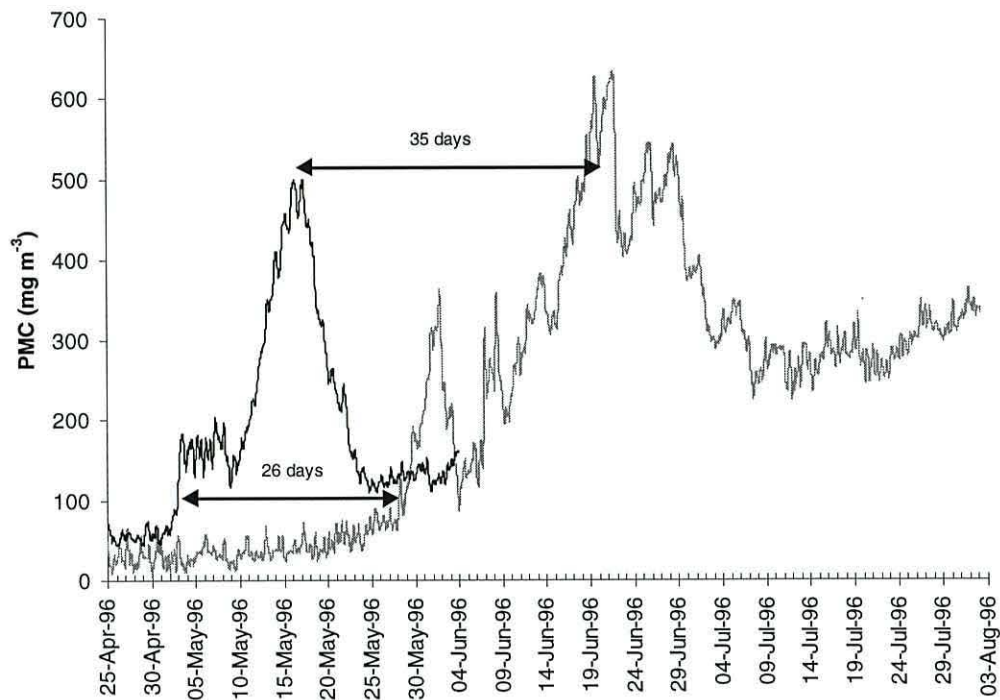ducing a residual flow. The net direction and rate of sediment transport is the result of many oceanographic processes that operate on different time and space scales. Although the residual circulation is typically only a few cm s^{-1} and is thus not strong enough to resuspend bottom sediments, it is important in determining the net direction of material transport over a long period of time. For example, very fine silts and clays that settle slowly are easily transported by a weak mean flow, and resuspension events caused by energetic internal waves or tides which are oscillatory by themselves result in a net transport of material when even a weak mean flow is superimposed. Therefore, although the residual circulation is not the whole transport story at the shelf break, it is an important component.

It is evident that the slope current dominated fluxes at the upper slope stations. The along-slope component was more than double that across the slope, and usually in the northward direction. At the deeper sites, along-slope fluxes remained greater than those across-slope but the difference was not as large. Cross-slope export of material was persistent at all stations during all the seasons for which data were obtained. A current flowing towards the north on a west-facing slope induces downslope Ekman transport in the BBL in the northern hemisphere (Apel, 1987). A reasonable explanation, therefore, for the persistent downslope near-bed flow is the presence of the poleward flowing slope current at the Hebridean margin. This flow, though weaker, was still apparent at the 1500 m isobath.

Averaging all near-bed mooring fluxes, at all sites and all times of the year, gives a mean off-shelf flux of 0.00288 g m^{-2} s^{-1}, or 249 g m^{-2} day^{-1}. The height of the BBL is proportional to (Apel, 1987):

$$h = \frac{ku*}{f} \tag{8.1}$$

where u* is the shear velocity, k is von Karman's constant (0.4), and f is the Coriolis parameter, with units of s^{-1}. Data from the STABLE rig provided an estimate of 0.01

m s^{-1} for the average shear velocity at the upper slope (Gatehouse & Huthnance, 1997). The height of the BBL calculated from equation 8.1 is of the order of 80 m, which corresponds well with observed BNL thickness. With a BBL of 80 m and a mean flux of 249 g m^{-2} day^{-1} we get off-shelf transport of the order of 20 kg m^{-1} day^{-1}. These figures represent back-of-the-envelope calculations but give a feel for the magnitude of material that moves downslope.

Vertical fluxes were estimated from sediment trap data between September 1995 and July 1996 (Perez-Castillo, 1999). The average total mass flux from the bottom trap was ~136 g m^{-2} y^{-1}, and 67 g m^{-2} y^{-1} at the trap at 1000 m (500 mab). The bottom trap gave a higher value due to the effects of resuspension and lateral transport near the bed. The average cross-shelf flux calculated from all the time series data at all the sites is 0.0288 g m^{-2} s^{-1} (90 kg m^{-2} y^{-1}). Thus lateral fluxes calculated in this study were almost three orders of magnitude greater than the observed vertical flux.

Few lateral flux estimates are available in the literature for comparative purposes. Laine *et al* (1994) calculated fluxes of 10 g m^{-2} day^{-1} across the Bermuda Rise, an order of magnitude less than this study. Thomsen (1999) estimated that 480-4800 g m^{-2} day^{-1} of particulate matter, in the form of aggregates, is transported laterally in the Rockall Trough by residual currents, and Puig *et al* (2000) measured mean horizontal particle fluxes of 216-345 g m^{-2} day^{-1} on the Barcelona continental slope. Thus the estimates from this study appear reasonable.

In the OMEX I study, which concentrated on the slope to the south west of Ireland, horizontal particulate organic carbon (POC) fluxes were estimated by multiplying mean POC concentrations and mean flow velocities in the BBL. Again, lateral fluxes were found to be orders of magnitude higher than the vertical fluxes, of the order of 25 kg POC m^{-2} y^{-1}, or 68 g POC m^{-2} day^{-1} (Thomsen & van Weering, 1998).

During the SES campaign, few PMC and POC samples were taken concurrently. However, a very good relationship (r = 0.94) was found between the samples available (Fig 8.14). Regression analysis allowed POC to be predicted from PMC in order to compare the flux estimates from the OMEX area with this study. Details of

the POC and PM samples used in the analysis are shown in Table 8.1.

Table 8.1: Details of PM and POC samples taken concurrently during the SES campaign.

Cruise	Station	Cast	Depth (m)	POC (mgC m^{-3})	PM (mg m^{-3})
CD93B	S300	166	5	122	709
CD93B	S300	166	267	52	343
CD93B	N1500	137	5	179	1138
CH123B	N1500	39	1495	16	1
CH123B	S200	80	6	33	170
CH123B	S200	80	224	29	35
CH128A	S140	14	30	250	2378
CH128A	S140	14	60	112	1239
CH128A	S140	14	138	59	420
CH128A	S300	5	5	243	1668
CH128A	S300	5	253	51	93
CH128A	S700	44	695	23	1
CH128A	S850	42	103	45	424
CH128A	S850	42	836	21	340
CH128A	S1000	41	300	35	427
CH128A	S1000	41	1000	30	361

The regression equation is:

$$POC \ (mgC \ m^{-3}) = 0.109 * PM \ (mg \ m^{-3}) + 15.3 \qquad (8.2)$$

Thus a POC flux of 68 gC m^{-2} day^{-1} equates to an PM flux of 618 g m^{-2} day^{-1} at the OMEX site. The magnitude of cross-slope flux at the Hebridean Shelf is therefore similar to that estimated south of the SES area in the OMEX I region. However, as the majority of POC/PM samples were Summer ones, this may only be representative of fluxes at times of high biogenic production.

The carbon dynamics and community structure of the benthos on the Hebridean slope were studied by Martyn Harvey and Lynda Mitchell from NERC-DML and SAMS-DML, respectively. The organic carbon 'demand' by the benthic community was estimated from sediment community oxygen consumption (SCOC) measurements by Martyn Harvey. He estimated that 22 g C m^{-2} y^{-1} is utilised by the benthic community. Perez-Castillo (1999) reported a vertical supply of 6 g C m^{-2} y^{-1}, which accounts for only 26 % of the carbon that is needed by the benthic community. It would appear that lateral transport plays a major role in supplying organic carbon to the benthos down the slope. A large biomass was observed at the mid-slope region being supported by the steady stream of material flowing down the slope (J. Gage, pers. comm.).
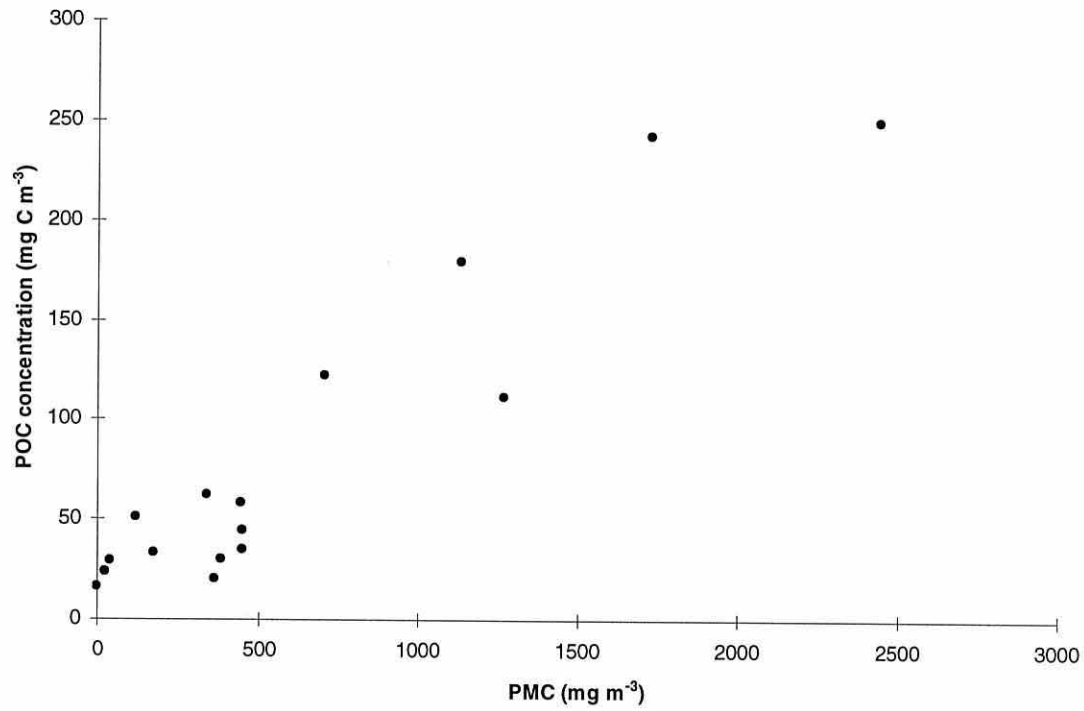
Figure 8.15: Relationship between particulate matter concentration and particulate organic carbon concentration in the SES box. Both properties were directly measured from the same CTD bottle.

8.6 Conclusions

The data from this study, and SES as a whole, have provided a valuable insight into the processes and exchanges occurring at the Hebridean shelf edge. The key features that emerged from the results of this study are summarised below, followed by suggestions that could benefit future studies of this nature.

The spatial distribution of PM at the Hebridean Shelf edge, both vertically and across the slope, was typical of many continental margins, with a three layer distribution in the vertical, and particle concentration tending to decrease seawards. PMC varied seasonally with the occurrence of phytoplankton blooms and storm resuspension events. On the upper slope, PM distribution was influenced by the poleward-flowing slope current, which is confined to the upper 500 m and produces a core of warmer, more saline water with higher PMC. Further down the slope, benthic nepheloid layers formed a characteristic feature throughout the year, but especially in Winter and late Spring. Intermediate nepheloid layers, following density surfaces, were also observed in the aftermath of a storm.

In Spring, phytoplankton blooms provide carbon-rich detritus, which settles rapidly to the bed forming a layer of fluff. However, median phytoplankton settling velocities measured in surface waters (< 0.2 m day^{-1}) were not consistent with the times apparently taken for phytodetritus to reach the bed. Measurements may have missed short-lived aggregation events. Time and personnel constraints during cruises meant that SVT sampling was somewhat limited. Future studies would benefit from higher resolution SVT sampling, focusing on near-bed as well as surface settling velocity distributions.

There is evidence that a rapid transit system conveys the detritus down the slope over a period of one to two weeks. In Winter, resuspension of material on the shelf and slope occurs intermittently resulting in intermediate and benthic nepheloid layers and additional export of material to the deep ocean. Significant resuspension due to tides or internal waves was not observed during this study.

119

Near bed PM flux calculations indicate that PM is persistently transported northwards along-slope by the slope current, and off-shelf in the benthic boundary layer, even at depths of 1500 m. Along-slope fluxes were 2-3 times greater than across-slope fluxes and were greatest on the shelf and upper slope. In common with previous margin studies, fluxes of material in a near-bed layer down the slope provided up to three orders of magnitude more material than the vertical supply. This accounts for some of the discrepancies found by other workers in SES where the vertical flux of carbon measured by sediment traps was not sufficient to supply the benthic community demand.

The maintenance of long time series is important in looking for seasonal and inter-annual variability in PM distribution and transport. The paucity of time series data from the deep stations (700-1500 m) means that there is uncertainty about the amount of material that is exported out of the SES box to the deep ocean. In SES the main instrument array along the S line extended as far as S700. Future studies should extend the main cross-slope instrument array to at least 1500 m. Longer sampling periods are required, in general, in order to observe interannual variability and the integrated effects of processes spanning different time scales.

PMC measurements in this study were largely obtained indirectly by transmissometers. Therefore there is no information on shorter term or seasonal variation in particle characteristics in the BBL. Instrument systems have been developed for *in situ* measurement of PM transport dynamics in the BBL (Thomsen, 1999) and future studies at this shelf break would benefit from a direct insight to PM behaviour close to the bed. However, this study has shown the importance of indirect PM measurements in obtaining accurate flux estimates and demonstrated the potential for combined particle size, settling velocity and transmissometer measurements.

REFERENCES

Aanderaa (1992). RCM 7 and 8 Operating manual, technical description no. 159. Aanderaa, Bergen, Norway.

Alldredge A.L. (1979). The chemical composition of macroscopic aggregates in two neritic seas. *Limnology and Oceanography*, **24:** 855-866.

Alldredge A.L., and M.W. Silver (1988). Characteristics, dynamics and significance of marine snow. *Progress in Oceanography*, **20**: 41-82.

Alldredge A.L., and C. Gotschalk (1989). Direct observation of the mass flocculation of diatom blooms: characteristics, settling velocities and formation of aggregates. *Deep-Sea Research.* **60**: 159-171.

Alldredge A.L., U. Passow, and B. Logan (1993). The existence, abundance, and significance of large transparent exopolymer particles in the ocean. *Deep-Sea Research I*, **40**: 1131-1140.

Anderson R.F., G.T. Rowe, P.F. Kemp, S. Trumbore and P.E. Biscaye (1994). Carbon budget for the mid-slope depocentre of the Middle Atlantic Bight. *Deep-Sea Research II*: **41**: 669-703.

Andrie C. and L. Merlivat (1988). Tritium in the western Mediterranean Sea during the 1981 *Phycemed* cruise. *Deep-Sea Research*, **35**: 247-267.

Antia A.N., B. von Bodungen, and R. Peinert (1999). Particle flux across the mid-European continental margin. *Deep-Sea Research*, **46:** 1999-2024.

Apel J.R. (1987). *Principals of ocean physics*. Academic Press, London.

Asper V.L. (1987). Measuring the flux and sinking speed of marine snow aggregates. *Deep-Sea Research*, **34**: 1-17.

Azetzu-Scott K., B.D. Johnson, and B. Petrie (1995). An intermittent, intermediate nepheloid layer in Emerald Basin, Scotian Shelf. *Continental Shelf Research,* **15(2/3)**: 281-293.

Baines P.G. (1986). Internal tides, internal waves, and near inertial motions. In: *Baroclinic Processes on Continental Shelves* (ed. C.N.K. Mooers): *Coastal and Estuarine Sciences*, **3**: 19-31: American Geophysical Union, Washington D.C.

Baker E.T., and J.W. Lavelle (1984). The effect of particle size on the light attenuation coefficient of natural suspensions. *Journal of Geophysical Research*, **89 (C5)**: 8199-8203.

Baker E. and B. Hickey (1986). Contemporary sedimentation processes in and around an active west coast submarine canyon. *Marine Geology*, **71**: 15-34.

Bartz R., J.R.V. Zaneveld and H. Pak (1978). A transmissometer for profiling and moored observations in water. *SPIE Ocean Optics V*, **160**: 102-108.

Biscaye P.E., R.F. Anderson, and B.L. Deck (1988). Fluxes of particles and constituents to the eastern United States continental slope and rise: SEEP-I. *Continental Shelf Research*, **8:** 855-904.

Biscaye P.E. and R.F. Anderson (1994). Fluxes of particulate matter on the slope of the southern Middle Atlantic Bight: SEEP II. *Deep-Sea Research II*, **41(2/3)**: 459-509.

Biscaye P.E., C.N. Flagg and P.G. Falkowski (1994). The Shelf Edge Exchange Processes Experiment, SEEP-II: and introduction to hypotheses, results and conclusions. *Deep-Sea Research II*: **41**: 231-252.

Bishop J.K.B., J.M. Edmond, D.R. Ketten, M.P. Bacon, and W.B. Silker (1977). The chemistry, biology and vertical flux of particulate matter from the upper 400 m of the equatorial Atlantic ocean. *Deep-Sea Research*, **25**: 511-548.

Bishop J.K.B. (1986). The correction and suspended particulate matter calibration of Sea Tech transmissometer data. *Deep-Sea Research*: **33**: 121-134.

Bishop J.K.B., R.C. Smith and K. Baker (1992). Springtime distributions and variability of biogenic particulate matter in Gulf Stream warm core ring 82B and surrounding NW Atlantic waters. *Deep-Sea Research* (Suppl. 1A), **S295-S325.**

Booth D.A. and D.J. Ellett (1983). The Scottish continental slope current. *Continental Shelf Research*, **2**: 127-146.

Bridge J.S. and D.F. Dominic (1984). Bed load grain velocities and sediment transport rates. *Water Resource Research*, **20(4)**: 476-490.

Brewer P.G., D.W. Spencer, P.E. Biscaye, A. Hanley, P.S. Sachs, C.L. Smith, S. Kadar and J. Fredericks (1976). The distribution of particulate matter in the Atlantic Ocean. *Earth and Planetary Science Letters.*, **32:**393-402.

Butman B. (1988). Downslope Eulerian mean flow associated with high-frequency current fluctuations observed on the outer continental shelf and upper slope along the northeastern United States continental margin: implications for sediment transport. *Continental Shelf Research*, **8**: 811-840.

Campbell D.E. and R.W. Spinrad (1987). The relationship between light attenuation and particle characteristics in a turbid estuary. *Estuarine, Coastal and Shelf Science*, **25**: 53-65.

Campbell A.R. (1996). Effects of turbulence on suspended sediment concentrations in a tidal flow. *Unpublished Ph.D. Thesis*, University of Wales, Bangor, U.K.

Churchill J.H., P.E. Biscaye, and F. Aikman (1988). The character and motion of suspended particulate matter over the shelf edge and upper slope off Cape Cod. *Continental Shelf Research*, **8**: 789-809.

Churchill J.H., C.D. Wirick, C.N. Flagg, and L.J. Pietrafesa (1994). Sediment resuspension over the continental shelf east of the Delmarva Peninsula. *Deep-Sea Research Part II - Topical Studies in Oceanography* **41 (2,3)**: 341-363.

Cooper L.N.H. and D. Vaux (1949). Cascading over the continental slope of water from the Celtic Sea. *Journal of the Marine Biological Association of the U.K.*, **28**: 719-750.

Csanady G.T., J.H. Churchill and B. Butman (1988). Near-bottom currents over the continental slope in the Mid-Atlantic Bight. *Continental Shelf Research*, **8**: 653-671.

Dickson R.R. and I.N. McCave (1986). Nepheloid layers on the continental slope west of Porcupine Bank. *Deep-Sea Research*, **33(6)**: 791-818.

Drake D.E. (1971). Suspended sediment and thermal stratification in the Santa Barbara Channel, California. *Deep-Sea Research*, **18**: 763-769.

Drake D.E., R.L. Kolpack, and P.J. Fischer (1972). Sediment transport on Santa Barbara-Oxnard Shelf, Santa Barbara Channel, California. In: *Shelf Sediment Transport: Process and pattern.* Swift D.J.P., Duane D.B., and Pilkey O.H. (eds). Dowden, Hutchinson and Ross, Stroudsburg, PA. 307-332

Durrieu de Madron X., F. Nyfeller, and C.H. Godet (1990). Hydrographic structure and nepheloid spatial distribution in the Gulf of Lions continental margin. *Continental Shelf Research*, **10**: 915-929.

Durrieu de Madron X. (1995). Calibration des mesures du néphélomètre intégrateur profond en terme de charge particulaire. *Technical Report 95/1*. Laboratoire de Sédimentologie et Géochimie Marines, Université de Perpignan, France.

Durrieu de Madron X., P. Castaing, F. Nyffeler, and T. Courp (1999). Slope transport of suspended particulate matter on the Aquitanian margin of the bay of Biscay. *Deep-Sea Research II*, **46**: 2003-2027.

Duursma E.K., and D. Eisma (1973). Theoretical, experimental and field studies concerning reactions of radioisotopes with sediments and suspended particles of the sea: Applications to field studies. *Netherlands Journal of Sea Research*, **6**: 265-324.

Dyer K.R. (1986). *Coastal and Estuarine Sediment Dynamics*, Wiley-Interscience, London.

Eckman J.E., A.R.M. Nowell, and P.A. Jumars (1981). Sediment destabilisation by animal tubes. *Journal of Marine Research*, **39**: 361-374.

Emery K.O., and S. Honjo (1979). Surface suspended matter off western Africa: Relations of organic matter, skeletal debris, and detrital minerals. *Sedimentology,* **26**: 775-794.

Eisma D. and G. Irion (1988). Suspended matter and sediment transport. In *Pollution of the North Sea, an assessment.* W. Salomons, B.L. Bayne, E.K. Duursma and U. Förstner (eds.), Springer-Verlag.

Eisma D. (1993). *Suspended matter in the aquatic environment.* Springer-Verlag, Berlin Heidleberg.

Etcheber H., J.C. Relexans, M. Beliard, O. Weber, R. Buscail, and S. Heussner (1999). Distribution and quality of sedimentary organic matter on the Aquitanian margin (Bay of Biscay). *Deep-Sea Research II,* **46**: 2249-2288.

Ewing M., and E.M. Thorndike (1965). Suspended matter in deep ocean water. *Science,* **147**: 1291-1294.

Falkowski P.G., P.E. Biscaye and C. Sancetta (1994). The lateral flux of biogenic particles from the eastern North American continental margin to the North Atlantic ocean. *Deep-Sea Research II,* **41(2/3)**: 583-601.

Folk R.L and W.C. Ward (1957). Brazos river Bar, a study in the significance of grain size parameters. *Journal of Sedimentary Petrology,* **27**: 3-26.

Gardner W.D., and L.G. Sullivan (1981). Benthic storms: temporal variability in a deep ocean nepheloid layer. *Science,* **213**: 329-331.

Gardner W.D. (1983). Suspended sediment transport in Baltimore Canyon and adjacent slope. Canyon and Slope Process study, Vol. II. Report to U.S. Department of the Interior, L.D.G.O., Palisades, New York, 135-241

Gardner W.D., P.E. Biscaye, J.R.V. Zaneveld, and M.J. Richardson (1985). Calibration and comparison of the LDGO nephelometer and the OSU transmissometer on the Nova Scotian Rise. *Marine Geology,* **66**: 323-344.

Gardner W.D. and I.D. Walsh (1990). Distribution of macroaggregates and fine-grained particles across a continental margin and their potential role in fluxes. *Deep-Sea Research,* **37**: 401-411.

Gatehouse D.K., and J.M. Huthnance (1997). Description and analysis of data recorded by STABLE II during *Challenger* cruise CH121 '95 and CH125 '96 SES, Malin Shelf. *Proudman Oceanographic Laboratory Internal Document No. 115.* 36pp.

Grant W.D., L.F. Boyer, and L.P. Sanford (1982). The effect of biological processes on the initiation of sediment motion in non-cohesive sediment. *Journal of Marine Research,* **40**: 659-677.

Gross T.F., A.J. Williams, and A.R.M. Nowell (1988). A deep-sea sediment transport storm. *Nature*, **331**: 518-521.

Gross T.F, and A.J. Williams (1991). Characterisation of deep sea storms. *Marine Geology*, **99**: 281-301.

Hall I.R., S. Schmidt, I.N. McCave and J.L. Reyss (2000). Particulate matter disequilibrium and $234^{Th}/238U$ disequilibrium along the Northern Iberian Margin: implications for particulate organic carbon export. *Deep-Sea Research I*, **47:** 557-582.

Harikrishnan M. (1998). Flow and water column structure at the Hebridean shelf edge. *Unpublished Ph.D. Thesis*. University of Wales, Bangor, U.K.

Harvey J.G. (1982). *Atmosphere and Ocean: Our Fluid Environments*. Artemis Press, 143 pp.

Heathershaw A.D. (1985). Some observations of internal wave current fluctuations at the shelf edge and their implications for sediment transport. *Continental Shelf Research*, **4**: 485-493.

Hecker B. (1990). photographic evidence for the rapid flux of particles to the sea floor and their transport down the continental slope. *Deep-Sea Research*, **37(12)**: 1773-1782.

Heussner S., X. Durrieu de Madron, O. Radakovitch, L. Beaufort, P.E. Biscaye, J. Carbonne, N. Delsaut, H. Etcheber, and A. Monaco (1999). Spatial and temporal patterns of downward particle fluxes on the continental slope of the Bay of Biscay (northeastern Atlantic). *Deep-Sea Research*, **46**: 2101-2146.

Hickey B., E. Baker, and N. Kachel (1986). Suspended particle movement in and around Quinalt Submarine Canyon. *Marine Geology*, **71**: 35-83.

Hill A.E. and J.H. Simpson (1994). The shelf edge current system. In: *LOIS Shelf Edge Study Programme*. Report of the SES Workshop at Proudman Oceanographic Laboratory, Bidston, U.K. April 11-13 1994.

Hill A.E., A.J. Souza, K. Jones, J.H. Simpson, G.I. Shapiro, R. McCandliss, H. Wilson and J. Leftley (1998). The Malin cascade in Winter 1996. *Journal of Marine Research*, **56**: 87-106.

Holmes R. (1994). Seabed topography and other geotechnical information for the Shelf Edge Study 55°N-60°N NW of Britain. In: *LOIS Shelf Edge Study Programme*. Report of the SES Workshop at Proudman Oceanographic Laboratory, Bidston, U.K. April 11-13 1994.

Honjo S. (1976). Coccoliths: production, transportation and sedimentation. *Marine Micropaleontology*, **1**: 65-79.

Honjo S., S.J. Manganinni and L.J. Poppe (1982). Sedimentation of lithogenic particles in the deep ocean. *Marine Geology.* **50**: 199-220

Humphery J.D. (1998). A photographic section through the SES area. In: *SES Winter Workshop Report.* Report of the SES workshop at Burton Manor, Wirral, 14-15 January 1998.

Humphery J.D., J.D. Gage, and R. Holmes (1998). The use of seabed photography to provide benchmark information for environmental impact studies. Proudman Oceanoographic Laboratory internal publication.

Hunter K.A. and P.S. Liss (1979). The surface charge of suspended particles in estuarine and coastal waters. *Nature*, **282**: 823-825.

Hunter K.A. and P.S. Liss (1982). Organic matter and the surface charge of suspended particles in estuarine waters. *Limnology and Oceanography*, **27**: 322-335.

Huthnance J.M. (1981). Waves and currents near the continental shelf edge. *Progress in Oceanography*, **10**: 31-42.

Huthnance J.M. (1984). Slope currents and "JEBAR". *Journal of Physical Oceanography*, **14:** 795-810.

Huthnance J.M., L.A. Mysak, and D.P. Wang (1986). Coastal trapped waves. In *Baroclinic Processes on Continental Shelves*, ed. C.N.K. Mooers, pp. 1-18. Washington D.C. AGU (*Coastal and Estuarine Sciences*, **3**).

Huthnance J.M. (1995). Circulation, exchange and water masses at the ocean margin: the role of physical processes at the shelf edge. *Progress in Oceanography*, **35**: 353-431.

Jago C.F., G. Novarino and G. Kennaway (1998). Biologically mediated particle aggregation and suspended particle dynamics in shelf seas. NERC final report.

Jerlov N.G. (1953). Particle distribution in the ocean. In: *Reports of the Swedish Deep-Sea Expedition*, Vol. 2, *Physics and Chemistry* **No.3**: 73-97.

Jerlov N.G. (1976). Marine Optics. Elsevier, Amsterdam, 231pp

Jones K. (1994). Phytoplankton and nutrient dynamics at the Hebridean Shelf edge. In: *LOIS Shelf Edge Study Programme.* Report of the SES Workshop at Proudman Oceanographic Laboratory, Bidston, U.K. April 11-13 1994.

Jones S.E. and C.F. Jago (1996). Determination of settling velocity in the Elbe Estuary using QUISSET tubes. *Journal of Sea Research*, **36(1/2)**: 63-67.

Jones S.E., C.F. Jago, A.J. Bale, D. Chapman, R.J.M. Howland and J. Jackson (1998). Aggregation and resuspension of suspended particulate matter at a seasonally

stratified site in the southern North Sea: physical and biological controls. *Continental Shelf Research*, **18**: 1283-1309.

Jumars P.A., and A.R.M. Nowell (1984). Effects of benthos on sediment transport: difficulties with functional grouping. *Continental Shelf Research*, **3**: 115-130.

Kenyon N. (1987). Mass-wasting features on the continental slope of northwest Europe. *Marine Geology*, **74**: 55-77.

Kranck K. and T.G. Milligan (1988). Macroflocs from diatoms: *in-situ* photography of particles in Bedford Basin, Nova Scotia. *Marine Ecology Progress Series*. **44**: 183-189.

Krause G. and K. Ohm (1984). A method to measure suspended load transports in estuaries. *Estuarine, Coastal and Shelf Science*, **19**: 611-618.

Krone R.B. (1978). Aggregation of suspended particles in estuaries. In: *Estuarine Transport Processes*. B. Kjerve ed., University of Southern Carolina Press. 117-190.

Laine E.P., W.D. Gardner, M.J. Richardson and M. Kominz (1994). Abyssal currents and advection of resuspended sediment along the north eastern Bermuda Rise. *Marine Geology*, **119**: 159-171.

Lall D. (1977). The oceanic microcosm of particles. *Science*, **198(4321)**: 520-527.

Lambert C.E., C. Jehanno, N. Silverberg, J.C. Brun-Cottan and R. Chesselet (1981). Log-normal distributions of suspended particles in the open ocean. *Journal of Marine Research*, **39**: 77-98.

Lampitt R.S. (1985). Evidence for the seasonal deposition of detritus to the deep-sea floor and its subsequent resuspension. *Deep-Sea Research*, **32**: 885-897.

McCave I.N. (1975). Vertical flux of particles in the ocean. *Deep-Sea Research*, **22**: 491-502.

McCave I.N. (1983). Particulate size spectra, behaviour and origin of nepheloid layers over the Nova Scotian continental rise. *Journal of Geophysical Research*, **88**: 7647-7666.

McCave I.N. (1984). Erosion, transport and deposition of fine-grained marine sediments. In: *Fine-grained sediments: deep water processes and facies*. Stow D.A.V. and Piper D.J.W. (ed.s). Geological Society of London Special Publication **15**: 35-69.

McCave I.N. (1985). Properties of suspended sediment over the HEBBLE area on the Nova Scotian Rise. *Marine Geology*, **66**: 169-188.

McCave I.N., I.R. Hall, A.N. Antia, L. Chou, F. Dehairs, R.S. Lampitt, L. Thomsen, T.C.E. van Weering and R. Wollast (submitted). Distribution, composition and flux of

particulate material over the European margin at 47°-50° N: Results from OMEX I. Submitted to *Deep-Sea Research II* (November 1998).

Meade R.H., P.L. Sachs, F.T. Manheim, J.C. Hathaway and D.W. Spencer (1975). Sources of suspended matter in waters of the Middle Atlantic Bight. *Journal of Sedimentary Petrology*, **45**: 171-188.

Mehta A.J., and E. Partheniades (1975). An investigation of the depositional properties of flocculated fine sediment. *Journal of Hydrological Research*, **13**: 361-381.

Millot C. (1990). The Gulf of Lions hydrodynamics. *Continental Shelf Research*, **10**: 885-894.

Monaco A., P. Biscaye, J. Soyer, R. Pocklington and S. Heussner (1990a). Particle fluxes and ecosystem response on a continental margin: the 1985-1988 Mediterranean ECOMARGE experiment. *Continental Shelf Research* **10(9-11)**: 809-839.

Monaco A., T. Courp, S. Heussner, J. Carbonne, S.W. Fowler, and B Deniaux. (1990b). Seasonality and composition of particulate fluxes during ECOMARGE-I, western Gulf of Lions. *Continental Shelf Research*, **10**: 959-987.

Monaco A., P.E. Biscaye and P. Laborde (1999). The ECOFER (ECOsystème du canyon du cap-FERret) experiment in the Bay of Biscay: introduction, objectives and major results. *Deep-Sea Research II*, **46**: 1967-1978.

Moody J.A., B. Butman, and M.H. Bothner (1987). Near-bottom suspended matter concentration on the continental shelf during storms: Estimates based on *in situ* observations of light transmission and a particle size dependent transmissometer calibration. *Continental Shelf Research*, **7**: 609-628.

Murray J.W. (1987). Coastally derived signals to the ocean interior: stable inorganic species. In: *Ocean Margins in GOFS*. U.S. GOFS Planning Report, **6**: 245pp.

New A.L. (1988). Internal tidal mixing in the Bay of Biscay. *Deep-Sea Research*, **37**: 691-709.

Newberger P.A., and D.R. Caldwell (1981). Mixing and the bottom nepheloid layer. *Marine Geology*, **41**: 321-336.

Nittrouer C.A. and L.D. Wright (1994). Transport of particles across continental shelves. *Reviews of Geophysics*, **32**: 85-113.

Nyfeller F., A. Wyttenbach, and J.M. Jaquet (1985). The benthic boundary layer: nepheloid and thermal structure, comparison of the suspended matter. Interim oceanographic description of the N.E. Atlantic site for the disposal of low-level radioactive waste. *O.E.C.D.*, **2**: 9-28.

Olsen M., and C. Lundsgaard (1991). Sedimentation of organic matter from the euphotic zone in Kattegat. In: *Sediment Trap Studies in the Nordic Countries. Proceedings of the Symposium: Sediment traps in marine ecological research and monitoring (1991).* P. Wassmann, A.S. Heiskanen, and O. Lindhal, (Eds). Kristineberg Marine Biological Station, Sweden, 21-25 November, 1990, 309pp.

Owen M.W. (1976). Determination of the settling velocities of cohesive muds. Hydraulic Research Station, Wallingford, Oxon., Report No. IT 161:1-8.

Pak H., l.A. Codispoti, and J.R.V. Zaneveld (1980a). On the intermediate particle maxima associated with oxygen-poor water off western South America. *Deep-Sea Research*, **27**: 783-797.

Pak H., J.R.V. Zaneveld and J. Kitchen (1980b). Intermediate nepheloid layers observed off Oregon and Washington. *Journal of Geophysical Research*, **85**: 6697-6708.

Passow U., A.L. Alldredge, and B.E. Logan (1994). The role of particulate carbohydrate exudates in the flocculation of diatom blooms. *Deep-Sea Research.* **41**: 335-357.

Perez-Castillo F. (1999). Sedimentation of organic matter on the Hebridean slope. *Unpublished Ph.D. Thesis*, University of Wales, Bangor, U.K.

Price J.F., and M.O.N. Baringer (1994). Outflows and deepwater production by marginal seas. *Progress in Oceanography*, **33**: 161-200.

Pugh D.T. (1987). *Tides, surges and mean-sea level.* J. Wiley publications, Chichester, New York.

Puig P., A. Palanques, J. Guillen and E. Garcia-Ladona (2000). Deep slope currents and suspended particle fluxes in and around the Foix submarine canyon (NW Mediterranean). *Deep-Sea Research*, **47**: 343-366.

Richardson M.J. (1987). Particle size, light scattering and composition of suspended particulate matter in the North Atlantic. *Deep-Sea Research*, **34**: 1301-1329.

Richardson M.J., G. Weatherly and W.D. Gardner (1993). Benthic storms in the Argentine Basin. *Deep-Sea Research*, **40(4/5)**: 975-987.

Riebesell U. (1991a). Particle aggregation during a diatom bloom. I: Physical aspects. *Marine Ecology Progress Series.* **69**: 273-280.

Riebesell U. (1991b). Particle aggregation during a diatom bloom. II: Biological aspects. *Marine Ecology Progress Series.* **69**: 281-291.

Riley G.A. (1963). Organic aggregates in seawater and dynamics of their formation and utilization. *Limnology and Oceanography*, **8**: 372-381.

Riley G.A. (1970). Particulate organic matter in seawater. *Advances in Marine Biology*, **82**: 1-110.

Sathyendranath S. and T. Platt (1990) The light field in the ocean. *Light and Life in the Sea*, P.J. Herring, A.K. Campbell, M. Whitfield and L. Maddock (eds.) Cambridge University Press.

Sea-Tech Transmissometer manual (1990). Sea Tech Inc., P.O. Box 779, Oregon, U.S.A.

Sherwin T. and J. Huthnance (1994). Three dimensional observations of the shelf edge internal wave field. In: *LOIS Shelf Edge Study Programme*. Report of the SES Workshop at Proudman Oceanographic Laboratory, Bidston, U.K. April 11-13 1994.

Shideler G.L. (1981). Development of the benthic nepheloid layer on the South Texas continental shelf, Western Gulf of Mexico. *Marine Geology*, **41**: 37-61.

Simpson J.H., and J.R. Hunter (1974). Fronts in the Irish Sea. *Nature*, **250**: 404-406.

Simpson J.H. (1994). Shelf Edge Study (SES) implementation plan. In: *LOIS Shelf Edge Study Programme*. Report of the SES Workshop at Proudman Oceanographic Laboratory, Bidston, U.K. April 11-13 1994.

Souza A.J., J.H. Simpson, M. Harikrishnan and J. Malarkey (1999). Structure and seasonality of the flow in the Hebridean shelf regime. *Oceanologica Acta*, in press.

Spinrad R.W., J.R.V. Zaneveld, and J.C. Kitchen (1983). A study of the optical characteristics of the suspended particles in the benthic boundary layer of the Scotian Rise. *Journal of Geophysical Research*, **88**: 7641-7645.

Tett P. (1987). Plankton. In '*Biological Survey of Estuaries and Coasts*. Ed. Baker, J. and Wolff, W.J. *Cambridge University Press*, pp. 280-341.

Tett P.B., I.R. Joint, D.A. Purdie, M. Baars, S. Oosterhuis, G. Daberi, F. Hannah, D.K. Mills, D. Plummer, A.J. Pomroy, A.W. Walne, and H.J. Witte (1993). Biological consequences of tidal stirring gradients in the North Sea. *Phil. Trans. Roy. Soc. Series A*, **343(1669)**: 493-508.

Thomsen L. and Tj.C.E van Weering (1998). Spatial and temporal variability of particulate matter in the benthic boundary layer at the N. W. European Continental Margin (Goban Spur). *Progress in Oceanography*, **42**: 61-76.

Thomsen L. (1999). Processes in the benthic boundary layer at continental margins and their implication for the benthic carbon cycle. *Journal of Sea Research*, **41**: 73-86.

Thorpe S.A. (1972). A sediment cloud below the Mediterranean outflow. *Nature*, **239**: 326-327.

Trent J.D., A.L. Shanks and M.W. Silver (1978). *In situ* and laboratory measurements on macroscopic aggregates in Monterey Bay, California. *Limnology and Oceanography*, **23**: 626-636.

Trowbridge J.H., B. Butman and R. Limeburner (1994). Characteristics of the near-bottom suspended sediment field over the continental shelf off northern California based on optical attenuation measurements during STRESS and SMILE. *Continental Shelf Research*, **14**: 1257-1272.

Tucholke B.E., and S. Eittreim (1974). The western boundary undercurrent as a turbidity maximum over the Puerto Rico Trench. *Journal of Geophysical Research*, **79**: 4115-4118.

Van Rijn L.C. (1993). *Principles of Sediment Transport in Rivers, Estuaries and Coastal Seas*. Aqua Publications, Amsterdam. 638 pp.

Van Weering T.C.E, I.N. McCave, and I.R. Hall (1998a). Ocean Margin Exchange (OMEX I) benthic processes study. *Progress in Oceanography*, **42**: 1-4.

Van Weering T.C.E., I.R. Hall, H.C. de Stigter, I.N. McCave and L. Thomsen (1998b). Recent sediments, sediment accumulation and carbon burial at Goban Spur, N.W. European continental margin (47-50°N). *Progress in Oceanography*, **42**: 5-35.

Walsh J.J. (1983). Death in the sea: enigmatic phytoplankton losses. *Progress in Oceanography*, **12**: 1-86.

Walsh J.J. (1988). *On the Nature of Continental Shelves*, Academic Press, San Diego, 520 pp.

Walsh J.J., P.E. Biscaye, and G.T. Csanady (1988). The 1983-1984 Shelf Edge Exchange Processes (SEEP)-I experiment: Hypotheses and highlights. *Continental Shelf Research*, **8**: 435-456.

Walsh J.J. (1994). Particle export at Cape Hatteras. *Deep-Sea Research II*, **41(2/3)**: 603-628.

Weeks A.R. (1989). Spatial and time dependent variations in suspended particulate material concentrations in the shelf seas. *Unpublished Ph.D. Thesis*, University of Wales, Bangor, U.K.

White M. (1994). Tidal and sub-tidal variability in the sloping benthic boundary layer. *Journal of Geophysical Research*, **99**: 7851-7864.

Whitehead J.A. (1987). Dense water off continents. *Nature*, **327**: 656
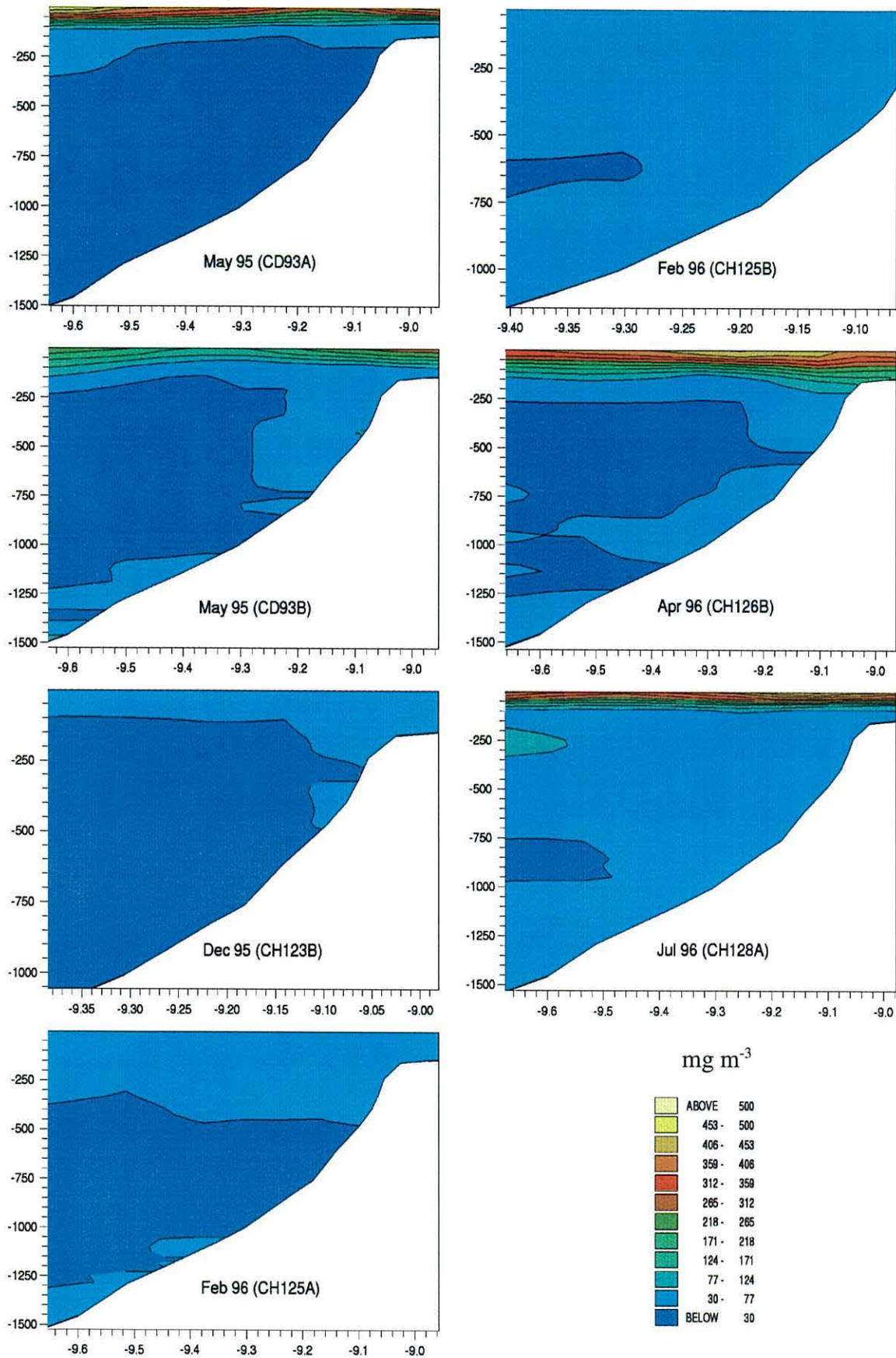
APPENDIX 1

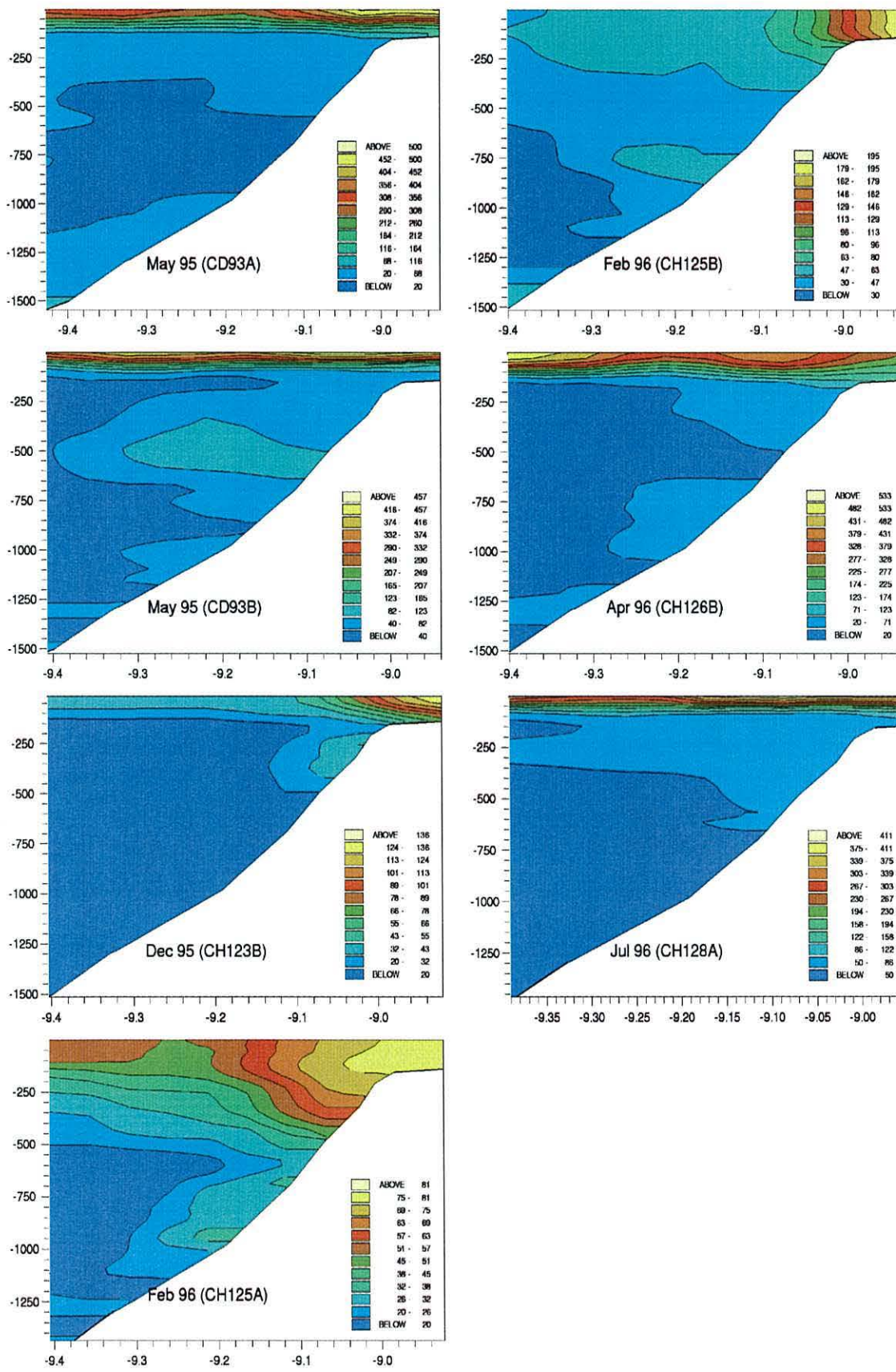Figure A.1: Particulate matter concentration sections along the S line across the shelf edge during SES.

Figure A.2: Particulate matter concentration sections along the N line across the shelf edge during SES. Contour scaling is different for each section in order to emphasise features in the distribution that might otherwise be masked.